WADD TECHNICAL REPORT 61-123

PROPERTIES OF YTTRIUM AND THE RARE EARTH METALS OXYGEN AND ALLOY SYSTEMS

OXYGEN AND ALLOY SYSTEMS

BERNARD LOVE

RESEARCH CHEMICALS
(A DIVISION OF NUCLEAR CORPORATION OF AMERICA)

AUGUST 1961

AERONAUTICAL SYSTEMS DIVISION

PDH

NOTICES

When Government drawings, specifications, or other data are used for any purpose other than in connection with a definitely related Government procurement operation, the United States Government thereby incurs no responsibility nor any obligation whatsoever; and the fact that the Government may have formulated, furnished, or in any way supplied the said drawings, specifications, or other data, is not to be regarded by implication or otherwise as in any manner licensing the holder or any other person or corporation, or conveying any rights or permission to manufacture, use, or sell any patented invention that may in any way be related thereto.

Qualified requesters may obtain copies of this report from the Armed Services Technical Information Agency, (ASTIA), Arlington Hall Station, Arlington 12, Virginia.

This report has been released to the Office of Technical Services, U. S. Department of Commerce, Washington 25, D. C., for sale to the general public.

Copies of ASD Technical Reports and Technical Notes should not be returned to the Aeronautical Systems Division unless return is required by security considerations, contractual obligations, or notice on a specific document.

WADD TECHNICAL REPORT 61-123

PROPERTIES OF YTTRIUM AND THE RARE EARTH METALS OXYGEN AND ALLOY SYSTEMS

OXYGEN AND ALLOY SYSTEMS

BERNARD LOVE

RESEARCH CHEMICALS
(A DIVISION OF NUCLEAR CORPORATION OF AMERICA)

AUGUST 1961

DIRECTORATE OF MATERIALS & PROCESSES
CONTRACT No. AF 33(616)-6829
PROJECT No. 7351

AERONAUTICAL SYSTEMS DIVISION
AIR FORCE SYSTEMS COMMAND
UNITED STATES AIR FORCE
WRIGHT-PATTERSON AIR FORCE BASE, OHIO

500 - December 1961 - 11-383 & 384

FOREWORD

This report was prepared by Research Chemicals under USAF Contract No. AF 33(616)-6829. This contract was initiated under Project No. 7351, "Metallic Materials," Task No. 73517, "Unique Metallic Materials and Techniques." The work was administered under the direction of the Directorate of Materials and Processes, Deputy for Technology, Aeronautical Systems Division, with Lt. S. A. Worcester acting as project engineer.

This report covers work conducted from October 1959 to October 1960.

The author, Bernard Love, was principal investigator on the program. Assistance was provided by members of the staff of Research Chemicals including Joseph Jenista, Craig Kirkpatrick, Wayne Lovald, Sten O. Samson, Edward Stoyack, Ronald C. Vickery, and William Ward.

ABSTRACT

Partial constitutional diagrams were established for a number of systems containing yttrium and the lanthanide elements. These studies were made as the first step in efforts to produce alloys with improved mechanical and atmospheric corrosion properties for use at elevated temperatures.

Alpha yttrium and erbium are completely soluble in all proportions. The yttrium-neodymium system is more complex. There is partial solubility at both ends of the system. An intermediate phase is present at the equi-atomic percentage composition. No marked beta phase stabilization was established.

The rare earth rich end of the yttrium, erbium, neodymium, and samarium systems with oxygen were investigated. The solubility of oxygen is low in the metals at temperatures up to the transformation temperature or 1000°C. The transformation temperature of neodymium is essentially unaffected, that of samarium is raised slightly. The nature of the elevated temperature portion of each system is less certain and two alternative phase diagrams are proposed. The preferred diagram indicates the presence of a high temperature interstitial monoxide.

The cobalt end of the cobalt-erbium system was investigated. A number of intermetallic compounds are formed. The first of these, $Co_{17}Er_2$, enters into eutectic reaction with cobalt. The solubility of erbium in cobalt is low, and the cobalt phase transformation is essentially unaffected by the presence of small additions of erbium. The cobalt-yttrium system appears to be similar.

Tantalum-lanthanum, tantalum-erbium, tantalum-yttrium, niobium-erbium, and niobium-yttrium systems were investigated. All systems were similar in their general characteristics. An extensive liquid immiscibility region is present which terminates in a monotectic very near the tantalum (niobium) end of the system. A eutectic is present at the rare earth end of the system. Room temperature solid solubility is very low, but there may be slight solubility at elevated temperature.

The alpha to beta transformation temperature was determined to be 848°C for neodymium, and 930°C for samarium. The transformation temperature of yttrium is approximately 20-30°C below the melting point of yttrium. Both the transformation and melting temperatures are somewhat dependent upon metal purity.

Atmospheric corrosion rates were determined in the above systems. Lower rates were found for certain niobium alloys, and for cobalt compositions, with added rare earths.

Improved mechanical properties were found for yttrium-erbium alloys and for yttrium-zirconium alloys ascribed to solid solution hardening. The latter age at room temperature, and rapidly over-age at elevated temperatures.

Procedures for purification of yttrium and erbium by vacuum distillation were developed. Improved methods for oxygen and tantalum analysis are described.

The addition of erbium to beryllium yields alloys indicating improved purity and grain refinement.

PUBLICATION REVIEW

This report has been reviewed and is approved.

FOR THE COMMANDER:

I. PERLMUTTER
Chief, Physical Metallurgy Branch
Metals and Ceramics Laboratory
Directorate of Materials & Processes

TABLE OF CONTENTS

TABLE OF CONTENTS (Continued)

TABLE OF CONTENTS (Continued)

LIST OF TABLES

LIST OF TABLES (Continued)

LIST OF FIGURES

LIST OF FIGURES (Continued)

LIST OF FIGURES (Continued)

LIST OF FIGURES (Continued)

LIST OF FIGURES (Continued)

LIST OF FIGURES (Continued)

LIST OF FIGURES (Continued)

LIST OF FIGURES (Continued)

INTRODUCTION

Background. The development of separations and reductions technology has recently made pure rare earth metals available in experimental and pilot plant quantities. The feasibility of extending these methods to commercial scale production has been established. A major program of investigation of the properties and potential applications of these materials has been undertaken by the Research Chemicals Division of Nuclear Corp. of America.

This research program has been greatly aided by the sponsorship of the Wright Air Development Division, Air Research and Development Command, Wright-Patterson Air Force Base, Ohio. A literature survey was made (25); and recently revised to be published as WADD 60-864. All of the rare earth metals were prepared, and analytic and metallographic examination techniques were developed. An extensive program to establish phase relationships between selected rare earth metals and zirconium, titanium, copper, tin, cobalt, vanadium, chromium, and beryllium was completed (26,27). Preliminary investigations of the mechanical properties of various rare earth metals and alloys were reported (26,28). Atmospheric corrosion rates were determined for the rare earth metals at both room and elevated temperatures and for dry and moist air exposure (26).

Scope of Current Program. The results of the above programs indicated areas of interest and potential value for further studies. Particular emphasis was placed upon improved atmospheric corrosion properties of materials for use in elevated temperature applications, and the effects of rare earth additions on the fabrication and mechanical properties of such materials. Included are studies in yttrium-lanthanide, and rare earth-oxygen systems; and systems of rare earths with cobalt, nickel, beryllium, tantalum, niobium, and zirconium. Requirements for high purity rare earth metals for these studies led to continued investigations of purification methods, and to development of vacuum distillation procedures.

Manuscript released by author 20 February 1961 for publication as a WADD Technical Report.

EXPERIMENTAL METHODS

Materials

Rare earth metals were prepared by Research Chemicals by metallothermic reductions as described in the following section. Typical analyses of the as-cast metal are given in Table I. The preparation of distilled metals is discussed in the section "Purification Studies".

The cobalt used for alloy preparations included high purity powder and rondels kindly furnished in research quantities by the Cobalt Information Center, Battelle Memorial Institute, Columbus, Ohio, and cobalt metal obtained from the General Chemical Division, Allied Chemical Corporation (B & A code 1588, 98-99%) and from Belmont Smelting and Refining Works, Brooklyn, New York. Other metals used included: zirconium, reactor grade, obtained from the Columbia-National Corporation, Pensacola, Florida; nickel, reagent grade, J. T. Baker Chemical Co., Phillipsburg, New Jersey; beryllium, premium grade (crushed lump), Brush Beryllium Co., Cleveland, Ohio; and tantalum sheet and niobium first melt bar stock from Fansteel Metallurgical Corporation, North Chicago, Illinois. Analyses of these materials are given in Table II.

Preparation of Rare Earth Metals

Complete details of preparation methods for the rare earth metals have been presented in previous reports (25, 26, 27, 28). A brief general description only is presented below.

Lanthanum, neodymium, yttrium, and erbium were prepared by the metallothermic reduction of the respective anhydrous fluorides. Rare earth oxides from the stocks of Research Chemicals were converted to chlorides, and the hydrated fluorides were precipitated by addition of hydrofluoric acid. These were washed, dried, and carefully dehydrated by heating in vacuum. The fused fluorides were heated under argon with a slight excess of calcium metal. After the reduction was completed the slag was removed and the metal remelted under vacuum and cast into split graphite or copper chill molds. Futher purification was effected by vacuum distillation. Details of this procedure are given in the section of this report "Purification Studies".

Samarium metal was prepared by the reduction of samarium oxide by lanthanum metal or by previously vacuum melted misch metal. The reduction was carried out in a high vacuum, the

samarium distilling from the reaction mixture as it was formed. The distilled metal was analyzed for oxygen and transported rare earths. These were usually found to be very low; if above a few hundred parts per million, the metal was redistilled.

Preparation of Alloys

All intermetallic alloys were prepared by the non-consumable arc-melting of mixtures of the respective metals. Rare earth metal - metal oxide systems were prepared by arc-melting mixtures of the metal and the corresponding sesquioxide.

Arc Melting Furnaces. Two furnaces were used during this study. The first, a small furnace with a water cooled copper hearth plate and a tungsten tipped counter electrode, has been previously described (26, 27).

The second furnace (Figures 1 and 2), although adaptable for use with a variety of molds, was constructed to permit the preparation of long ingots of refractory materials for mechanical testing. The body of the furnace was constructed from an 18" length of heavy walled brass tubing. One end was permanently sealed with water and power inlets in place. The hearth translation drive passed through a double O-ring sealed port. The stinger was constructed from concentric tubes which allows for passage of cooling water as well as providing support for the offset (1") tungsten electrode. The stinger may be moved vertically to establish the desired arc length, and it may be rotated for positioning of the tip at any point on the circle described by the offset. The capacity of the furnace is eight one inch diameter buttons, or two bars 6" x 3/4" x 1/2" deep. The distinguishing feature of the furnace is the translating hearth plate. In operation the stinger is positioned as indicated above to melt the material in one end of the mold, and the hearth plate is then translated so that the molten portion of the bar moves from one end to the other. The sample may be inverted and remelted several times if desired, the molten zone being moved either in the same direction each time, or backwards and forwards. Due precautions were taken to insure the absence of air, the actual melting being carried out under reduced pressure using a 75% helium - 25% argon mixture. The final specimens were sectioned and examined metallographically for homogeneity. Only the tantalum and niobium based alloys were non-homogeneous in spite of repeated meltings.

Heat Treatment. Alloys subjected to homogenizing anneals or heat treat and quench procedures were sealed in Vycor. The tubes were evacuated to less than one micron pressure, back-filled with argon, re-evacuated, then sealed. When a volatile component

(i.e. samarium) was present the tubes were back filled to approximately one-half atmosphere pressure with the 75% helium-25% argon mixture.

Air quenching was accomplished by removing the samples from the furnace and allowing them to cool in air to room temperature. Severe quenching was accomplished by plunging the sealed capsules into water and breaking the Vycor. This water quenching technique produced some surface corrosion, but examination indicated only very slight penetration from the surface.

Some alloys, heat treated at 1000°C or higher, showed evidence of increased oxygen content after heat treatment. The source of the contaminating oxygen may be reaction of the alloy with the SiO_2, or may be diffusion of air through the Vycor. Evidence for the former was occasionally found in the presence of a fine gray powder, identified as silicon, within the tubes.

Terminology. The primary concern in all of the alloy systems investigated in this program was at one end of the constitutional system only. To emphasize the matrix element of concern, all systems were therefore identified with the matrix element first and the alloying element second, rather than the more conventional alphabetical order.

All references to compositions in the text, in tables, or in figures, are in terms of weight percent unless otherwise specified.

Chemical and Spectrographic Analysis

Chemical and spectrographic analyses were performed on all metals and alloys as required. It may be noted that nominal alloy compositions are quite adequate for interpretation and evaluation of results in some experiments. Thus cobalt alloys containing 5, 10, 15, 20 and 25% erbium all corroded more rapidly than cobalt metal at elevated temperature, and at increasing rates with increasing erbium content. Exact analyses of such alloys would provide no additional significant data and were therefore not made.

Most of the analytic procedures used have been fully described in earlier reports (25,26,27,28). These are briefly discussed below. Greater detail is provided for new or modified procedures.

Sampling. Sampling methods were based on the type of material to be analyzed, particularly with respect to the quantity available and the homogeneity expected.

For the cast pure metals, solid pieces were cut for the determination of total rare earths, carbon nitrogen, and oxygen.

Representative samples for spectrographic analysis were obtained by combining the drilling chips obtained from several small diameter holes.

Alloys were cut with a fine bladed saw, and the resulting small chips (representing a relatively large area) were reserved for spectrographic and chemical analyses as required. Solid samples were used for oxygen and nitrogen analyses to minimize possible errors due to atmospheric corrosion. Metals and alloys subjected to mechanical test were sampled from the reduced section of the tensile specimen after fracture.

Rare Earth Analysis. The rare earth content of the rare earth metals used was determined by dissolution of the metal in acid, precipitation of the rare earth with oxalic acid from slightly acid solution, ignition of the resulting oxalate, and gravimetric determination as oxide. These determinations were made primarily to insure the absence of any gross errors or contamination.

The rare earth content of compositions in rare earth-oxygen systems was regularly determined by the same method, as confirmatory checks of the analyzed oxygen values.

Rare earth-nickel and rare earth-cobalt alloys were dissolved in hydrochloric acid, and the rare earths separated from the nickel or cobalt by precipitation and reprecipitation with ammonium hydroxide. The second hydroxide precipitate was dissolved in acid, and the rare earths determined gravimetrically after precipitation as oxalate and ignition to oxide as described above.

Neodymium and erbium in their respective yttrium alloys were determined spectrophotometrically. The alloys were dissolved in nitric acid and the solutions diluted to measured volume. The optical density of the solutions was determined at 742 millimicrons for neodymium and 523 millimicrons for erbium. The corresponding element concentrations were determined from standard curves prepared from known quantities of the respective elements.

Cobalt Analysis. The alloy was dissolved in hydrochloric acid, and the cobalt was precipitated with a alpha-nitroso-beta-naphthol. The precipitate was filtered and ignited. The ignition product was fused with potassium pyrosulfate. The melt was allowed to cool, then taken up with water. The solution thus obtained was made alkaline with sodium hydroxide and the cobalt oxidized to the cobaltic state by sodium peroxide. The excess peroxide was destroyed by boiling, potassium iodide added, and the solution acidified. Under these conditions the cobaltic ion oxidized an equivalent amount of iodide to iodine, which was then titrated with sodium thiosulfate.

Nickel Analysis. The alloy was dissolved in dilute nitric acid, the solution was diluted and filtered. Any insoluble residue was ignited, fused with potassium pyrosulfate, dissolved in water, and combined with the original filtrate. A suitable aliquot was taken and the rare earths complexed with ammonium citrate. The solution was made very slightly alkaline with ammonium hydroxide and the nickel precipitated with dimethylghoxime. The precipitate was filtered, dried, and the nickel determined gravimetrically.

Tantalum Analysis. Quantitative tantalum analysis was made by the tartaric acid-tannin method (39,40). The alloy was treated with dilute hydrochloric acid and the insoluble residue (tantalum) was filtered, ignited to oxide, and fused with potassium pyrosulfate. The cooled melt was taken up in tartaric acid solution, diluted, acidified, and boiled to effect hydrolysis. The precipitate was filtered and reserved. The solution was combined with the filtrate from the original alloy dissolution, made neutral with ammonium hydroxide, buffered with ammonium chloride plus ammonium acetate, and the soluble tantalum precipitated with tannin. The tannin precipitate was ignited, fused, dissolved, and treated with ammonium oxalate to remove rare earths. Tantalum was then again recovered by tannin precipitation. This precipitate was combined with the reserved major hydrolysis product, ignited, and weighed as oxide.

The oxide was fused with potassium pyrosulfate, and the melt dissolved in a dilute solution of tartaric acid plus ammonium oxalate. Ammonium hydroxide and hydrogen sulfide were added. The resulting precipitate was filtered, ignited, weighed and subtracted as an impurity correction (principally iron, calcium, and silicon oxides) from the tantalum oxide value as obtained above.

Zirconium Analysis. Alloy samples were treated with dilute sulfuric acid. This treatment disintegrated the sample, the rare earths and some of the zirconium going into solution, and some of the zirconium remaining as an insoluble precipitate. Without filtering, the zirconium in solution was precipitated with cupferron. The solution was now filtered, and the precipitated zirconium plus the undissolved zirconium was ignited at a relatively low temperature (approximately 500°C). The resulting oxides were fused with potassium pyrosulfate. The fusion production was dissolved in dilute sulfuric acid, and the zirconium precipitated with diammonium phosphate. The zirconium precipitate was ignited, and the zirconium determined gravimetrically as pyrophosphate.

Carbon Analysis. Carbon was determined by the direct combustion-carbon train method (2). The metal or alloy sample was carefully cleaned, placed in an Alundum boat with granular

tin catalyst, and burned at 1300° - 1450°C in a stream of purified oxygen. The combustion products were purified and the carbon dioxide absorbed in Ascarite and weighed in the conventional manner.

Nitrogen Analysis. Nitrogen was determined by the usual Kjeldahl method (2,40). The sample was dissolved in a mixture of hydrochloric and fluoboric acids in the presence of a selenium catalyst (Hengar granule). An excess of sodium hydroxide was added, and the liberated ammonia distilled into a boric acid solution which was then titrated with standard sulfuric acid.

Oxygen Analysis. The complete procedure for the analysis of oxygen in rare earth metals and alloys has been given previously (26). In summary the method consists of heating the metal to 1900°C or higher in contact with graphite in a platinum bath. The heating step may be carried out either in a vacuum or in an argon atmosphere. The carbon monoxide formed is passed through a heated tube containing iodine pentoxide which oxidizes the carbon monoxide to carbon dioxide and simultaneously liberates an equivalent amount of iodine. The iodine is absorbed in a potassium iodide solution and is then titrated for determination of the equivalent amount of oxygen initially present.

Analysis in inert atmosphere has been found superior to analysis in vacuum. The blank is reduced and is much more constant. The method has been used routinely to determine oxygen contents as low as 100 ppm for samples weighing approximately 1 gram. Greater sensitivity if required, may be obtained by using larger samples.

Spectrographic Analysis. All spectrographic analyses were made by d.c. arc excitation of materials in graphite electrodes. The spectrograph used was a Baird Associates 3 meter model GX-1. Details of operating conditions are given in Table III.

Most analyses were made using first order dispersion. The limits of tantalum detection by these techniques appeared to be approximately 0.05 - 0.10%. Development of procedures for distillation of the rare earths improved the quality of the metals and introduced a requirement for greater sensitivity. A number of different procedures were evaluated, the one finally selected being consistent with the general procedure and providing approximately a ten-fold increase in sensitivity.

Ten milligrams of sample, blended with an equal amount of powdered graphite, are burned to completion in a 10 ampere direct current arc. Full intensity (no sector) exposure is diffracted in the second order. Under these conditions several tantalum emission lines are detected at concentrations of 0.01% or less

in rare earth matrices. The wave lengths of the lines most commonly used for analysis are 2635.58, 2647.46, 2675.90, 2685.11, 2694.76, and 2714.67 angstroms (all values are from the MIT tables (15).

The pure metals were analyzed by comparing the spectra of the metal with an immediately adjacent spectrum of the pure oxide. The presence of impurities was immediately revealed by the additional lines found in the metal spectra. Estimations of the concentration of these impurities were made by comparison with spectra of standards prepared by the addition of known amounts of other elements to rare earth oxides. Spectrographic analyses of alloys were similarly made by comparing spectra of the alloys with those of the pure oxides and the pure alloy elements.

Metallographic Examination

The problems occurring in the metallographic examination of rare earth containing alloys are similar to those for the pure rare earth metals. Techniques for examining rare earth metals have been previously described (26,27), and have formed the basis for the procedures used throughout this work. Improvements have been made, however, as described below. Additionally, most of the rare earth alloys of concern in this program involved the less reactive metals, and it has been possible to utilize somewhat more reactive media than possible for the more active metals. Neodymium alloys must still be treated with somewhat more care.

Sectioning. Alloys containing yttrium, erbium, and samarium were sectioned with a high speed abrasive cut-off wheel. A water soluble oil was used as lubricant and coolant. The more corrosive, high neodymium alloys were generally cut more slowly by hack saw with mineral oil lubricant.

Mounting. The samples were mounted in "Lucite" or "Bakelite" by conventional methods. "Lucite" was generally used because of its transparancy.

Rough Grinding. After mounting, the specimens were ground on a belt sander to obtain a smooth, clean, level surface. Kerosene was used as a coolant to prevent overheating and oxidation, and to wash abraded particles away. With reasonable care it represents no exceptional fire hazard.

Fine Grinding. Fine grinding was carried out on rotating polishing wheels. Initial grinding began on a 240 grit silicon carbide abrasive disc for approximately 2-3 minutes. Succeeding steps used 320, 400, and 600 grit silicon carbide abrasive discs.

Kerosene was used as a coolant during all the final grinding steps. The specimens were thoroughly rinsed with kerosene between each step to eliminate carry-over of abrasives from the preceding papers. Most specimens were ground using a Buehler "Automet" attachment. Six specimens could be prepared simultaneously under controlled and reproducible conditions.

Mechanical Polishing. The metals were polished in two successive steps; a rough polishing step using 6 micron diamond abrasive on a "Metcloth" or "Nylon" covered polishing wheel, and a final polishing step with 1 micron diamond abrasive on a "Microcloth" covered polishing wheel. Wheel speeds were relatively slow, 150-250 R.P.M.; very light pressure was used. A steady flow of kerosene was maintained during polishing operations.

Chemical Polishing. Chemical polishing was found effective for removing the fine grinding scratches and preparing a highly polished surface on tantalum and niobium alloys. The polishing solution (10 cc hydrofluoric acid, 10 cc nitric acid, and 30 cc lactic acid) was applied with a cotton swab. Alternate fine polishing and swabbing was sometimes necessary to remove the last embedded abrasive particles and to prevent relief.

Electropolishing. Electrolytic polishing techniques were found applicable to cobalt and nickel alloys, and to some rare earth based alloys. The specimen was made the anode in an electrolytic cell; a tantalum electrode was used as the cathode. The electrolyte used for cobalt and its alloys was orthophosphoric acid; for nickel, a solution of 39 parts concentrated sulfuric acid in 29 parts distilled water; for rare earths, a solution of 15 parts nitric acid in 85 parts methanol. The applied voltages ranged from 1-25 V., and were adjusted to provide a current density of 0.03 amps/in^2.

Etching. Chemical etching was generally not necessary for the chemically polished or electrolytically polished specimens. Etchant solutions used, as well as the chemical polishing solutions and electrolytic solutions, are summarized in Table IV.

Microscopy. The microscopy was performed with a Bausch & Lomb metallograph model MILS. Preliminary visual observations of samples in preparation were made on the metallograph or with a Unitron inverted metallurgical microscope. The light source for the metallograph was a ribbon filament incandescent lamp. All metallographic work was conducted under bright field illumination. All photographs were taken with the customary green-yellow filter.

Photography and Recording. Microstructures were recorded on 4 x 5 and 5 x 7 metallographic plates which were tank developed in Eastman D-19 developer. Contact prints were made on glossy

single weight Azo paper. Prints were trimmed and mounted on 5 x 8 cards and identified as to print number, sample number, sample source, etch, magnification, and other pertinent information.

Thermal Analysis

Melting Point Determinations. Liquidus temperatures for alloy systems were obtained in a small melting point furnace (27). Each alloy specimen was inserted as a resistor between two water cooled, tungsten tipped electrodes. Current up to 200 amperes was passed through the specimen, and melting characteristics and temperatures were obtained by two workers simultaneously observing through a cathetometer and an optical pyrometer. The method is simple, rapid, and convenient. Problems associated with container materials and attack of thermocouples by reactive metals are eliminated.

The principal errors are those associated with the optical determination of the temperature of materials with unknown emissivities, and the visual detection of the exact moment of complete liquidus.

The determination by optical pyrometry of the temperature of specimens heated in a furnace is made difficult by problems of emissivity of the material investigated. The furnace temperature is usually different from that of the specimen, and the varying reflectivities of different materials give different indicated temperatures. It is noted that in the resistance method the specimen is heated internally and is protected within the furnace chamber from external sources of radiation. For the rare earth metals, and for a number of rare earth intermetallic compositions, thermal analysis determinations were frequently made by both the resistance melting point method and differential thermal analysis. Comparison of the data obtained indicates that emissivity is not a serious problem in these systems for temperatures to approximately 1500°C. For intermetallic systems (and the metal-metal oxide systems with high metal content) the temperature readings are considered accurate to perhaps ± 20°C. It is noted that the above discussion is not applicable to certain rare earth-metalloid systems which become strongly photo-emissive at elevated temperature.

Ascertainment of the liquidus condition presents no problem for compositions which are essentially single phase, or for which the difference between the solidus and liquidus temperatures is small. If the difference between the solidus and liquidus temperatures is large, however, a considerable fraction of the material will melt before the actual liquidus temperature is reached, and

the determination of this temperature may be difficult. In the resistance method here described the melting point is taken as the temperature at which the specimen becomes sufficiently liquid so that surface tension draws the material up into a globule. Usually the metal will simultaneously drop through the gap between the electrodes and break the circuit. This temperature may aptly be termed the "globule point", although to avoid confusion in the subsequent test it is referred to as the melting point or liquidus temperature. It may be noted that an analogous difficulty exists in the more commonly used method of Pirani and Alterthum (34), in which a solid specimen is heated in a furnace, and the temperature at which the solid appears to collapse is taken as the liquidus temperature.

It is difficult to assign one firm estimate as to the accuracy of the method since it is so dependent upon the nature of the system being investigated. For the analyses made in this program the estimated overall accuracy is $\pm 30\text{-}50^{\circ}C$.

Differential Thermal Analysis. Samples for differential thermal analysis were placed in small (approximately 1/4" x 1/2" x 1/4" deep) tantalum foil cups. These were spot-welded to a platinum/platinum-13% rhodium thermocouple. Reference neutral bodies were placed in similar cups welded to the bucking thermocouple. Reference metal bodies were selected from arc-melted tantalum, vanadium, or titanium (beta stabilized with 25% molybdenum).

The samples were placed in a tube furnace in a stream of purified argon. The furnace was heated by silicon carbide elements to a maximum temperature of approximately $1500^{\circ}C$. For many samples, unfortunately, the thermocouple elements were apparently chemically attacked by rare earth vapors and embrittled. For these compositions thermocouple failure occurred before the maximum furnace temperature could be reached. Power input was controlled through a motor driven, geared variable transformer so that a near constant heating rate of $10^{\circ}C$/minute was obtained from room temperature to maximum temperature. The cooling rate could not be similarly controlled, but was adjusted to be between 5 and $25^{\circ}C$/ minute by appropriate settings of the transformer. All samples were heated to slightly above their melting points, to failure of the thermocouple, or to $1500^{\circ}C$.

The thermocouple potential was recorded as one tracing on a two point "Wheelco" recorder. The differential EMF was amplified by a "Kintel" electronic galvanometer, model 204A, which was modified to permit the output signal to record directly as the second tracing on the recorder. The amplified signal was further biased to zero at the center of the recorder chart, and thus eliminated the need for switching polarity to keep the tracing on chart. Electronic shielding was provided to keep the noise level at

lowest possible values. Operating under the conditions as described above, differential signals of 2-3 microvolts could be detected below 1000°C, and signals of 5 microvolts could be detected between 1000 and 1500°C. Such signals correspond to temperature differences of 0.2 - 0.3°C between the specimen and neutral body.

Corrosion Tests

Alloy specimens for atmospheric corrosion (oxidation) tests were cut in the form of flat rectangular plates, and were polished by the techniques used for metallographic examination. Final polishing was by hand with 600 grit silicon carbide abrasive. Excess kerosene was removed by rinsing with acetone and wiping dry or, subsequently, by simply wiping. Samples were stored under argon until tested. Dimensions were determined by measurement, and the total surface areas were calculated.

Tests were run in a large tube type furnace. A slow stream of air, pre-dried by passage through a "Drierite" column, was maintained throughout all runs. The test specimens were placed at an angle in small crucibles to permit maximum air circulation. The crucibles were centered in the furnace in a preheated massive holder to help minimize temperature variations. Initial runs were made at 600°C. Materials which showed low rates of oxidation at this temperature, or for which there was only minor effects detectable upon rare earth additions were also run at 900°C. The furnace temperature was found to be constant within ±2°C at both temperatures. Initial exposure times were usually for 2 hours. Successive exposures were for progressively longer periods depending upon the observed rate of corrosion.

After exposure, the crucibles were immediately covered and transferred to a dessicator to cool. Weight increases were calculated as grams per square decimeter (milligrams for the more resistant alloys) and plotted against time.

X-Ray Diffraction

X-ray diffraction was used as an aid in establishing solubility limits in the metallic systems, and to determine the presence and nature of intermetallic compounds. Many different materials were investigated and several different techniques were used, each with procedural variations dependent upon the type of material and the information desired. The following discussion indicates the general procedures and conditions used.

Analyses were conducted using a General Electric Co. model XRD-5 X-ray diffractometer, a General Electric Co. powder camera, and a Charles E. Supper Co., Weissenberg single crystal camera. X-rays were excited from a standard CA-7 copper target tube at 45 KV and 18 milliamperes. The radiation was filtered through 0.0035" nickel foil.

In diffractometer use, the optical system operating conditions included 1-3° diverging slits, 0.02-0.1° receiving slits, and a 4° take off angle. The radiation was again filtered to exclude excited fluorescence and picked up by a General Electric #2 krypton proportional counter tube. Scanning rates (2θ) were 2° per minute providing medium resolution for phase identifications (2θ = ± 0.05°), and 0.2° per minute providing high resolution for lattice parameter measurements (2θ = ± 0.01°). Chart speed was 1" per minute. Samples were either polished flat plates or powders packed into a flat holder.

While diffractometer procedures are more rapid than powder camera procedures, and allow the use of flat plate samples, the data obtained is less precise. Errors are due to absorption by flat plate samples, to the fact that the flat plate is not entirely on the axis of rotation, and to errors in the mechanical construction of the goniometer. When more precise data was required, therefore, the powder camera was used.

Samples for the powder camera were alloy chips, powder wedges, or powders packed in capillary tubes. "Kodak no-screen" film was used, developed for 5 minutes at 68°F in Kodak liquid X-ray developer. Suitable extrapolation functions based on the methods of Bradley and Jay (5) or Nelson and Riley (32) were used for lattice parameter calculation refinements.

The Weissenberg camera, used primarily for the erbium-cobalt system, also used "Kodak no-screen" film with the same developing treatment. Single crystals were analyzed by Laue, oscillation, and rotation techniques.

Analytic Samples, Solid. In order to correlate the microstructures observed with the crystal structures determined by X-ray diffraction, large flat plate samples were prepared which could be examined both metallographically and by diffraction. The samples were mounted and polished as for metallographic examination, and differed from the usual metallographic specimens only in that the area was sufficiently large to intercept a large portion of the X-ray beam. Previous experiments (26) had indicated that lattice parameters determined from a solid sample and those from a powder sample of the same material were in good agreement. The principal deficiency of the solid sample techniques (other than precision as indicated above) was that samples showed some preferred

orientation. Amplitudes of the peaks, therefore, could not be used for intensity measurements.

Analytic Samples, Powder. When precise intensity data was required, to establish the structure of intermetallic compounds for example, analyses were made on powdered samples. Some metals and alloy compositions also crystallized with grains so large that the preferred orientation of the area examined resulted in insufficient peaks for analysis. Such alloys were also examined by powder techniques.

The metals were crushed, ground, or filed to minus 100 mesh. The powders were washed with carbon tetrachloride, sealed in Vycor tubing under vacuum, and stress relieved by heating to approximately 400°C.

Elevated Temperature Studies. A sample furnace constructed by Tempres Inc., University Park, Pa., was installed on the General Electric diffractometer. The sample is held in platinum or tantalum holders mounted on a quartz or mullite holding rod. Samples may be flat plate or powder, and both were used in this study. Heating is by platinum resistance windings imbedded in ceramic. A saturable reactor type controller maintained temperatures within ±2°C to 1000°C and within ±5°C to 1400°C. The outside of the furnace is air cooled.

An inert atmosphere is maintained around the sample and sample holder within the furnace by providing a rapid flow of argon. Owing to furnace design, however, (refractories within the furnace, imperfect sealing, etc.) some corrosion was always observed on the test specimens. These corrosion products made interpretation more difficult, but the major metal phases present could almost always be identified. It is emphasized that X-ray diffraction is essentially a surface analysis. The formation of very thin corrosion films result in diffraction patterns of the corrosion products. The films, however, may still be too thin to separate from the base metal for chemical analysis.

A diffraction pattern was first obtained at room temperature for all test specimens as mounted in the high temperature head. Without disturbing the specimen, patterns were then made at various elevated test temperatures on both the heating and cooling cycles. When cool, a second room temperature pattern was obtained. The specimen, if solid, was then repolished and a final diffraction pattern made. This sequence of tests permitted the unambiguous definition of metal phase changes, and the distinction of patterns arising from surface corrosion effects.

Mechanical (Tensile) Properties

Tensile Coupons. The geometry of the test specimens used for the determination of tensile properties in this program is illustrated in Figure 3. The reduced diameter is 1/4 inch and the gauge length is one inch. This specimen requires much less metal than the standard 0.505" diameter, 2" gauge length coupon, and is considered large enough to provide accurate strength and ductility values.

Test Method. All tensile tests were conducted in a Tinius-Olsen, 60,000 lb. capacity, Super 'L', Universal testing machine equipped with a loading rate indicator and recorder. Ultimate tensile strength, elongation, and reduction in area were determined for all specimens. A constant loading rate of 2250 lbs. per minute was used in all tests. Elongation ductility was determined by measuring the position of scribe marks on the gauge length after fracture. Reduction of area values were obtained from measurements of the diameter of the specimens after failure. Modulus of elasticity values were determined from the recorded loan-strain curves.

Where possible, the yield strength at 0.2% offset was determined using the Model S-3, 1" gauge length electronic extensometer. Many alloys were very brittle, however, and broke with no observed yield. Subsequent tests on each group of these alloys were therefore run without the extensometer to prevent its damage, and no yield values were obtained.

Elevated Temperature Tests. Elevated temperature tensile tests were conducted using a portable furnace (Marshall Products Co., Columbus, Ohio). The furnace temperature was controlled by a Minneapolis Honeywell-Brown "Pyr-O-Vane" controller. Three chromel-alumel thermocouples were attached to the specimens; one in the center of the reduced section, and the others just outside the gauge length near the shoulders. Glass and asbestos insulated #28 AWG thermocouple wire was used. A Leeds and Northrup portable potentiometer was used to determine the temperature along the gauge length.

"Kaowool" insulation was inserted into the top and bottom of the furnace to prevent drafts. The specimens were tested when the temperature variation of the specimen from the nominal test temperature was within $\pm 2^{\circ}C$ at the center of the specimen, and the indicated temperature variation along the gauge length was within $\pm 3^{\circ}C$. The conditions of restricted air circulation and relatively short time at elevated temperature minimized atmospheric corrosion effects. A very thin, adherent film was formed, and no evidence of scaling or penetration was observed.

RESULTS AND DISCUSSION

PURIFICATION STUDIES

Rare Earth Metals

Distillation. Rare earths were used as minor additions to base metals for many of the tests and investigations in this project. In other investigations the rare earth matrix metals were alloyed with large percentages of other elements or compounds. For these systems, the regular 99+ percent grade metals were considered sufficiently pure. Where the effect of trace additions was to be investigated, rare earth metals of higher purity were required.

Samarium, as previously indicated, was prepared by reduction of the oxide and simultaneous distillation. Samarium is one of the more volatile rare earths, and vacuum distillation proceeds readily at approximately 1300°C. If oxide or other rare earths (from the reductant) are carried into the distillate, a redistillation procedure efficiently removes these impurities.

Erbium and yttrium are much less volatile, but procedures were developed for their distillation. Distillation was carried out in a heavy walled tantalum crucible equipped (in the first runs) with a molybdenum cap - subsequently replaced by tantalum. The lower part of the crucible was heated by induction to 1600-1800°C for erbium, and 1750-1850°C for yttrium. A vacuum of <0.3 microns pressure was maintained during distillation. Table V indicates the results of the initial distillations of erbium and yttrium made from sub-grade starting feeds. The final analyses are compared with the feed analyses and with typical good grades of as-cast metals. The analysis range indicated for the distilled metals represents the compositional range for various areas of deposit.

It is observed that the distillation effectively separated the metals from the less volatile oxides and from tantalum. Iron distilled and concentrated with the recovered metal. A trace of molybdenum was found in condensate adjacent to the cover. Subsequent runs made with tantalum covers indicated tantalum contents generally less than 0.01%.

The microstructure of distilled erbium is seen in Figure 4. Photomicrographs are presented of the metal in various preparative states for illustrative purposes. Figure 4a, of unetched metal, may be compared with Figure 5, which shows a nominal 99.5% erbium in the unetched state, to illustrate the decreased amount of second phase impurities. Figure 4b shows the erbium microstructure after

etching with concentrated nitric acid. Grains are revealed, as is the subgrain structure. In Figure 4c, the same portion of the specimen seen in Figure 4b is viewed under polarized light. The subgrain structure is lost, but grain contrast is increased.

The microstructure of distilled yttrium (unetched) is seen in Figures 69 and 70. The distilled metal deposited as large crystalline grains, and the entire field of view in these photomicrographs is of a single grain. Comparison of second phase impurities with those in the nominal purity metal can be made by comparing with Figure 14.

Neodymium has a lower vapor pressure than erbium or yttrium; its melting point (1019°C) is very much lower than that of yttrium (1509°C) or erbium (1497°C). The low vapor pressure requires heating to high temperatures to obtain a reasonable volatilization rate; the low melting point, however, requires a relatively cool condensing surface. The combined effect of these two factors is to require an extreme thermal gradient. Attempts to distill neodymium in the same equipment used for erbium and yttrium were not successful. The equipment was modified several times by the addition of radiation shields inside the crucible and by the provision of heat sinks or radiators on the cover. Effective distillation, however, could not be attained.

Zone Refining. The zone refining of yttrium has been investigated and reported (17). The results obtained did not indicate promise for the removal of the principal impurities in the rare earths used in this program. The physical processes group at Research Chemicals, however, has been engaged in a study of the effect of heating and electric current variables on zone refining processes. One procedure which appeared to have some promise was tried on yttrium.

An arc-melted bar of yttrium, approximately 6" x 1/2" x 1/2" was fitted with water cooled electrical contacts and placed vertically in an inert atmosphere chamber. A direct current of 400 amperes at 2.4 volts was passed through the bar. An induction heated zone was simultaneously passed through the bar. The rate of travel was approximately 4.4 in/hr, and 11 passes were made. The temperature was deliberately held below the melting point of the yttrium, the maximum in the induction zone being kept at 1250°C.

The yttrium rod was sectioned and examined metallographically for variations in impurity distribution. No such variations were found, and it must be concluded that the results of this preliminary test were negative.

Beryllium

Previous investigations of the beryllium-erbium and beryllium-ytterbium systems (26,27) had indicated the possibility of improving the purity and ductility of beryllium by melting with rare earth metals. That work was based on small, arc-melted buttons which provided sufficient material for metallurgical examination only. Further investigation was considered desirable, and larger buttons were prepared to provide for adequate chemical, metallurgical, and mechanical testing.

Three inch diameter buttons were prepared by arc-melting beryllium with 1/2, 1, 2-1/2, and 5% erbium. The buttons were sectioned and portions prepared for metallographic and X-ray diffraction analysis.

X-ray diffraction indicated the presence of beryllium and the $Be_{13}Er$ compound. No other compounds were detected.

Metallographic examination indicated that the compound is present as a fine particle precipitate, widely dispersed, in contrast to the large crystals previously observed. The microstructure of the base beryllium metal and of the 1% and 2-1/2% erbium alloys is shown in Figures 6-8. Small cubic crystals of the compound are noted in the alloys, particularly in Figure 7.

It is again noted that the 1% alloy appears to be "cleaner" than the base beryllium metal. Effective separation of slag did not occur, however, and discrete areas of high impurity content were mixed with areas which appeared to have been purified. The mixtures were too intimate to permit effective separation for analytic purposes.

Considerable porosity was also evident. The dark circles in the photomicrographs (Figures 7 and 8) are microscopic voids. Porosity on a macroscopic scale also occurred and is shown in Figures 9 and 10. Macroscopic hardness values were determined across the polished cross section of all alloy compositions. No significant difference was found between the various compositions or across any one specimen. Cracks are also present and appear to be larger in the arc-melted beryllium than in the beryllium-rare earth compositions. Some grain refinement is noted in the rare earth alloys (Figure 10 compared to Figure 9), and it is possible that the grain refinement and lowered cracking severity are related.

Since clean separation of the impurity phases did not occur, chemical analyses would be meaningless and were therefore not made. Similarly the presence of voids did not permit the preparation of sound mechanical test specimens.

PHASE DIAGRAMS

Tentative partial phase diagrams have been established for the rare earth rich end of the yttrium, erbium, neodymium, and samarium systems with oxygen; of the base metal rich end of nickel, cobalt, niobium, and tantalum systems with rare earths; and of the entire yttrium-erbium and yttrium-neodymium systems. The diagrams were compiled from the best data as determined by X-ray diffraction, metallographic examination, and thermal studies.

The scope of work performed on each system was dictated by the consideration of the ultimate objectives of this work, that is, the rapid screening of a number of systems in order to establish the practicality of producing materials of structural significance. The pertinent ends of these systems were examined only up to the composition of the first compound, if one occurred, although in some cases additional compositions were examined to help establish the nature of this compound. Similarly, complete investigations of areas above eutectic temperatures were not made, since these areas are not generally of importance for structural purposes.

Full advantage was taken of the diversity of analytic methods available to minimize much of the work customarily done in establishing a complete constitutional diagram. The use of the high temperature X-ray diffractometer minimized the need for a large number of alloy preparations followed by anneals at various temperatures and by metallographic examination. It is considered that the essential information leading to possibly improved structural properties has been obtained for the systems investigated.

THE HIGH TEMPERATURE (BETA) PHASE OF RARE EARTH METALS

The various allotropic crystallographic phases present in the metal systems will be fully discussed in each respective system. The data for the pure metals are summarized below.

The alpha to beta transformation for samarium was found to be 930°C, that for neodymium was found to be 848°C, both determined by differential thermal analysis. Spedding and co-workers (42,45) have reported values of 917° and 862°C respectively.

Eash and Carlson (10) have reported a phase transformation in yttrium at 1490°C. The melting point of yttrium is reported as 1509°C for vacuum distilled metal and 1540°C for metal melted in tantalum (20). Our observations of melting points for as-cast yttrium have ranged between 1520° and 1540°C. Differential thermal analysis has indicated a transformation occurring approximately 20-30°C below the melting point of the particular specimen, in good agreement with the literature values reported above.

The high temperature structure of neodymium was confirmed by elevated temperature X-ray diffraction examination. The high temperature samarium structure could not be established (discussed in the samarium-oxygen system), and the yttrium transformation occurs above the temperature limits of the X-ray equipment.

Beta phase stabilization was not observed in any of the neodymium, samarium, or yttrium systems investigated.

Differential thermal analysis signals have also been obtained for some specimens of erbium at temperatures ranging from 1450-1500°C (melting temperatures 1500-1540°C). These have not been consistent, however, and have not been found in all samples tested. The signals are small, and it is not certain that they represent crystallographic transformations.

Spedding and Daane (20) have reported that transformations from hexagonal to body centered cubic structures occur in the heavy rare earths at that temperature at which the c/a ratio of the hexagonal cell becomes 1.601 ± 0.001. They report that the c/a ratio for erbium increases more slowly with temperature than does the ratio for the other elements, that the value 1.601 is not reached, and that the high temperature transformation has not been observed. It is known that the addition of interstitial impurities to some hexagonal elements (i.e. titanium) increases the "c" parameter much more than the "a" parameter, and thus increases the c/a ratio. The various erbium specimens examined were of varying degree of purity. Although the solubility of the interstitial impurities is very low at room temperature, they may become significant at temperatures near the melting point. It is interesting to speculate that such solubility may influence the c/a ratio sufficiently to provide conditions under which a crystallographic transformation might occur.

RARE EARTH ALLOY STUDIES

YTTRIUM - RARE EARTH COMPOSITIONS

Alloying to form solid solutions often leads to improvement of the mechanical properties of metals. For the hexagonal rare earth metals, the c/a ratio is approximately 1.57-1.58 at room temperature, somewhat less than the 1.63 value for a perfect close packed hexagonal structure. It is possible that solid solution alloying would improve this ratio and thus lead to better properties. Consideration of atomic radius, electro-negativity, and valence values leads to predictions of complete mutual solubility for the systems yttrium-erbium and yttrium-neodymium, but the degree of improvement of mechanical properties, or the effect on corrosion resistance or fabricability is less certain. The systems yttrium-erbium and yttrium-neodymium were accordingly investigated.

The System Yttrium-Erbium

General Characteristics. Alpha yttrium and erbium are completely soluble in all proportions. There are no intermediate compounds. No evidence was found for the stabilization of beta yttrium nor was positive evidence found for the existence of beta erbium.

Phase Diagram. A tentative equilibrium diagram for the system yttrium-erbium is presented in Figure 11 as constructed from differential thermal analysis and melting point determinations, metallographic examination, and X-ray analysis at room and elevated temperatures. Complete solid solubility is shown between alpha yttrium and erbium. The existence of beta yttrium is noted, but no evidence for stabilization of beta yttrium was detectable. The spread between the solidus and liquidus is relatively slight.

Thermal Analysis. The melting points of alloy compositions, as determined by the resistance method are presented in Table VI. Except for the 50-50 weight percent composition, they appear to be constant within experimental error. The melting appeared to be quite sharp indicating very little temperature difference between the solidus and liquidus temperatures.

Differential thermal analysis measurements were made on compositions at 10 percent increments. Considerable difficulty was encountered in this system with thermocouple failure above approximately 1300°C. Several compositions, however, did reach to

approximately 1500°C. No evidence of phase transitions was found for any of the alloys.

X-Ray Diffraction. Room temperature X-ray diffraction examination showed only a single phase, hexagonal close packed structure for all compositions in both as-cast and heat treated conditions. The observed 2θ values for the various diffraction maxima are indicated in Table VII, and the $\Delta 2\theta$ values for erbium containing compositions (referred to yttrium) are given in Table VIII. The latter values are presented graphically in Figure 12. The slopes of the curves in Figure 12 are plotted against composition in Figure 13 (two sets of curves, A and B, are presented, since the curves in Figure 12 are not straight lines). It is noted that the curves in Figure 13 do not have discontinuities, indicating continuous solid solubility, and that when plotted on an atomic percent basis they form straight lines indicating conformance to Vegard's law.

High temperature X-ray diffraction studies indicated the continuous presence to 1200°C of the hexagonal close packed metal structure. Surface oxidation of some samples produced the normal body centered cubic sesquioxide. Additionally, atmospheric corrosion produced surface contamination, identified as having a face centered cubic cell. For the yttrium-40% erbium alloy this cell dimension was 4.93A at 1000°C, contracting to 4.85A at 25°C. The X-ray data for these calculations are presented in Tables IX and X. The crystal structure of yttrium nitride (YN) has been reported as face centered cubic with a_o=4.87A (22). This is considered to be an interstitial type compound, and it is believed that oxygen could substitute for part, or perhaps all, of the nitrogen. (The film produced was very thin and stoichiometric chemical analysis was not possible). The face centered cubic structure observed is therefore considered to be a contamination product, and is not indicated in the phase diagram.

Thermal coefficient of expansion determinations for hexagonal materials require accurate measurements of peaks for indices 001 and hk0. Although shifts in peak position were observed in the elevated temperature scans, the peaks were not well shaped, and expansion coefficients were not determined.

Physical Appearance. All alloy compositions were metallic in appearance, and had the typical silvery luster of the individual elements.

Microstructures. The microstructures of yttrium, erbium, and yttrium-erbium alloys are revealed in two sets of photomicrographs. Figures 14-21 are of arc-melted metals and alloys, polished but unetched, photographed at 100X to show general characteristics. Figures 22-29 are of metals and alloys after 40 hours heat treatment at 1000°C followed by slow cooling (100°C per hour). The

specimens were etched with nitric acid and photographed at 250X to reveal greater detail.

The alloys were prepared from nominal purity metals containing 1/4-1/2% each of oxygen and tantalum. Comparison of Figures 14 and 22 for yttrium with 20 and 29 for erbium indicates that the distribution of impurities is somewhat different in the two metals. In yttrium most of the impurities collect in the grain boundaries and in preferred locations (as platelets) within the grains. In erbium there is a tendency for much more uniform distribution. Impurities are present as a fine dispersion throughout the grains, much less being in the grain boundaries and as platelets. The alloys, in agreement with previously discussed evidence for continuous solid solution, show a progression through the series; the yttrium-10% erbium alloy being similar to yttrium, the yttrium-90% erbium alloy similar to erbium, and the intermediate alloys of intermediate character.

The nitric acid etchant attacks the grains unequally as a function of grain orientation, so that some grains appear darker than others. It is noted that the oxide platelets appear to be wider, or absent in these darker grains, indicating that the orientation of these grains is such that the platelets are in, or nearly in the plane of the metal surface.

Some alloy specimens, etched in the arc-melted condition with nitric acid, revealed a structure which could be interpreted either as "eutectoid-like" or as having a considerable amount of eutectic present (Figures 30 and 31). After heat treatment at 1000°C and slow cooling, these structures were much less evident (Figures 32 and 33). Traces of this structure are also seen in Figure 22 for pure yttrium. The structure may be related to beta to alpha transformations, but as indicated above, no firm diffraction or thermal evidence has been found to indicate significant beta stabilization.

The System Yttrium-Neodymium

General Characteristics. The yttrium-neodymium system is characterized by a uniform decrease in melting point from yttrium to neodymium; by significant, although undetermined, solid solubility of neodymium in yttrium with perhaps lesser solubility of yttrium in neodymium; and by the presence of an intermediate phase at the equal atomic percent (38 wt. % yttrium-62 wt. % neodymium) composition. Stabilization of beta yttrium could not be established. At the neodymium end of the system the addition of 10% or less of yttrium does not markedly affect the neodymium alpha to beta transformation temperature.

Phase Diagram. The data obtained by metallographic, thermal, and X-ray analyses are summarized as the tentative, partial equilibrium diagram presented in Figure 34.

A low temperature compound (gamma) is present which decomposes at approximately 550°C. The gamma compound may have reasonable limits of composition (i.e. it may be an intermediate solid solution), and a dashed region is therefore shown at either side. The alpha phases of both yttrium and neodymium show regions of solubility for each other, but there is also an extensive two phase region at room temperature for each element with gamma. At moderately elevated temperatures, crystallographic interpretation is difficult, but it is believed that a rather wide two phase region exists between the two alpha solid solutions.

The alpha to beta transformation for neodymium occurs at 860°C, and is relatively unaffected by the addition of up to 10% yttrium. It is tentatively shown as increasing to 1110°C as the yttrium content subsequently increases to 40%. The alpha-beta transformation for yttrium is shown at 1490°C. It is likely that the beta yttrium region extends down to link with the beta neodymium region, but no experimental evidence for this could be obtained.

The melting point of the system decreases regularly from that of yttrium to that of neodymium; the spread between the solidus and liquidus lines is small.

Thermal Analysis. Thermal analysis data for the yttrium-neodymium system is presented in Table XI. Melting points as determined by differential thermal analysis and by the globule technique are in reasonably good agreement except for the yttrium-80% neodymium alloy, where the value determined by the globule technique appears to be low, and where no reliable data was obtained by differential thermal analysis. The melting temperatures decrease regularly from yttrium to neodymium. The melting appeared to be quite sharp indicating little temperature difference between the solidus and liquidus temperatures.

Differential thermal analysis showed strong deflection signals for the transformations in neodymium and yttrium-90% neodymium. The signals at 1040° and 1110° for the yttrium-70% and -60% neodymium alloys were much weaker, and are assigned only tentatively to an alpha-beta transformation. The signal at 550°C for the yttrium-60% neodymium alloy was definite, and appears to coincide with the disappearance of the gamma phase as noted in elevated temperature X-ray analysis.

X-Ray Diffraction. X-ray diffraction analysis in the yttrium-neodymium system is considerably more complex than in the yttrium-erbium system. First, the crystal structures of yttrium and

neodymium are different. Second, a new (gamma) phase is present in the system, which is stable only up to moderate temperatures. The diffraction pattern for this structure is characterized by the presence of a large number of low intensity peaks. Unambiguous identification of the crystal structure would involve complex single crystal analysis - beyond the scope of this program. Comparison of the diffraction pattern of alloys containing little free neodymium or yttrium, however, with that for samarium indicates very close similarity. The observed gamma phase has therefore been tentatively identified as having a samarium structure. Spedding and Daane too, have recently reported that a compound with the samarium structure exists in the yttrium-lanthanum system and probably also in the systems of yttrium with cerium, praseodymium, and neodymium (19). Third, alloys in the yttrium-neodymium system, particularly those of high neodymium content, are subject to much more rapid atmospheric attack at elevated temperatures than alloys in the yttrium-erbium system. The corrosion products may be of the interstitial monoxide, nitride, or oxy-nitride type, or they may be sesquioxides. The corrosion products of yttrium rich alloys moreover, may be different from those of neodymium rich alloys.

The combined effect of all of these variables is to produce very complex diffraction patterns which in some cases may be interpreted in more than one way. The identifications indicated below are the results of considerable study, and frequently take into consideration other metallurgical data, or knowledge of the general behavior of rare earth metals. In some cases alternate assignments of diffraction peaks are indicated.

The room temperature patterns of yttrium, the yttrium-10% neodymium, and the yttrium-20% neodymium alloys all show a single phased, hexagonal close packed yttrium structure. Patterns of alloys containing 30-50% neodymium are two phased, the samarium structure occurring together with the yttrium structure. The yttrium-60% neodymium composition is essentially single phased with the samarium structure. Alloys containing 70-90% neodymium again are two phased; the samarium structure being present with increasing amounts of the hexagonal (lanthanum type) neodymium structure. In an effort to determine the limit of solubility of yttrium in neodymium, alloys of neodymium containing 2, 4, 6, 8, and 10% yttrium were prepared and examined. Diffraction patterns of these alloys showed the presence of the neodymium structure, together with a second phase which was not present in sufficient quantity to be accurately indexed. The lattice spacings of neodymium in this series appeared unchanged from that of pure neodymium. It should be noted, however, that the atomic radii of neodymium and yttrium differ by only 1%, and large changes would not be expected.

Yttrium and alloys containing up to 80% neodymium were examined at 1025°C. Alloys containing up to and including 60% neodymium all had the hexagonal close packed yttrium structure, the 70 and 80% neodymium alloys showed the neodymium structure. The yttrium-90% neodymium alloy, and pure neodymium metal were examined at 925°C (to keep below the melting point). A body centered cubic structure was identified with a lattice parameter of 4.12A. This is in good agreement with the same structure and a lattice parameter of 4.13A (temperature not specified) reported by Daane (18) for beta neodymium. The yttrium-70% neodymium alloy, which showed primarily the samarium structure at room temperature and the neodymium structure at 1025°C, was re-examined at intermediate temperatures. The structure at 525°C was still essentially the samarium structure; at 625°C, however, only the neodymium structure was observed. These values correlate well with the transition observed by DTA at 550°C. The phases present at the various temperatures are summarized in Table XII.

Data obtained in the X-ray analysis of the atmospheric corrosion products from neodymium are summarized in Tables XIII and XIV. A face centered cubic structure is observed with a_o=5.13A at 925°C and 5.08A at 25°C. This structure would be characteristic of an interstitial type monoxide, nitride, or oxy-nitride.

The X-ray diffraction pattern at 1025°C from neodymium alloys containing yttrium show diffraction peaks from the alpha neodymium structure, the face centered cubic structure (NdO? NdN?) indicated above, and from an additional face centered cubic cell having a_o=4.93A. This latter corresponds to the corrosion product observed in the yttrium-erbium system. The data are summarized in Table XV.

The assignment of structures and diffraction peak locations for corrosion products preceded the complete interpretations and identifications of the metallic phases present as discussed above. The assignment of diffracting planes to the observed diffraction maxima for the yttrium-60% neodymium alloy, for example, is given in Table XVI. It is observed that all diffraction maxima are accounted for, and that there are no peaks from the samarium structure. It may be noted that peaks due to the metal phase may be assigned to either the neodymium or yttrium structure. Similarly Table XVII illustrates the identification and calculation of the lattice constants of the body centered cubic, high temperature form of neodymium in the yttrium-90% neodymium alloy.

Physical Appearance. All alloy compositions were metallic in appearance, and had the typical silvery luster of the individual elements.

Microstructures. The microstructures of yttrium-neodymium alloys, as arc-melted, are shown in Figures 35-41 inclusive. All specimens were etched with concentrated nitric acid, which, as noted under procedures, has a side effect of emphasizing the presence of oxides or corrosion products. The high neodymium alloys also corrode quite rapidly, even at room temperature. Such corrosion spreads from oxide sites (26) and specimens therefore appear to have more impurity phase than is actually present. The principal purpose of the metallographic examination, however, is the delineation of the metallic structure. The manner of distribution of impurity phases may be helpful in this, and is therefore of importance.

The yttrium-10% neodymium alloy (Figure 35) shows the structure typical of yttrium (Figure 22) except that there appears to be somewhat less than usual amounts of intergranular impurities and therefore somewhat poorer grain definition. The yttrium-50% neodymium and yttrium-60% neodymium alloys (Figures 37 and 38) show a structure found typical for many alloys in this composition range, and identified by X-ray analysis as having the samarium structure. The grains are considerably smaller than for either yttrium or neodymium, and the (oxide) impurities tend to solidify as dendrites rather than as the typical platelets or uniform intergranular deposits. The intermediate composition, yttrium-40% neodymium (Figure 36) shows an intermediate structure with poorly defined grains, and oxides present both intergranularly and as dendrites.

At the neodymium end of the system, Figure 41 illustrates the yttrium-90% neodymium structure, again quite typical of the pure neodymium structure. In the yttrium-80% alloy (Figure 40) the oxides again come out as dendrites with the base metal appearing somewhat different and suggestive of a phase transformation having occurred. The yttrium-70% neodymium microstructure (Figure 39) is strongly suggestive of a transformed structure and almost resembles the "basket-weave" transformed alpha titanium structure.

It is noted that there are two transformations occurring in this system. The first, on cooling, is the beta to alpha; the second is the alpha to gamma. With the alpha to gamma transformation occurring as low as 550°C, it was considered that the transformation rate might be sluggish, and that quenching might retain the alpha structure. The specimen of yttrium-60% neodymium alloy was therefore heat treated at 1000°C for 40 hours and air quenched. The resulting structure (Figure 42) is quite similar to the as arc-melted structure for the same composition (Figure 38), except for the redistribution of the non-metallic impurity phase. X-ray diffraction again indicated essentially the samarium structure, and it is therefore apparent that the beta to gamma transformation must be quite rapid.

Investigations of the neodymium alloys containing less than 10% yttrium revealed some unusual and interesting microstructures. Figure 43 of the yttrium-98% neodymium alloy is illustrative. It is noted that there are apparently two distinct systems of granular orientation. The first, outlined by a heavy concentration of intergranular material, is a system of irregularly shaped grains. The second, outlined by a much thinner line of intergranular material results in a pattern of grains with quite straight sides and with many of the grain boundaries intersecting at nearly 120°, typical for a hexagonal crystallite. Although no positive mechanism producing this microstructure has been determined, it is postulated that the irregularly shaped grains are formed first on cooling of the melt. Most of the impurities are rejected into the grain boundaries. When the metal cools through the beta to alpha transformation region, enough energy is released to permit a considerable amount of grain re-orientation. A smaller amount of impurities is rejected to form the new, thinner grain boundaries. Comparison of the magnitudes of DTA deflections for the transformation and for the melting of neodymium does indicate that the heat of transformation is large. Daane (44) has indicated that for the cerium group metals the heat of transformation may be of the order of magnitude of 50% that of the heat of fusion.

RARE EARTH ALLOY STUDIES

RARE EARTH - OXYGEN SYSTEMS

The engineering application of metals may be influenced by the oxygen content of the system at both high and low levels. Recent developments in metal-metal oxide systems, particularly aluminum-aluminum oxide, have indicated that compositions containing considerable percentages of oxygen can be prepared which exhibit markedly improved properties over those of the base metal at elevated temperatures. At low levels of oxygen content, the mechanical properties of metals, and especially ductility, may be markedly affected by the form in which the oxygen is present. Information as to solubility limits, the nature of oxygen containing compounds, and the changes which occur as a function of thermal history may contribute to the development of more useful alloy systems. In view of the rather encouraging elevated temperature properties found for the rare earth metals (26, 28) it was considered desirable to obtain further information as to the nature of rare earth-oxygen systems.

Selected for study were: erbium, representing a typical heavy rare earth metal with the hexagonal close packed structure; neodymium, a typical light rare earth metal with the lanthanum hexagonal structure; samarium, because of its anomalous oxidation behaviour (26); and yttrium because its lower specific gravity increases its potential for early technological application.

The following discussion will first treat with the experiments made, and the results obtained, for each system. Concluding remarks will summarize the data with respect to the phase diagrams proposed.

Rare Earth-Rare Earth Oxide Equilibria

A number of different methods may be considered for obtaining metal-oxygen compositions in true equilibrium. The method used in this program was the non-consumable arc-melting of rare earth metals with their oxides. Photomicrographs of the resulting structures suggested that the oxide had dissolved in the metals at the high temperatures attained, and that furthermore the character of the oxide particles had changed sufficiently so that it was likely that there was a true metal-oxygen equilibrium.

Two experimental tests were made to establish whether equilibrium was attained between the oxygen in the rare earth oxide and the rare earth metal with which it was arc-melted. In the first, yttrium metal was arc-melted with erbium oxide, and erbium metal was arc-melted with yttrium oxide. X-ray diffraction analysis of the resulting compositions indicated metal lattice parameters

intermediate between those of yttrium and erbium. The crystal structures of the two metals and of the two oxides are the same. The experimental evidence indicates the four species are in equilibrium at elevated temperature.

$$Y + Er_2O_3 \rightleftharpoons Er + Y_2O_3$$

The second experiment indicated further that oxygen has high mobility in these systems. Yttrium and neodymium metals have different crystal structures as do the respective yttrium and neodymium oxides. An yttrium metal-neodymium oxide composition was arc-melted. X-ray diffraction analysis of the resulting alloy indicated the presence of neodymium metal and yttrium oxide as well as yttrium metal and neodymium oxide, and therefore established that exchange had occurred:

$$Y + Nd_2O_3 \rightleftharpoons Nd + Y_2O_3$$

The arc melting procedure produces a molten pool at very high temperature. The combined results of the above experiments and the metallographic observations strongly suggest that under these conditions the oxygen from a rare earth oxide is quite mobile, and is free to combine and react under equilibrium conditions.

The System Erbium-Oxygen

General Characteristics. The systems erbium-oxygen and yttrium-oxygen are quite closely analogous in many respects. Although each is described separately, some details of the metallurgical analysis may be found more completely described in one, others in the other. It is suggested that the two be considered together.

The partial equilibrium diagram for the erbium-oxygen system is based on observations made to temperatures of approximately 1200°C, and deductions as to processes and conditions existing above this temperature. At least two different equilibrium diagrams could be constructed consistent with the observed data. The first would be characterized by considerable solubility of oxygen in the beta metal phase (for elements with a beta allotrope). The second, and preferred diagram, would indicate the presence of a high temperature interstitial monoxide.

Extensive solubility of oxygen in the beta phase of erbium or yttrium appears unlikely for several reasons. First, it is noted that the solubility of oxygen in erbium at room temperature is very low, and that neither microstructures nor high temperature diffraction analysis support extensive solubility in the alpha phase metal at elevated temperatures. If solubility in the alpha phase is low, then significant solubility of oxygen in the beta phase would imply the possibility of significant beta phase stabilization. Such stabilization has not been observed in this laboratory nor reported in the literature (it is noted that earlier conjecture regarding beta stabilization of erbium is related to the total of all interstitial type impurities). The beta phase in erbium has not been unqualifiedly established, and the beta phase in yttrium shows no evidence for stabilization as a function of oxygen content. Second, it is noted that the neodymium-oxygen and samarium-oxygen systems can be examined in the beta phase region since this occurs at lower temperatures. Granted differences in the alpha crystal structure of these metals, there is no significant solubility nor beta stabilization observed.

The existence of rare earth monoxides at elevated temperatures, however, has been observed by a number of investigators. Chupka and co-workers (6) have reported the reaction of lanthanum with lanthanum sesquioxide to produce lanthanum monoxide at elevated temperatures. Yosim and Milne (49) report data on the vaporization of lanthanum monoxide formed in equilibrium with oxygen from sesquioxide. Eick, Baenziger, and Eyring have reported the preparation and crystal structures of SmO and EuO (11), and Achard and Tsoucaris have reported an X-ray study of ytterbium suboxide (1). The structure of NdO has been reported as fcc, with a_o=5.07A (Battelle Memorial Institute). Walsh and co-workers (48) reported extensively on the vaporization of lanthanum, yttrium, and neodymium oxides and indicate that both experimental evidence and thermodynamic considerations support the existence of the monoxides. Walsh has further observed that at temperatures above 1800°C the sesquioxides react at significant rates with tantalum to produce rare earth monoxide and tantalum monoxide. The temperatures attained in our arc melting preparations are well above this, and it appears reasonable to assume that rare earth metals may similarly reach a monoxide equilibrium. On the other hand, decomposition of yttrium or erbium compounds containing oxygen, i.e. oxalates, carbonates, etc., results only in the formation of the sesquioxides. Room temperature oxidation similarly results only in the formation of the sesquioxides. No monoxide structures have been observed at room temperature in the rare earth-oxygen preparations, nor has it been possible to quench in the monoxide phase. The monoxide is therefore not considered stable at room temperature, and the equilibrium diagrams will show its existence only at elevated temperatures.

Phase Diagram. The solubility of oxygen in erbium at room temperature is less than 0.03%. The solubility at elevated temperatures could not be determined, but general observations of heat

treated and quenched erbium specimens indicate that the solubility must be less than 0.2% at 1000°C. A (cubic) sesquioxide is present, and monoxide is inferred from available data. No evidence was found for a high temperature (beta) form of erbium. Figure 44 shows a tentative phase diagram compatible with the observed data. The portion of the diagram below 1200°C has been shown to be a simple, two phase mixture of hexagonal close packed erbium and cubic erbium sesuioxide.

Thermal Analysis. Differential thermal analysis in this system was limited by frequent failure of thermocouples due to chemical attack. No evidence was found for phase transformations or reactions in those specimens which did reach the melting point. Melting point data was obtained for some compositions by differential thermal analysis. The melting points of all oxide compositions were also determined by the resistance method, and of several compositions by observations in an induction heated furnace. The best averaged results are indicated in Table XVIII.

X-Ray Diffraction. Room temperature diffraction of all compositions containing 0.34% or more of oxygen showed the presence of two (and only two) phases; hexagonal close packed erbium and cubic erbium sesquioxide. In the sample containing 0.34%, the 222, 440, 400, and 622 reflections of the oxide were observed. The lattice parameters of distilled erbium (0.03% oxygen) were identical with those of erbium containing 0.34% or more of oxygen. On this basis X-ray diffraction results indicate oxygen solubility in erbium as less than 0.03%.

Elevated temperature X-ray analysis indicated the continued presence of hexagonal close packed erbium in all compositions up to 90% erbium oxide at temperatures to 1000°C, and in several selected compositions investigated to 1200°C. The cubic sesquioxide structure was found in compositions containing 10% or more sesquioxide, and suspected but not confirmed in lower compositions where identification was more difficult due to the formation of a new phase attributed to atmospheric corrosion of the metal surface.

The new phase has a face centered cubic structure with a_o=4.878A. Diffraction data for this phase is presented in Table XIX which is for an erbium-1% Er_2O_3 composition held at 1000°C until the diffraction pattern from the erbium metal had virtually disappeared. The (chemical) composition of this phase has not been unambiguously established. Since the erbium-erbium interatomic distance in this cell is determined as 3.45A, and the calculated interatomic distance for erbium with coordination number 12, is 3.48A, it is most likely that the cell is a face centered cubic structure of erbium, stabilized by the presence of a large percentage of interstitial compound formers such as oxygen or nitrogen. All of the rare earth nitrides have been prepared and investigated, and all have face centered cubic structures. Whether oxygen contributes

to the stabilization of this phase has not been established. That the new structure is probably a corrosion product is indicated by its formation during the holding period at elevated temperatures, its existing presence when the sample is cooled to room temperature, and its absence when the sample is re-examined after repolishing. It is noted that for compositions containing appreciable amounts of sesquioxide the reaction sesquioxide plus metal to yield monoxide during the heating cycle, and its reversal during the cooling cycle, would yield essentially similar diffraction results. This is especially true if the finely divided metal phase resulting from the disproportionation reacts rapidly in air forming nitride on the specimen surface during the cooling cycle.

The various phases found present in erbium-erbium oxide compositions are indicated for both room temperature and 1000°C in Table XX.

Physical Appearance. Compositions containing up to, and including, 40% erbium sesquioxide had a lustrous, silvery, metallic appearance. The 50% composition was shiny but gray, the 60-90% compositions were shiny black. All compositions appeared to be uniform, homogeneous, and without cracks or other physical defects.

Microstructures. Metallographic examination of both as arc-melted and heat treated erbium-erbium oxide compositions showed the presence of two phases. A small, but detectable, quantity of second phase was present in the distilled metal containing 0.03% oxygen (Figure 4), confirming the low solubility found by X-ray diffraction.

Compositions containing up to approximately 20% erbium oxide showed a metal matrix with oxide present both in grain boundaries and as platelets within the grains. From approximately 20-50% a metal matrix was observed with almost all of the oxides as platelets; not longer nor more numerous, but much wider than in the lower compositions. Very little oxide was in the grain boundaries, distinction between grains being based on the orientation of the platelets. The existence of these platelets within the grains is very difficult to explain for a system without the monoxide phase. If only metal and sesquioxide were present, it would be expected that the sesquioxide would separate from the melt as a primary phase.

Above 60% oxide content, the matrix consists of primary grains of oxide with metal inclusions, and an intergranular metal phase. No platelets are observed in the metal phase. The structures of typical compositions containing 10-75% erbium oxide are illustrated in Figures 45-52 inclusive. Figure 47, of the 25% sesquioxide composition at high magnification, indicates that the oxide has a lamellar structure. Just such a structure might be expected if a solid state reaction (inverse peritectoid) occurred in which one phase dissociated to two phases. Although less apparent, some evidence of the lamellar structure is also seen in the high magnification photomicrographs of the 60 and 75% sesquioxide

compositions (Figures 50 and 52).

The effect of heat treatment (40 hours at 1000°C, air quenched) on the microstructure is seen in Figures 53-55. It is noted that the platelet structure was partially spheroidized. In Figure 53, of the 10% oxide composition, the shorter platelets have apparently transformed more completely than the long thin platelets. Figure 54 at 100X, and Figure 55 at 750X magnification, show the rounded particles in various stages of formation and separation from the platelets.

The System Yttrium-Oxygen

General Characteristics. This system was found to be quite similar to the erbium-oxygen system. The solubility of oxygen in yttrium is low. Below 1200°C the system is composed of two phases; hexagonal close packed yttrium and cubic yttrium sesquioxide. The existence of a monoxide at elevated temperatures is proposed.

Phase Diagram. A tentative, partial equilibrium phase diagram for the system yttrium-oxygen, compatible with the observed data, is presented in Figure 56. The solubility of oxygen in yttrium is very low. At temperatures to 1200°C only two phases, hexagonal close packed yttrium and cubic yttrium sesquioxide, are present. The melting point rises from essentially that of pure yttrium to that of the sesquioxide. A monoxide is present. Yttrium also exists in the high temperature body centered cubic structure (beta) but the types of equilibrium reactions between the yttrium allotropes and the monoxide and sesquioxide have not been established.

Thermal Analysis. Melting points were determined by the resistance method (globule technique) and confirmed for the lower oxygen contents by some of the differential thermal analysis results. The melting point data is summarized in Table XXI.

Differential thermal analysis was carried to the temperature limit of the equipment (1540°C) unless specimens melted below this temperature, or unless thermocouple failure occurred first. No differential signals were obtained which could be distinguished from random noise levels, and thus no transitions could be located by this technique.

X-Ray Diffraction. Room temperature X-ray diffraction analysis indicated the presence of hexagonal close packed yttrium and of cubic yttrium sesquioxide in all alloy compositions. The lattice parameters of yttrium in the alloy compositions were unchanged from those of pure yttrium.

Elevated temperature diffraction analysis immediately introduced complexities. As in the case of erbium, atmospheric corrosion of the surface took place. The corrosion products, however,

were identified as consisting of two new phases (Table XXII). Both were face centered cubic. One phase, with a unit cell a_o=4.93A, very closely resembled the ErN structure discussed under erbium, and is similarly identified as probably being YN; although here too the possibility of substitution of oxygen for nitrogen is implied. It may be noted that Svec (20) reports that YN, as found in YH_2, has a cell constant of 4.95A, and reports unpublished results of Daane giving 4.905A for YN. The second phase, with a unit cell a_o=5.49A at 1000°C and 5.40A at room temperature, is too large to allow simple sodium chloride packing, and more closely resembles the fluorite structure. After these phases were identified, the original room temperature diffractograms were re-examined, and the presence of very small amounts was established in some of the arc-melted alloys. Table XXIII lists the various phases detected in the arc-melted alloys, the alloys examined at 1000°C, re-examined after cooling to room temperature, and finally examined after repolishing.

The nature of the larger cell could not be established. It is most logically a product of atmospheric corrosion, and this implies a compound with nitrogen, oxygen, or hydrogen (from water vapor) individually, or in combinations. Some consideration had been given to hydride formation since cerium dihydride had been reported (24) to have a face centered cubic structure with a_o=5.55A. Allowing for the lanthanide contraction, it was believed that the cell size observed for the yttrium compound would be in approximate agreement. Svec (20), however, during investigations of the reaction between yttrium and water, reported that the cell size of the dihydride was 5.194A, and the cell size of the dihydride expanded by the solution of oxygen was 5.285A. These values are significantly below that observed, and it therefore, does not appear likely that the compound is a hydride. The observed presence of traces of this structure in the original arc-melted compositions is also difficult to reconcile with their method of preparation, and the structure has not been found present in any yttrium specimens not melted with oxide. A further point of uncertainty is introduced in the comparisons of the phases observed in the 1% and 2% yttrium oxide compositions as determined at 1000°C and then cooled to room temperature (Table XXIII). The development of a major sesquioxide phase not present at 1000°C is noted. This could be due to the unknown phase being a nitride (or hydride) reacting with moisture in the air, to a nonequilibrium monoxide continuing to oxidize to the sesquioxide, or to a transformation, by disproportionation, of the monoxide into metal and the cubic sesquioxide.

In summary it is noted that X-ray diffraction indicates that the equilibrium phases in the yttrium-oxygen system are hexagonal close packed yttrium and cubic yttrium sesquioxide to at least 1200°C. The thin oxidation film which forms on yttrium at elevated temperatures apparently is two phased. One is a face centered cubic structure closely resembling YN, the other is an unidentified

face centered cubic structure which may be a non-equilibrium oxygen containing compound.

Physical Appearance. Compositions containing up to, and including, 40% yttrium sesquioxide had a lustrous, silvery, metallic appearance. The 50% composition was shiny, but gray, the 60-90% compositions were shiny black. All compositions appeared to be uniform, homogeneous, and without cracks or other physical defects.

Microstructures. Metallographic examination of yttrium-yttrium oxide compositions showed the presence of two phases. Figures 57-60 illustrate compositions containing 10-50% oxide, and indicate a metal matrix with oxide platelets progressively increasing in volume. The 50% microstructure indicates some change in oxide habit. Figures 57 and 59 are particularly illustrative of the platelet structure, the platelets apparently being cut in various grains at various angles - from near normal to near parallel.

Figures 61-63 illustrate the 10-30% oxide compositions at much greater magnification (750X). Details of the oxide platelets are revealed which indicate that the oxide has a lamellar structure, very possibly due to a reaction of an inverse peritectoid type. It is noted that if the monoxide phase is only stable at elevated temperatures as proposed, it must decompose to form metal plus sesquioxide.

Compositions containing 60% or more of oxide have been observed in two habits. Figures 64 and 65 illustrate an oxide matrix structure at 100X and 500X respectively. This structure is rather similar to that observed in the erbium-erbium oxide system (Figures 49 and 51). Figures 66 and 67 illustrate a metal matrix with dendritic oxide. The figures at higher magnification again indicate the lamellar or transformed oxide structure. The yttrium-60% yttrium sesquioxide composition has less oxygen than equivalent for the monoxide. Since the upper peritectic transformation temperature is still indeterminate, however, it is not certain whether the first oxide to separate would be the sesquioxide or the monoxide.

Increasing the sesquioxide percentage to 90%, where the sesquioxide would be the first equilibrium form to solidify, results in the microstructure seen in Figure 68 at 500X magnification. The lamellar structure is much less evident, appearing only in isolated small areas. This appears to provide added support to the thesis that the lamellar structure is truly a result of the reaction: yttrium monoxide decomposing to yttrium plus sesquioxide. The black areas in the gray oxide have not been fully defined. Examined visually at 500X, the oxide appears to have areas of varying transparency and reflectivity. It is possible that the difference between the black and gray areas is due to such variations, as produced in the oxide during cooling from an almost pure oxide melt.

Figures 69 and 70 illustrate the structure of distilled yttrium at two different magnifications. Yttrium condenses as a coarsely crystalline deposit. The total area in both photographs is within one grain. The oxide content in this metal was 0.04%. Calculation of the platelet area corresponds closely to this value and indicates that the solubility of oxygen in yttrium must be very low. Some small, white inclusions, with a gray surrounding halo are also noted. The chemical and spectrographic analyses did not indicate any impurity which might be responsible, but it is noted that analysis is not made for fluoride. This is very likely present in the as-cast metal, and having approximately the same volatility at elevated temperatures, would distill, in part, along with the yttrium. If these inclusions are yttrium fluoride, the fluoride content is estimated at $\leqslant 0.03\%$.

The System Neodymium-Oxygen

General Characteristics. Analysis of alloy compositions in the neodymium-oxygen system is complicated by the relatively rapid rate of atmospheric corrosion even at room temperature. Some of the X-ray diffraction results may be interpreted to indicate the presence, at least under certain conditions, of the monoxide. Metallographic evidence, however, seems to indicate that the sesquioxide is relatively a more important phase, and that there is either no monoxide phase or that the monoxide is stable over a smaller temperature interval than in the yttrium-oxygen or erbium-oxygen systems. Two alternative systems are therefore proposed.

Phase Diagrams. One tentative, partial, equilibrium phase diagram prepared for the system neodymium-oxygen is presented in Figure 71. The solubility of oxygen in neodymium is low. At room temperature alpha neodymium and hexagonal neodymium sesquioxide forms a two phase region. The transformation temperature of neodymium is 848°C and this is essentially unchanged by the presence of oxygen. The melting point of neodymium is 1020°C. This is apparently lowered slightly to 1010°C by the presence of the oxide. A monoxide phase is present which decomposes, on cooling, to neodymium metal and sesquioxide. The transformation temperature is tentatively placed within the beta neodymium region. The sesquioxide transformation temperature is not indicated since it is apparently to some considerable extent a variable with time, temperature, and previous thermal history (discussion and references under X-ray diffraction).

A second, alternative phase diagram is presented in Figure 72. The principal difference is the absence of the monoxide phase.

Thermal Analysis. The results of differential thermal analysis determinations are presented in Table XXIV. The alpha-beta transformation in neodymium was determined as 848°C. The 2% neodymium oxide composition transformation was somewhat lower (825°C),

but compositions from 5-15% oxide transformed at 845°C. The melting temperature of the metal and of the 2% oxide composition was determined as 1020°C; for the 5-15% compositions it was found to be 1010°C, and this is considered to be the solidus (eutectic?) temperature. Literature values for the transition and melting temperatures are 862° and 1019° respectively (21, 45).

X-Ray Diffraction. Room temperature X-ray diffraction analysis indicated the presence of the hexagonal sesquioxide in all compositions, and the presence of alpha neodymium in the high metal compositions. The pattern for neodymium metal becomes weaker very rapidly as the oxide content increases, and it is not detected in compositions prepared with more than 50% sesquioxide. The lattice constants for the neodymium metal phase remain constant indicating no change due to solid solubility.

Neodymium sesquioxide absorbs moisture (and then carbon dioxide) from the air quite rapidly (26). The diffractograms of specimens which had been exposed to air for several hours before or during diffraction runs revealed extra peaks which disappeared on heating. The nature of the hydrated oxide was not investigated.

The results of X-ray diffraction analysis are summarized in Table XXV for the sequence; room temperature, elevated temperature, cooled to room temperature, and repolished. The analysis was considerably complicated by the rapid corrosion. It is noted, however, that the corrosion product up to 900°C was not the face centered cubic structure observed in the yttrium and erbium systems, but was determined to be the hexagonal sesquioxide. Oxide compositions examined at 1000°C did reveal a face centered cubic structure, however, and the disappearance of both the metal and sesquioxide phases is strongly suggestive of their reaction to form monoxide. The face centered cubic phase remained present after cooling, but disappeared upon repolishing. This now suggests that the face centered cubic phase may have been a corrosion product (nitride?) which in this case only formed at elevated temperatures and was the dominant diffracting phase after formation. Another speculative possibility is that the monoxide disproportionated to form sesquioxide and metal on cooling; the metal, being finely subdivided, reacted on the surface to form a new interstitial compound (the nitride?). The nature of the face centered cubic phase is therefore still indeterminate. The lattice parameter has been established as 5.115A at 1000°C and 5.025A at 23°C, but the composition is not known.

Neodymium sesquioxide has been reported in three crystallographic structures. Blum and McGuire (3) have reported a transformation from the C type (cubic) to the A type (hexagonal) at approximately 600°C. Shafer and Roy (41) report the formation of the B type (orthorhombic) under hydrothermal conditions. Roth and Schneider (37) have recently reported that the C type is formed when neodymium oxalate is ignited at temperatures below 600°C,

that the A type is formed at 1300°C, and that both C and A are formed at intermediate temperatures. Since the A type did not revert back to the C, Roth concluded that the A (hexagonal) is the stable isomorph.

The production of oxides by ignition of rare earth compounds is difficult at low temperatures, especially if the compounds contain water (of hydration) or dissociate through release of water. The possibility of oxide structures other than the hexagonal existing at room or slightly elevated temperatures, however, indicated the need for investigating oxides formed at low temperature. The observations of the rapid oxidation of neodymium metal in the presence of traces of air suggested that X-ray studies might be made at relatively low temperatures to determine the type of oxide formed "in situ".

In the 2θ region 45° - 50° (for copper K alpha radiation) diffraction peaks for neodymium (105), hexagonal oxide (110), and cubic oxide (433) occur close together, yet distinguishable from each other. A neodymium metal specimen was therefore set up, heated to 200°C, and successive scans of this area were made at suitable time intervals. The relative intensities of the three peaks are indicated in Table XXVI, which indicates that only the hexagonal oxide is formed. At the conclusion of the experiment a complete (0-90°) scan was made, and analyzed for positive identification of the oxidation product. The results, Table XXVII, confirm the formation of the hexagonal neodymium sesquioxide. It is therefore concluded that the cubic and orthorhombic structures are produced only under special conditions, and are not equilibrium forms in the metal-oxygen system.

Microstructures. Microstructures of neodymium and neodymium-oxygen compositions reveal different structures from those observed in the yttrium and erbium systems. The structure of the metal itself shows less concentration of impurities as platelets, and a greater concentration in grain boundaries and as randomly scattered inclusions within the grains. Development of the microstructure is more difficult because of the rapid oxidation of neodymium and the tendency for oxidation to occur along preferred planes and impart a platelet appearance. Figures 73-75 illustrate the microstructure of neodymium containing approximately 3000 ppm oxygen (equivalent to about 2% sesquioxide). The metal specimens were carefully etched, and photographed as rapidly as possible. The etching action tends to accentuate the impurity areas, and make the metals appear less pure than they are, but by the same process well delineates the location of the impurities. Figure 73 illustrates cast neodymium etched with nital, and is rather typical of the cast structure. Figure 74 is cast neodymium metal with large grains formed by slow cooling. The central grain illustrates a transformation structure. Figure 75 is of arc-melted metal etched with a dilute nitric-acetic acid solution. Some of the oxide has precipitated as very small platelets, but the platelets do not appear to have the same structure as in yttrium and erbium.

Some typical examples of the nature of oxide precipitates from high oxide compositions are seen in Figure 76-78. In these figures the amount of oxide appears to be greater than the nominal composition would indicate. In part this is due to the rapid surface oxidation of the metal in these compositions. Figure 76 illustrates the neodymium-10% neodymium oxide composition. The oxide has precipitated from the melt as primary dendritic grains. In the 25% neodymium oxide composition (Figure 77), the dendritic grains are larger and have occluded metal from the melt. In the 50% oxide composition (Figure 78), the oxide appears to constitute almost the entire matrix. Careful examination, however, indicates that approximately 25% of the area is intergranular material (metal) and that another 25% is occluded metal (partly oxidized after polishing) within the grains.

The System Samarium-Oxygen

General Characteristics. The data obtained for this system, as for the neodymium system, may be interpreted on the basis of either of two equilibrium diagrams; one in which the alpha and beta forms of samarium are in equilibrium with samarium sesquioxide, and a second, preferred, which has a monoxide compound present.

The nominal percentage compositions of samarium-samarium sesquioxide alloys are reasonably close to actual when equal to or less than 5%. The volatility of samarium metal, however, produced losses for compositions in which the oxide content was great enough to significantly increase the arc-melting temperature. Based on weight loss data and metallographic evidence, compositions containing 15%, 25%, and 35% nominal sesquioxide are estimated to actually contain approximately 25%, 50%, and 90% oxide respectively.

Phase Diagrams. One tentative, partial, equilibrium phase diagram proposed for the system samarium-oxygen, including the monoxide, is presented in Figure 79. The second is presented in Figure 80.

The solubility of oxygen in samarium is low. At room temperature, alpha (rhombohedral) samarium and monoclinic samarium sesquioxide are in equilibrium. Samarium transforms to a beta phase (body centered cubic) at 930°C, and this temperature is raised, as a function of oxygen added, to 1000°C for a composition containing approximately 25% samarium sesquioxide (15% nominal). The melting temperature of samarium is 1070°C. The melting temperatures of compositions containing up to 25% sesquioxide are not materially changed.

A monoxide is proposed in Figure 79. The limits of stability of this compound were not established. It is therefore indicated in dashed lines, as is the extent of the alpha-beta transformation of samarium, since this isothermal may extend to the sesquioxide or may be intercepted by the monoxide phase. As in the neodymium system, the crystallographic change in

the sesquioxide is not indicated.

Thermal Analysis. The results of differential thermal analysis and melting point determinations are presented in Table XXVIII. The transformation temperature and melting point of distilled samarium were found to be 930° and 1070°C respectively. Literature values for these temperatures are reported as 917° and 1072°C respectively (42, 47). The transformation temperature rises slowly with increasing oxide content to 1000°C for the approximately 25% sesquioxide composition.

The solidus temperature appears to be essentially unchanged for compositions to 25% sesquioxide, differential thermal analysis indicating 1070-1080°C. The melting temperatures determined by the resistance method are apparently slightly low, but indicate that the liquidus temperature probably does not rise rapidly at the low oxygen end of the system.

X-Ray Diffraction. Four distinct crystallographic phases were expected in this system; two of samarium metal and two of samarium sesquioxide. The high temperature form of the metal, however, was not detected. Instead, a face centered cubic structure was observed, which could have been either an equilibrium monoxide, a corrosion product monoxide or nitride, or both.

Preliminary to investigation of the metal-oxygen systems, samarium sesquioxide was prepared and diffracted in order to establish the crystallographic forms which could exist. The sesquioxide prepared by ignition of the oxalate at 800°C was found to be cubic (the "C" structure). After heating to 1223°C during a 1/2 hour period it was found to have undergone a transformation to the monoclinic ("B") structure. The reaction was not reversible, the monoclinic form remaining after cooling to room temperature. This transformation is in agreement with the observations of Roth and Schneider (37) who report an irreversible reaction at about 950°C, and is contrary to the report of a reversible reaction by Goldschmidt, et al (14). Roth also related the ease of transformation to the degree of crystallinity, that is, poorly crystallized "C" structure oxide was reported to transform more readily than well crystallized oxide. Since no quantitative data was presented, it is difficult to make comparisons. The "C" oxide examined in this work, however, was observed to have a high degree of crystallinity and yet was observed to transform within the time necessary (about 30 minutes) to heat it to 1223°C. The oxide was finely divided, and it is possible that rate of transformation is determined by particle size as well as state of crystallinity.

Analysis of the pure samarium metal at room temperature indicated a complex rhombohedral structure. There are a large number of diffracting planes resulting in a diffraction pattern having a large number of low intensity peaks.

Room temperature analysis of samarium-samarium sesquioxide compositions indicated the presence of rhombohedral samarium and monoclinic sesquioxide in a two phase structure. Since these alloys were prepared from samarium metal plus cubic sesquioxide, it is indicated that the equilibrium condition of the oxide in equilibrium with metal is also the monoclinic structure.

X-ray analysis at elevated temperatures was not very satisfactory for this system. Interpretation of metal phases was difficult in the limited time available due to the presence of many low intensity peaks from the oxide, and the pattern due to the large quantity of face centered cubic phase which formed. As for the neodymium-neodymium oxide alloy system, it was not possible to define unambiguously the composition of this phase, nor to establish whether it is first formed as an equilibrium product between metal and sesquioxide or as a corrosion product. The lattice parameter determined for the face centered cubic structure at 900°C was 5.05A. This compares with 5.015-5.050A reported for samarium monoxide by Ellinger and Zachariasen (12). It is noted, however, that Klemm and Winkelmann (23) also report a face centered cubic structure for the mononitride having a_o=5.046A.

Microstructures. Metallographic examination indicated two phase structures for all compositions. For low oxide content the structure is metal matrix with oxide inclusions. For high oxide content the structure is oxide matrix with the metal primarily as an intergranular phase. Selected compositions are illustrated in Figures 81-84. Distilled samarium metal is seen in Figure 81. The original (beta) grain structure is barely discernible through the transformation structure. Figures 82-84 illustrate compositions with increasing oxygen content. Evidence for the monoxide to metal plus sesquioxide disproportionation is much less evident, although some grains, particularly in Figure 83 for the nominal 25% sesquioxide composition, show the lamellar structure found in the erbium and yttrium compositions.

Figure 85 illustrates a portion of the samarium-1% samarium sesquioxide structure, and indicates that this composition is well above the solubility limit for oxygen in samarium.

Summary Discussion of Rare Earth-Oxygen Systems

The room temperature portions of the phase diagrams of rare earth-oxygen systems, as established by examination in normal atmospheres, appears to consist of a simple equilibrium between the metal (with very low oxygen solubility) and the sesquioxide. The elevated temperature portion of the phase diagrams has been less clearly established.

Evidence for the existence of a monoxide phase has been found in the literature, and is implied by the experimental data established in this research program. The existence of lanthanum, neodymium, samarium, europium, ytterbium, and, tentatively, yttrium monoxides is reported in the literature as determined through experiments on the rates of volatilization of the metals and oxides, and in some cases through preparations and determinations of the crystal structures of the compounds. The crystal structures, where established, were face centered cubic structures of the same type found in elevated temperature X-ray diffraction studies made in this program. The latter studies, however, could not be made in the complete absence of atmospheric contaminants, and the results do not unambiguously rule out nitride formation.

Metallographic examination of compositions in the yttrium-oxygen and erbium-oxygen systems indicates that the oxide phase is primarily distributed as platelets within the metal grains. Examination of the platelets under high magnification indicates a lamellar structure. These observations are consistent with the concept of a monoxide being present at elevated temperatures which, on cooling, reacts in the solid state to form two phases (metal plus sesquioxide). It is noted at this point that yttrium and erbium sesquioxides, and erbium metal, have been reported as existing in only one crystallographic form, and that yttrium has a phase transformation which is apparently within only 20°C of its melting point.

The appearance of the oxide phase in photomicrographs of neodymium-oxygen and samarium-oxygen compositions is considerably different from the platelet structure noted above. In the neodymium system the oxide appears as dendrites or as globules with metal inclusions. In the samarium system the oxide appears as elongated grains, or, in the higher oxygen compositions, as globules.. Little or no lamellar structure is observed. It is here noted that both neodymium and samarium metals have considerably lower melting points than yttrium and erbium, that each has a phase transformation approximately 150°C below the melting point with considerable heat of reaction, and that the sesquioxides may exist in two different crystallographic states, with the equilibrium transformation temperature in each case below the melting point of the respective metal. The effects of the various transformations on the physical structure of the oxides is not known.

In none of the four systems examined was evidence found for any significant metal phase stabilization which would have implied high temperature oxygen solubility.

On the basis of all evidence obtained, it is considered that the rare earth-oxygen systems investigated probably contain a monoxide phase in addition to metal and sesquioxide phases. Positive identification of this phase has not been achieved. Metallographic evidence for the presence of monoxide in the neodymium and samarium systems is not as certain as for the yttrium and erbium systems. An alternative phase diagram, less preferred, is therefore also suggested for these two elements.

RARE EARTH ALLOY STUDIES

COBALT AND NICKEL ALLOYS

Cobalt is a hard, oxidation resistant element with a relatively high melting point (1495°C). It has recently found wide use, both as an alloying constituent and as a matrix element of high temperature alloys. The rare earth ends of the yttrium-cobalt and erbium-cobalt systems have been reported (27). In view of cobalt's demonstrated importance in high temperature alloy technology it was considered pertinent to investigate the cobalt end of a cobalt-rare earth system.

Nickel too, has found important application in high temperature alloys. The addition of cerium to nickel based resistance elements has been reported to decrease the oxidation rates of these elements at elevated temperatures (16). Since the yttrium-nickel system was under investigation in another laboratory (9), phase diagram studies were not made. The effect of rare earth additions on the atmospheric corrosion resistance of nickel, however, was investigated, and some of the alloy compositions were investigated metallographically.

The System Cobalt-Erbium

General Characteristics. Cobalt forms a number of intermetallic compounds with erbium. A eutectic is formed with the first of these, $Co_{17}Er_2$. The solubility of erbium in cobalt is low. The phase transformation in cobalt is essentially unaffected by the presence of small percentages of erbium; it could not be detected in compositions containing 5% or more of erbium.

The Phase Diagram. A tentative partial equilibrium diagram for the system cobalt-erbium is presented in Figure 86.

The alpha-beta transformation for cobalt was found to be 405°C. This was lowered to 400°C for the 1% erbium alloy and 395°C for the 2% erbium alloy. The transformation was not detected in compositions containing 5% or more of erbium. It is possible that the transformation temperature drops off very sharply as in the cobalt-iron system (30), but it is more likely that the rate of transformation simply becomes very slow with increasing erbium content. A second transition was found by differential thermal analysis at 1100°C in cobalt metal and the 1% and 2% erbium alloys. Both phase changes and magnetic changes have been reported by various investigators for cobalt and dilute cobalt alloys in this temperature region (7). Since the Curie temperature of cobalt is 1120°C

(and in the absence of positive evidence for a crystallographic phase change) the transition is considered to be associated with a magnetic change.

The solubility of erbium in cobalt is low. Analysis of the microstructures (see below) indicates that the solubility, both at room and elevated temperatures, is considerably less than 1/2%.

Three compounds, $Co_{17}Er_2$, Co_5Er, and Co_4Er, are proposed for the portion of the system examined. The two higher cobalt content compounds at least, probably decompose peritectically. A eutectic is present near 20% erbium. The eutectic temperature is 1320°C.

Thermal Analysis. Compositions of cobalt with up to 15% erbium were examined by differential thermal analysis, and the melting points were determined by the resistance method. The data obtained are indicated in Table XXIX.

Exothermic signals (during the heating cycle) were observed at 405°, 400°, and 395°C for cobalt, and the 1% and 2% erbium alloys respectively. A second signal was observed for these compositions at 1100°C. These two signals are considered as locating the alpha-beta transformation in the first case, and a magnetic ordering transformation in the second. Neither transformation was observed in the high purity metal. The transformations of cobalt have been reported as sluggish and may be incomplete (4,33). Such effects may make them difficult to detect by thermal methods. The transformations were not observed in compositions containing 5% or more of erbium, and it is believed that the alpha to beta transformation temperature is lowered (thus also becoming more sluggish) in the manner defined as "type 1, open beta field" (7).

An exothermic reaction occurs at 1320°C with increasing magnitude as the erbium content increases. This is ascribed to the eutectic reaction.

The melting points of the alloys, as determined by the resistance method, decreases quite regularly with increasing erbium content.

X-Ray Diffraction. Analysis of alloys containing 15-40% erbium, in the as arc-melted condition, indicated the presence of two compounds. Comparison of the diffraction patterns of these compounds with those found in the cobalt-gadolinium system (35) indicated that the two cobalt-erbium compounds are probably isomorphous with Co_5Gd and Co_4Gd, and they are correspondingly identified as Co_5Er and Co_4Er. A new compound was observed when the 15% and 25% erbium alloys were annealed. This was found isomorphous with the monoclinic $Co_{17}Th_2$ structure reported by Florio and Rundle (13), and is correspondingly identified as $Co_{17}Er_2$.

Identification of the monoclinic structure by X-ray diffraction is indicated in Table XXX. Identification of $Co_{17}Er$, Co_5Er, and Co_4Er in as arc-melted cobalt-25% erbium is indicated in Table XXXI.

Identification of the cobalt metal phase is made complex by the X-ray fluorescence produced during analysis which increases the background noise level. The face centered cubic (beta) structure is easily detected, but determination of the hexagonal (alpha) structure is more difficult. Only the face centered cubic form of cobalt was detected in all of the compositions examined.

Physical Appearance. The arc-melted 98-99% cobalt base metal had a dull silver appearance (cut and polished surface). Alloys containing 1/4%-20% erbium had a shiny silver surface when cut and polished in the same manner.

Microstructures. The microstructures of cobalt and cobalt-erbium alloys are illustrated in Figures 87-101. The structure of the starting cobalt metal (as arc-melted) is seen in Figures 87 and 88. The 1/4% alloy (Figures 89 and 90) appears quite clean, apparently containing less impurities than the base cobalt metal. Beginning with the 1/2% erbium alloy, increasing amounts of second phase are observed until the eutectic composition is reached at cobalt-20% erbium (Figure 99). Close examination of the 1/4% alloy indicated that the erbium containing second phase may also be present in this composition, but since the base erbium metal was so apparently impure it is difficult to ascertain the true nature of the second phase.

The solubility of erbium in cobalt must therefore be less than 1/2% and may be less than 1/4%. Furthermore, if the first 1/4% erbium addition has acted as a scavenger and been slagged off, much of the initial addition is no longer in the alloy, and the solubility must then be considerably less than 1/2%. Comparison of the microstructures of the alloy series also indicates that the second phase in the 1/2% composition is a eutectic phase rather than compound precipitated from solid solution. This indicates that the solubility of erbium in cobalt must be low at elevated temperature (1320°C) as well as at room temperature.

An unusual detail of microstructure, consisting of parallel bands, was observed in the cobalt-1/2% erbium alloy. These are seen in Figure 91 and at greater magnification in Figure 92. This is the only composition in which these bands were observed, and they were observed present only in a small portion of the area examined. It is possible that hexagonal twinning may be represented in an area too small to give positive identification of the hexagonal structure by X-ray diffraction.

Increasing amounts of eutectic are seen in Figures 93-98 of the 1%, 5%, and 15% alloys. Figure 94 at 500X indicates decreasing evidence for transformation in the 1% alloy compared to the 1/4%

and 1/2% alloys, and in Figure 96, for the 5% alloy, no evidence of a transformed structure is seen in the cobalt grains. Figure 99 indicates that the 20% erbium is essentially completely eutectic. The 25% alloy is seen in Figure 100 as largely compound phase. Detail of a high eutectic portion is seen in Figure 101 at 750X.

Cobalt-Yttrium Alloys

Although the cobalt-yttrium constitutional diagram was not to be constructed, a number of alloys were prepared for atmospheric corrosion tests. These were examined metallographically for comparison with the cobalt-erbium structures.

Figures 102-105 illustrate the structures of the cobalt alloys containing 1/4, 1, 5, and 10 weight percent of yttrium respectively. Since the atomic weight of yttrium is just slightly over one-half that of erbium, these compositions, on an atomic basis, correspond very nearly to the 1/2, 2, 10, and 20 weight percent erbium compositions. The structures are seen to correlate very closely.

Nickel-Yttrium Alloys

Domagala and co-workers (9) have reported the phase diagram for the yttrium-nickel system. A eutectic is reported at 90% nickel, between nickel (solid solution) and the first compound YNi_9. The solid solubility limit was reported as less than 1 weight percent yttrium in nickel.

Compositions prepared for atmospheric corrosion tests were also examined metallographically. Figures 106-109 illustrate the microstructures of nickel and nickel with 1/4%, 1%, and 5% yttrium. The 5% yttrium alloy appears to be close to 50% eutectic and substantiates Domagala's value of 10% for the eutectic composition. It is also noted that the 1% yttrium composition has a typical dendritic nickel matrix with considerable eutectic present. The 1/4% yttrium composition consists of primary nickel with a dispersed second phase. The distribution of the second phase strongly suggests its having formed as a small amount of eutectic rather than having precipitated from solid solution, and thus sets the maximum limit of solid solubility for yttrium in nickel as less than 1/4 weight percent at both room and elevated temperatures.

RARE EARTH ALLOY STUDIES

TANTALUM AND NIOBIUM ALLOYS

Tantalum and niobium are closely related transition elements which have recently become commercially available. The metals have high melting points; 3000° and approximately 2475°C, respectively (31), and the metals and their alloys have attracted considerable interest for elevated temperature applications. Such applications, unfortunately, are limited by rather rapid atmospheric attack.

Experience in the production of rare earth metals in tantalum or niobium crucibles indicates considerable attack at elevated temperatures. Although contraindicated by theoretical considerations, this suggests the possibility of some solubility or of compound formation, and attendent effects on mechanical properties or corrosion rates. Partial equilibrium phase diagrams for systems of rare earths with tantalum and niobium were consequently determined, to help elucidate the observed behavior of alloys, and to serve as a basis for future alloy investigations.

Tantalum-lanthanum, tantalum-erbium, tantalum-yttrium, niobium-erbium, and niobium-yttrium systems were investigated. Preliminary examination indicated general similarity as discussed under "General Characteristics" below. Specific details as obtained for each system are subsequently described in the paragraphs for the various procedures. Two phase diagrams are constructed, one of the tantalum-erbium system, the other of the niobium-erbium system. It is considered that the essential features at the tantalum and niobium ends of these systems would be similar for the various rare earths, the major differences being associated with the varying melting points and allotropic structures of the individual rare earths.

General Characteristics. The principal feature of tantalum-rare earth and niobium-rare earth phase diagrams is the presence of an extensive liquid immiscibility region. This region extends from very near pure tantalum (niobium) to 80% or higher rare earth. The lower limit of the two liquid region is a monotectic horizontal involving the reaction:

$$\underset{\text{(Ta rich)}}{\text{Liquid}} \longrightarrow \underset{\text{(RE rich)}}{\text{Liquid}} + \underset{\text{(ss)}}{\text{Ta}}$$

A eutectic is present at the rare earth rich end of the system. The room temperature solid solubility is very low at both ends of the system, but there may be slight solubility of rare earth in

tantalum near the monotectic temperature, and of tantalum in rare earth at the eutectic temperature.

Phase Diagrams. A tentative, equilibrium phase diagram for the system tantalum-erbium is presented in Figure 110, and the tantalum end of the system in greater detail in Figure 111 (idealized). During the course of this work Lundin (29) presented the phase diagram for the system tantalum-yttrium (Figure 112). The basic features are quite similar except for the expression of possible slight solubility at the monotectic and eutectic temperatures in our work.

An extensive liquid immiscibility region exists, covering the composition range from approximately 2-3% erbium to slightly less than 90% erbium. The lower limit of the two liquid region is the monotectic isotherm which is presumed to be only slightly lower in temperature than the melting point of tantalum (3000°C).

The solubility of erbium in tantalum is very low at room temperature. The solubility at elevated temperature was difficult to establish. Photomicrographs (discussed below) indicate a maximum solubility of 1%, but it is probable that the actual solubility is lower. Lundin (29) indicates that the solubility of yttrium in tantalum is less than 0.1%.

A eutectic is present at approximately 90% erbium, the eutectic temperature being only slightly lower than the melting point of erbium. The composition of Liquid 2 at the monotectic temperature is almost the same as its composition at the eutectic temperature.

The solubility of tantalum in erbium is very low at room temperature, but there may be slight solubility near the melting point.

The tentative equilibrium phase diagram for the niobium-erbium system is presented in Figure 113. It is quite similar to the tantalum-erbium diagram, one point of difference being a somewhat greater change in the width (composition limits) of the Liquid 2 region as a function of temperature. The solubility of rare earths in niobium at elevated temperatures was not determined, but it appears to be low.

Savitskii, Terekhova, and Burov (38) have reported investigations of the niobium rich end of systems with lanthanum and cerium. They report a phase diagram similar to that reported herein, with the solubility of lanthanum and cerium less than 0.05%, and with the two liquid immiscibility region beginning at 0.1-0.2% lanthanum, and 1-2% cerium respectively.

Thermal Analysis. Most of the alloys investigated were at the tantalum (niobium) end of the systems. The important features at this end of the systems are all at very high temperatures. Differential thermal analysis indicated no evidence for reactions occurring below 1500°C in any composition.

The melting points of rare earth metals containing up to several percent tantalum appear to be very close to that of the pure rare earth metals, indicating that the eutectic temperature is only slightly lower than the melting point of the pure metal.

X-Ray Diffraction. X-ray diffraction of tantalum compositions containing up to 40% lanthanum indicated the presence of tantalum and lanthanum only. No intermediate compounds were detected. There was no shift in the position of the diffraction peaks for lanthanum, indicating no detectable solubility. For tantalum, only the 161.6° (2θ) peak (hkl = 411,300) was slightly shifted, to indicate a slight contraction of the lattice, and implying some purification by scavenging. The effect is very small, being observed only for this (highest) 2θ peak where any shift would be maximized.

Yttrium and erbium as normally prepared may contain 0.25-0.5% tantalum. X-ray diffraction of these metals indicates that the tantalum is not in solution, but is present as the element. Lanthanum as normally prepared contains less than 0.1% tantalum, too low to be detected by X-ray diffraction. Two percent of tantalum was introduced into lanthanum by holding it molten in a tantalum crucible for two hours at 1600°C. X-ray diffraction analysis of this material indicated the presence of elemental tantalum. The lanthanum parameters were unchanged indicating no detectable solubility.

Alloys of tantalum with lanthanum showed evidence of very rapid oxidation, even at room temperature. This was believed due principally to exposure and oxidation of the finely divided lanthanum phase. Alloys were therefore prepared from tantalum with yttrium and with erbium. X-ray examination of the latter gave results exactly analogous to the tantalum-lanthanum system. Both metals were found in the elemental state with essentially unchanged lattice parameters.

Alloys of niobium with 10-90% erbium were examined by X-ray diffraction. The results were again analogous to those observed above. Elemental niobium and erbium were present, the lattice parameters were essentially unchanged from those of the pure metals, and no intermetallic compounds nor intermediate phases were detected.

Physical Appearance. All alloy compositions produced typically metallic buttons. When cut and polished, evidence of gross segregation was visually apparent in compositions of tantalum or

niobium with 5% or more of rare earths. Compositions containing less than 5% rare earths appeared pitted. Since the pure tantalum did not have these pits it is presumed they represent areas from which the rare earth rich phase was eroded. The macroscopic appearance of a two phase alloy is illustrated in Figure 114 of a niobium-20% erbium composition.

Microstructures. The microstructure of compositions cooled from the liquid immiscibility region are illustrated in Figures 115-117. Figure 115 indicates the interface in a tantalum-erbium composition. The appearance of the two phases is rather typical for all compositions. Very little dendritic growth of tantalum is observed in the erbium rich phase, suggesting very little change in composition of the Liquid 2 liquidus curve between the monotectic and the eutectic temperatures.

Figure 116 shows the interface between the two liquids in a niobium-10% erbium alloy. The niobium phase shows a considerable amount of entrapped Liquid 2. The erbium rich phase shows a considerable amount of niobium present which may have been likewise entrapped, or which may have precipitated during cooling. It is noted that the specific gravity of niobium is 8.6, not greatly different from that of erbium, 9.1. Since the two liquid solutions would have even closer specific gravities, physical separation of the two liquids might be relatively slow.

Figure 117 illustrates the interface in a niobium-50% erbium alloy. Here the precipitation of niobium from the erbium rich liquid is clearly visible both as crystallites seeded by the massive niobium, and as dendrites precipitated within the liquid. This separation of niobium was characteristic in the erbium rich liquid phase of many of the high erbium alloys, and is considered to be evidence for the Liquid 2 liquidus curve changing composition significantly between the monotectic and eutectic temperatures.

Figure 118 illustrates the microstructure of a typical area in arc-melted tantalum. The phase boundary between several large grains is noted. The quantity of second phase observed is approximately average. Some areas appeared to contain almost no second phase, others appeared to have slightly more.

Figures 119 and 120 illustrate the microstructures of tantalum alloys containing 0.07% and 0.8% erbium respectively, and are representative of the entire cross section of the arc-melted buttons. A second phase is present, appearing as dark etch pits randomly distributed throughout the grains. There appears to be no particular concentration of second phase within the grain boundaries (the bold appearance of some of the grain boundaries is due to physical relief). It is tempting to consider this random distribution of second phase as evidence for the solubility of

erbium in tantalum at elevated temperature followed by precipitation as the tantalum cooled. Such precipitates, however, are usually finely divided, and in the concentrations here present may even be difficult to detect. The relatively large size of some of the second phase areas suggests that some other mechanism may operate. Such a mechanism (considered with reservations) may be the solidification from Liquid 1 (see Figure 111) of primary tantalum, the production of the monotectic liquid, and its subsequent monotectic reaction to produce additional tantalum plus Liquid 2. One reservation to this process is the lack of second phase material in the intergranular boundaries. During the solidification of the primary tantalum it would be expected that the liquid phase, ultimately with the monotectic composition, would be forced into the intergranular areas, and these should show high concentration of Liquid 2. The solidification, however, occurs at elevated temperature, and - particularly if the monotectic temperature is close to the melting point of tantalum - is undoubtedly very rapid. Under these conditions the liquid may become entrapped.

As the erbium content is increased, a new structure becomes apparent. This is illustrated in Figures 121 and 122 of tantalum - 1.0% and - 4% erbium content respectively. The new structure is characterized by the presence of a complex sub-grain pattern rather reminiscent of compositions containing considerable eutectic. There is also considerable grain refinement. In compositions containing 15-80% of erbium almost the entire tantalum rich phase has this structure. It is illustrated again for the 15% erbium alloy in Figure 124 at 100X and in greater detail in Figure 125 at 500X. It is considered that this microstructure represents the tantalum rich phase of the two immiscible liquids. As the liquid phases reach the monotectic temperature the tantalum rich liquid undergoes the monotectic reaction producing tantalum (perhaps a very dilute solid solution) and Liquid 2, which in this case is now most certainly trapped within the tantalum grains. Some of the structure characteristic of the lower erbium compositions is also still present. Figure 123 illustrates a second area of the same specimen of tantalum-4% erbium alloy seen in Figure 122.

The above microstructures suggest that the maximum solubility of erbium in tantalum at the monotectic temperature is 1%, and that it is probably considerably less. The monotectic composition is between 0.8% and 4% erbium. Allowing for the difficulty of attaining true equilibrium it is probably between 2% and 3%.

Investigations at the high rare earth end of the system were not very comprehensive. The nominal niobium-90% erbium composition, however, as prepared for corrosion tests, was examined metallographically. Figure 126 illustrates the microstructure of a

portion of this alloy although it is not certain that it represents equilibrium conditions. A small droplet of niobium is observed which may have been unmelted metal. The erbium phase has scattered, fairly well defined erbium grains, and areas which appear to be eutectic in nature. There is also present some niobium which may have precipitated from solid solution.

ATMOSPHERIC CORROSION STUDIES

One of the properties of great interest in current technology is the resistance of materials to atmospheric corrosion, especially at elevated temperatures. The systems studied in this program include compositions potentially having improved corrosion resistance. A complete study of the fundamental corrosion mechanisms for these systems was beyond the scope of this program. The systems were examined, however, for a practical evaluation of resistance to sustained atmospheric exposures at elevated temperature.

Rare Earth - Oxygen Systems

Neodymium-Neodymium Oxide. The rate of atmospheric corrosion of neodymium-neodymium oxide compositions at 600°C increases with increasing oxide concentration (Figure 127). It is noted that the curves for neodymium and the neodymium-10% neodymium oxide composition indicate increased rates of corrosion as a function of time. This too corresponds to faster corrosion rates with increased oxygen content. The curves for compositions containing 15%, 25%, and 35% neodymium oxide have approximately the same slope. The curves become horizontal when all of the metal has corroded. Compositions containing 50% or more of oxide were too brittle to permit sample preparation, and were therefore not tested.

Neodymium metal after 2 hours at 600°C had a heavy coating of corrosion product which became a separated crust after 6 hours exposure. The entire specimen was fragmented after 12 hours. The same behavior was noted for the oxide compositions, but the process was accelerated as a function of increasing oxide composition.

The corrosion product for all compositions had the typical light blue color of neodymium oxide except as sometimes dulled by the grayness of interspersed metal.

Erbium-Erbium Oxide. The atmospheric corrosion behavior of erbium-erbium oxide compositions at 600°C (Figure 128) is similar to that of the neodymium-neodymium oxide compositions in that the rate increases with increasing oxide content. The actual corrosion rates are slower by approximately an order of magnitude. Compositions containing 50-90% erbium oxide all corrode at nearly the same rate.

The surface of erbium metal after two hours exposure was blackened and appeared to have a thin, tightly adherent coating. After 6 hours light pink spots, with a typical sesquioxide

appearance, were observed. The entire surface was pink after twelve hours. Longer exposure produced a crust, followed by complete fragmentation of the specimen.

Compositions containing 10-35% oxide all had pink surfaces after two hours; crusting and fragmentation were observed on longer exposures, and at an accelerated rate with increasing oxide content.

The appearance of erbium - 50% erbium oxide specimens, as polished, was "shiny gray" rather than the "shiny silver" of the pure metal and the lower oxide compositions. The addition of 60-90% oxide produced a "shiny black" appearance. These compositions did not turn pink after atmospheric attack at 600°C but gradually cracked and fragmented. The colors of the corroded specimens were gray to black, similar to those of the starting compositions.

Yttrium-Yttrium Oxide. The rates of atmospheric corrosion of yttrium and yttrium-yttrium oxide compositions are shown in Figure 129. The rates of corrosion increase with increasing oxide content. The change in rate of corrosion as a function of time is much less pronounced for yttrium than for neodymium and erbium, and the rate curve may be considered a straight line within the limits of accuracy of measurement.

The changes in appearance of yttrium and the yttrium-yttrium oxide compositions during test were analogous to the changes in the erbium-erbium oxide system. Yttrium metal first darkened, then became spotted with white sesquioxide which gradually spread to cover the entire surface, and deepened with fragmentation of the metal. The high oxide content alloys (as prepared) were gray to black in appearance, and the corrosion products were also gray to black rather than white.

Samarium-Samarium Oxide. The rates of corrosion of samarium and samarium-samarium oxide compositions at 600°C are shown in Figure 130. The compositions are nominal starting compositions and the oxide values are probably slightly low due to volatilization of samarium metal during arc melting. The corrosion rates for all of the lower oxide compositions are quite similar, both in nature and magnitude, to that for samarium. The nominal 15% oxide composition corrodes more rapidly.

An initial rather rapid weight loss for samarium and for the low oxide compositions suggests that the rate of volatilization of samarium metal in air at 600°C is more rapid than the rate of oxidation. As the surface does become oxidized, however, weight gains and losses are balanced, or the protective coating prevents further volatilization.

All of the compositions prepared were initially "shiny silver" with the typical very slightly golden cast of pure samarium. As corrosion progressed, the surfaces first darkened to a gray-black color, then developed spotted areas of the almost white sesquioxide which gradually spread to cover the entire surface for the 10 and 15% oxide compositions.

Rare Earth-Tantalum and Rare Earth-Niobium Systems

The rare earth-tantalum and rare earth-niobium systems are two phase systems with essentially no solid solubility of rare earths in the earth metals. The presence of an extensive two liquid phase region further results in macroscopic phase separations for compositions containing more than a few percent rare earths. Rare earth containing alloys consequently solidify as segregated alloys containing a rare earth rich phase (which may be almost entirely a eutectic structure) and a tantalum (or niobium) rich phase. Each of these macroscopically separated phases may further contain entrapped droplets of the other phase. From a corrosion point of view the phases are essentially those of the respective elemental metals except for the effects of state of subdivision. Indeed it was found that all of the alloys tested corroded somewhat more rapidly in air than did the respective individual metals.

Tantalum-Lanthanum. Alloys of tantalum with from 1 to 40% lanthanum were prepared for the phase diagram studies. When prepared for metallographic examination, the lanthanum phase corroded very rapidly even at room temperature. Since it appeared obvious that increased corrosion resistance for tantalum would not be obtained with these alloys, they were not tested at elevated temperatures. It was not certain, however, whether possible scavenging effects of small additions might improve corrosion resistance. The one percent composition and alloys containing nominally 1/10% and 1/3% lanthanum were therefore tested. Figure 131 indicates that all compositions corroded somewhat more rapidly than the base metal.

Tantalum-Yttrium. Several alloys of tantalum with yttrium appeared to be much more stable at room temperature than the tantalum-lanthanum alloys. A number of compositions were therefore prepared and tested at 600°C. The results, shown in Figure 132, indicate that tantalum and yttrium metals have coincidentally approximately the same rate of corrosion at 600°C, but that all of the alloys corroded more rapidly on prolonged exposure. No correlation was observed between composition and rate of corrosion. Some evidence was noted for possibly improved corrosion resistance during the first few hours of test, but the results again were not

consistent with composition, and may have been within the limits of error for the non-homogeneous system.

All alloys were originally "shiny silver" in appearance. The initial corrosion appeared as white spots which gradually spread to form a crust.

Niobium-Erbium. Alloys of erbium with niobium corroded more rapidly than either base metal (Figure 133). Again, as in the tantalum-yttrium system, there was no correlation of corrosion rate with composition.

The corrosion product of the niobium was cream colored, that of the erbium pink, and of the alloys an intermediate yellow-pink depending upon composition.

Niobium Alloy - Rare Earth Compositions. Two niobium base alloys have recently been proposed as useful structural materials based on their mechanical properties at elevated temperature. Preliminary investigations were made of the effect of rare earth additions on the atmospheric corrosion properties of these alloys.

The first alloy contained 15% tungsten, 5% molybdenum, 2% platinum, balance niobium. To this alloy was added small amounts (1/4%, 1%, and 2%) of erbium and of yttrium. The results of atmospheric corrosion tests at 600°C are seen in Figures 134 and 135. The addition of erbium to the alloy did not markedly affect the corrosion rate. One percent erbium increased the rate slightly, 1/2% and 2% decreased the rate. Yttrium appeared to be somewhat more effective. The 1/2% and 2% alloys had slightly decreased corrosion rates, the rate for the 1% yttrium alloy was only about 1/3 the rate for the base alloy.

The second alloy tested contained 20% tungsten, 2% titanium, balance niobium. Two arc-melted heats of this alloy were prepared. Again additions of 1/2%, 1%, and 2% of erbium and of yttrium were made, and the compositions tested at 600°C. The results are shown in Figures 136 and 137. It is observed that the two heats of the base niobium alloy corroded at considerably different rates. From X-ray and metallographic examination it appeared that the alloys were homogeneous and single phased. No explanation for the variance can presently be offered. All of the erbium and yttrium containing alloys corroded much more slowly. There was very little difference between the rates for the various compositions (relative to the base alloy), the average rate being about 20% of that for the better of the two base alloys, and less than 10% of that for the poorer base alloy.

As corrosion progressed, the surface of the niobium alloys first turned dark, then gradually developed a dull gray crust for the tungsten and titanium alloy, and an olive green crust for the

tungsten, molybdenum, platinum alloy. Alloys containing yttrium had scattered white spots, and alloys containing erbium had scattered pink spots indicating that the rare earth was present as a separate metal or compound phase.

Rare Earth-Cobalt and Rare Earth-Nickel Systems

Cobalt and cobalt base alloys are used in many applications at elevated temperatures. The possibility of improving atmospheric corrosion resistance through the addition of rare earths was examined by testing cobalt alloyed with erbium and with yttrium.

Cobalt-Erbium. The corrosion rates of cobalt, erbium, and their alloys at 600°C is shown in Figure 138. Compositions containing one percent or less of erbium corrode more slowly than the base cobalt metal, compositions containing 5% or more of erbium corrode more rapidly.

The lustrous, shiny surface of the uncorroded alloys first tarnished to a dull, blue-gray film. The corrosion film then grew thicker, becoming a mottled blue (with pink) for the low erbium alloys, and a definite blue for the higher erbium alloys. The oxide film formed is strongly coherent and its coefficient of expansion is apparently significantly different from the base metal. When the test specimens were removed from the furnace and cooled, the oxide broke away in flakes. In some cases the flakes vigorously popped away from the metal and the results were subject to some error (this led to covering the crucibles immediately after removal from the furnace). The corrosion rate curves appeared to be reasonably smooth, however, and relative losses in the initial time periods appeared to be minor.

The apparent improvement in corrosion rate at 600°C (approximately a factor of two for low erbium compositions) was considered sufficient in magnitude to be of practical interest. A further test of these compositions was made at 900°C to ascertain whether protection also existed at this temperature. The results shown in Figure 139 indicate that the rate of corrosion of cobalt is approximately 40-50 times greater at 900°C than at 600°C. Erbium additions of 1-5% apparently are still effective in reducing the rate by about a factor of two.

The appearance of the corrosion film obtained at 900°C was quite comparable to that obtained at 600°C, except that the color was somewhat less blue and more gray, and the pink mottled effect was less pronounced.

Cobalt-Yttrium. The rate of atmospheric corrosion of cobalt-yttrium alloys is shown in Figure 140. Flaking in this system was more severe, and data could not be obtained for the 1 and 5% yttrium alloys. The cobalt-1/4% yttrium alloy was apparently attacked more slowly than pure cobalt for the first few days, but the rate of attack subsequently increased. All other alloys corroded more rapidly (in comparing yttrium additions with erbium additions it must be noted that on an atomic basis 1% yttrium is equivalent to almost 2% of erbium).

The cobalt-yttrium alloys were also tested at 900°C. The results, shown in Figure 141, indicate that the corrosion rate of cobalt at this temperature was also reduced (again by a factor of approximately two) by the addition of up to 5% yttrium.

Except for the more severe flaking as noted above, the nature of the corrosion products appeared quite similar at both 600 and 900°C to those observed in the cobalt-erbium system.

Nickel-Yttrium. The rate of atmospheric corrosion of nickel-yttrium alloys at 600°C is shown in Figure 142. Additions of yttrium up to one percent show little effect, larger additions rapidly increase the rate of attack. The rate of attack at 900°C is shown in Figure 143. There is a slight improvement for the 1/4% and 1% yttrium alloys, but the difference may be within the limits of experimental error. Nickel with 5% yttrium oxidizes more rapidly than the base metal.

Upon corrosion, the shiny surface of the metal turns dull gray to dull black in color, occasionally with a greenish tinge. Compositions with the higher yttrium contents appeared generally darker than those with low yttrium content.

Yttrium - Rare Earth Systems

Atmospheric corrosion tests were made on alloys in the yttrium-erbium and yttrium-neodymium systems along with the measurements and examinations made for ascertaining the nature of the constitutional diagrams. For the yttrium-erbium system, one objective was to ascertain possible effects of slight lattice distortions. For the yttrium-neodymium system, objectives were to establish the effects of modifications of crystal structure as produced by another "rare earth", and to establish whether unusual effects might occur for the intermediate compound.

Yttrium-Erbium. The atmospheric corrosion rate of yttrium-erbium compositions was determined on a set of alloys prepared by arc melting the appropriate relative amounts from one lot of each metal. Figure 144 indicates the weight increase per unit time for

the various nominal compositions. The addition of up to 20 weight percent of erbium to yttrium, or of up to 40 weight percent of yttrium to erbium, had little effect upon the corrosion rate of each matrix metal. The intermediate compositions had intermediate corrosion rates. The effect is perhaps more clearly shown in Figure 145, which indicates weight increase as a function of composition after 12 hours exposure.

Yttrium-Neodymium. A series of yttrium-neodymium compositions were prepared and tested at 600°C. These first results showed no consistent trend, and, with one exception, were all of approximately the same order of magnitude. The exception was the yttrium-60% neodymium alloy for which the rate of corrosion was much lower. Since this composition is very near the 1:1 atomic ratio at which a new crystal structure exists, the lower rate was considered as possible due to the presence of this new structure. Additional alloys in the composition range 30-80 weight percent neodymium were therefore prepared and tested.

The results of all tests are shown in Figure 146. For clarity the weight gain per unit area after six hours exposure at 600°C has been plotted against the composition. Since the exact composition may here have considerable significance, all alloys were analyzed, and the data are presented by actual, rather than nominal, composition. No consistent pattern of corrosion rate as a function of composition is evident, and the results do not duplicate well for similar compositions in the center of the system. The values for pure yttrium and neodymium are in good agreement with data for these elements in the other systems.

It is considered that the rate of atmospheric corrosion of the intermediate compositions may be significantly influenced by the nature of the phases present in the alloys. Single or two phase regions exist in this system depending upon the exact composition and the thermal history of the alloys. As noted in the constitutional diagram discussion, there is also the possibility of allotropic crystallographic transformations occurring at or near the test temperature.

The Effect of Some Sample Preparation Variables on the Corrosion Rate of Yttrium

In course of the tests described above, a number of different lots of rare earth metals were used. One sample from each lot was tested as a control for the alloys prepared from that lot. In general the corrosion rates for the various lots of each metal were in good agreement with each other, and were in agreement with rates previously reported (26).

The rate of corrosion for the yttrium metal used in preparing the yttrium-erbium alloy series, however, was considerably higher than the rate for other yttrium specimens. The test specimens in this system had been rinsed in acetone after polishing, and had subsequently been stored under argon for several weeks before the corrosion test was started. To check the effects of these variables on corrosion rates, one sample of yttrium metal was cut into four specimens. Two were rinsed with acetone after polishing, and two were rinsed with kerosene, then wiped dry. One of each pair was tested for corrosion rate immediately, the others were stored under argon for one month and then tested. The results are shown in Figure 147. It is seen that all specimens corroded at approximately the same rate, indicating relatively little effect due to these variables (and also reasonable duplication of results). The rate for this lot of yttrium was in agreement with that previously obtained (26), and with the rate obtained for yttrium in the yttrium-yttrium oxide series and in the yttrium-tantalum series.

Analysis of the yttrium metal used in preparation of the yttrium-erbium series indicated a typical purity level, with no indication of the presence (or absence) of any constituents which might inordinately influence oxidation rate. The reasons for the rapid rate therefore remain unexplained.

The Effect of Purity on the Corrosion Rates of Yttrium and Erbium

Pure (distilled) samarium metal had previously been shown to corrode very slowly in air at 600°C, and it had been theorized that one explanation for the slower rate in comparison with other rare earths might be related to its purity (26). The corrosion rate of samarium to which significant amounts of oxide were added (15% oxide, equivalent to approximately 2% oxygen) was indeed very much greater than that for the distilled metal. The corrosion rates for metals containing less than 5% added oxide, however, were not markedly changed. It has been noted that the microstructure of samarium containing small amounts of oxide (Figures 82,85) is not the same as the microstructure of other rare earth metals containing small amounts of oxide (Figures 45, 57). In particular the lamillar platelet type inclusions are not present in samarium.

Development of techniques for distilling yttrium and erbium made it possible to examine these metals and compare their corrosion rates with the as-cast metals. The results are shown in Figures 148 and 149 for yttrium and erbium respectively. The rate of corrosion of distilled yttrium was markedly lower than that

for the as-cast metal. The rate of corrosion of the distilled erbium was higher than that for the pre-distilled metal.

The results for yttrium were expected, and in agreement with general observations in the laboratory that cut and polished distilled metals appeared to stay bright longer than as-cast metals. The results for erbium were of course completely unexpected. Examination of the erbium and yttrium metals, however, indicated that a reasonable explanation could be found in the physical structure of the metals as deposited during the distillation process. The melting points of yttrium and erbium are at very nearly the same temperature (1509° and 1497°C respectively). The vapor pressure of yttrium is very much lower than that of erbium, however, and it is consequently distilled at a higher pot temperature. The condensing yttrium absorbs a good deal of radiant heat, and individual grains fuse. The metal is essentially in a cast state (frozen from melt) and the effective surface exposed in the corrosion test is that of the specimen. The erbium, however, distilled at a lower pot temperature, condensed below its melting point as an aggregate of coarse crystals. Although a polished specimen was prepared for corrosion testing, attack could still occur between the crystals, opening up a much larger surface area to further attack. Examination of the corroded specimens did indeed indicate that attack on the yttrium was essentially limited to the surface, while corrosion of the erbium had penetrated intergranularly and broken up the metal into a large number of individual crystals, each corroding on its entire surface.

THE MECHANICAL PROPERTIES OF SOME RARE EARTH ALLOYS

Tensile property determinations of rare earth metals and their alloys as previously reported (26,28) were extended to the systems currently under consideration. The alloys investigated are reactive at elevated temperature with most of the available container materials. Additionally many alloys were prepared from metals which are still rather costly. To avoid the possibility of contamination during the usual melting and casting procedures, and to minimize wastage of metal, many of the alloys were arc-melted (non-consumably) into bars approximating the final dimensions of the test coupons.

A comprehensive test program was initially outlined. It was soon found, however, that testing in each system was best developed slowly, with each step predicated on the previous results obtained. In some systems, for example, the alloys turned out to be so brittle that they could not be machined and further testing was abandoned; in others, the porosity of machined samples indicated that tensile data would be valueless. In the discussion below, each system is considered individually, and all experimental results are detailed.

The Yttrium-Erbium System

A series of alloys was prepared consisting of yttrium and erbium at 20% composition intervals. Test specimens of the pure metals were also prepared by arc-melting, and carried through the succeeding operations for comparative purposes. The pure metals and alloy compositions were subjected to a homogenizing anneal at 1000°C (1832°F) for 24 hours followed by a water quench. The ultimate tensile strength values obtained for these materials are given in Table XXXII.

The values obtained for yttrium and erbium are in general agreement with those previously reported (26,28). The values for the yttrium-20% erbium composition were considerably lower than for pure yttrium, but the specimens broke outside the gauge length, and it is not certain whether the values were a function of the composition or of the sample preparation method. The tensile strength of the yttrium-80% erbium composition was only very slightly below that of the pure erbium.

The highest tensile values were obtained for compositions containing 40% and 60% erbium. Since there are no compounds or intermediate phases present in this system, the higher values are ascribed to solid solution hardening. Tensile values at 400°F (204°C) averaged approximately 75% of room temperature values.

The tensile yield strength was determined only for the yttrium-80% erbium alloy. The value obtained (41,500 psi), was very near the ultimate tensile strength (42,000 psi). The ductility was found to be low, and subsequent tests did not include yield determinations in order to avoid extensometer damage.

The ductility of all nominal purity samples, as measured by elongation and reduction in area, was very low at room temperature. The ductility at elevated temperatures was somewhat better as would be expected, but the materials must be considered brittle as here prepared and tested. One tensile specimen was prepared from distilled erbium. Analysis indicated an oxygen content of 0.01%, total rare earth impurities 0.2 %, and total non-rare earth metallic impurities 0.1 % (tantalum 0.01%). The test results are summarized in Table XXXII. Tensile and yield strengths are somewhat lower than for the nominal >99% purity erbium, but ductility as measured both by elongation and reduction in area is improved.

Neodymium and Neodymium-Oxygen Compositions

A neodymium-1% neodymium sesquioxide composition was prepared by arc-melting, subjected to a homogenizing anneal for 24 hours at 833°C (1532°F), and air cooled. After machining, the specimen was observed to be porous and was not tested. A neodymium metal specimen prepared in a similar manner as a control was found to be sound. The ultimate tensile strength of this material was determined to be 15,000 psi (Table XXXII) somewhat lower than the 25,000 psi previously reported (26) for as cast neodymium. The elongation was 22% compared with approximately 10% for the as-cast metal, however, indicating greater ductility.

Erbium and Erbium-Oxygen Compositions

An erbium-1% erbium sesquioxide composition was prepared by arc-melting, subjected to a homogenizing anneal for 24 hours at 1000°C (1832°F), and air-cooled. The ultimate tensile strength of this material (Table XXXII) was 39,300 psi, slightly lower than for pure erbium.

Cobalt-Erbium and Cobalt-Yttrium Alloys

Cobalt-1% erbium and cobalt-1% yttrium alloys were prepared by arc-melting in the 1/2" x 1/2" x 6" mold. The test ingots appeared to be structurally sound. Attempts to produce an ingot from the base cobalt metal failed, all ingots having considerable porosity. The difference in fabricability may be related to

refinement of the cobalt by small additions of rare earths as noted in the metallographic discussion of the cobalt-rare earth systems.

The erbium and yttrium alloys were heat treated for 24 hours at 1000°C (1832°F) and air cooled. Ultimate tensile strengths (Table XXXII) were 30,500 psi for the erbium alloy, and 29,600 psi for the yttrium alloy. The yield strength of the erbium alloy was 29,800 psi (0.2% offset). Ductility was very low for both compositions. Comparative values for the base cobalt metal could not be obtained, but literature values for cobalt are indicated as of the same order as obtained above for the alloys (30).

Nickel-Erbium and Nickel-Yttrium Alloys

Attempts were made to prepare nickel, nickel-1% erbium, and nickel-1% yttrium alloys by arc-melting in the 1/2" x 1/2" x 6" mold. All specimens showed excessive porosity.

Yttrium-Zirconium Alloys

The phase diagram of the yttrium-zirconium system contains a receding solvus line, and indicates sufficient solubility of zirconium in yttrium at elevated temperatures to suggest age hardening possibilities. Three alloy compositions were prepared containing nominal 1 1/2%, 3 1/2%, and 6% zirconium additions. The 1 1/2% composition was selected as being near the solid solubility limit at room temperature. The 3 1/2% composition is within the solid solubility limit at 1000°C, but exceeds the solid solubility at room temperature. The 6% composition exceeds the solubility limit at 1000°C and below.

Ultimate tensile properties were determined for these alloys as arc-melted and as solution heat treated for 7 hours at 1000°C (1832°F) followed by a water quench. The results (Table XXXIII) indicate that the 6% alloy had the highest strength, and that the solution heat treated specimens were stronger than the as-cast specimens. No satisfactory correlation however, could be made for the results for the 1 1/2% and 3 1/2% zirconium alloys. The high value for the 6% zirconium in yttrium alloy correlates with previous results (28) for the erbium-zirconium system, in which it was found that highest tensile values were obtained for an alloy containing zirconium in excess of elevated temperature solubility limits. Ductility, as measured by elongation, was low for all alloys.

Considering now the age hardening possibilities in the system, hardness values were determined for the solution heat treated alloys. They were then subjected to aging treatments

of 15 minutes at temperatures of 300° and 600°C (572°, 1112°F). For all compositions the hardness decreased, indicating an overaged condition and suggesting that the alloys were age hardenable at room temperature. Specimens from the 1 1/2%, 3 1/2%, and 6% zirconium compositions were therefore again solution heat treated at 1000°C for 2 hours and water quenched. Hardness measurements were made immediately, and again after 65 hours. Hardness values increased from R_A = 36, 38, and 44 to 43, 44, and 54 respectively.

A more comprehensive examination of age hardening characteristics was made for carefully analyzed alloys. The alloy compositions were found to be: yttrium-2.4%, -3.9%, and -5.7% zirconium. Each bar was divided into two parts. All specimens were sealed in Vycor under argon, solution heat treated for 20 hours at 1000°C (1832°F) and water quenched. Immediately after quenching, one specimen of each composition was placed in a mixture of dry ice and acetone and reserved for comparison hardness at a later date. The hardness of the other specimen of each composition was determined immediately and then again at progressively longer time intervals. The results obtained are presented in Table XXXIV.

It is noted that all three alloys became progressively harder. The 5.7% zirconium alloy reached an essentially constant value after about one day, the 3.9% alloy after about 4 days, and the 2.4% alloy after about 5 days. A small section of each of these specimens was overaged by heating to 538°C (1000°F) for 16 hours and air cooling. The hardness of these specimens was near to or less than that of the original heat treated and quenched specimens. The reserved halves of the original alloys which had been kept in dry ice and acetone for up to 158 hours showed very little change in hardness from the quenched state.

In summation, the aging investigations indicate that yttrium-zirconium alloys age harden in from 1-7 days at room temperature and overage rapidly at moderately elevated temperatures. It is now certain that alloys tested for mechanical properties after homogenizing anneals or stress relief anneals were actually in an overaged condition.

SUMMARY AND CONCLUSIONS

The study of yttrium and the rare earth elements has been continued in a number of diverse aspects. High purity metal has been produced, and improved methods of analysis and metallography developed. A number of binary systems have been investigated to establish constitutional phase diagrams and to determine corrosion and mechanical properties.

Procedures were developed for the purification of erbium and yttrium by vacuum distillation at elevated temperature (1600 - 1850°C). The principal impurities in the as-cast metals are oxygen and tantalum, each commonly present to the extent of approximately 0.2 - 0.5%. The oxygen content of the distilled metals was reduced by approximately an order of magnitude; the tantalum content of the distilled metals was generally reduced to 0.01% or less.

An attempt to purify yttrium by the combined effect of zone refining and the passage of a direct current was unsuccessful.

Experiments in the purification of beryllium by melting with rare earths continued to provide metallographic evidence that such purification occurred. The non-consumable arc-melting procedures available, however, produced porous specimens not suitable for mechanical property evaluation.

The analytic method for oxygen determination was improved by modifying the procedure to provide for melting the metal and removing the oxygen as carbon monoxide in a stream of inert gas rather than in a vacuum. This resulted in a lower and more constant blank, and provided for routine analysis of oxygen contents as low as 0.01%. The limit of spectrographic detection of tantalum was also reduced to 0.01% by developing a procedure for diffraction analysis at full intensity exposure (no sector). Interference due to broadening of spectral lines was overcome by examination in the second order.

Several changes in metallographic procedures provided for more rapid and improved microscopic examination. Water soluble oil was used as lubricant and coolant for the less corrosive metals and alloys. Final polishing was performed with diamond abrasive to provide sharper microstructures. Chemical polishing techniques based on a hydrofluoric-nitric-lactic acid solution were used for tantalum and niobium alloy systems, and electropolishing procedures were developed for cobalt, nickel, and rare earth alloys.

Tentative binary constitutional phase diagrams (either partial or complete) have been established for selected yttrium-lanthanide, rare earth-oxygen and rare earth-base metal systems. Analysis was based primarily on metallographic, thermal, and room and elevated temperature X-ray diffraction studies.

The alpha to beta transformation temperature was determined to be 848°C for neodymium, and 930°C for samarium. The transformation temperature of yttrium is approximately 20-30°C below the melting point of yttrium. Both the transformation and melting temperatures are somewhat dependent upon metal purity.

Alpha yttrium and erbium are completely soluble in all proportions. The yttrium-neodymium system is more complex. There is partial solubility at both ends of the system. An intermediate phase is present at the equi-atomic percentage composition. No marked beta phase stabilization was established.

The rare earth rich end of the yttrium, erbium, neodymium, and samarium systems with oxygen were investigated. Compositions were prepared by arc-melting the respective metal with its oxide after preliminary experiments indicated high mobility for the oxygen and rapid equilibration under the conditions used. The solubility of oxygen is low in the metals at temperatures up to the transformation temperature or 1000°C. The transformation temperature of neodymium is essentially unaffected, that of samarium is raised slightly. The nature of the elevated temperature portion of the systems is less certain. Two alternative phase diagrams are proposed. The preferred diagram indicates the co-existence at room temperature of the metal and sesquioxide phases. An interstitial monoxide is present at elevated temperatures. The second, less favored, diagram is suggested as a possibility for the samarium and neodymium systems. It indicates only the presence of metal and sesquioxide phases.

The cobalt end of the cobalt-erbium system was investigated. A number of intermetallic compounds are formed. The first of these, $Co_{17}Er_2$, enters into eutectic reaction with cobalt. The solubility of erbium in cobalt is low, and the cobalt phase transformation is essentially unaffected by the presence of small additions of erbium. Metallographic examination of cobalt-yttrium compositions indicated close similarity with the cobalt-erbium system.

Metallographic examination of nickel compositions with added rare earths confirm published reports for the presence of a eutectic near the nickel end of the system. The solubility of yttrium in nickel is low both at room and elevated temperatures.

Tantalum-lanthanum, tantalum-erbium, tantalum-yttrium, niobium-erbium, and niobium-yttrium systems were investigated. All systems were similar in their general characteristics. An extensive liquid immiscibility region is present which terminates in a monotectic very near the tantalum (niobium) end of the system. A

eutectic is present at the rare earth end of the system. Room temperature solid solubility is very low, but there may be slight solubility at elevated temperature.

The rate of atmospheric corrosion was determined for a large number of compositions in dry air at elevated temperature. Most studies were made at 600°C, a few, as noted below, at 900°C.

Rare earth-rare earth oxide compositions (yttrium, neodymium, samarium, and erbium) all corroded more rapidly than the metals alone. The corrosion rate increased with increasing oxygen content. It was also noted that the corrosion rate of distilled yttrium was much lower than that of the as-cast metal.

Rare earth-tantalum and rare earth-niobium compositions corroded more rapidly than either the respective rare earth metal or tantalum (niobium)alone. The increased rate is ascribed to the presence of finely dispersed phases as produced by cooling from the immiscibility region. Once corrosion starts the effective surface exposed is much greater than the gross surface as measured.

Two niobium based alloys were also investigated with rare earth additions. Addition (up to 2%) of erbium or yttrium to a niobium base alloy containing 15% tungsten, 5% molybdenum, and 2% platinum did not markedly affect the corrosion rate. Similar additions to a niobium alloy containing 20% tungsten and 2% titanium, however, reduced the corrosion rate at 600°C to approximately 10-20% that of the base alloy.

Cobalt compositions with 1% or less of erbium or yttrium corroded more slowly at both 600° and 900°C than the base cobalt metal. Compositions containing more than 1% rare earth corroded more rapidly. The addition of 1% or less of yttrium to nickel had little effect on the corrosion rate at either 600° or 900°C. Larger additions increased the corrosion rate.

The addition of moderate quantities of yttrium to erbium or of erbium to yttrium produced little change in corrosion rate. Intermediate compositions had corrosion rates intermediate between those of the base yttrium and erbium metals. In the yttrium-neodymium system no correlation could be made between corrosion rate and composition. Single or two phase regions may exist in this system depending upon temperature and composition, and possibly on the thermal history of the alloys. Additionally some compositions may have allotropic phase changes at temperatures near to the corrosion test temperature.

Efforts were made to determine the tensile properties of alloy compositions in all of the systems discussed. Alloys were prepared by arc-melting into near test specimen dimensions. These were then subjected to a homogenizing anneal at 1000°C and water quenched. Many of the resulting alloys showed excessive porosity or were otherwise unsuited for tensile test. Significant results obtained are indicated below.

In the yttrium-erbium system maximum tensile strength, apparently due to solid solution hardening, was obtained for compositions containing 40-60 weight percent erbium. Neodymium-oxygen and erbium-oxygen compositions had lower tensile strengths than the respective metals.

The tensile strengths of cobalt alloys containing 1% erbium or yttrium were approximately the same as indicated literature values for pure cobalt metal. It may be noted that the alloys, as arc-melted and heat treated, appeared to be physically sound. Similar specimens prepared from the base cobalt metal were porous. The difference in fabricability may be related to refinement of the cobalt by small additions of rare earths.

A number of yttrium alloys containing varying additions of zirconium were prepared and subjected to heat treat and quench procedures in order to evaluate solid solution hardening and age hardening possibilities. Many of the alloys showed markedly higher tensile values than was characteristic for the pure yttrium. No correlation could be obtained, however, between composition, heat treatment, and tensile properties. Metallurgical examination suggested the possibility of overaging having occurred. Subsequent tests indicated that aging does indeed occur fairly rapidly at room temperature, and very rapidly at even moderately elevated temperatures (such as might be used for stress relief), and that all compositions tested were actually in either a fully aged or overaged condition.

BIBLIOGRAPHY

(1) Achard, J.C., and Tsoucaris; Compt. rend. 246, (2) 285 (1958)

(2) ASTM Methods for Chemical Analysis of Metals, American Society for Testing Materials, Philadelphia, Pa. (1956)

(3) Blum, S.L., and McGuire, E.A.; Ceram. Bull. 39, No. 6, 310 (1960)

(4) Bozorth, R.M.; Ferromagnetism, D. Van Nostrand Co., Princeton, N.J. (1951)

(5) Bradley, A.J., and Jay, A.H.; Proc. Phys. Soc. (London) 44, 563 (1932)

(6) Chupka, W.A., Inghram, M.G., and Porter, R.F.; J. Chem. Phys. 24 (4) 792 (1956)

(7) Cobalt and its Alloys; Cobalt Information Center, Battelle Memorial Institute, Columbus, Ohio

(8) Daane, A.H., Iowa State University of Science and Technology, Ames, Iowa; Personal communication

(9) Domagala, R.F., Rausch, J.J., and Levinson, D.W.; ASM Preprint No. 187 (1960)

(10) Eash, D.T., and Carlson, O.N.; Trans. ASM, 1097 (1960)

(11) Eick, H.A., Baenziger, N.C., and Eyring, L.; J. Am. Chem. Soc. 78, 5147 (1956)

(12) Ellinger, F.H., and Zachariasen, W.H.; J. Amer. Chem. Soc. 75, 5650 (1953)

(13) Florio, J.V., and Rundle, R.E.; ISC 273, Iowa State College, Ames, Iowa (1952)

(14) Goldschmidt, V.M., Ulrich, F., and Barth, T.; Skrifter Norske Videnskaps - Akad. Oslo, I, Mat. - Naturv, Kl. 1925, No. 5, 5-24

(15) Harrison, G.R.; Massachusetts Institute of Technology Wavelength Tables. John Wiley and Sons, New York (1956)

(16) Horn, L.; Z. Metallk. 36, 142 (1944); 40, 73 (1949)

(17) Huffine, C.L.; Presented at the joint ASM-AEC Symposium on the Rare Earths and Related Metals, Chicago, Ill. (Nov. 1959)

(18) Iowa State College, Ames, Iowa; ISC 1049 (June, 1958)

(19) Iowa State College, Ames, Iowa; ISC 1116 (April, 1959)

(20) Iowa State University of Science and Technology, Ames, Iowa; IS-15 (1959)

(21) Johnson, R.G., Hudson, D.E., Caldwell, W.C., Spedding, F.H., and Savage, W.R.; J. Chem. Phys. 25, 917 (1956)

(22) Kempter, C.P., Krikorian, N.H., and McGuire, J.C.; J. Phys. Chem. 61, 1237 (1957)

(23) Klemm, W., and Winkelmann, G.; Z. anorg. Chem. 288, 87 (1956)

(24) Kost, M.Ye., and Gol'der, G.A.; Z. neorg. khim. 4, (7), 1488 (1959)

(25) Love, B.; Selection and Evaluation of Rare or Unusual Metals for Application to Advanced Weapons Systems,

WADC Technical Report 57-666 Part I, Wright Air Development Center, Wright-Patterson Air Force Base, Ohio (1958)
(26) Love, B.; Selection and Evaluation of Rare or Unusual Metals, the Metallurgy of Yttrium and the Rare Earth Metals, WADC Technical Report 57-666 Part II, Wright Air Development Center, Wright-Patterson Air Force Base, Ohio (1959)
(27) Love, B.; The Metallurgy of Yttrium and the Rare Earth Metals, Phase Relationships; WADD Technical Report 60-74 Part I, Wright Air Development Division, Wright-Patterson Air Force Base, Ohio (1960)
(28) Love, B.; The Metallurgy of Yttrium and the Rare Earth Metals, Mechanical Properties; WADD Technical Report 60-74 Part II, Wright Air Development Division, Wright-Patterson Air Force Base, Ohio (1960)
(29) Lundin, C.E.; Presented at the Joint ASM-AEC Symposium on Rare Earths and Related Metals, Chicago, Ill. (Nov. 1959) to be published
(30) Lyman, T. (Ed.); Metals Handbook, pg. 1192, American Society for Metals, Cleveland, Ohio (1948)
(31) Miller, G.L.; Tantalum and Niobium, Academic Press Inc., New York (1959)
(32) Nelson, J.B., and Riley, D.P.; Proc. Phys. Soc. (London) 57, 160 (1945)
(33) Pearson, W.B.; A Handbook of Lattice Spacings and Structures of Metals and Alloys, Pergamon Press, New York, N.Y. (1958)
(34) Pirani, M., and Alterthum, H.; Z. Elektrochem. 29, 5 (1923)
(35) Research Chemicals; Ferromagnetic Gadolinium Alloys, RC 127, Research Chemicals Div. of Nuclear Corp. of America, Burbank, Calif. (Dec. 1959)
(36) Roth, R.S.; Natl. Bur. of Standards, Wash, D.C., Personal communication
(37) Roth, R.S., and Schneider, S.J.; J. Res. Natl Bu. Stds; A. Physics and Chemistry 64A, No. 4, 309 (1960)
(38) Savitskii, E.M., Terekhova, V.F., and Burov, I.V.; Zhur. Neorg, Khim. 4, No. 6, 1462 (1959)
(39) Schoeller, W.R., and Powell, A.R.; Analysis of Minerals and Ores of the Rarer Elements. Hafner Publishing Co., N.Y. (1955)
(40) Scott, W.W.; Standard Methods of Chemical Analysis, D. Van Nostrand, New York (1939)
(41) Shafer, M.W., and Roy, R.; J. Am. Ceram. Soc. 42, 563 (1959)
(42) Spedding, F.H., and Daane, A.H.; in Progress in Nuclear Energy, Vol. 1, Series V, Pergamon Press, N.Y. (1950)
(43) Spedding, F.H., and Daane, A.H.; ISC-1116, Iowa State College, Ames, Iowa (1959)
(44) Spedding, F.H., Daane, A.H., and Herrmann, K.W.; Acta Cryst. 9, 559 (1956)
(45) Spedding, F.H., Daane, A.H., and Herrmann, K.W.; J. Metals 9, Trans. AIME 209, 895 (1957)

(46) Spedding, F.H., Legvold, S., Daane, A.H., and Jennings, L.D.; in Progress in Low Temperature Physics, Vol. II, Ch. XII, Ed. by Gorter (1956)
(47) Spedding, F.H., McKeown, J.J., and Daane, A.H.; J. Phys. Chem. 64, 289 (1960)
(48) Walsh, P.N., Goldstein, H.W., and White, D.; J. Am. Ceram. Soc. 43 (5), 229 (1960)
(49) Yosim, S.J., and Milne, T.A.; Atomics International Div. of North American Aviation Inc. Report No. NAA-SR-2124 (1957)

TABLE I

TYPICAL ANALYSES OF RARE EARTH METALS: AS CAST*

	Neodymium	Samarium**	Erbium	Yttrium
Oxygen	0.05-0.20	0.02-0.10	0.2-0.5	0.2-0.5
Nitrogen	<0.01	<0.01	<0.01	<0.01
Carbon	$\leqslant 0.01$	$\leqslant 0.01$	$\leqslant 0.01$	$\leqslant 0.01$
Tantalum	0.01-0.1	$\leqslant 0.01$	0.25	0.25
Calcium	0.01	0.02	<0.01	0.01
Magnesium	0.01	0.02	<0.01	0.01
Iron	$\leqslant 0.01$	$\leqslant 0.01$	$\leqslant 0.01$	$\leqslant 0.01$
Other Rare Earths, total:				
99.9% Grade	<0.1	<0.1	<0.1	<0.1
99 % Grade	<1.0		<1.0	<1.0

* Arc-melting introduced traces of copper ($\leqslant 0.01$)
Tungsten could not be detected spectrographically

** Prepared by metallothermic reduction and distillation

TABLE II

ANALYSES OF METALS USED FOR ALLOY PREPARATIONS

Cobalt

	Belmont Smelting & Refining Works (1)	(3)	Cobalt Information Center (2)	(3)
Cobalt	98.25%		99.92 %(5)	
Nickel	0.53	0.5 %	0.005	0.005 %
Magnesium	0.09	<0.01	0.00 (6)	0.0001
Silicon	0.20	0.02	0.009 (6)	0.004
Calcium	0.22	<0.03	0.00 (6)	0.0001
Manganese	0.04	<0.01	0.00	0.001
Iron	0.12	0.80 (4)	0.010	0.01
Copper	0.03	<0.01	0.001	0.003
Aluminum			0.001 (6)	0.001
Lead			<0.01	0.001
Zinc			≤0.01	<0.05
Sodium			≤0.01	<0.01
Carbon	0.23		0.007	
Sulfur	0.013		0.010	Cr 0.005

(1) Typical analysis quoted by supplier.
(2) Analysis quoted by supplier.
(3) Spectrographic Analysis by Research Chemicals.
(4) Chemical Analysis by Research Chemicals.
(5) Quoted "by difference".
(6) Quoted as MgO, SiO_2, CaO, and Al_2O_3 respectively.

Beryllium *

Assay	99%
Iron	0.05 - 0.20
Aluminum	0.05 - 0.20
Silicon	0.05 - 0.20
Oxygen	(Not Indicated)

* Quoted as typical: Brush Beryllium Company.

TABLE II (Continued)

ANALYSES OF METALS USED FOR ALLOY PREPARATIONS

Zirconium*

Aluminum	0.0075%
Chlorine	0.13
Chromium	0.02
Cobalt	0.002
Hafnium	0.01
Iron	0.15
Lead	0.01
Magnesium	0.06
Manganese	0.005
Nickel	0.007
Nitrogen	0.005
Oxygen	0.14
Silicon	0.01
Titanium	0.005
Vanadium	0.005
Calcium	0.003
Carbon	0.05
Copper	0.005
Molybdenum	0.005
Phosphorus	0.01
Sodium	0.005
Tungsten	0.005
Zinc	0.01

Niobium**

Oxygen	0.05%
Nitrogen	0.05
Carbon	0.02
Iron	0.02
Titanium	0.02
Zirconium	0.02
Tantalum	0.08
Nickel	0.01
Tungsten	0.01

Tantalum**

Tantalum	99.9+%
Iron	< 0.03
Carbon	< 0.03

* Maximum Content Specification for Reactor Grade Sponge.
** Quoted typical analysis by Fansteel Metallurgical Corporation.

Nickel***

Nickel (Assay)	99.8 %
Lead	0.005
Cobalt	0.005
Iron	0.05

*** Quoted typical analysis by J. T. Baker Chemical Company.

TABLE III

OPERATING CONDITIONS FOR BAIRD SPECTROGRAPH

Sample Charge	1 : 1 graphite - sample
Weight of Charge	3 to 20 mgm.
Spectrograph	Baird Associates, 3 meter
Grating	15,000 lines per inch
Order and Dispersion	First, 5.4 Angstroms /mm Second, 2.7 Angstroms /mm
Upper electrode (cathode)	3/16" graphite rod. tapered 15° with 1/16" hemispherical tip
Lower electrode (anode)	3/16" graphite rod. 3/32" deep x 1/8" diameter cup. Undercut.
Analytical Gap	5 mm.
Slit Width	25 microns
Excitation	D.C. arc. 10 amps maintained during excitation
Length of Exposure	Samples arced to completion (neck of electrode burned away)
Exposure Control	Rotating Sector
Emulsion	Spectrum analysis No. 1, 4" x 10" glass plates. 2200 - 4600 A.
Development	3 min. Eastman D-19 developer
Densitometry	Applied Research Laboratories Comparator-Densitometer

TABLE IV

ETCHING AND POLISHING SOLUTIONS FOR METALLOGRAPHY

Material	Chemical Polish Solution
Tantalum, Niobium	10 cc hydrofluoric acid, 10 cc nitric acid, 30 cc lactic acid.
	Electrolytic Polish Solution
Cobalt	orthophosphoric acid
Nickel	39 cc sulfuric acid plus 29 cc distilled water
Rare Earths	15 cc nitric acid plus 85 cc methanol
	Etchants
Rare Earths	concentrated nitric acid
Nickel	Carapella's Reagent; 5 grams ferric chloride in 99 cc ethanol plus 2 cc hydrochloric acid
Beryllium	5 cc hydrofluoric acid plus 95 cc methanol

TABLE V

ANALYSIS OF DISTILLED ERBIUM AND YTTRIUM

Erbium

	Normal Grade	Distillation Feed	Distilled Metal
Oxygen	0.3	0.53	0.019-0.029
Tantalum	0.25	1.	N.D. <0.1
Iron	≤0.01	0.04	0.01 -0.05
Molybdenum			0. -0.03

Yttrium

	Normal Grade	Distillation Feed	Distilled Metal
Oxygen	0.3	1.	0.010-0.027
Tantalum	0.25	1.	N.D. <0.1
Iron	≤0.01	0.05	0.05 -0.07
Molybdenum			0. -0.03

TABLE VI

THERMAL ANALYSIS IN THE YTTRIUM-ERBIUM SYSTEM

Alloy Composition	Melting Point by Globule Technique Average of 2 determinations, °C
Yttrium	1520
90% Yttrium -10% Erbium	1510
80% Yttrium -20% Erbium	1500
70% Yttrium -30% Erbium	1500
60% Yttrium -40% Erbium	1490
50% Yttrium -50% Erbium	1560 (?)
40% Yttrium -60% Erbium	1485
30% Yttrium -70% Erbium	1520
20% Yttrium -80% Erbium	1530
10% Yttrium -90% Erbium	1480
Erbium	1520

TABLE VII

OBSERVED 2θ VALUES FOR YTTRIUM-ERBIUM ALLOYS

	Percent Erbium in Yttrium									
Index	Y	10%	20%	30%	40%	50%	60%	80%	90%	Er
100	28.2°	28.4°	28.4°	28.4°	28.5°	28.8°	28.6°	28.8°	28.9°	28.9°
002	31.0		31.1	31.4		31.5	31.6	31.8	31.9	31.9
101	32.3	32.5	32.3	32.6	32.7	32.8	32.8	33.0	33.2	33.1
102	42.5	42.7	42.5	42.8	42.9	43.0	43.1	43.4	43.6	43.6
110	49.9	50.2	50.2	50.2	50.4	50.5	50.6	50.9	51.1	51.2
103	56.1	56.4	56.3	56.5	56.7	56.8	56.9	57.3	57.5	57.7
200	58.4	58.6	58.6	58.6			59.1	59.5	59.8	59.9
112	60.0	60.4	60.2	60.4	60.6	60.7	60.9	61.3	61.5	61.6
201	60.8		61.0	61.1	61.2	61.4	61.5	62.0	62.0	62.3
004	64.9		65.0	65.4		65.6	66.0	66.2	66.4	
202	67.6	67.9		68.1	68.3	68.4	68.6	69.1	69.4	69.6
104	72.1	72.5	72.5		72.9	73.1	73.3	73.8	74.2	74.3
203	78.4	78.8	78.7	78.9		79.4	79.5	80.1	80.4	80.7
210	80.3	80.7	80.7			81.3	81.4	82.0	82.4	82.7
211	82.3	82.8	82.9	83.0	83.3	83.4	83.6	84.2	84.6	84.8
114	86.0		86.5	86.7	87.0	87.3	87.5		88.6	88.8
212	88.5	89.0	88.9			89.7	90.0	90.8	91.0	91.4
105	90.9	91.6				92.2	92.6		94.1	94.0
204	92.8	93.4		93.6		94.1	95.2	96.2	96.4	
300	93.9	94.4	94.6							
213	98.9	99.4	99.4	99.7	100.1		100.6	101.4	101.8	102.2
302	102.2	102.7	102.6	103.0	103.2	103.6	104.0	104.8	105.4	105.9

TABLE VIII

Δ 2θ VALUES FOR YTTRIUM-ERBIUM ALLOYS

		Percent Erbium in Yttrium								
Index	Y	10%	20%	30%	40%	50%	60%	80%	90%	Er
100	28.2°	0.2°	0.2°	0.2°	0.3°	0.6°	0.4°	0.6°	0.7°	0.7°
002	31.0		0.1	0.4		0.5	0.6	0.8	0.9	0.9
101	32.3	0.2	0.0	0.3	0.4	0.5	0.5	0.7	0.9	0.8
102	42.5	0.2	0.0	0.3	0.4	0.5	0.6	0.9	1.1	1.1
110	49.9	0.3	0.3	0.3	0.5	0.6	0.7	1.0	1.2	1.3
103	56.1	0.3	0.2	0.4	0.6	0.7	0.8	1.2	1.4	1.6
200	58.4	0.2	0.2	0.2			0.7	1.1	1.4	1.5
112	60.0	0.4	0.2	0.4	0.6	0.7	0.9	1.3	1.5	1.6
201	60.8		0.2	0.3	0.4	0.6	0.7	1.2	1.2	1.5
004	64.9		0.1	0.5		0.7	1.1	1.3	1.5	
202	67.6	0.3		0.5	0.7	0.8	1.0	1.5	1.8	2.0
104	72.1	0.4	0.4		0.8	1.0	1.2	1.7	2.1	2.2
203	78.4	0.4	0.3	0.5		1.0	1.1	1.7	2.0	2.3
210	80.3	0.4	0.4			1.0	1.1	1.7	2.1	2.4
211	82.3	0.5	0.6	0.7	1.0	1.1	1.3	1.9	2.3	2.5
114	86.0		0.5	0.7	1.0	1.3	1.5		2.6	2.8
212	88.5	0.5	0.4			1.2	1.5	2.3	2.5	2.9
105	90.9	0.7				1.3	1.7		3.2	3.1
204	92.8	0.6		0.8		1.3	2.4	3.4	3.6	
300	93.9	0.5	0.7							
213	98.9	0.5	0.5	0.8	1.2		1.7	2.5	2.9	3.3
302	102.2	0.5	0.4	0.8	1.0	1.4	2.2	2.6	3.2	3.7

TABLE IX

X-RAY DIFFRACTION DATA AT 1000°C
FOR A 60% YTTRIUM-40% ERBIUM ALLOY

Observed 2θ	Observed $Sin^2\theta$	hkl*	$Sin^2\theta$ Calc.	hkl**	$Sin^2\theta$ Calc.**	$\Delta Sin^2\theta$ Calc-obs
28.0°	0.0585	100	0.0589			0.0004
30.6	0.0696	002	0.0698			0.0002
31.3	0.0728			111	0.0733	0.0005
32.0	0.0760	101	0.0763			0.0003
36.4	0.0976			200	0.0977	0.0001
42.0	0.1284	102	0.1286			0.0002
49.7	0.1766	110	0.1766			0.0000
52.5	0.1956			220	0.1954	0.0002
55.4	0.2161	103	0.2158			0.0003
59.6	0.2470	112	0.2464			0.0006
60.4	0.2530	201	0.2529			0.0001
62.4	0.2684			311	0.2687	0.0003
63.8	0.2792	004	0.2792			0.0000
65.6	0.2934			222	0.2932	0.0002
67.1	0.3054	202	0.3052			0.0002
71.1	0.3380	104	0.3379			0.0001
77.5[a]	0.3918			400		0.0000
77.7[a]	0.3935	203	0.3924		0.3909	0.0009
85.1	0.4573	114	0.4557			0.0016
89.5	0.4957	105	0.4949			0.0008

* hkl values for hcp (Y-Er). $Sin^2\theta$ calc. from determined lattice parameters; a_o = 3.67 A, c_o = 5.83 A.

** hkl values for fcc structure. $Sin^2\theta$ calc. from the determined lattice parameter; a_o = 4.933A.

a Overlapping diffraction peaks.

TABLE X

ROOM TEMPERATURE X-RAY DIFFRACTION DATA FOR THE FCC STRUCTURE FOUND ON A 60% YTTRIUM-40% ERBIUM ALLOY

Observed 2θ	Observed $Sin^2\theta$	hkl	Calc.* $Sin^2\theta$	$\Delta Sin^2\theta$ Calc-Obs
32.1°	0.0765	111	0.0759	0.0006
37.2	0.1017	200	0.1012	0.0005
53.5	0.2026	220	0.2024	0.0002
63.7	0.2785	311	0.2783	0.0002
66.8	0.3030	222	0.3036	0.0006
78.9	0.4038	400	0.4048	0.0010

* $Sin^2\theta$ calc. from the determined lattice parameter; a_o = 4.85A

TABLE XI

THERMAL ANALYSIS IN THE YTTRIUM-NEODYMIUM SYSTEM

Alloy Composition	Differential Thermal Analysis °C		Melting Point By Resistance Technique °C
	Transformation	Solidus	
Yttrium		1520	1520
Yttrium-10% Neodymium		> 1300	
Yttrium-20% Neodymium		> 1300	
Yttrium-30% Neodymium		> 1300	1470
Yttrium-40% Neodymium		> 1300	1400
Yttrium-50% Neodymium		1230*	1320
Yttrium-60% Neodymium	550 1110 (?)	1200	1190
Yttrium-70% Neodymium	1040 (?)	1150	
Yttrium-80% Neodymium		> 1100	1060
Yttrium-90% Neodymium	870	1100	1125
Neodymium	860	1020	1040

* 1230° on heating, 1320° on cooling.

TABLE XII

METAL STRUCTURES OBSERVED BY X-RAY DIFFRACTION
IN THE YTTRIUM-NEODYMIUM SYSTEM

Alloy Composition	Temperature °C				
	25°C	525°C	625°C	925°C	1025°C
Yttrium	1				
Yttrium-10% Neodymium	1				1
Yttrium-20% Neodymium	1				1
Yttrium-30% Neodymium	1,3				1
Yttrium-40% Neodymium	1,3				1
Yttrium-50% Neodymium	1,3				1
Yttrium-60% Neodymium	3			1	1
Yttrium-70% Neodymium	2,3	3	2		2
Yttrium-80% Neodymium	2,3				2
Yttrium-90% Neodymium	2,3			4	
Neodymium	2			4	

1. Hexagonal close packed - yttrium structure.
2. Hexagonal (Lanthanum type)-neodymium structure.
3. "Rhombohedral" - samarium structure.
4. Body centered cubic - beta neodymium structure.

TABLE XIII

X-RAY DIFFRACTION AT 900°C OF THE ATMOSPHERIC CORROSION PRODUCT FROM NEODYMIUM

Observed 2θ	Observed $Sin^2\theta$	hkl	s	$Sin^2\theta/s$	Calc. $Sin^2\theta$	$\Delta Sin^2\theta$ Calc-Obs
30.2°	0.0679	111	3	0.0226	0.0677	0.0002
*30.6	0.0696					
35.0	0.0904	200	4	0.0226	0.0903	0.0001
50.3	0.1806	220	8	0.02258	0.1806	0.0000
59.8	0.2485	311	11	0.02259	0.2483	0.0002
62.7	0.2707	222	12	0.02256	0.2709	0.0002
73.9	0.3613	400	16	0.02258	0.3612	0.0001
81.8	0.4287	331	19	0.02256	0.4289	0.0002
84.4	0.4512	420	20	0.02256	0.4514	0.0002
94.8	0.5418	422	24	0.02258	0.5418	0.0000
102.7	0.6100	511,333	27	0.02259	0.6094	0.0006
			Avg.	0.02257	a_o = 5.131 A	

* Possibly Beta Neodymium

TABLE XIV

X-RAY DIFFRACTION AT 25°C OF THE ATMOSPHERIC CORROSION PRODUCT FROM NEODYMIUM

Observed 2θ	Observed $Sin^2\theta$	hkl	s	$Sin^2\theta/s$	Calc. $Sin^2\theta$	$\Delta Sin^2\theta$ Calc-Obs
30.5°	0.0692	111	3	0.0231	0.0690	0.0002
35.3	0.0919	200	4	0.0230	0.0920	0.0001
*45.7	0.1508					
50.8	0.1840	220	8	0.02300	0.1840	0.0000
**54.0	0.2061					
60.4	0.2530	311	11	0.02300	0.2530	0.0000
63.5	0.2769	222	12	0.02308	0.2760	0.0009
74.7	0.3687	400	16	0.02301	0.3680	0.0007
			Avg.	0.02300	a_o = 5.082A	

* Possibly Nd (104)
** Possibly Nd (106)

TABLE XV

X-RAY DIFFRACTION DATA AT 1025°C FOR AN YTTRIUM-70% NEODYMIUM ALLOY

Observed Data		Diffraction Peaks Assigned to α Neodymium		Diffraction Peaks Assigned to NdO(NdN)			Diffraction Peaks Assigned to YO(YN)		
2θ	$\sin^2\theta$	hkl	Calc. $\sin^2\theta$	hkl	s	$\frac{\sin^2\theta}{s}$	hkl	s	$\frac{\sin^2\theta}{s}$
30.3°	0.0683	004	0.0683	111	3	0.0228			
31.4	0.0732						111	3	0.0244
31.9	0.0755	102	0.0754						
35.0	0.0904			200	4	0.0226			
36.4	0.0976	103	0.0970				200	4	0.0244
41.7	0.1267	104	0.1266						
52.2	0.1935						220	8	0.0242
54.8	0.2118	106	0.2120						
59.1	0.2433	114	0.2433						
62.3	0.2676						311	11	0.02433
65.4	0.2919						222	12	0.02433
76.9	0.3866	206	0.3869						
				Average		0.0227	Average		0.0244
			Calc. a_o = 3.67A c_o = 11.80A		Calc. a_o = 5.11 A			Calc. a_o = 4.93A	

TABLE XVI

ASSIGNMENT OF DIFFRACTION PEAKS FOR THE YTTRIUM-60% NEODYMIUM ALLOY AT 625°C

2θ	Hex Neodymium	Hcp Yttrium	fcc YO = YN	fcc NdO = NdN
28.0°	100	100		
30.3				111
31.4			111	
31.8	102	101		
35.3				200
36.4			200	
41.6	104	102		
49.2	110	110		
50.6				220
52.5			220	
54.7	106	103		
58.9	114	112		
59.9				311
62.4			311	
63.2				222
63.6			222	

All observed diffraction peaks are indexed as noted. The "samarium structure" has therefore transformed and is not present at this temperature.

TABLE XVII

IDENTIFICATION OF PHASES AND CALCULATION OF LATTICE CONSTANTS FOR AN YTTRIUM-90% NEODYMIUM ALLOY AT 925°C

Observed Data		Assigned to NdO=NdN			Assigned to YO=YN			Assigned to β Nd				
2θ	$Sin^2\theta$	hkl	s	$Sin^2\theta$ s	hkl	s	$Sin^2\theta$ s	hkl	s	$Sin^2\theta$ s	Calc. $Sin^2\theta$	Δ $Sin^2\theta$
30.8°	0.0705							110	2	0.03525	0.0702	0.0003
31.3	0.0727				111	3	0.02423				0.0730	0.0003
35.2	0.0914	200	4	0.02285							0.0910	0.0004
36.4	0.0976				200	4	0.02440				0.0973	0.0003
44.0	0.1403							200	4	0.03508	0.1403	0.0000
50.5	0.1821	220	8	0.02276							0.1820	0.0001
52.4	0.1949				220	8	0.02436				0.1946	0.0003
54.6	0.2104							211	6	0.03507	0.2105	0.0001
60.0	0.2500	311	11	0.02273							0.2503	0.0003
62.3	0.2676				311	11	0.02433				0.2676	0.0000
64.0	0.2808							220	8	0.03510	0.2806	0.0002
65.3	0.2912				222	12	0.02427				0.2920	0.0008
77.3	0.3901				400	16	0.02438				0.3893	0.0008
85.6	0.4616				331	19	0.02429				0.4623	0.0007
		Average		0.02275			0.02433			0.03508		
		a_o = 5.11A			a_o = 4.94A			a_o = 4.12A				

TABLE XVIII

THERMAL ANALYSIS IN THE ERBIUM-ERBIUM OXIDE SYSTEM

Composition	Melting Point °C Solidus by Differential Thermal Analysis	Melting Point °C Melting Temperature by Resistance Method
Erbium (Distilled)	1510	
Erbium - 3% Er_2O_3		1550
Erbium - 5% Er_2O_3		1570
Erbium -10% Er_2O_3	1490	
Erbium -15% Er_2O_3	1500	
Erbium -25% Er_2O_3	1540	
Erbium -35% Er_2O_3		1660
Erbium -50% Er_2O_3		1910
Erbium -60% Er_2O_3		2000
Erbium -75% Er_2O_3		2180

TABLE XIX

X-RAY DIFFRACTION DATA AT 1000°C OF THE CORROSION PRODUCT ON ERBIUM-1% Er_2O_3

Observed Data 2θ	$Sin^2\theta$	hkl	s	$\frac{Sin^2\theta}{s}$	$Sin^2\theta$ calc.	$\Delta Sin^2\theta$ calc-obs.
28.9°	0.0622	222*				
31.7	0.0745	111	3	0.0248	0.0744	0.0001
32.5	0.0783	101**				
33.5	0.0831	400*				
36.8	0.0996	200	4	0.0249	0.0998	0.0002
48.2	0.1667					
53.1	0.1998	222	8	0.02498	0.1998	0.0000
57.3	0.2298	530*				
63.2	0.2746	311	11	0.02496	0.2747	0.0001
66.4	0.2998	222	12	0.02498	0.2997	0.0001
78.4	0.3995	400	16	0.02497	0.3996	0.0001
87.1	0.4747	331	19	0.02498	0.4745	0.0002
87.9	0.4992	420	20	0.02496	0.4994	0.0002
			Average	0.02497		

a_o = 4.878A

* Er_2O_3

** Er

TABLE XX

CRYSTALLOGRAPHIC PHASES OBSERVED BY X-RAY DIFFRACTION IN THE ERBIUM-OXYGEN SYSTEM

Composition	Temperature 23°C	1000°C
Erbium (0.03% O_2)	A	A,c
Erbium- 1% Er_2O_3	A,b	A,c,b(?)
Erbium- 2% Er_2O_3	A,b	A,c,b(?)
Erbium- 5% Er_2O_3	A,b	A,c,b(?)
Erbium-10% Er_2O_3	A,b	A,c,b
Erbium-25% Er_2O_3	A,B	A,b,c
Erbium-50% Er_2O_3	A,B	A,B,c
Erbium-75% Er_2O_3	B,A	B,A,c
Erbium-90% Er_2O_3	B,a	B,a,c

A. Hexagonal close packed erbium.
B. Cubic Er_2O_3
C. Face centered cubic (ErN ?)

Upper case designates Major Constituent.
Lower case designates Minor Constituent.
Phases are listed in order of estimated abundance.

TABLE XXI

THERMAL ANALYSIS IN THE YTTRIUM-YTTRIUM OXIDE SYSTEM

Composition	Melting Temperature By Resistance Method °C
Yttrium	1510
Yttrium - 15% Y_2O_3	1540
Yttrium - 20% Y_2O_3	1620
Yttrium - 30% Y_2O_3	1680
Yttrium - 40% Y_2O_3	1700
Yttrium - 50% Y_2O_3	1870
Yttrium - 60% Y_2O_3	1950
Yttrium - 70% Y_2O_3	2100
Yttrium - 80% Y_2O_3	2200
Yttrium - 90% Y_2O_3	> 2200

No transformations were detected in this series of compositions by differential thermal analysis to 1500°C.

TABLE XXII

IDENTIFICATION OF PHASES AND CALCULATION OF LATTICE CONSTANTS FOR AN YTTRIUM-1% YTTRIUM OXIDE COMPOSITION AT 1000°C

Observed data		Diffraction	Assignment	Calc.	$\Delta \sin^2\theta$
2θ	$\sin^2\theta$	hkl	Phase	$\sin^2\theta$	Calc.-obs
28.2°	0.0593	111	*	0.0591	0.0002
31.5	0.0736	111	YN		
31.9	0.0755	101	Y		
32.6	0.0788	200	*	0.0788	0.0000
36.5	0.0981	200	YN		
41.8	0.1273	102	Y		
46.8	0.1577	220	*	0.1576	0.0001
52.6	0.1963	220	YN		
55.5	0.2168	311	*	0.2168	0.0000
58.2	0.2365	222	*	0.2365	0.0000
60.0	0.2500	201	Y		
62.6	0.2699	311	YN		
65.7	0.2945	222	YN		
68.4	0.3159	400	*	0.3153	0.0006
75.5	0.3748	331	*	0.3744	0.0004
77.7	0.3934	420	*	0.3941	0.0003
86.1	0.4660	331	YN		
86.8	0.4721	422	*	0.4729	0.0008
89.9	0.4992	420	YN		
93.7	0.5323	511,333	*	0.5320	0.0003
100.2	0.5885	422	YN		

* Unidentified structure

a_o = 4.925A For YN Fcc structure.
a_o = 5.49A For unidentified structure.

TABLE XXIII

CRYSTALLOGRAPHIC PHASES OBSERVED BY X-RAY DIFFRACTION IN THE YTTRIUM-OXYGEN SYSTEM

Composition	Arc-melted Specimens; Temperature of Examination, °C			
	25°	1000°	Cooled to 25°	Repolished at 25°
Yttrium	A	A	A	A
Yttrium- 1% Y_2O_3	A,c,d,b?	D,C,a	D,B,c	A,c,b
Yttrium- 2% Y_2O_3	A,b,d	D,C,a,b?	B,c,d,a	A,b,d
Yttrium- 5% Y_2O_3	A,b,c	B,c,a,d	B,a,c,d?	A,b
Yttrium-10% Y_2O_3	A,b,d?	B,a,c,d	B,C,a,d	A,c,d?
Yttrium-15% Y_2O_3	A,b,d?	B,c,a,d	B,c,a	A,b
Yttrium-25% Y_2O_3	A,b	B,c,a,d	B,c,a,d	A,b
Yttrium-35% Y_2O_3	A,b	B,c,a,d	B,c,a,d?	A,b
Yttrium-50% Y_2O_3	A,B,c	B,c,a	B,c,a	A,B,c
Yttrium-60% Y_2O_3	B,A,c	B,c,a	B,c,a	B,A,c
Yttrium-75% Y_2O_3	B,a	B,a	B,a	B,a
Yttrium-90% Y_2O_3	B,a	B,a	B,a	B,a

A Hexagonal close packed yttrium.
B Cubic yttrium sesquioxide.
C Face centered cubic (YN).
D Face centered cubic.

Upper case designates Major Constituents.
Lower case designates Minor Constituents.
Phases are listed in order of estimated abundance.

TABLE XXIV

THERMAL ANALYSIS IN THE NEODYMIUM-NEODYMIUM OXIDE SYSTEM

Composition	Differential Thermal Analysis Temperatures °C	
	Transformation	Solidus (Eutectic)
Neodymium	848	1020
Neodymium- 2% Nd_2O_3	825 (?)	1020
Neodymium- 5% Nd_2O_3	845	1010
Neodymium-10% Nd_2O_3	845	1010
Neodymium-15% Nd_2O_3	845	1010

TABLE XXV

CRYSTALLOGRAPHIC PHASES OBSERVED BY X-RAY DIFFRACTION IN THE NEODYMIUM-OXYGEN SYSTEM

Composition	Arc-melted Specimens; Temperature of Examination; °C				
	25°	900°	1000°	Cooled to 25°	Repolished at 25°
Neodymium	A	B,c,d*			A
Neodymium-20% Nd_2O_3	A,C		D	D	A,c
Neodymium-30% Nd_2O_3	A,C		D	D	A,C
Neodymium-40% Nd_2O_3	A,C		D	D	A,C
Neodymium-50% Nd_2O_3	C,A		D	D	C,A
Neodymium-60% Nd_2O_3	C,a		D,C	-	C,d(?)
Neodymium-70% Nd_2O_3	C		D,c	D,c	C
Neodymium-80% Nd_2O_3	C		D,c	D,c	C
Neodymium-90% Nd_2O_3	C	C	-	D,c	C

A. Alpha Neodymium; hexagonal (lanthanum) structure.
B. Beta Neodymium; body centered cubic structure.
C. Neodymium sesquioxide; Hexagonal
D. Face centered cubic structure; composition not established (NdN? NdO?)

Upper case designates Major Constituents
Lower case designates Minor Constituents

* 925°C

TABLE XXVI

X-RAY DIFFRACTION STUDY OF NEODYMIUM OXIDATION AT 200°C

	Relative Intensity		
Time	Nd(105)	Hexagonal Sesquioxide(110)	Cubic Sesquioxide(433)
8:40	100	0	0
9:10	93	0	0
9:40	73	23	0
10:40	73	53	0
11:40	73	60	0
12:40	62	62	0
1:40	62	62	0

TABLE XXVII

X-RAY DIFFRACTION DATA FOR THE SURFACE OF NEODYMIUM OXIDIZED IN AIR AT 200°C

Observed Data 2θ	Observed Data $Sin^2\theta$	Diffraction hkl	Assignment Phase	Calc. $Sin^2\theta$*	$\Delta Sin^2\theta$ Calc-obs.
27.0°	0.0545	100	Nd_2O_3	0.0544	0.0001
28.4	0.0602	100	Nd	0.0591	0.0011
29.9	0.0665	002	Nd_2O_3	0.0656	0.0009
30.4	0.0687	004	Nd	0.0680	0.0007
30.8	0.0705	101	Nd_2O_3	0.0709	0.0004
32.2	0.0769	102	Nd	0.0761	0.0008
36.4	0.0976	103	Nd	0.0974	0.0002
47.6	0.1628	110	Nd_2O_3	0.1635	0.0007
48.2	0.1667	105	Nd	0.1654	0.0013
50.0	0.1786	110	Nd	0.1773	0.0013
53.8	0.2047	103	Nd_2O_3	0.2020	0.0027
55.1	0.2139	106	Nd	0.2121	0.0018
57.1	0.2284	112	Nd_2O_3	0.2291	0.0007
57.6	0.2321	201	Nd_2O_3	0.2343	0.0021
59.5	0.2463	114	Nd	0.2453	0.0010
63.0	0.2730	203 107	Nd Nd	0.2747	0.0017
68.4	0.3159	104	Nd_2O_3	0.3170	0.0011
84.4	0.4512	213	Nd	0.4519	0.0003

* $Sin^2\theta$ for neodymium calculated from: a_o =3.658A c_o =11.799A, (28).

$Sin^2\theta$ for Nd_2O_3 calculated from: a_o = 3.80A, c_o = 6.01A, as determined from above observed (not refined) 2θ values.

TABLE XXVIII

THERMAL ANALYSIS IN THE SAMARIUM-SAMARIUM OXIDE SYSTEM

Composition	Differential Thermal Analysis Transformations °C	Solidus	Melting Point By Resistance Technique
Samarium	930, (470?)	1070	
Samarium- 1% Sm_2O_3	945	1070	1030
Samarium- 2% Sm_2O_3	970	>1080	1065
Samarium- 5% Sm_2O_3	985, (425?)		1040
Samarium-10% Sm_2O_3	970	1080	
Samarium-15% Sm_2O_3	1000, (425?)	1080	1190

TABLE XXIX

THERMAL ANALYSIS IN THE COBALT-ERBIUM SYSTEM

Composition	Differential thermal Analysis °C Transformations	Eutectic	Melting Point by Resistance Technique °C
Cobalt - High Purity	Not Detected		
Cobalt - 98-99%	405 1100	-- --	1460
Cobalt - 1% Erbium	400 1100	1320	1420
Cobalt - 2% Erbium	395 1100	1320	1430
Cobalt - 5% Erbium	Not Detected	1320	1420
Cobalt -10% Erbium	Not Detected	1320	1365
Cobalt -15% Erbium	Not Detected	1320	

TABLE XXX

X-RAY DIFFRACTION IDENTIFICATION OF PHASES PRESENT IN AN ANNEALED COBALT-15% ERBIUM ALLOY

Observed Diffraction Peaks	Calculated Position of Diffraction Peaks Face Centered Cubic Cobalt		Monoclinic $Co_{17}Er_2$ ($Co_{17}Th_2$)	
2θ	hkl	2θ	hkl	2θ
30.6°			221	30.3°
31.4			202	31.6
37.5			$20\bar{2}$	37.1
43.8			003	43.6
44.3	111	44.3°	421	44.1
51.6	200	51.6		
52.3			$40\bar{2}$	52.2
59.4			204 004	59.3
70.0			$44\bar{2}$	69.7
80.0			801	79.7
92.5	311	92.5		

TABLE XXXI

X-RAY DIFFRACTION IDENTIFICATION OF PHASES PRESENT IN AN ARC-MELTED COBALT-25% ERBIUM ALLOY

Observed Diffraction Peaks 2θ	Calculated Position of Diffraction Peaks Monoclinic $Co_{17}Er_2$ ($Co_{17}Th_2$) hkl	2θ	Hexagonal Co_5Er hkl	2θ	Hexagonal Co_4Er hkl	2θ
30.8°	221	30.3°	101	30.7°		
34.8					111	34.2°
37.5	$20\bar{2}$	37.1				
41.7					003	41.7
42.8	040	42.7	200	42.7		
43.8	003	43.6	111	43.4		
49.3	422	49.2				
57.0	$42\bar{2}$	56.9				
59.9	004	59.3	112	59.7	104	59.9
67.7	$62\bar{1}$	67.2				
69.8	260	69.5			311	69.8
70.9	261	70.4	301	70.7		
80.1	801	79.7			223	80.3
93.6			400	93.4	106	93.6
Relative Intensities	**strong**		**weak**		**v. weak**	

TABLE XXXII

MECHANICAL PROPERTIES OF SOME RARE EARTH ALLOYS

Nominal Composition	Ultimate Tensile strength psi	Elongation % in 1" Gauge length	Percent reduction in area	Test temperature °C (°F)
Yttrium	35,000	2.	-*	Room
	32,500	4	2.4	204 (400)
Yttrium-20% Erbium	23,000(a)	-*	-	Room
	18,800(a)	-	-	204 (400)
Yttrium-40% Erbium	51,200	2	-	Room
	27,800	-	-	204 (400)
Yttrium-60% Erbium	48,200	2.	-	Room
	33,100	2.	2.8	204 (400)
Yttrium-80% Erbium	42,000(b)	2	-	Room
	30,100	5	4.8	204 (400)
Erbium	44,500	2	-	Room
	45,800	2	-	93 (200)
	32,800	5	8.8	204 (400)
Cobalt-1% Erbium	30,500(c)	1	-	Room
Cobalt-1% Yttrium	29,600(a)	-	-	Room
Neodymium	15,000	22	24.7	Room
Erbium-1% Er_2O_3	39,300	-	-	Room
Erbium (Distilled)	23,360(d)	11	10	Room

* - indicates very low (< 1%) elongation or reduction in area.
a Bad break in tensile specimen (outside gauge length).
b Yield strength 41,500 psi (0.2% offset).
c Yield strength 29,800 psi (0.2% offset).
d Yield strength 17,600 psi (0.2% offset).

TABLE XXXIII

MECHANICAL PROPERTIES OF YTTRIUM-ZIRCONIUM ALLOYS

Composition	Ultimate tensile strength psi	Elongation % in 1" gauge length
	As Arc Melted	
Yttrium-1½% Zirconium	22,800	1
Yttrium-3½% Zirconium	22,600	-*
Yttrium-6 % Zirconium	35,200	1
	Solution Heat Treated	
	7 Hours at 1000°C (1832°F), water quenched.	
Yttrium-1½% Zirconium	37,500	-
Yttrium-3½% Zirconium	31,200	1
Yttrium-6 % Zirconium	40,500	-

* - indicates very low (<1%) elongation.

TABLE XXXIV

THE AGE HARDENING OF YTTRIUM-ZIRCONIUM ALLOYS

Composition	Hardness, R_A values after indicated times from solution heat treatment at 1000°C (1832°F) and water quench (hours and minutes) 0:15	1:30	4:45	20:45
Erbium-2.4% Zirconium	30	32	37	39
Erbium-3.9% Zirconium	42	42	44	44
Erbium-5.7% Zirconium	47	48	49	57

Composition	99:	118:	936:	Overaged *
Erbium-2.4% Zirconium	47	52	51	33
Erbium-3.9% Zirconium	50	50	50	34
Erbium-5.7% Zirconium	57	58	57	42

Composition	Hardness of specimens kept in dry ice and acetone after indicated times: 118 hours	158 hours
Erbium-2.4% Zirconium	36	36
Erbium-3.9% Zirconium	39	40
Erbium-5.7% Zirconium	47	47

* 20 days (480 hours) at room temperature plus 16 hours at 538°C (1000°F) and air cooled.

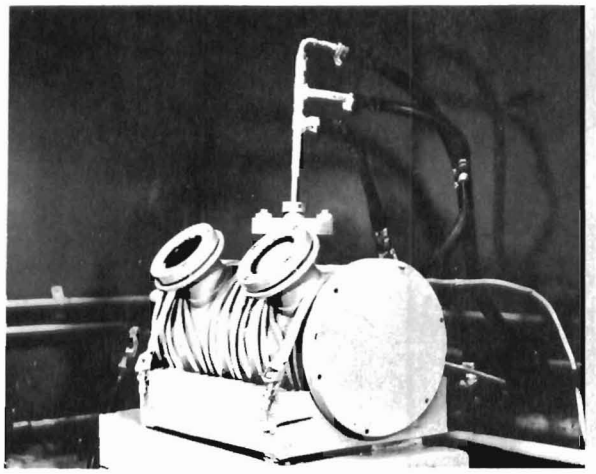

Figure 1. Non-consumable Arc Melting Furnace. Exterior view.

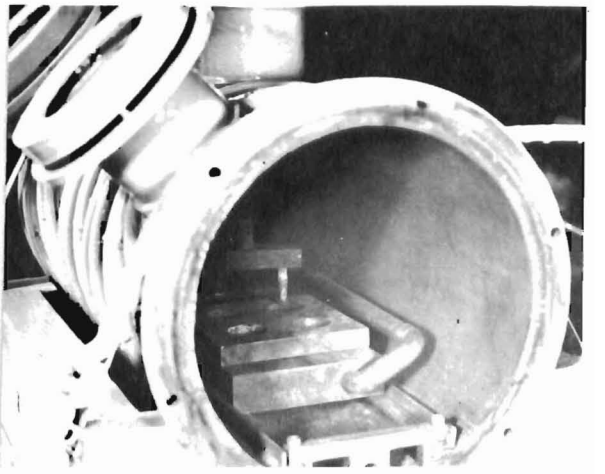

Figure 2. Non-consumable Arc Melting Furnace. Interior view.

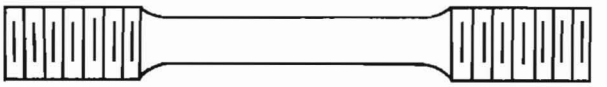

Figure 3. Tensile Test Coupon.

Overall length:	2.75" Minimum
Reduced section:	Length; 1.250" Min. Diameter; 0.250" ± 0.001" at center Taper; Uniform from shoulder, 0.001" to 0.002"
Shoulder radius:	0.250"
Threads:	3/8" Diameter - 16 NC

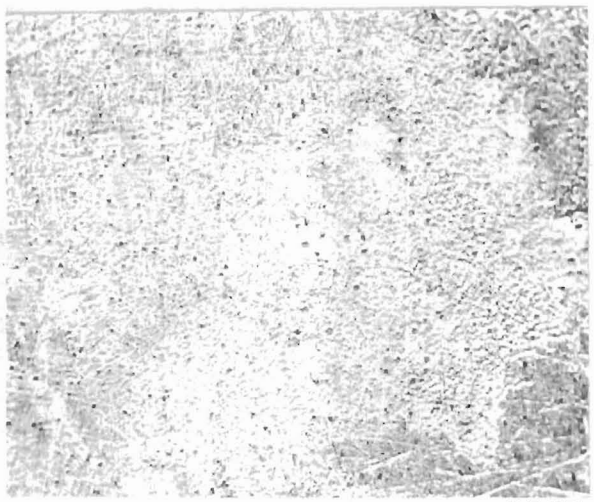

2595

Figure 4a. Unetched, bright field illumination, 100X.

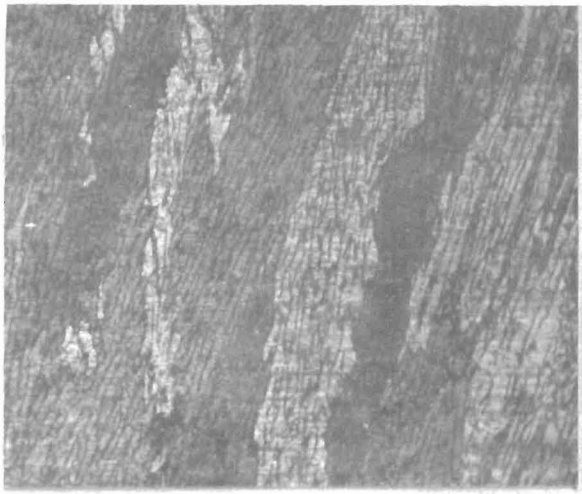

3652

Figure 4b. Nitric acid etch. Bright field illumination, 100X.

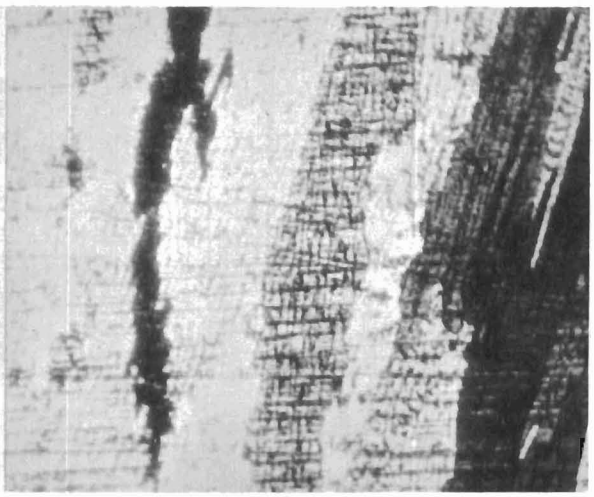

3653

Figure 4c. Nitric acid etch. Polarized light, 100X.

Figure 4. Distilled erbium metal, arc-melted. Photomicrographs after the various indicated treatments.

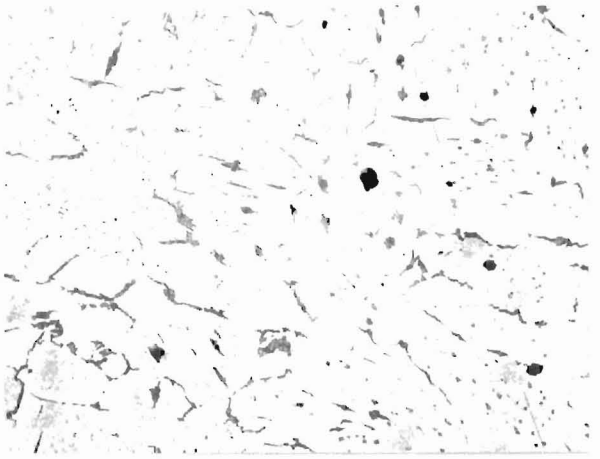

2620

Figure 5. Erbium metal as arc-melted. Unetched. 100X.

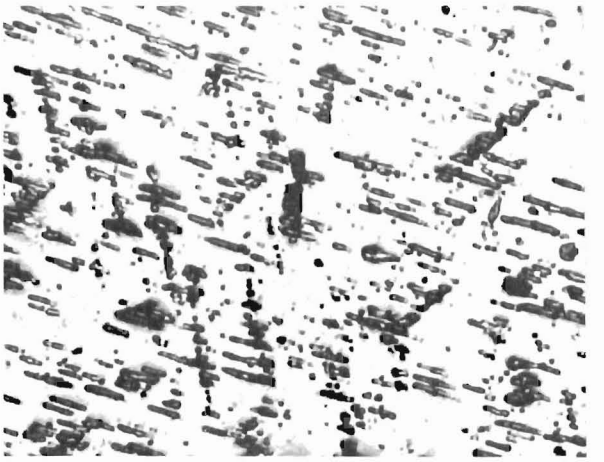

3223

Figure 6. Beryllium metal, as arc-melted. 5% HF in methanol etch. 500X.

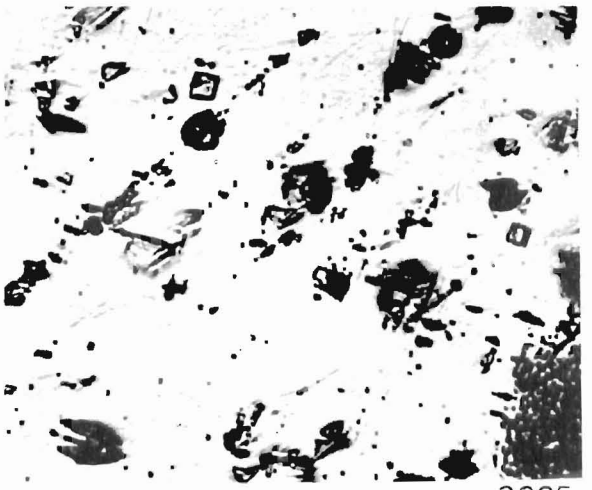

3225

Figure 7. Beryllium - 1% erbium, as arc-melted. Cubic crystals are $Be_{13}Er$. Microporosity appears as black circles. 5% HF in methanol etch. 500X.

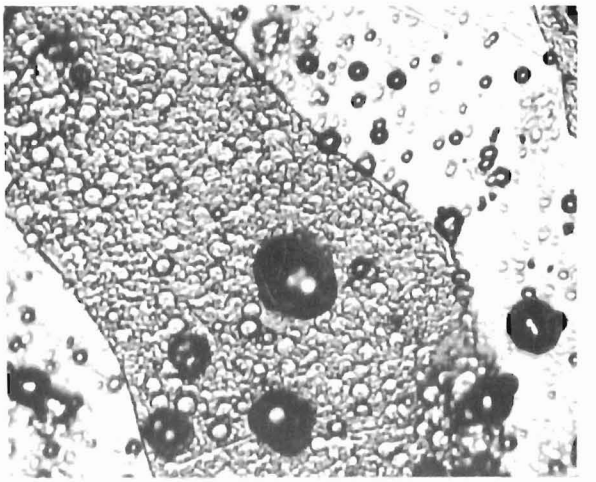

3224

Figure 8. Beryllium - 2.5% erbium, as arc-melted. Microporosity appears as black circles. 5% HF in methanol etch. 500X.

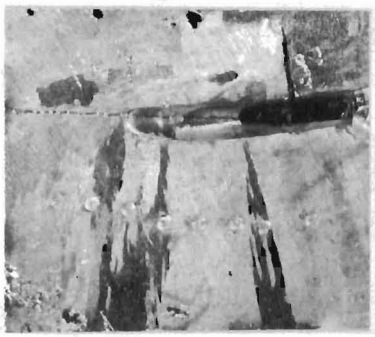

3294

Figure 9. Beryllium metal, as arc-melted. Large cavity and cracks observed in upper portion of specimen, smaller cavities along top and bottom edges. Hardness indentations in center, oblique illumination. 5% HF in methanol etch. 5X.

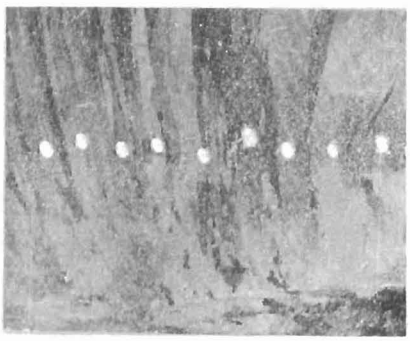

3293

Figure 10. Beryllium - 1% erbium, as arc-melted. Hardness indentations in center. Microporosity observed as fine white spots throughout specimen. No macroscopic cracks are evident and some grain refinement has apparently occurred. 5% HF in methanol etch, oblique illumination. 5X.

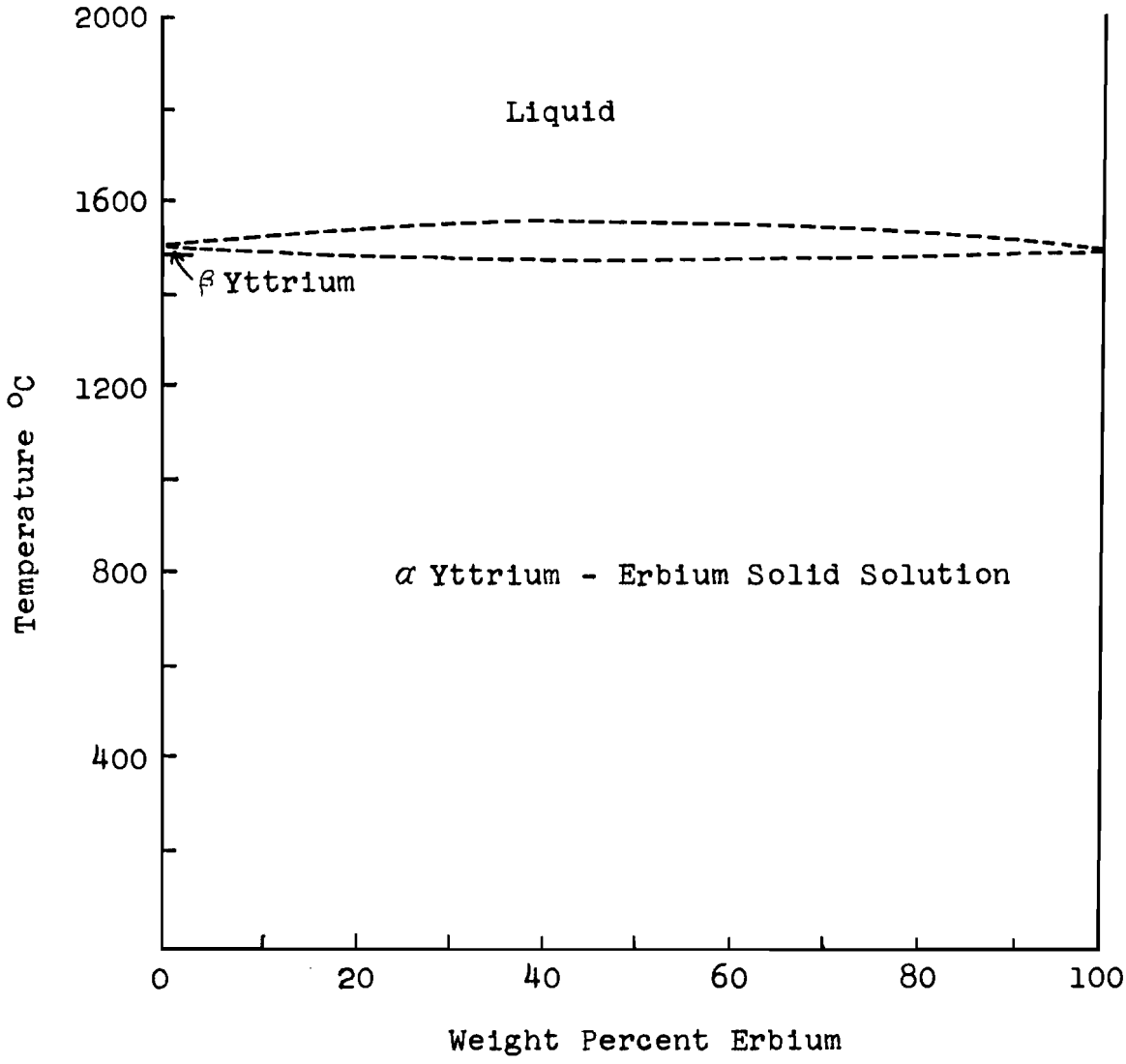

Figure 11. Constitutional Diagram for the Yttrium - Erbium System

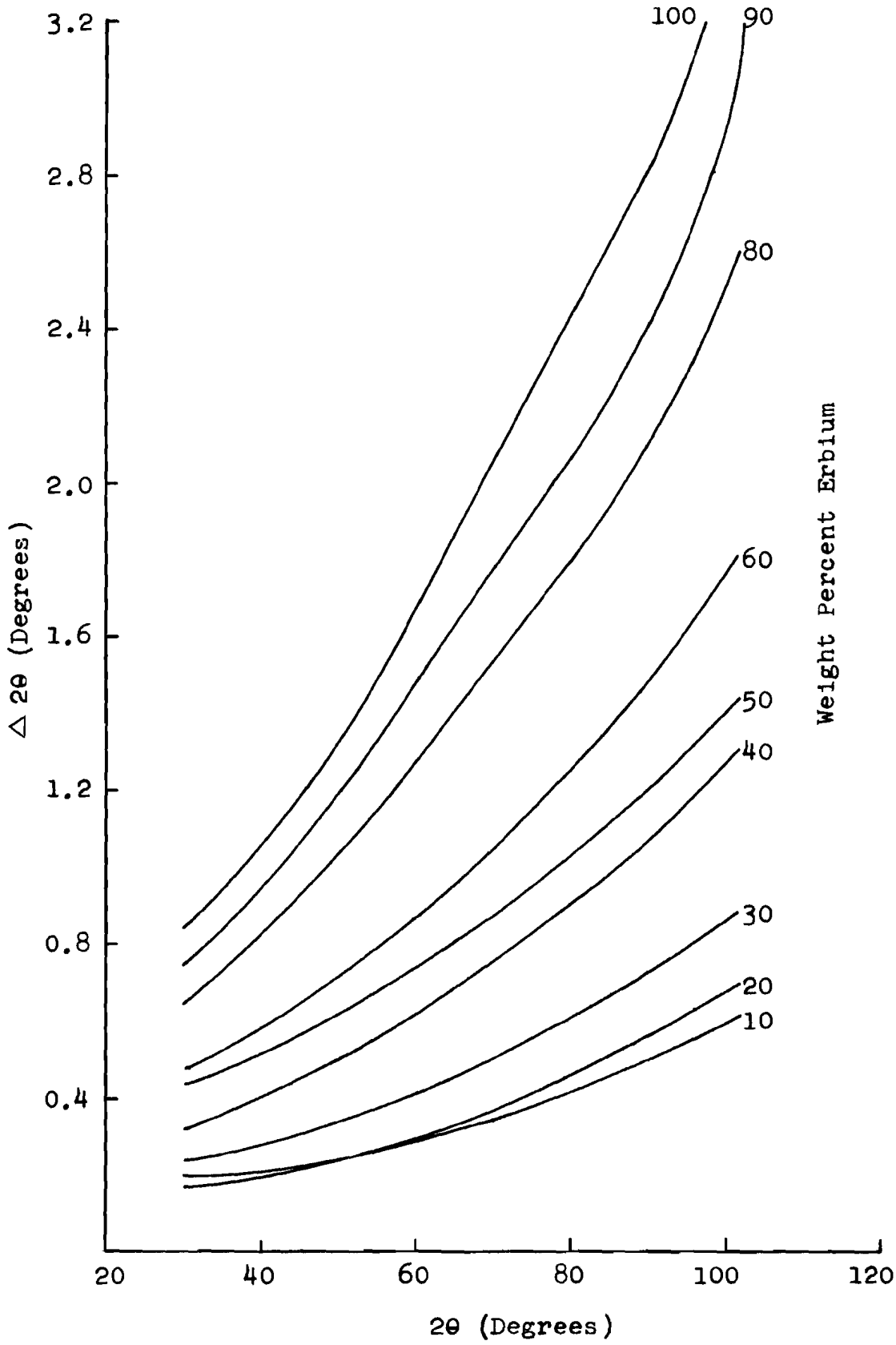

Figure 12. The Shift in Position of Yttrium Diffraction Peaks as a Function of 2θ for Various Erbium Contents.

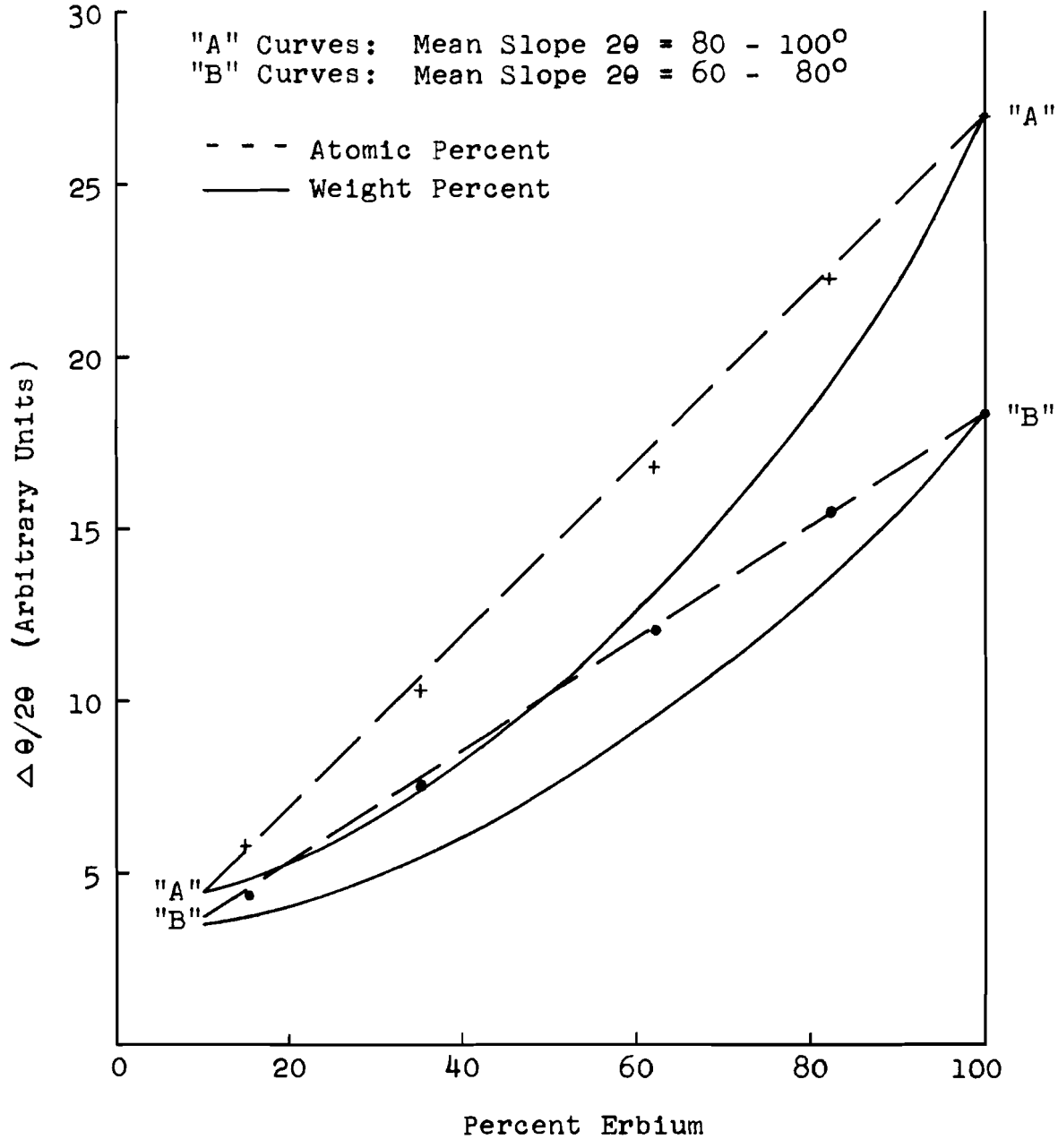

Figure 13. The Slope of the 2θ Displacement Curves for Yttrium Diffraction Peaks as a Function of Erbium Content

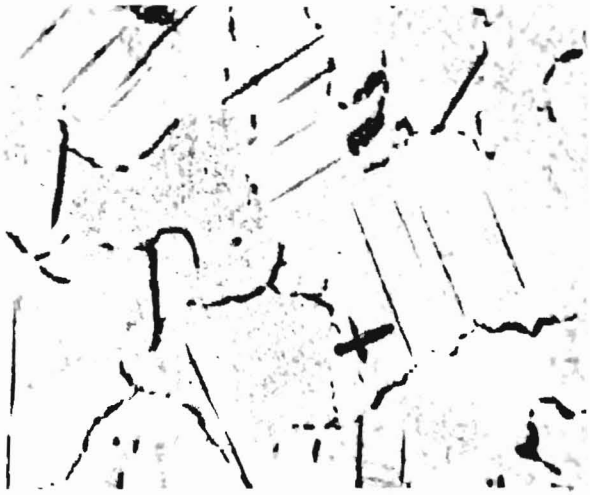

2608

Figure 14. Yttrium metal as arc-melted. Unetched. 100X.

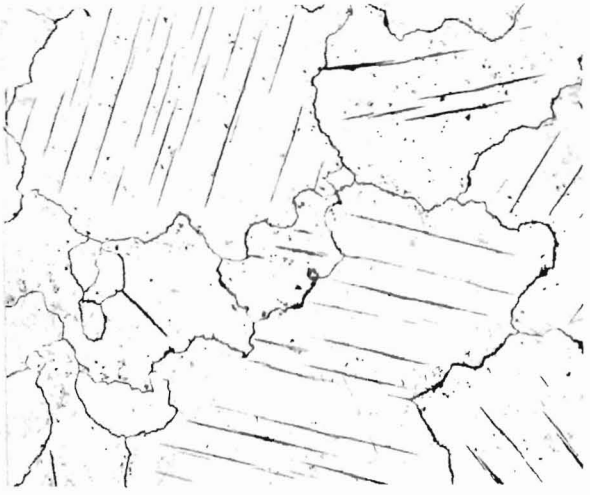

2609

Figure 15. Yttrium - 10% erbium, as arc-melted. Unetched. 100X.

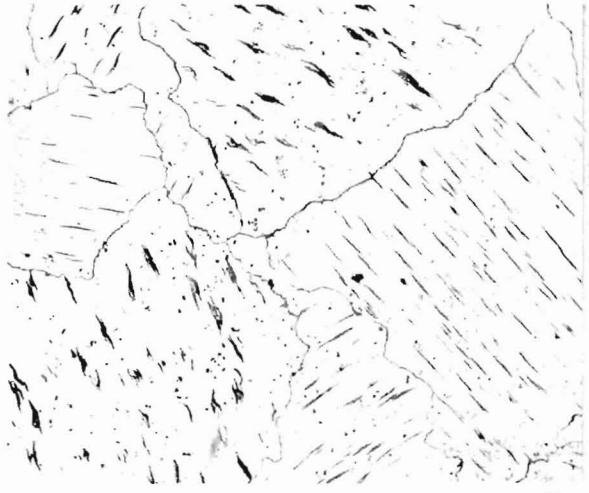

2612

Figure 16. Yttrium - 25% erbium, as arc-melted. Unetched. 100X.

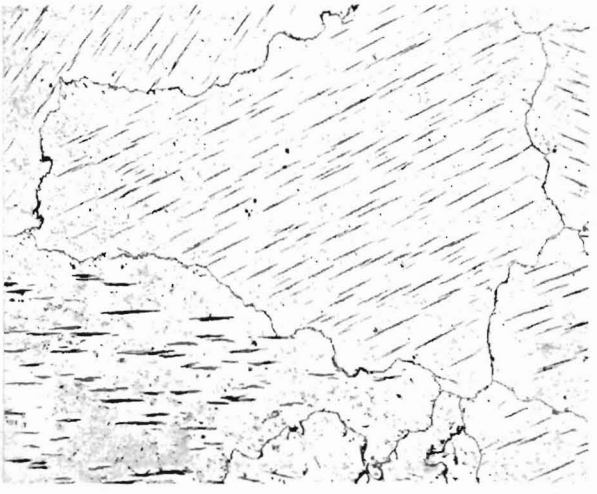

2613

Figure 17. Yttrium - 50% erbium, as arc-melted. Unetched. 100X.

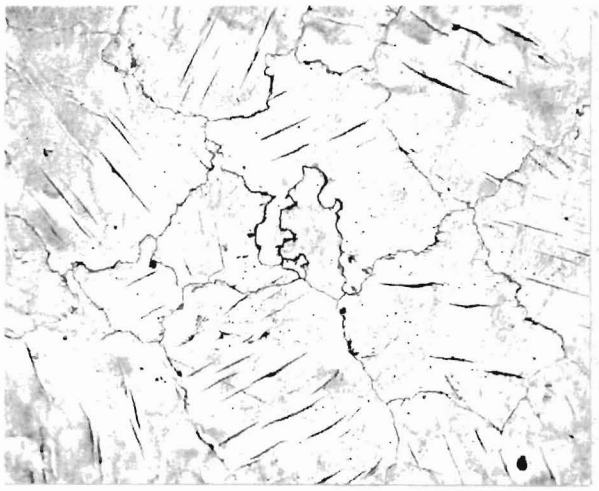

2617

Figure 18. Yttrium - 75% erbium, as arc-melted. Unetched. 100X.

2616

Figure 19. Yttrium - 90% erbium, as arc-melted. Unetched. 100X.

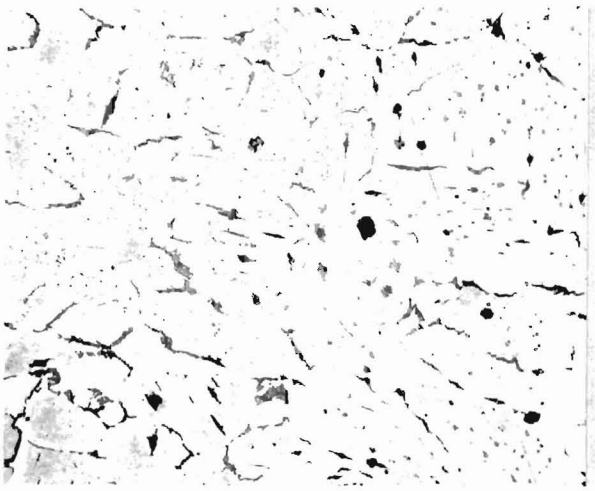

2620

Figure 20. Erbium metal, as arc-melted. Unetched. 100X.

2595

Figure 21. Distilled erbium metal, as arc-melted. Unetched. 100X.

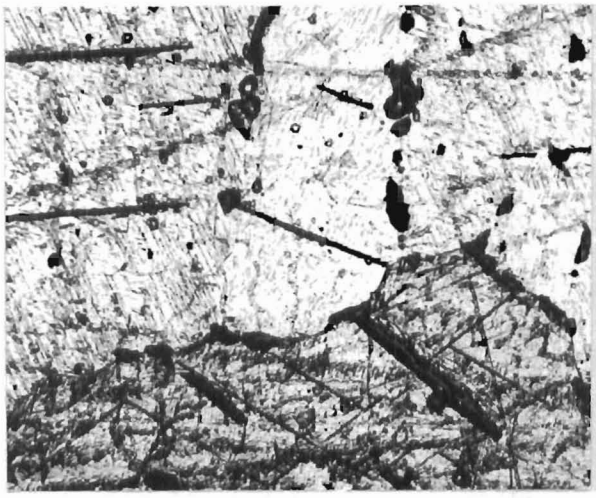

3241

Figure 22. Yttrium metal, heat treated at 1000°C, slow cooled. Nitric acid etch. 250X.

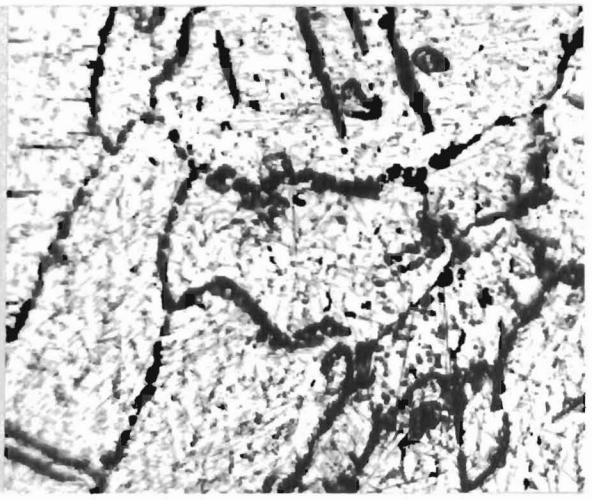

3366

Figure 23. Yttrium - 10% erbium, heat treated at 1000°C, slow cooled. Nitric acid etch. 250X.

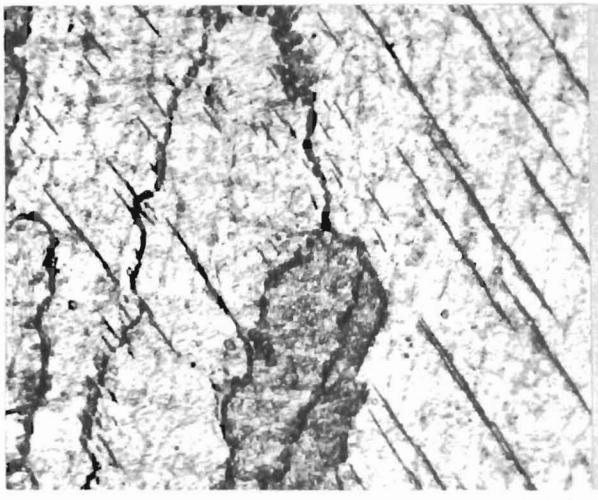

3373

Figure 24. Yttrium - 20% erbium, heat treated at 1000°C, slow cooled. Nitric acid etch. 250X.

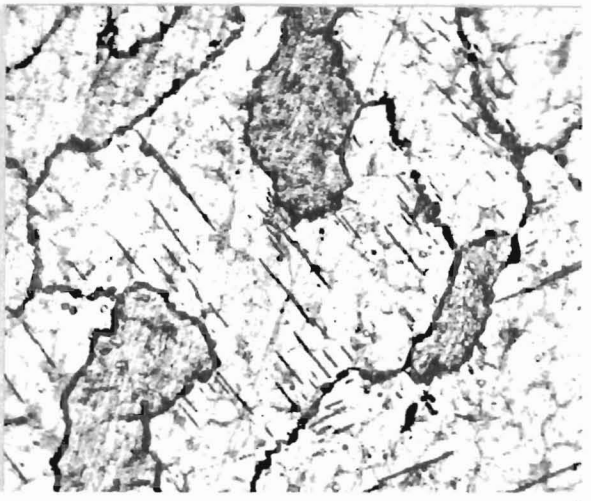

3378

Figure 25. Yttrium - 30% erbium, heat treated at 1000°C, slow cooled. Nitric acid etch. 250X.

3380

Figure 26. Yttrium - 50% erbium, heat treated at 1000°C, slow cooled. Nitric acid etch. 250X.

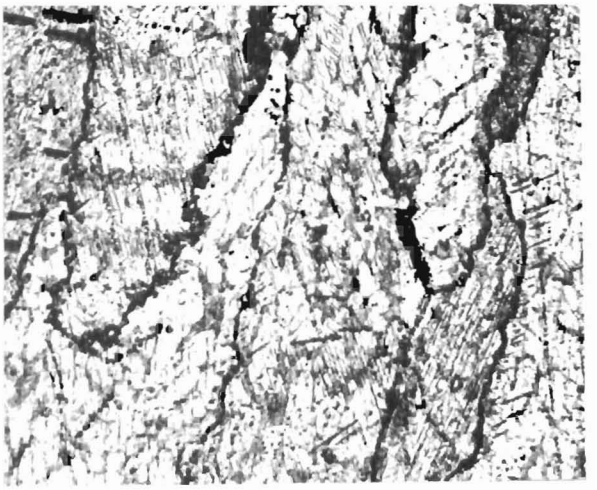

3381

Figure 27. Yttrium - 60% erbium, heat treated at 1000°C, slow cooled. Nitric acid etch. 250X.

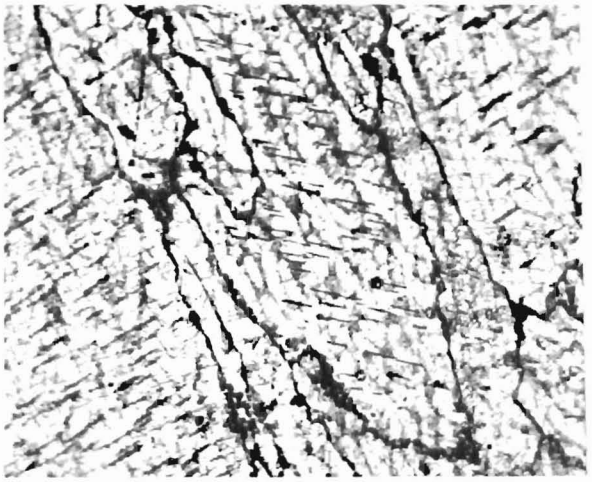

3382

Figure 28. Yttrium - 90% erbium, heat treated at 1000°C, slow cooled. Nitric acid etch. 250X.

3206

Figure 29. Erbium, heat treated at 1000°C, slow cooled. Nitric acid etch. 250X.

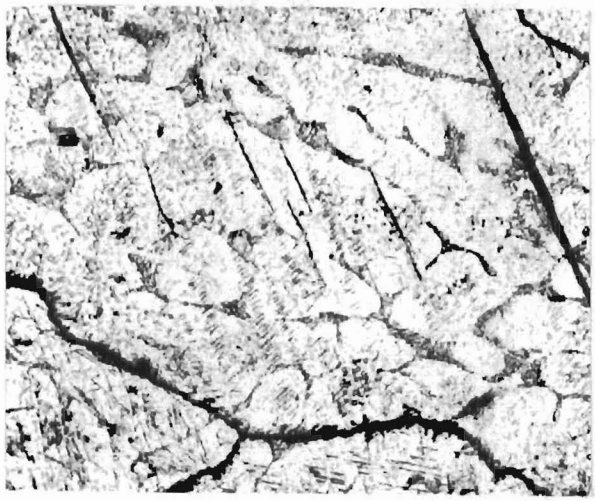

2969

Figure 30. Yttrium - 30% erbium as arc-melted. Concentrated HNO_3 etch. 500X.

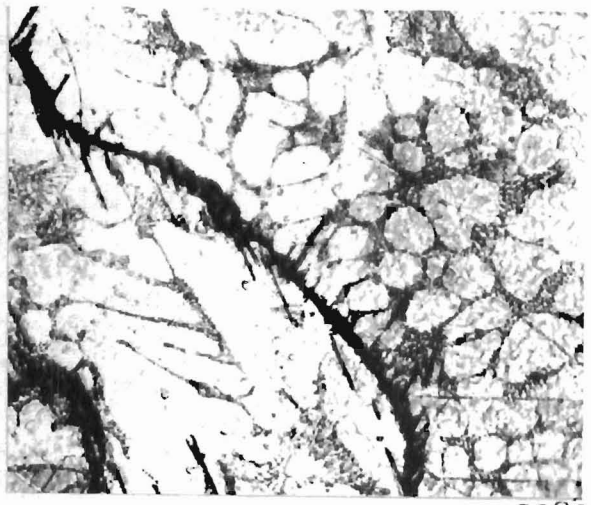

2989

Figure 31. Yttrium - 40% erbium as arc-melted. Concentrated HNO_3 etch. 500X.

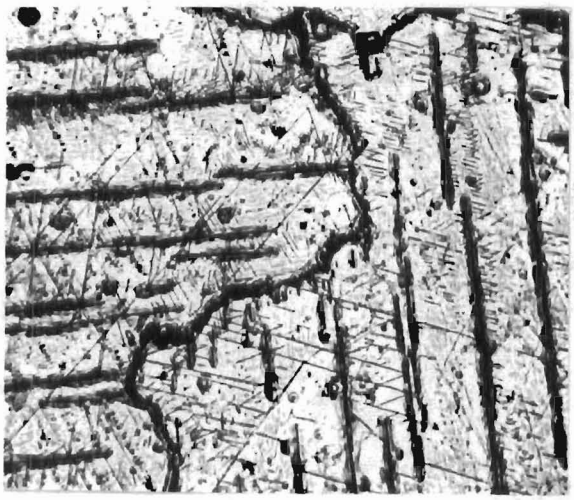

3237

Figure 32. Yttrium - 30% erbium, heat treated at 1000°C and slow cooled. (Partial breakup of oxide platelets to spheres is noted and change in appearance of the erbium metal). Concentrated HNO_3 etch. 250X.

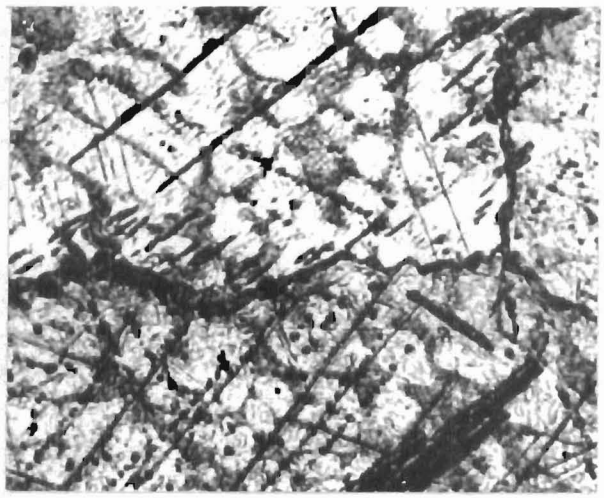

3236

Figure 33. Yttrium - 40% erbium, heat treated at 1000°C and slow cooled. (The quantity of "eutectoid" appearing structure is less than in the arc-melted condition). Concentrated HNO_3 etch. 500X.

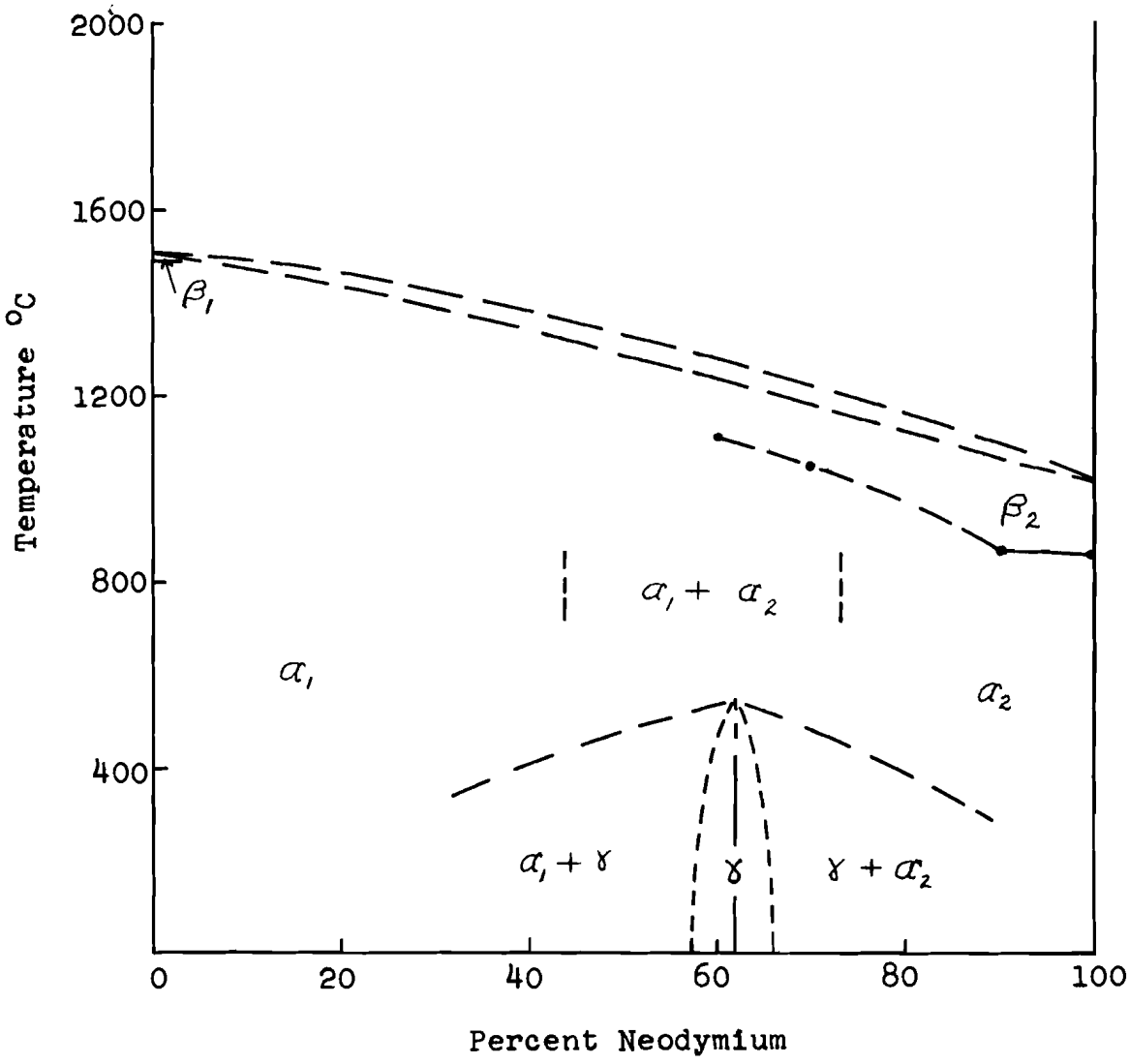

Figure 34. Tentative Constitutional Diagram for the Yttrium - Neodymium System

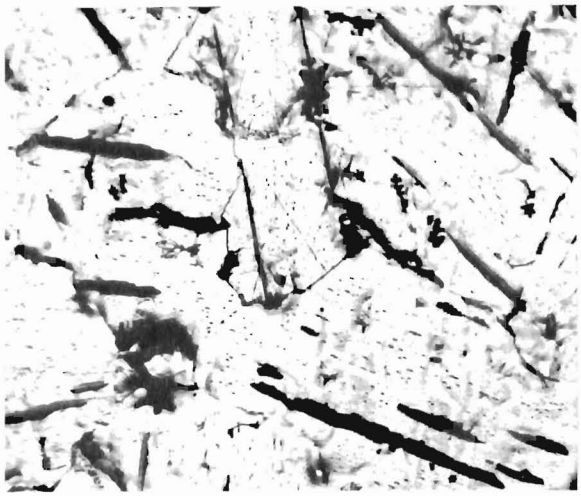

3417

Figure 35. Yttrium - 10% neodymium, as arc-melted. (Structure typical of yttrium with perhaps somewhat poorer grain definition). Nitric acid etch. 250X.

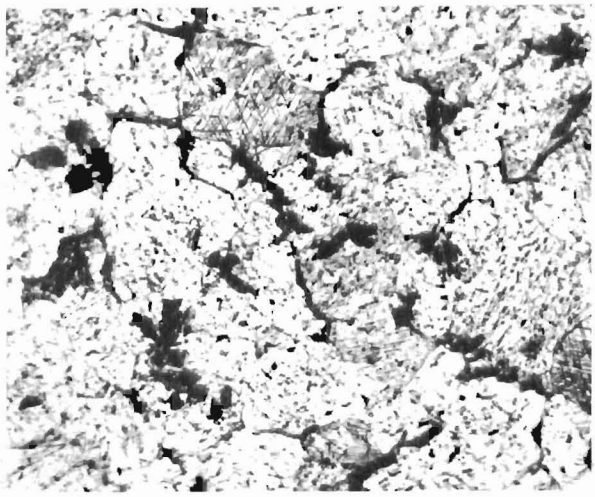

3420

Figure 36. Yttrium - 40% neodymium, as arc-melted. (Poorly defined grains, impurities in grain boundaries and as dendrites). Nitric acid etch. 250X.

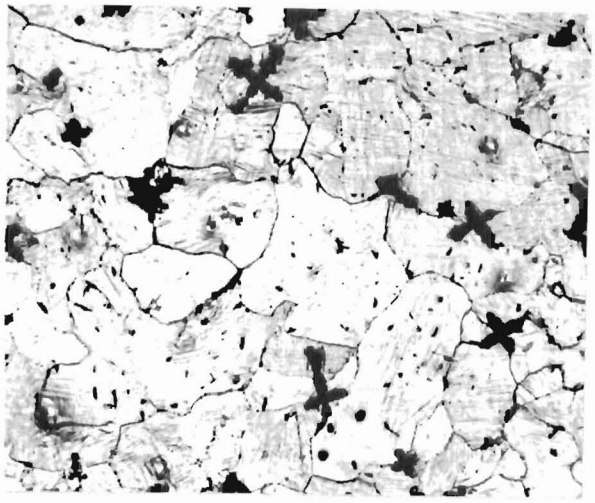

3421

Figure 37. Yttrium - 50% neodymium, as arc-melted. (Well defined grains, smaller than either yttrium or neodymium, traces of transformation structure, impurities as dendrites). Nitric acid etch. 250X.

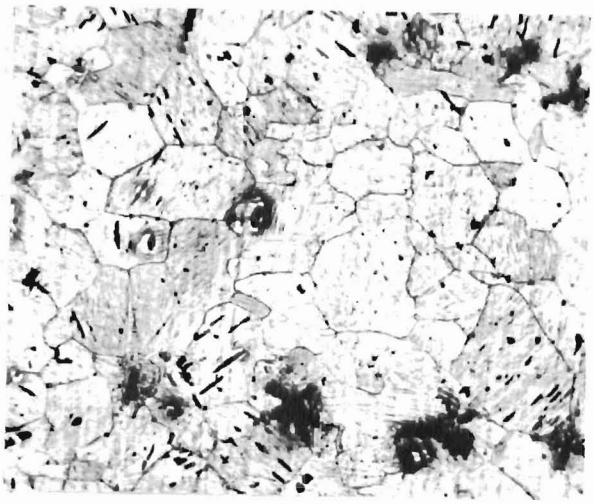

3422

Figure 38. Yttrium - 60% neodymium, as arc-melted. (Well defined small grains, traces of transformation structure, impurities mostly as dendrites). Nitric acid etch. 250X.

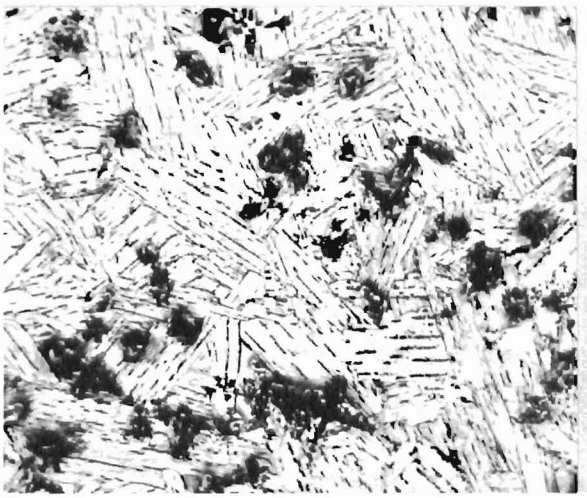

3428

Figure 39. Yttrium - 70% neodymium, as arc-melted. (Transformed structure, impurities as platelets and dendrites). Nitric acid etch. 250X.

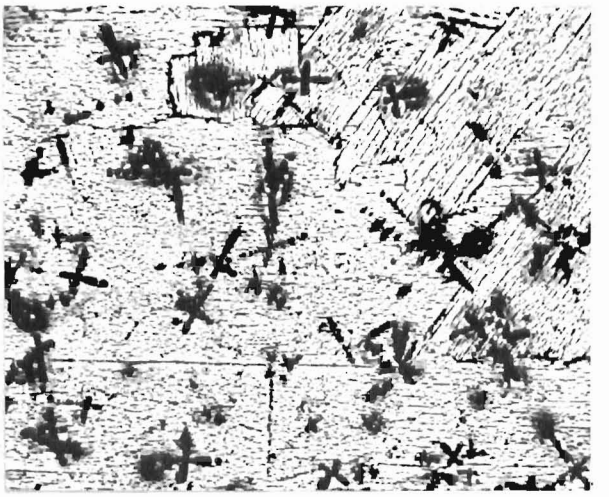

3429

Figure 40. Yttrium - 80% neodymium, as arc-melted. (Partly transformed structure, impurities as fine platelets and dendrites). Nitric acid etch. 250X.

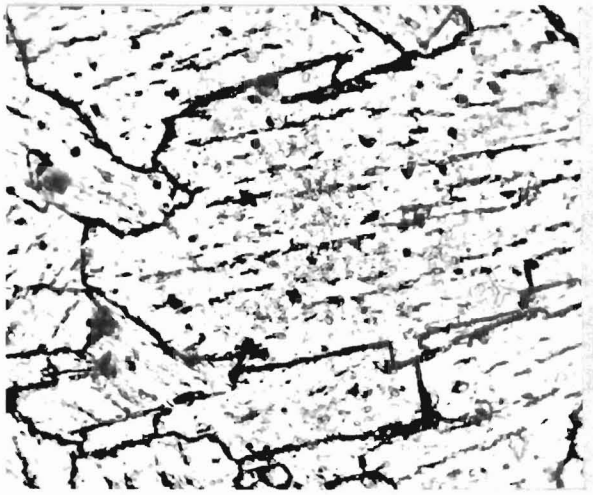

3263

Figure 41. Yttrium - 90% neodymium, as arc-melted. (Typical neodymium structure with platelets). Nitric acid etch. 500X.

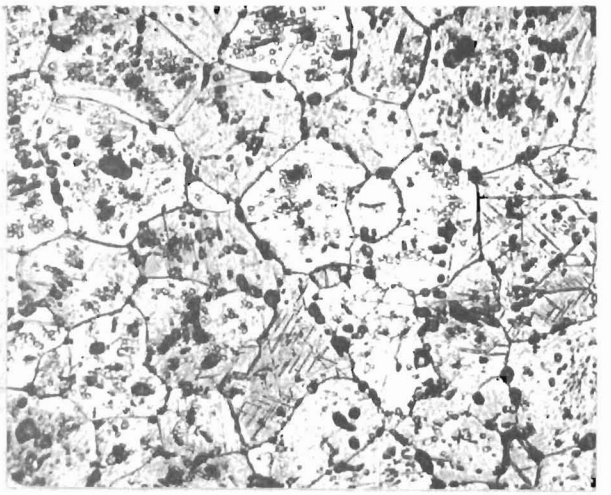

3245

Figure 42. Yttrium - 60% neodymium. (Heat treated 40 hours at 1000°C and air quenched. Metal structure similar to that of as arc-cast specimen (Figure 38). Redistribution and spheroidization of impurities). Nitric acid etch. 250X.

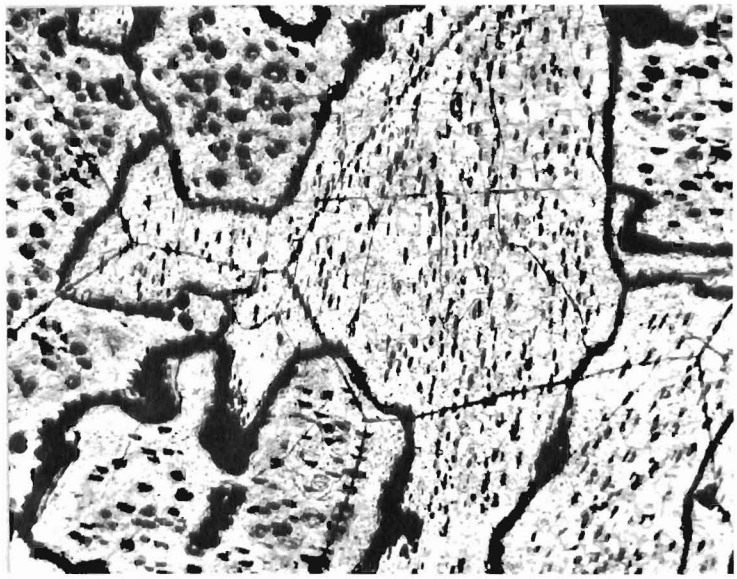

3271

Figure 43. Yttrium - 98% neodymium, as arc-melted. Two systems of granular orientation. Irregularly shaped grains with heavy grain boundaries. Platelets are distributed throughout each grain. Secondary grains, outlined by thin grain boundaries, with straight sides and intersecting angles typical for hexagonal grain shapes.

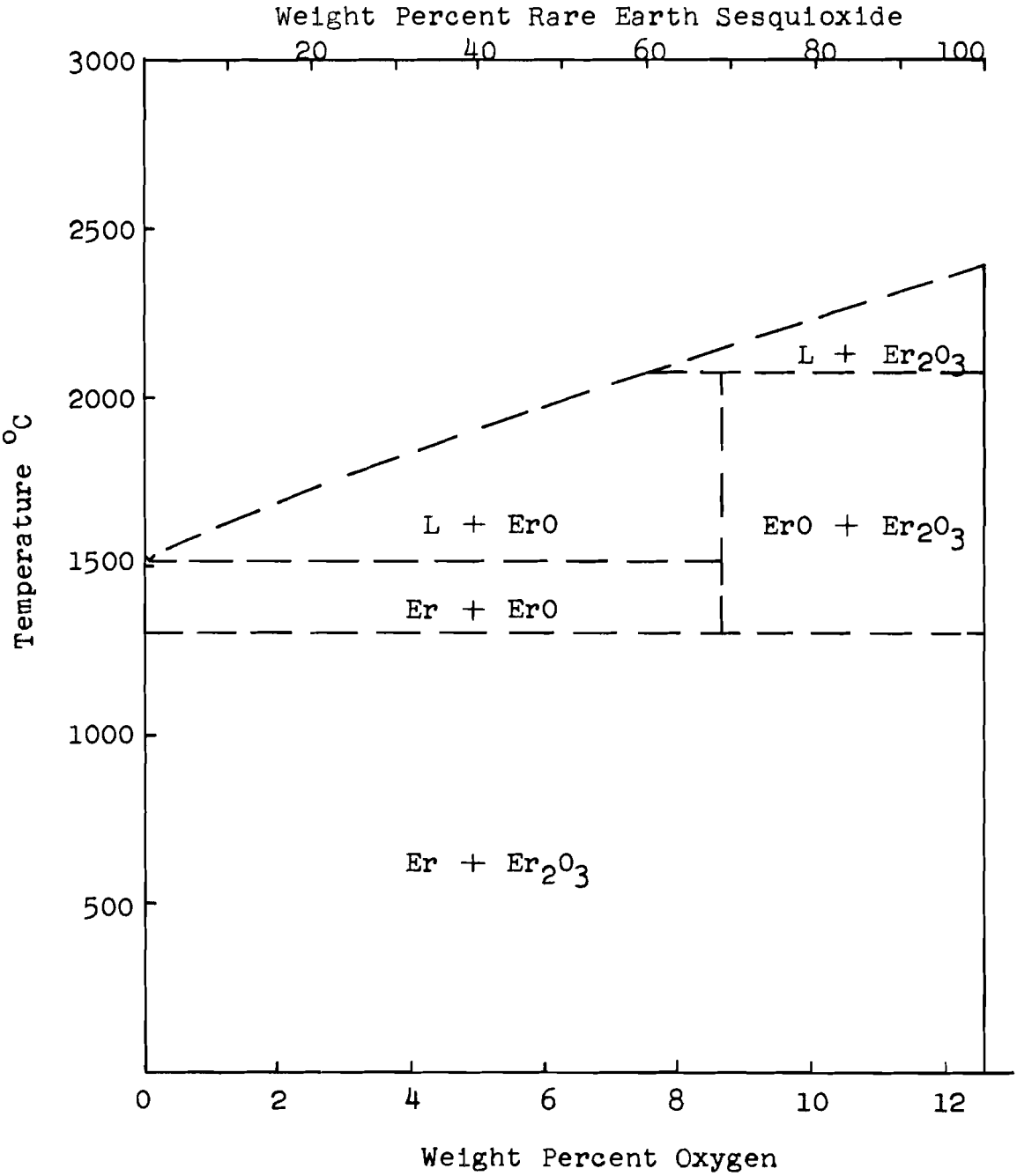

Figure 44. Tentative Partial Constitutional Diagram for the Erbium - Oxygen System

2652

Figure 45. Erbium-10% Er_2O_3, as arc-melted. Oxide principally in grain boundaries and as platelets within grains. Unetched. 100X.

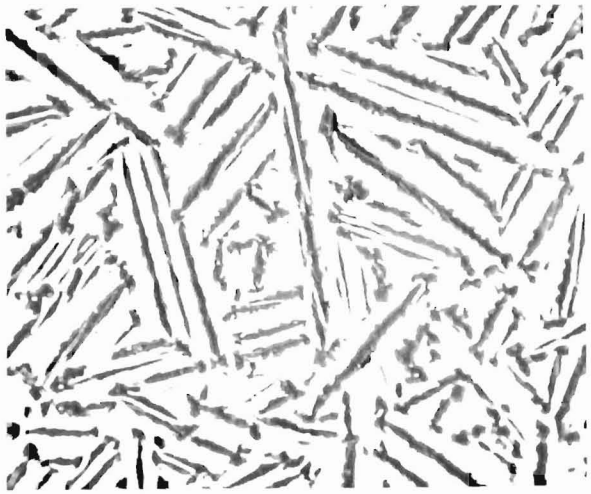

2658

Figure 46. Erbium-25% Er_2O_3, as arc-melted. Oxide as platelets. No concentration of oxide in grain boundaries as present in Figure 45. Unetched. 100X.

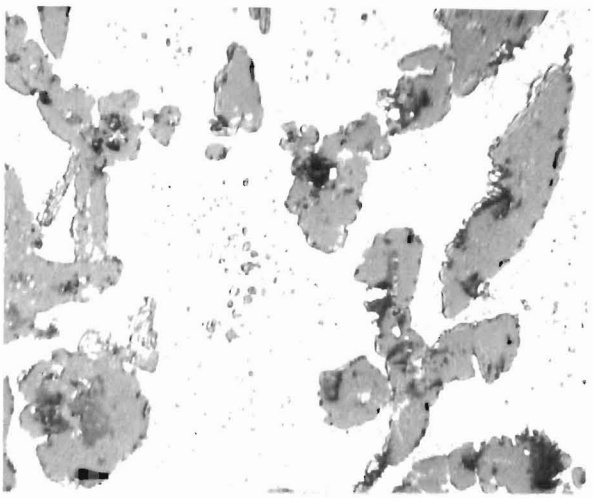

3474

Figure 47. Erbium-25% Er_2O_3, as arc-melted. Detail of oxide platelets showing lamellar structure. Unetched. 750X.

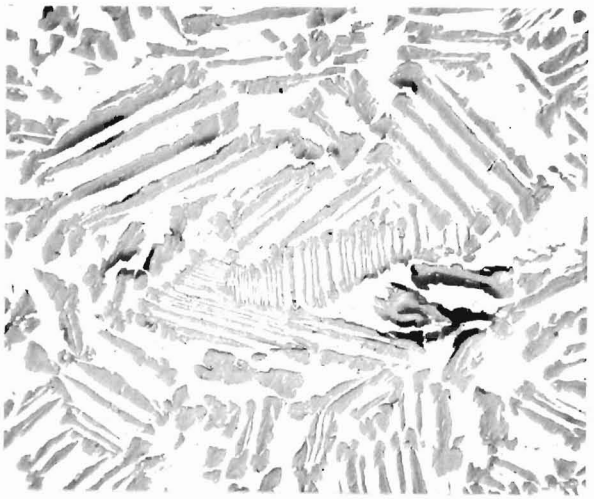

2661

Figure 48. Erbium-35% Er_2O_3, as arc-melted. Oxide as platelets. Unetched. 100X.

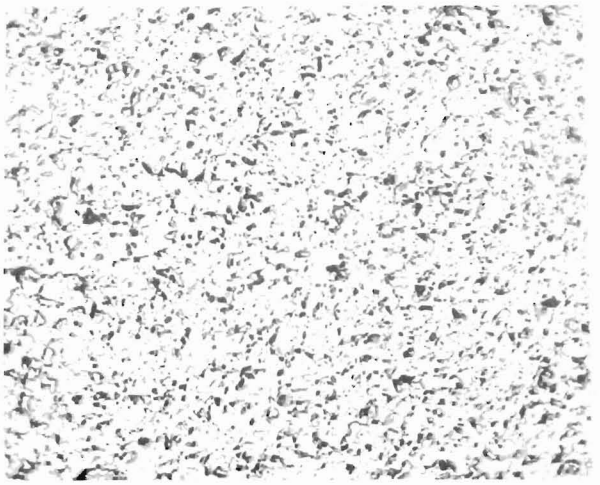

3119

Figure 49. Erbium-60% Er_2O_3, as arc-melted. Mixed oxide-metal matrix. Unetched. 100X.

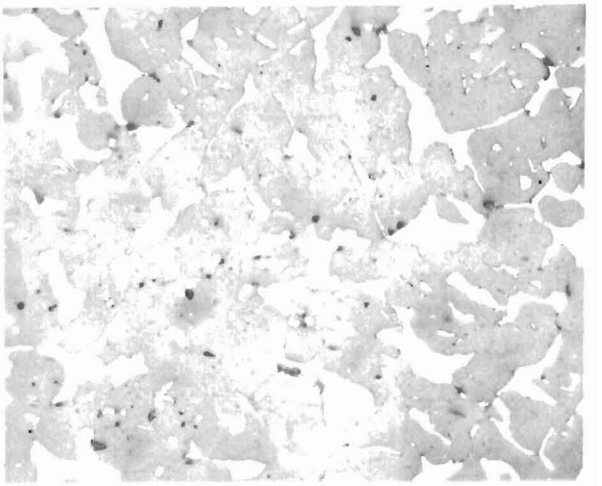

2668

Figure 50. Erbium-60% Er_2O_3, as arc-melted. Mixed oxide-metal matrix. Metal phase (white) does not have platelet inclusions. Unetched. 500X.

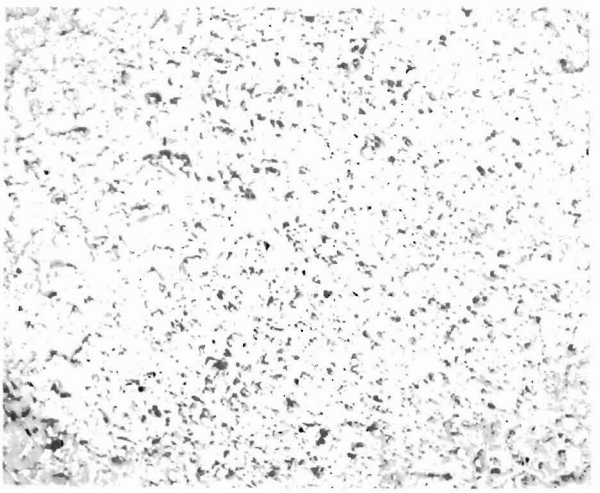

3118

Figure 51. Erbium-75% Er_2O_3, as arc-melted. Oxide matrix with metal inclusions. Unetched. 100X.

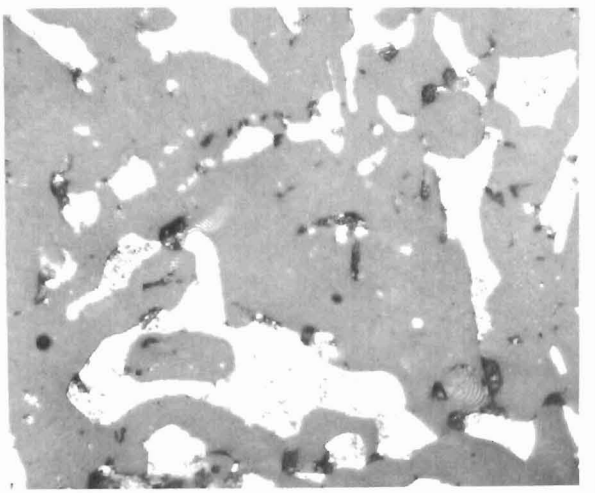

3131

Figure 52. Erbium-75% Er_2O_3, as arc-melted. Oxide matrix with metal inclusions. Possible lamellar structure indicated for oxide. No platelets in metal phase. Unetched. 500X.

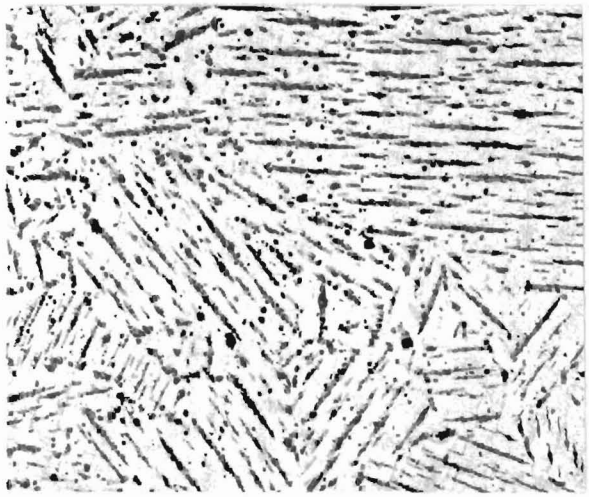

3114

Figure 53. Erbium-10% Er_2O_3. Heat treated 40 hours at 1000°C, air quenched. Spheroidization of smaller oxide particles and portions of the platelets. Unetched. 100X.

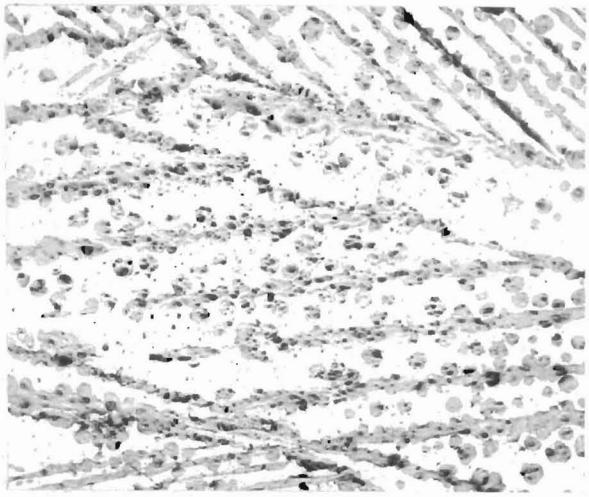

3117

Figure 54. Erbium-35% Er_2O_3. Heat treated 40 hours at 1000°C, air quenched. Spheroidization of smaller oxide particles and extensive reforming in platelets. Unetched. 100X.

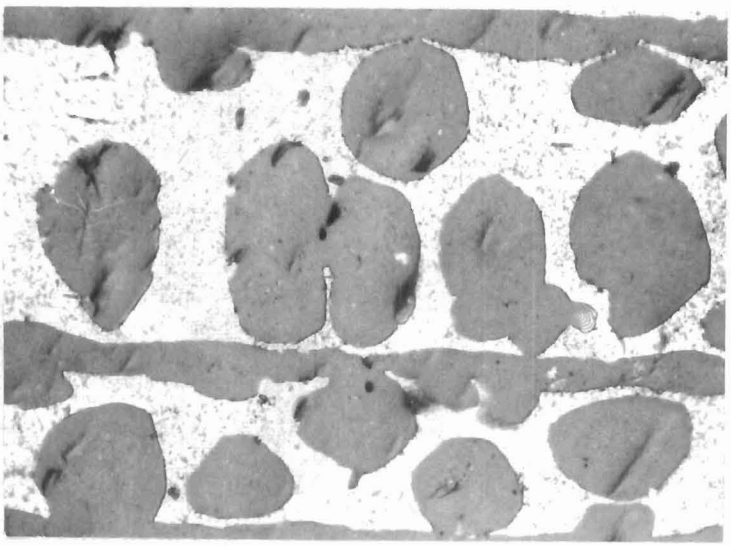

3126

Figure 55. Erbium-35% Er_2O_3. Heat treated 40 hours at 1000°C, air quenched. Enlarged detail of spheres formed and forming from platelets. Unetched. 750X.

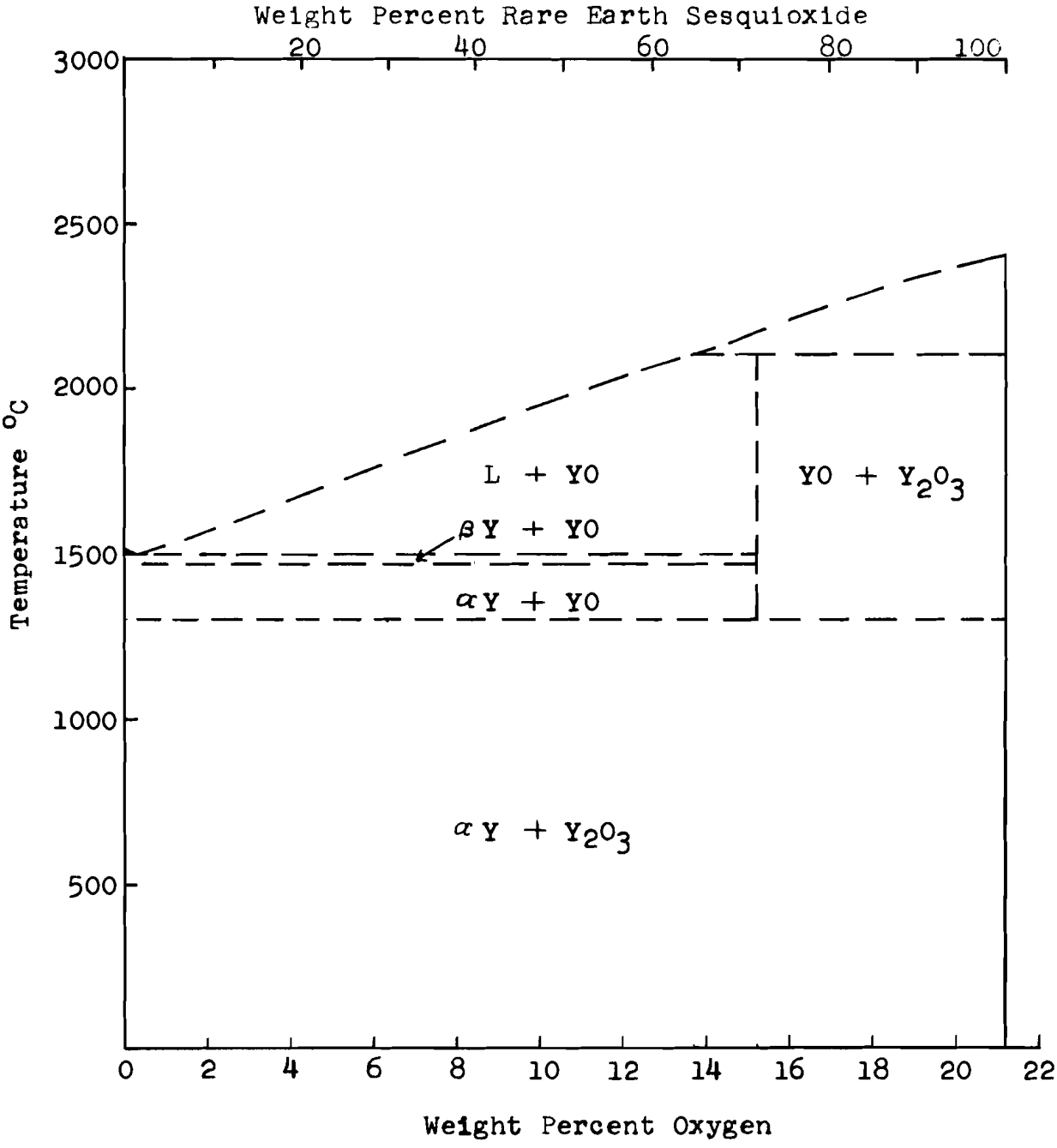

Figure 56. Tentative Partial Constitutional Diagram for the Yttrium - Oxygen System

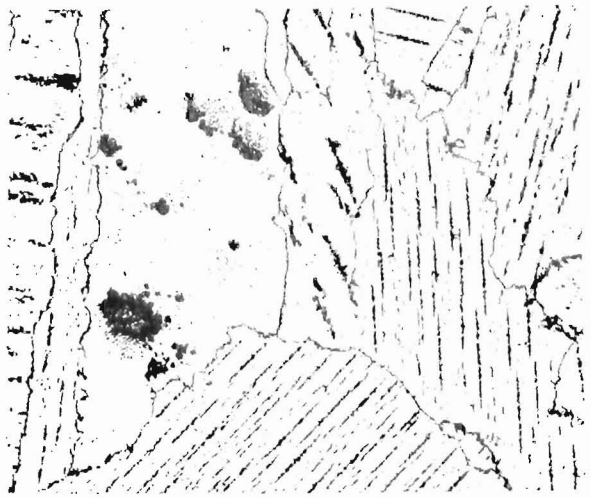

3132

Figure 57. Yttrium-10% Y_2O_3, as arc-melted. Oxide platelets sectioned transverse and parallel to major plane. Unetched. 100X.

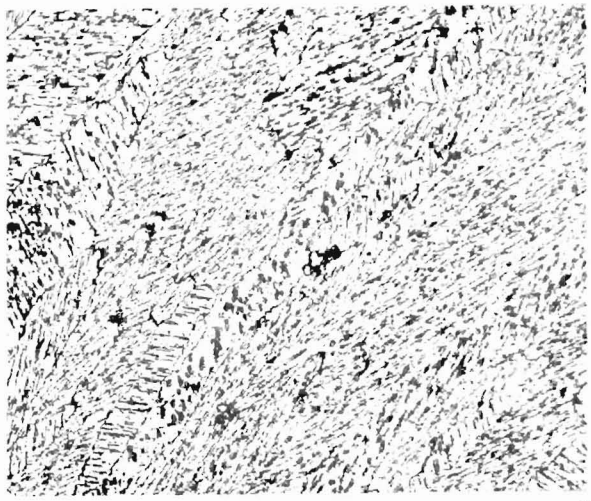

3136

Figure 58. Yttrium-20% Y_2O_3, as arc-melted. Oxide platelets sectioned at various angles. Unetched. 100X.

3140

Figure 59. Yttrium-30% Y_2O_3, as arc-melted. Oxide platelets sectioned at various angles, and parallel to major plane. Unetched. 100X.

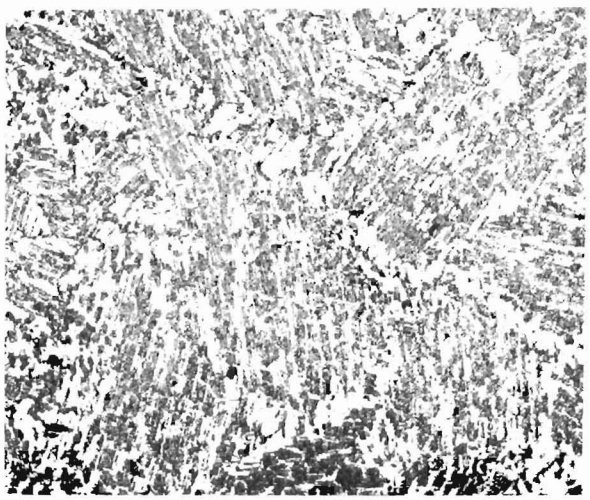

3148

Figure 60. Yttrium-50% Y_2O_3, as arc-melted. Unetched. 100X.

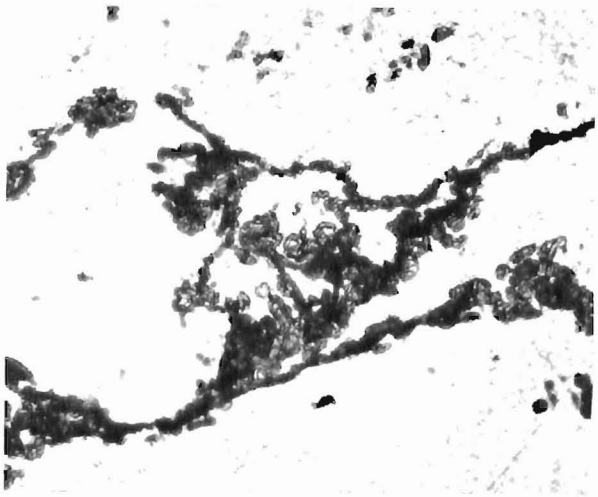

3134

Figure 61. Yttrium-10% Y_2O_3, as arc-melted. Oxide inclusion showing lamellar or transformed structure. Unetched. 750X.

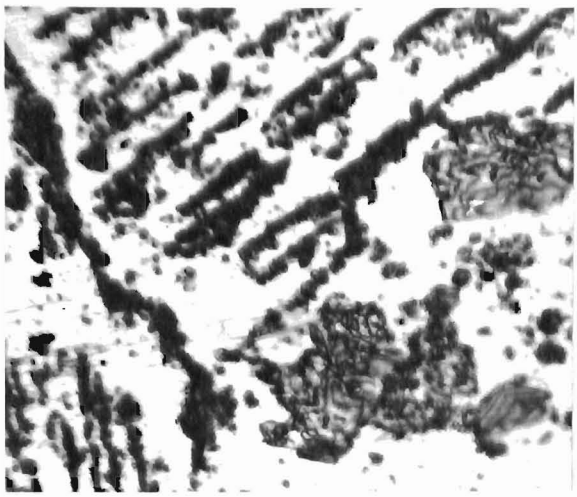

3138

Figure 62. Yttrium-20% Y_2O_3, as arc-melted. Oxide platelets transverse and parallel. Unetched. 750X.

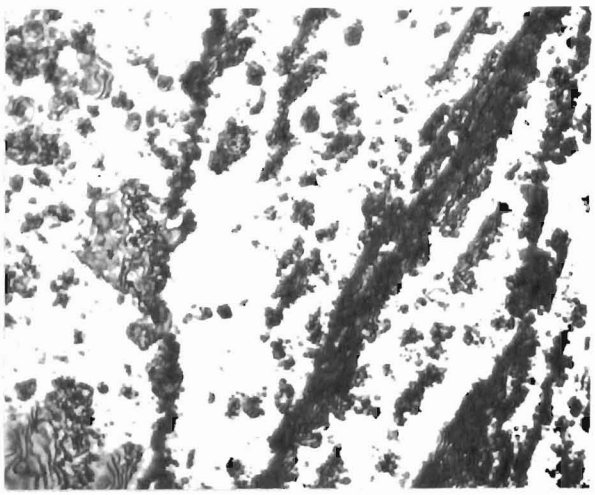

3142

Figure 63. Yttrium-30% Y_2O_3, as arc-melted. Oxide platelets transverse and parallel. Unetched. 750X.

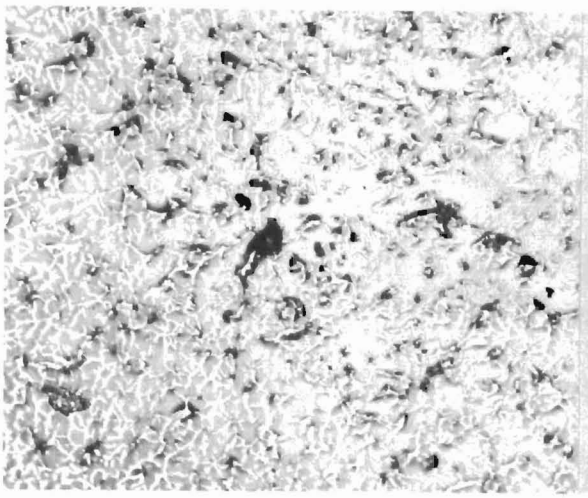

2703

Figure 64. Yttrium-60% Y_2O_3, as arc-melted. Oxide matrix with metal inclusions. Unetched. 100X.

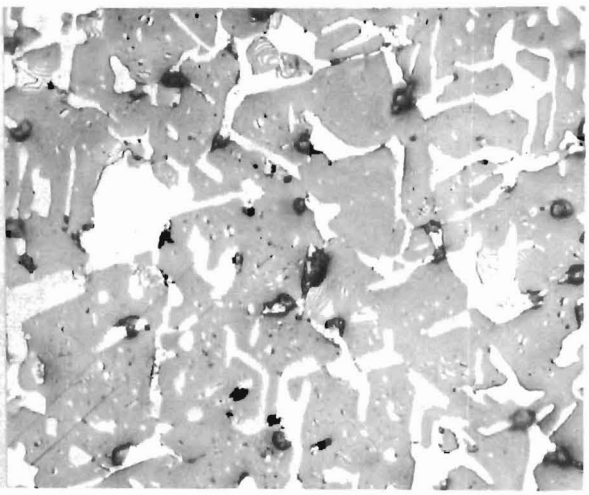

2702

Figure 65. Yttrium-60% Y_2O_3, as arc-melted. Oxide matrix with metal inclusions. Lamellar or transformed structure in oxide. No platelets in metal. Unetched. 500X.

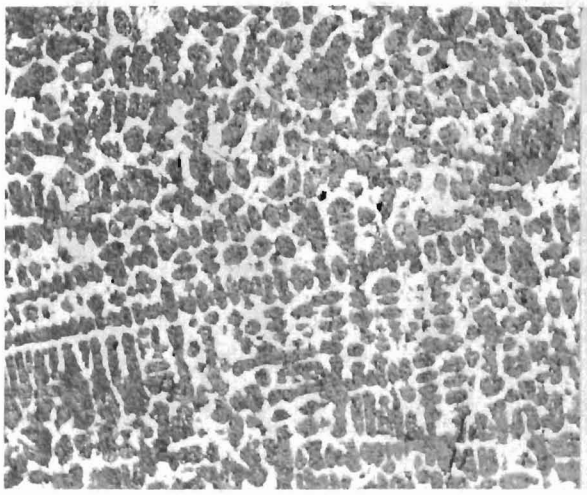

3411

Figure 66. Yttrium-60% Y_2O_3, as arc-melted. Metal matrix with dendritic primary oxide. Unetched. 100X.

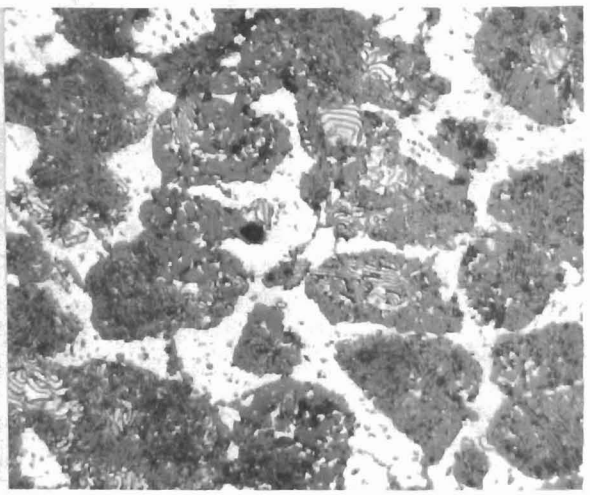

3412

Figure 67. Yttrium-60% Y_2O_3, as arc-melted. Metal matrix with dendritic primary oxide. Lamellar or transformed oxide structure. 500X.

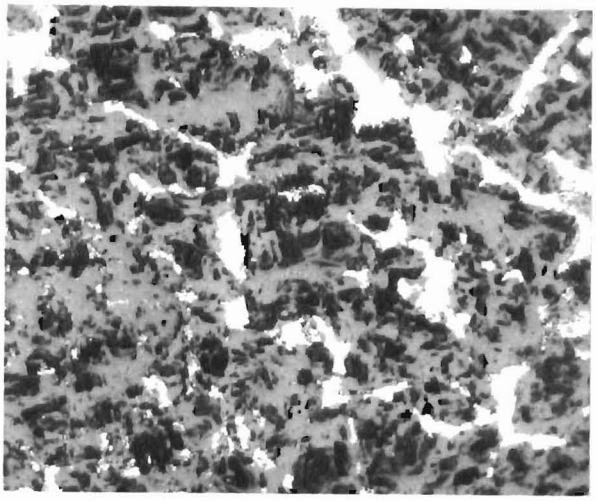

3402

Figure 68. Yttrium-90% Y_2O_3, as arc-melted. The nature of the dark areas within the oxide (gray) has not been defined. Visually they appear to have a different reflectivity. Unetched. 500X.

3479

Figure 69. Distilled yttrium, oxygen content 0.04%. Entire area within one grain. Oxide platelets plus small crystallites. Unetched. 250X.

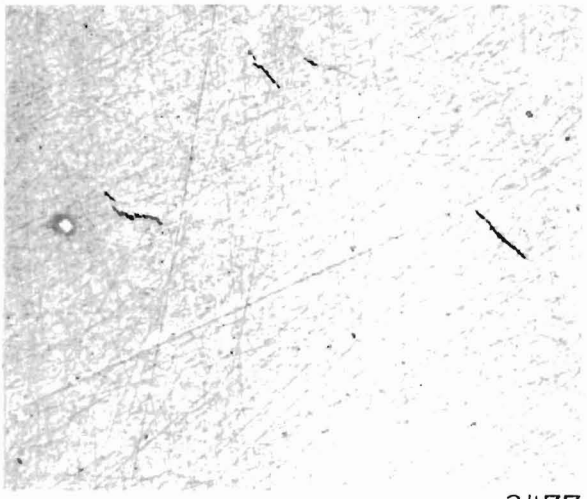

3477

Figure 70. Enlarged detail of specimen as seen in Figure 69. Platelets plus crystallite. Unetched. 500X.

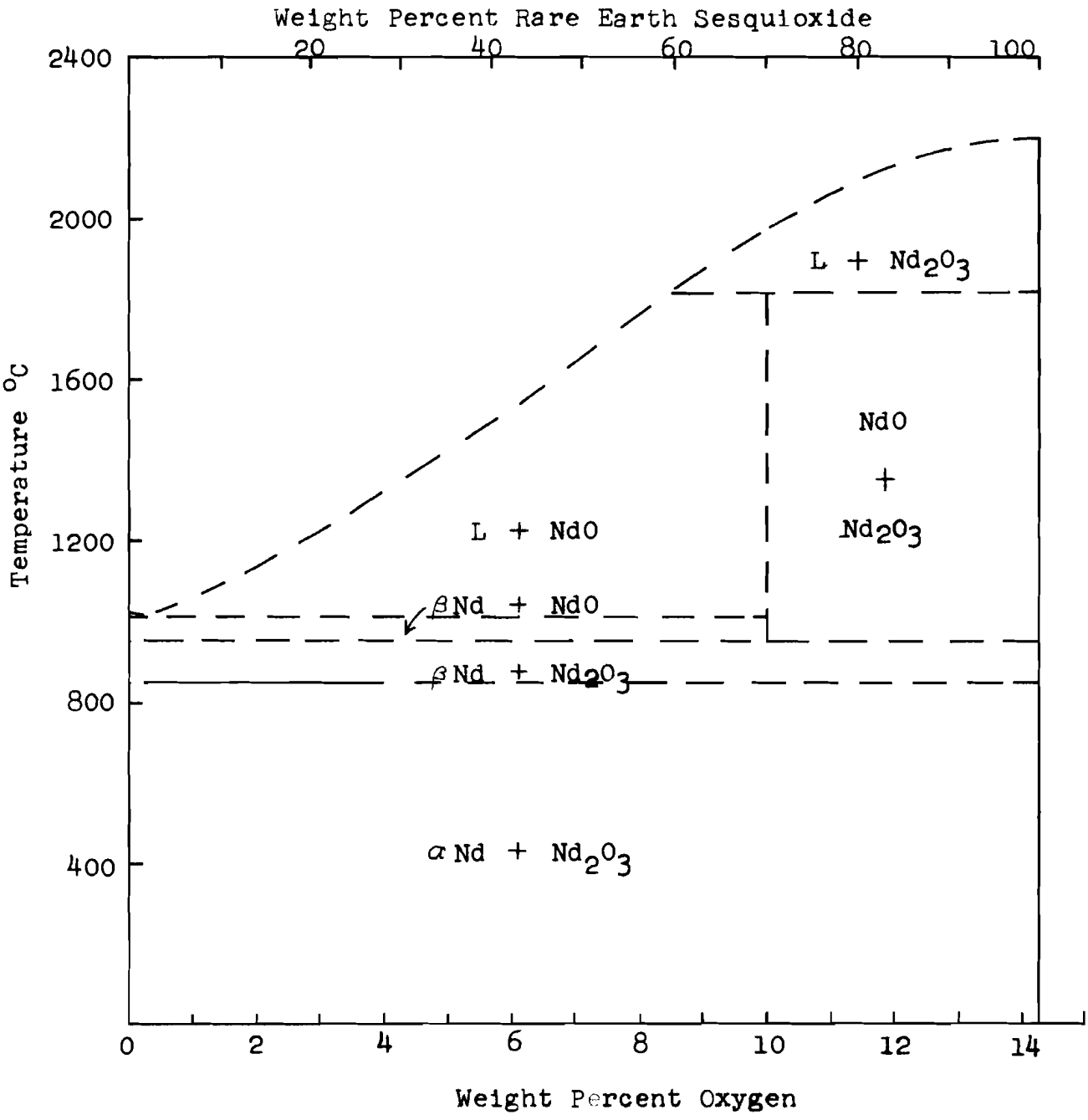

Figure 71. One of two Tentative Partial Constitutional Diagrams for the Neodymium - Oxygen System. See Figure 72.

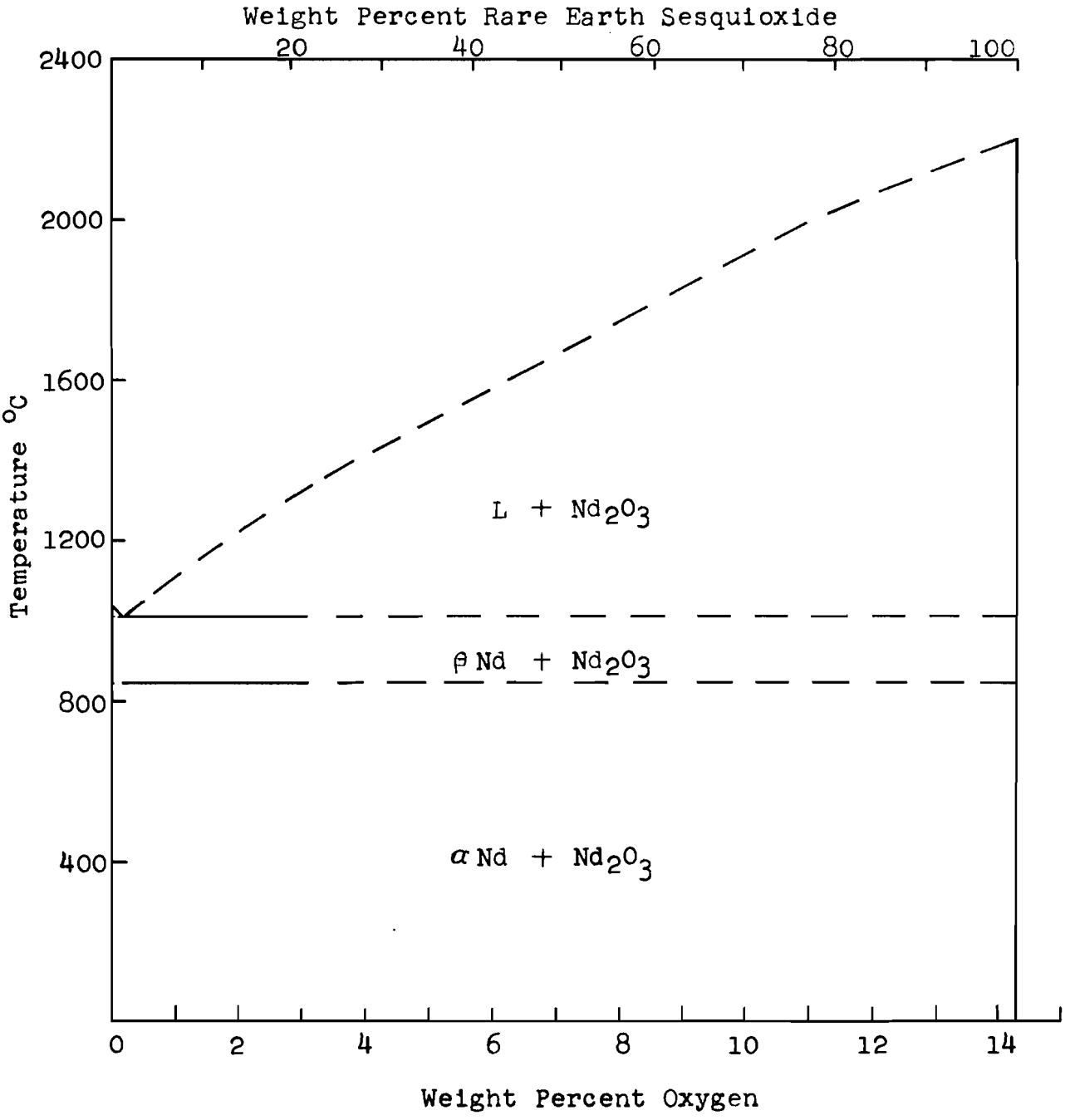

Figure 72. One of two Tentative Partial Constitutional Diagrams for the Neodymium - Oxygen System. See Figure 71.

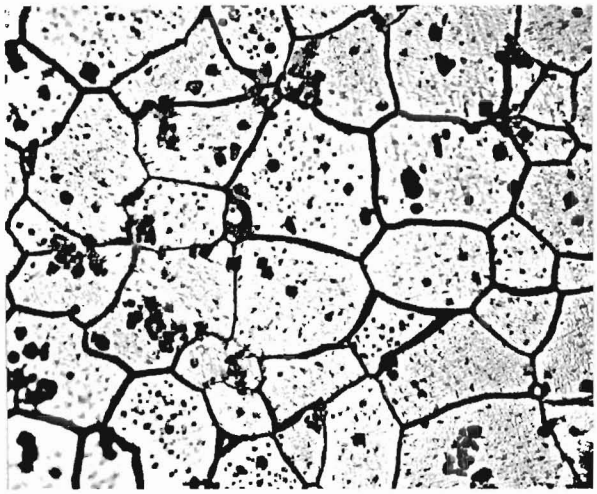

1325

Figure 73. Neodymium metal, as-cast. Oxides in grain boundaries and dispersed within grains. 10% nital etch. 250X.

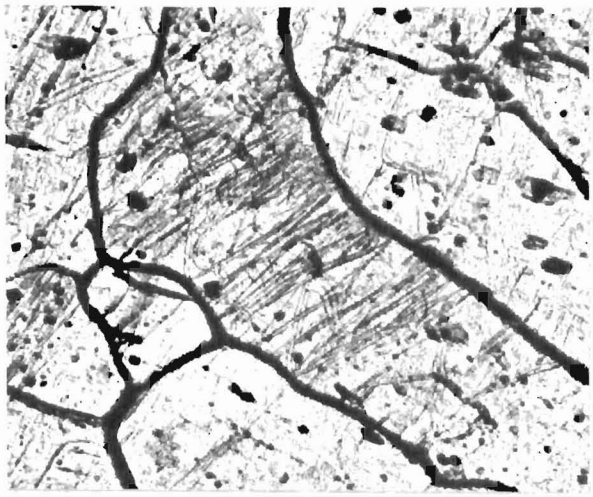

843

Figure 74. Neodymium metal, as-cast. Large grains formed by slow cooling, transformation structure. Hydrofluoric-nitric acid etch followed by repolish. 100X.

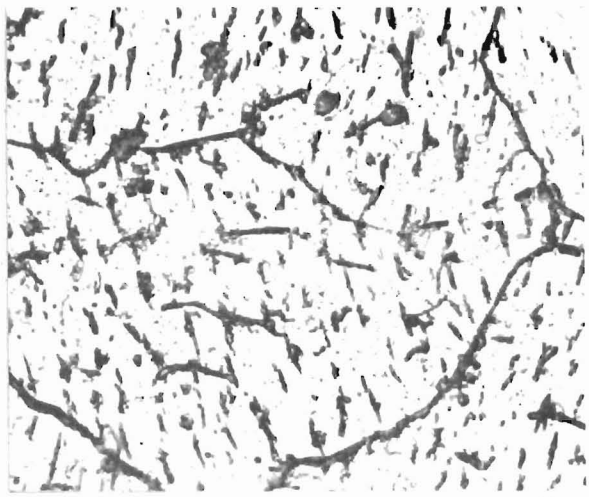

2847

Figure 75. Neodymium metal, as arc-melted. Oxides dispersed and as very small platelets. 1% nitric plus 1% acetic acids etch. 500X.

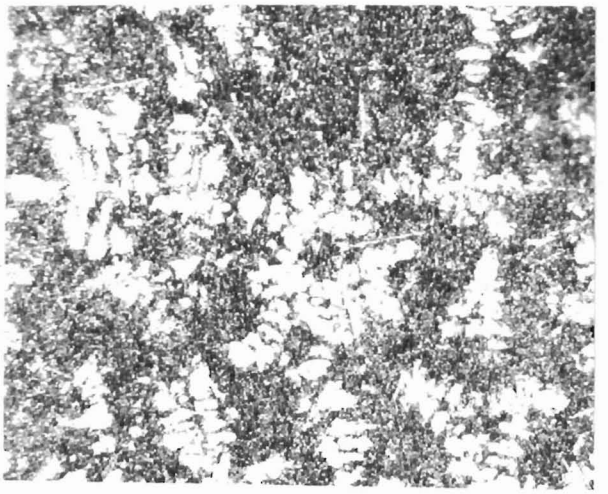

2791

Figure 76. Neodymium-10% Nd_2O_3, as arc-melted. Oxide dendrites in neodymium matrix. Unetched. 500X.

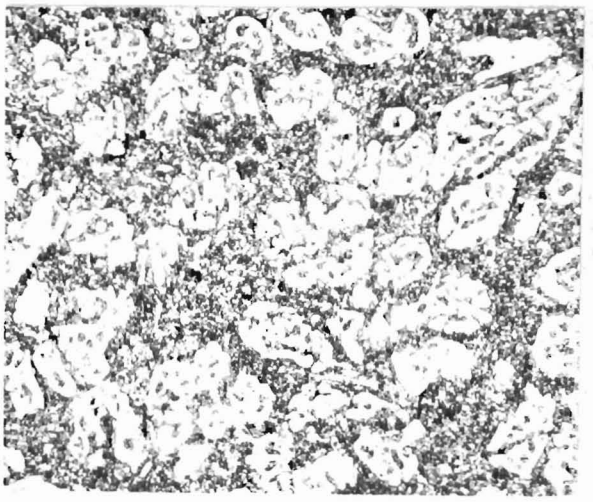

2787

Figure 77. Neodymium-25% Nd_2O_3, as arc-melted. Oxide grains in a dendritic structural pattern. Neodymium matrix and neodymium inclusions in the oxide grains. Unetched. 500X.

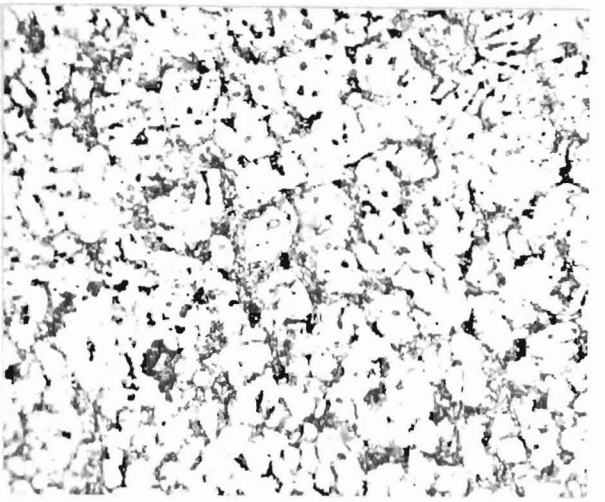

2774

Figure 78. Neodymium-50% Nd_2O_3, as arc-melted. Large oxide grains (melted? sintered?) with occluded and intergranular metal. 500X

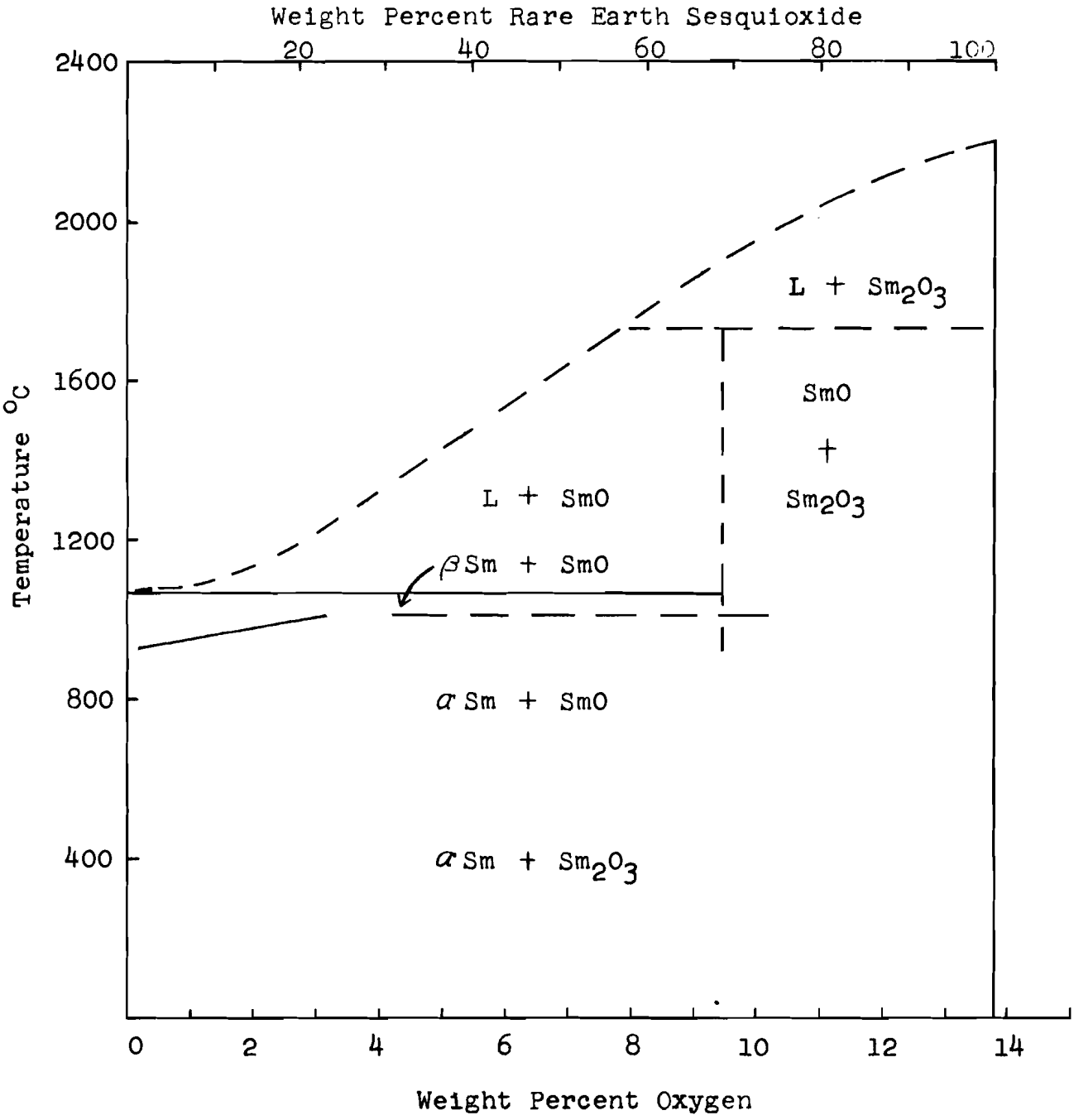

Figure 79. One of two Tentative Partial Constitutional Diagrams for the Samarium - Oxygen System. See Figure 80.

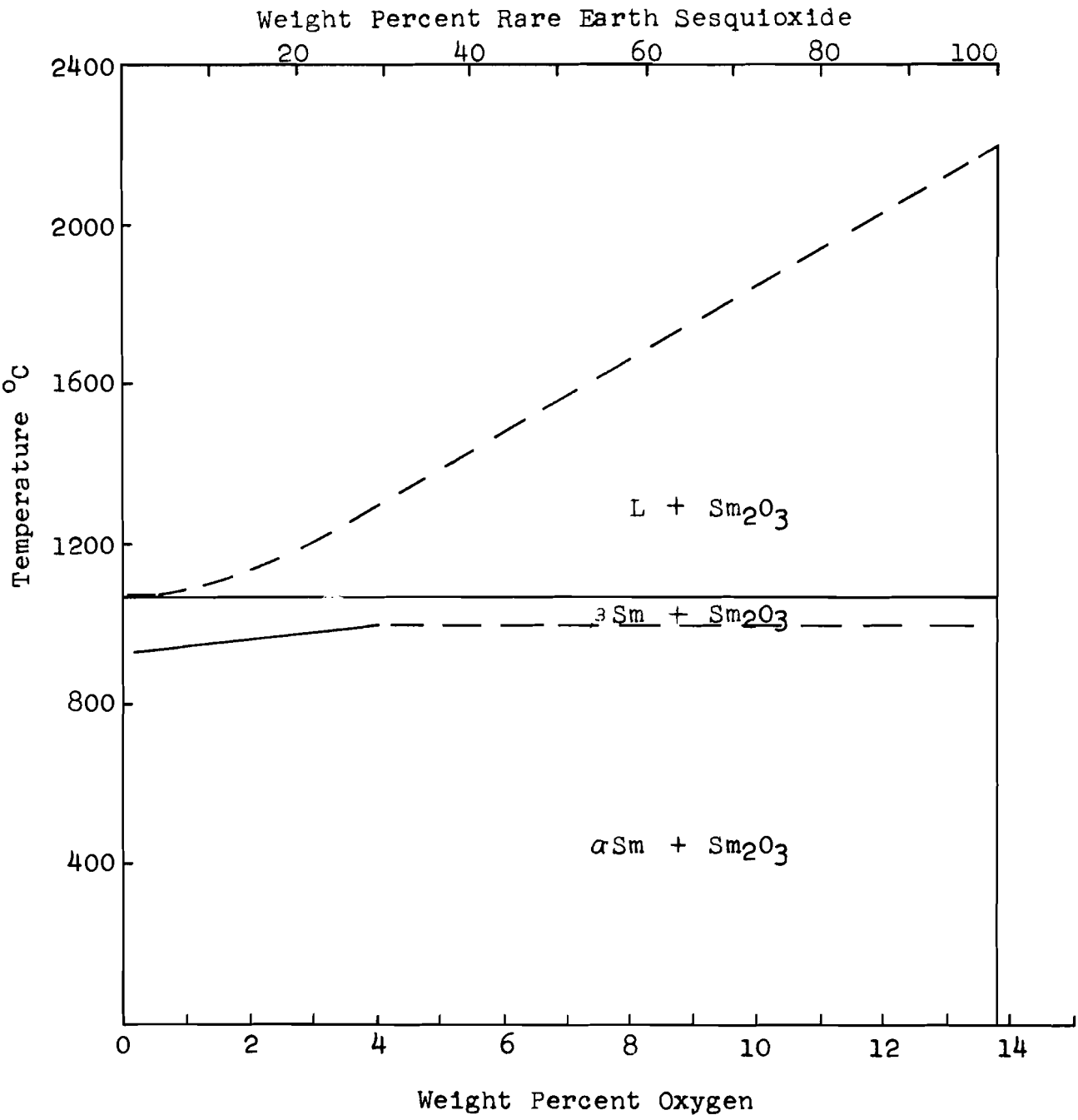

Figure 80. One of two Tentative Partial Constitutional Diagrams for the Samarium - Oxygen System. See Figure 79.

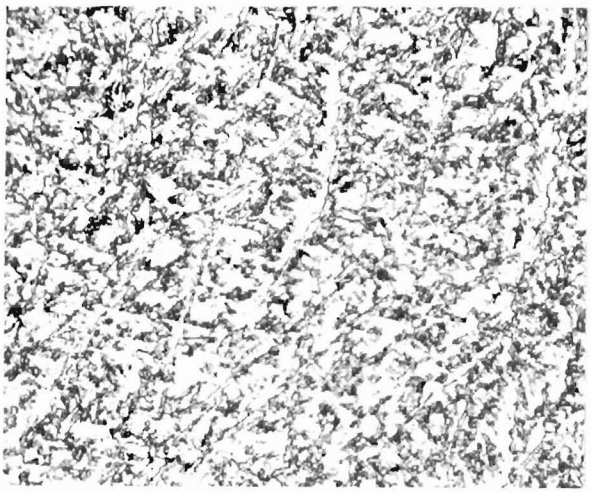

2821

Figure 81. Distilled samarium metal, arc-melted. Transformed structure, original (beta) grains barely detectable. Unetched. 500X.

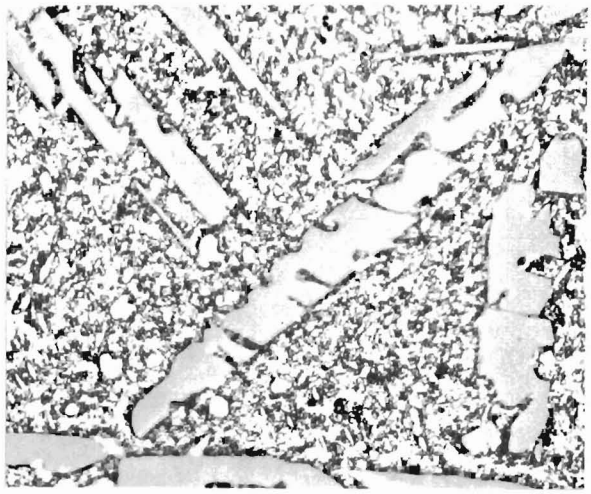

2813

Figure 82. Nominal composition samarium-15% samarium sesquioxide; actual composition approximately 25% sesquioxide. Monoclinic sesquioxide grains in transformed metal matrix. Unetched. 500X.

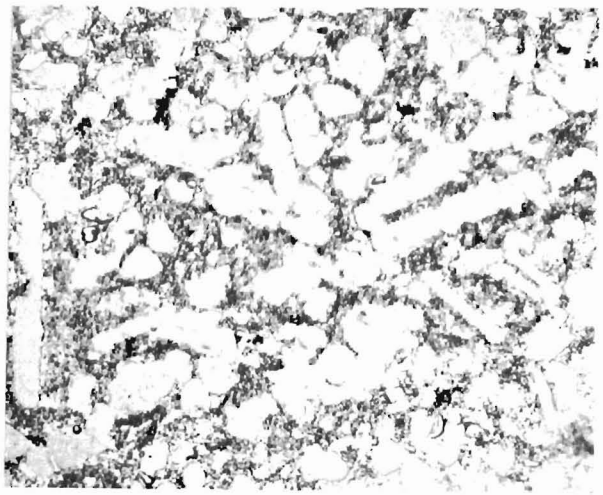

2816

Figure 83. Nominal composition samarium-25% samarium sesquioxide; actual composition approximately 50% sesquioxide. Monoclinic sesquioxide with transformed metal. Some of the oxide grains are long needles as observed in Figure 82 above, many are rounded grains, some of which appear to have undergone reaction. Unetched. 500X.

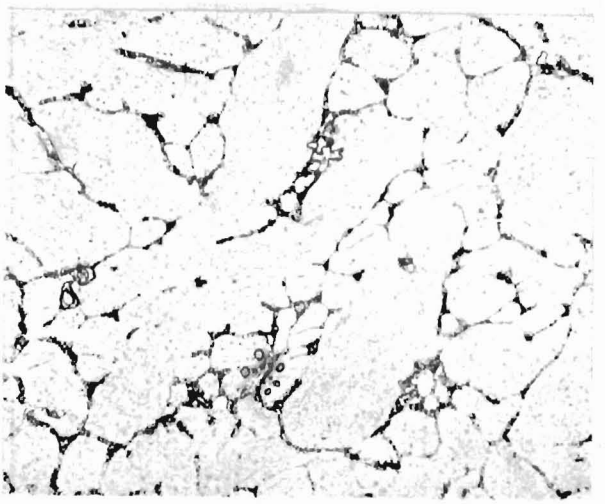

2817

Figure 84. Nominal composition samarium-35% samarium sesquioxide, actual composition approximately 90% sesquioxide. Coalesced monoclinic sesquioxide with samarium metal primarily as intergranular material. 500X

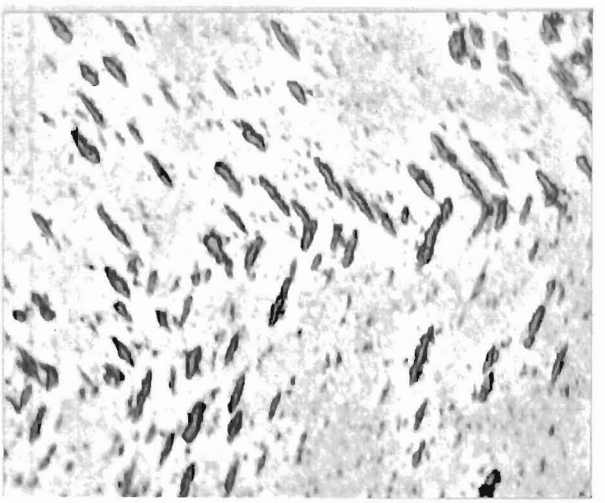

3483

Figure 85. Nominal composition samarium-1% samarium sesquioxide. Monoclinic sesquioxide present indicating low solubility of oxygen in samarium. Unetched. 500X.

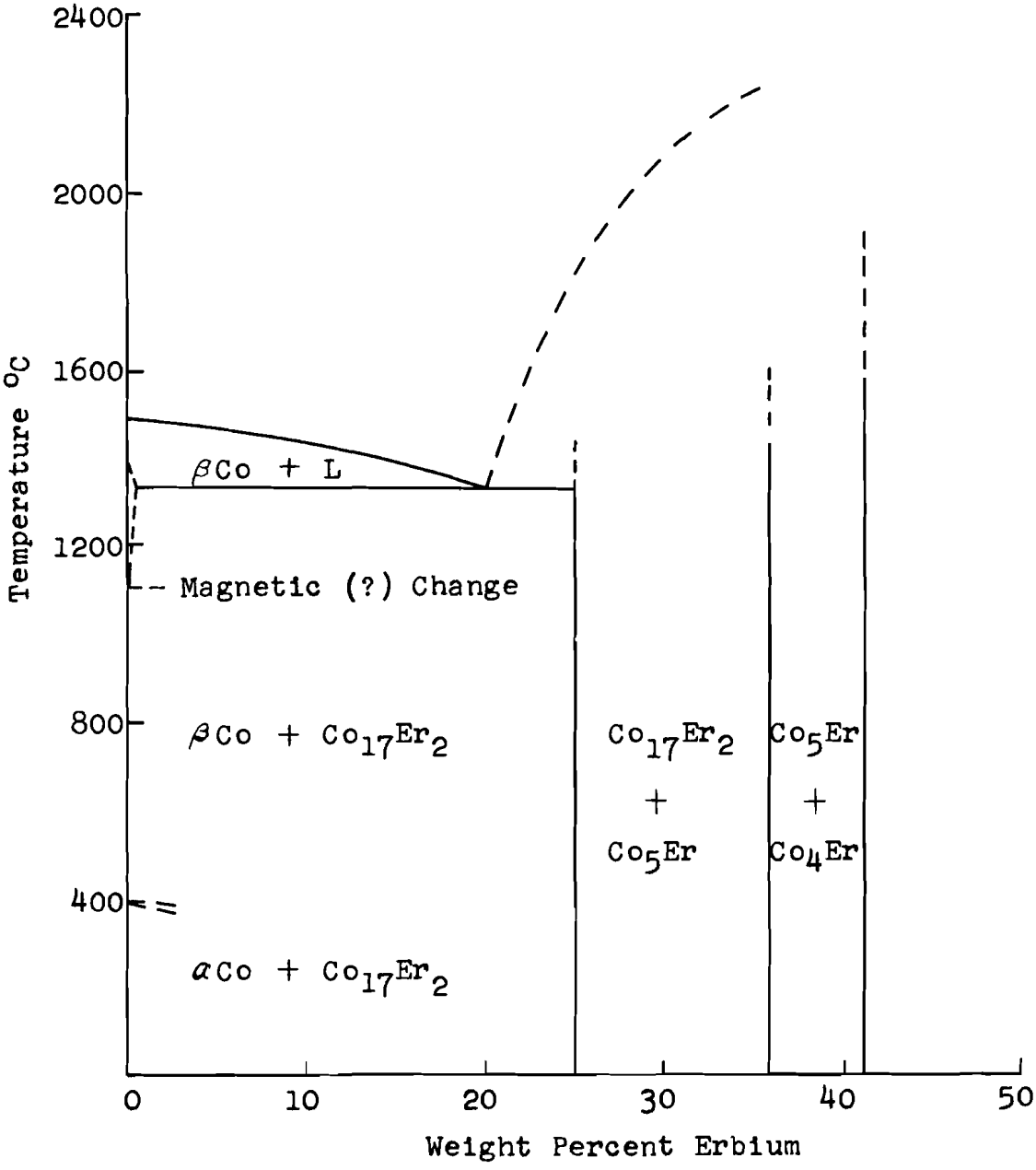

Figure 86. Partial Constitutional Diagram for the Cobalt - Erbium System

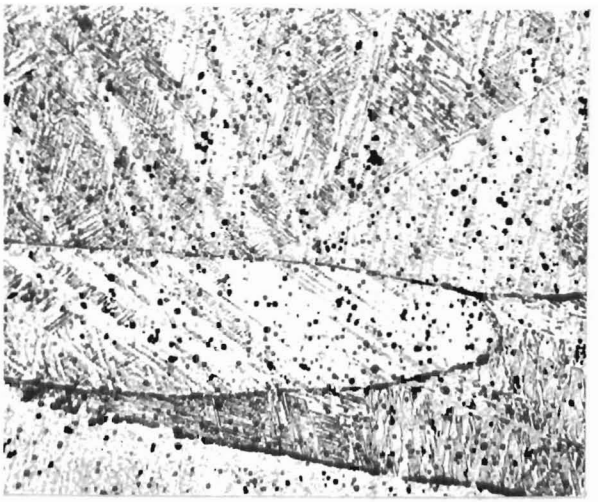

3099

Figure 87. Cobalt metal, 98-99% grade, as arc-melted. Electro-polished, 150X.

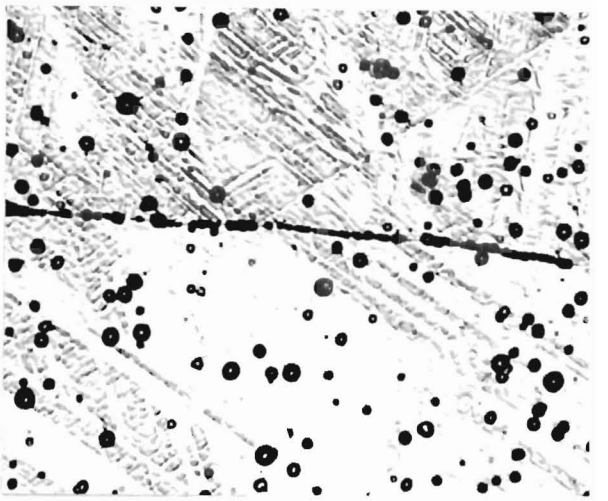

3100

Figure 88. Cobalt metal, 98-99% grade, as arc-melted. Electro-polished. 500X.

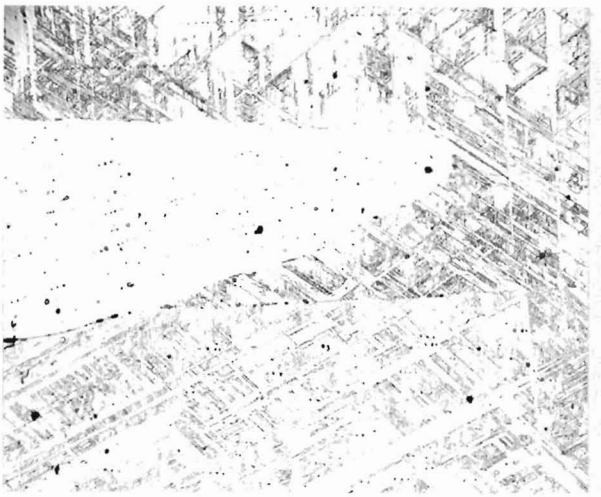

3109

Figure 89. Cobalt-$\frac{1}{4}$% erbium, as arc-melted. Electro-polished. 100X.

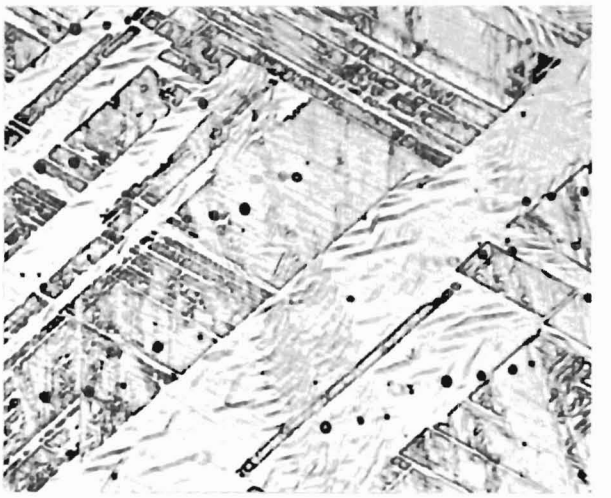

3108

Figure 90. Cobalt-$\frac{1}{4}$% erbium, as arc-melted. Electro-polished. 500X.

3110

Figure 91. Cobalt-½% erbium, as arc-melted. Primary cobalt, largely with transformed structure. Eutectic definitely visible plus an unexplained banded structure present in one small area only. Electro-polished. 100X.

3111

Figure 92. Cobalt-½% erbium, as arc-melted. Detail of eutectic and banded structure. Electro-polished. 500X.

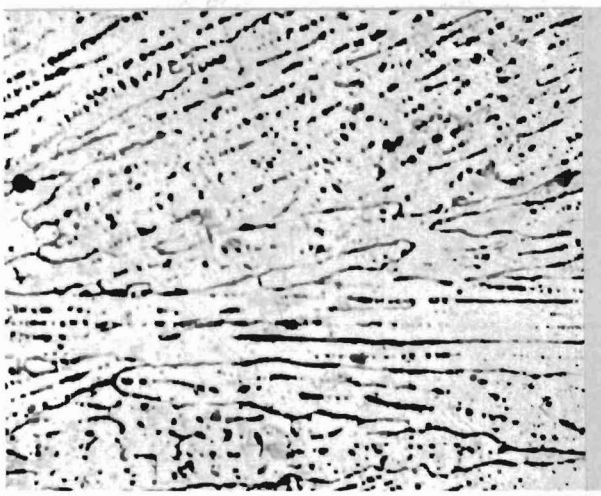

3113

Figure 93. Cobalt-1% erbium, as arc-melted. Primary cobalt plus eutectic. Electro-polished. 100X.

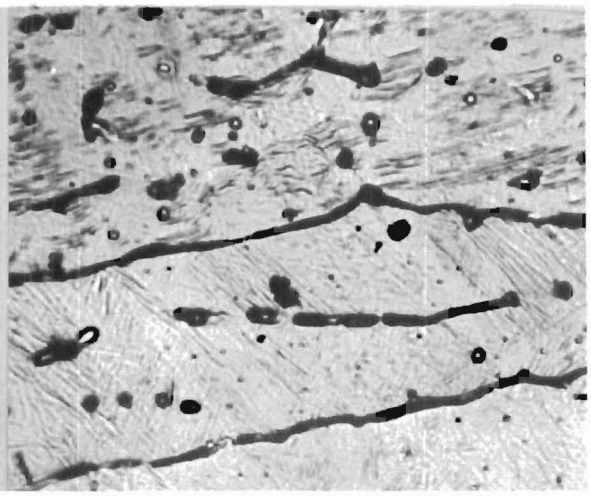

3112

Figure 94. Cobalt-1% erbium, as arc-melted. Primary cobalt plus eutectic. Transformation structure still visible in primary grains. Electro-polished. 500X.

3172

Figure 95. Cobalt-5% erbium, as arc-melted. Primary dendritic cobalt with eutectic. Electro-polished. 100X.

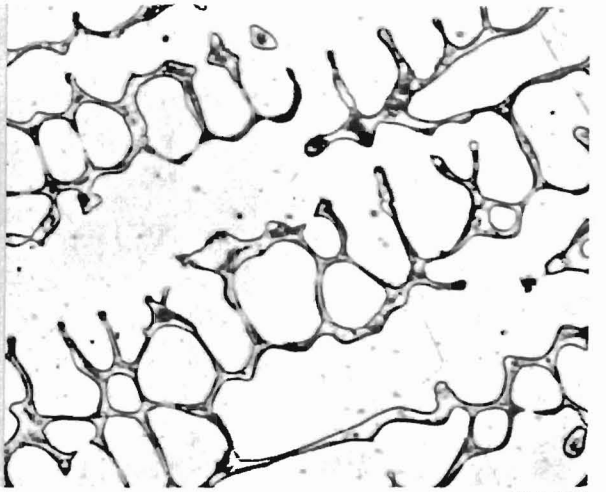

3173

Figure 96. Cobalt-5% erbium, as arc-melted. Primary dendritic cobalt with eutectic. Transformed structure no longer visible in cobalt grains. Electro-polished. 500X.

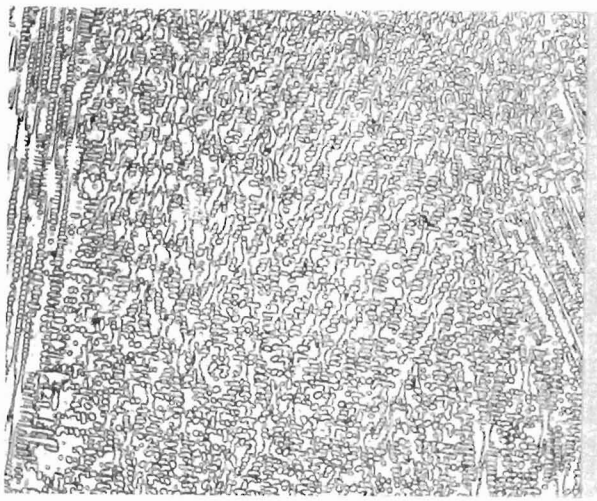

3179

Figure 97. Cobalt-15% erbium, as arc-melted. Dendritic cobalt in eutectic. Electro-polished. 100X.

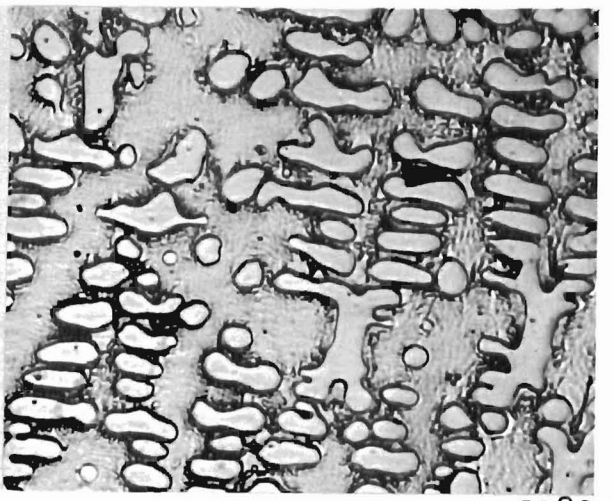

3180

Figure 98. Cobalt-15% erbium, as arc-melted. Dendritic cobalt in eutectic. Electro-polished. 500X.

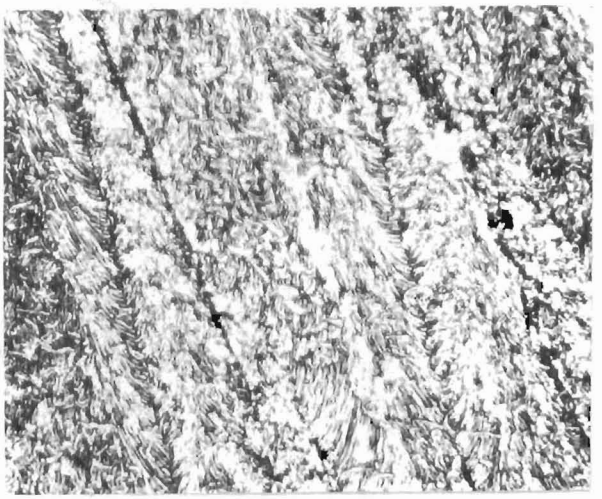

3178

Figure 99. Cobalt-20% erbium, as arc-melted. This composition is very near to 100% eutectic. Electro-polished. 750X.

2808

Figure 100. Cobalt-25% erbium, as arc-melted. Compound plus eutectic. Cobalt #1 etch (60 ml hydrochloric, 15 ml nitric, and 15 ml acetic acids with 15 ml distilled water). 100X.

3184

Figure 101. Cobalt-25% erbium, as arc-melted. Detail of eutectic rich region. Electro-polished. 750X.

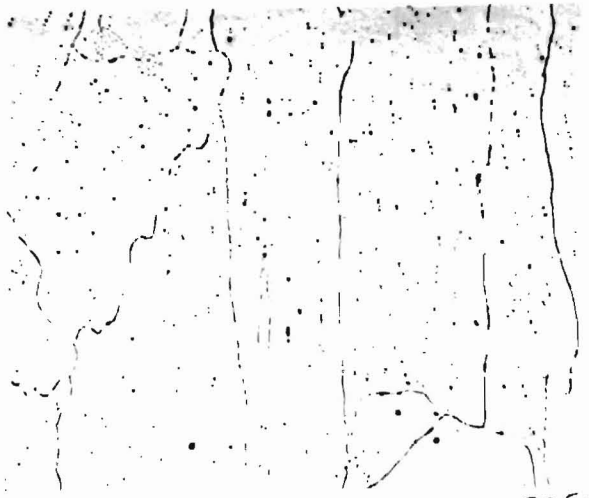

3169

Figure 102. Cobalt-$\frac{1}{4}$% yttrium, as arc-melted. Primary cobalt plus eutectic. Electro-polished. 100X.

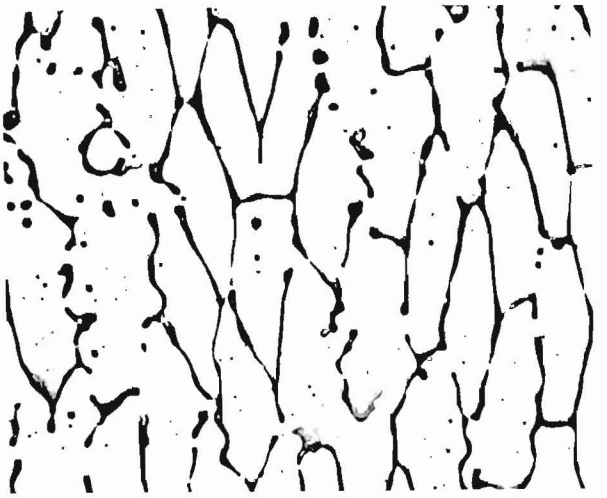

3104

Figure 103. Cobalt-1% yttrium, as arc-melted. Primary cobalt plus eutectic. Electro-polished. 250X.

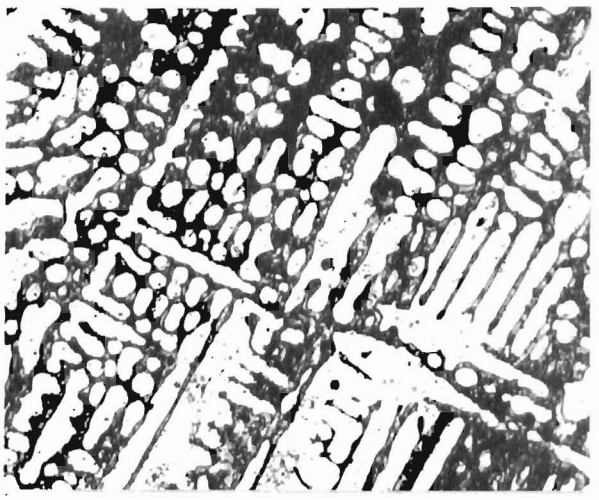

3093

Figure 104. Cobalt-5% yttrium, as arc-melted. Dendritic cobalt grains in eutectic. Unetched. 500X.

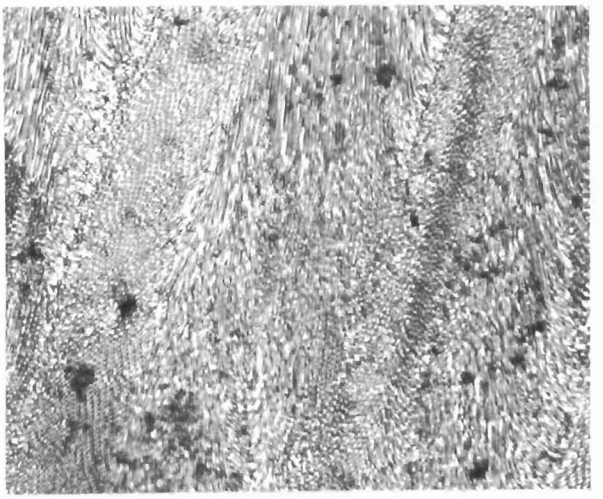

3171

Figure 105. Cobalt-10% yttrium, as arc-melted. Eutectic structure. Electro-polished. 750X.

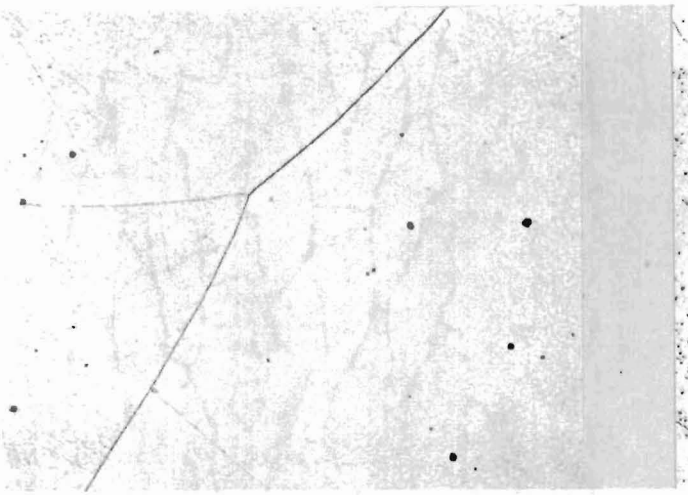

3195

Figure 106. Nickel, as arc-melted. Electro-polished, Carapella's etch. 250X.

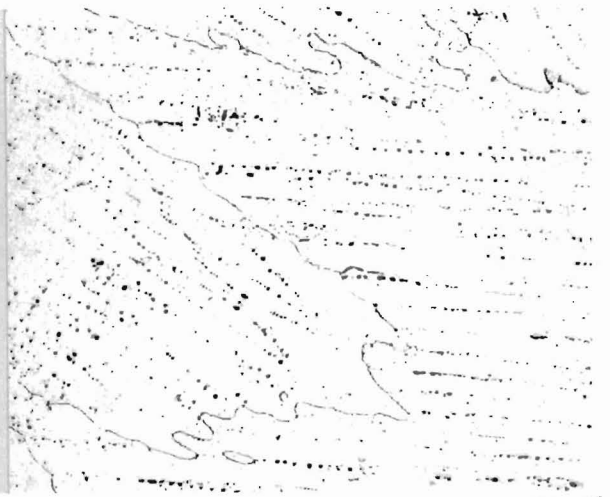

3196

Figure 107. Nickel-$\frac{1}{4}$% yttrium, as arc-melted. Primary nickel with small amount of second phase eutectic. Electro-polished, Carapella's etch. 100X.

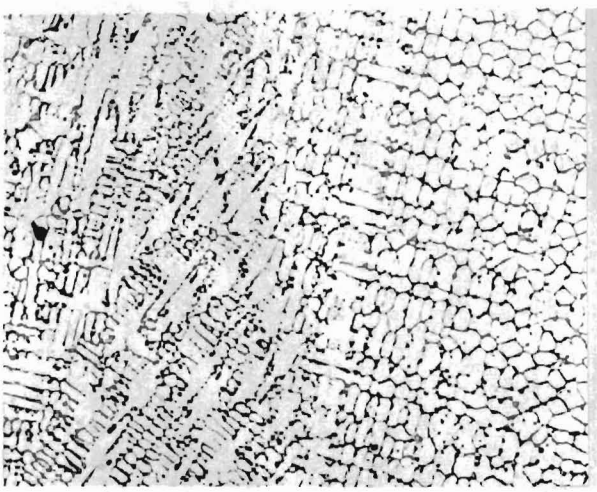

3200

Figure 108. Nickel-1% yttrium, as arc-melted. Dendritic primary nickel plus eutectic. Electro-polished, Carapella's etch. 100X.

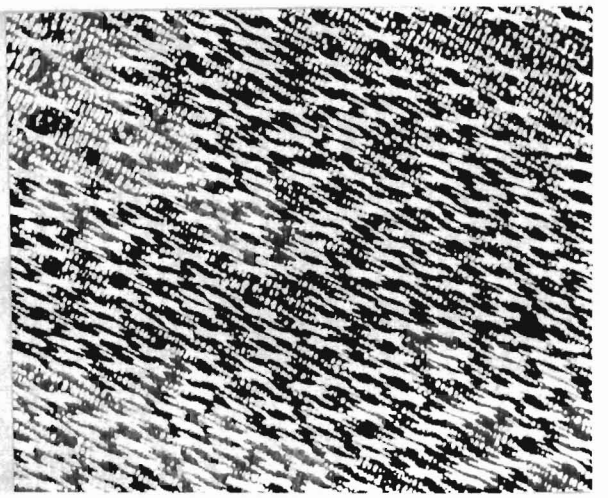

3203

Figure 109. Nickel-5% yttrium, as arc-melted. Dendritic primary nickel in eutectic. Electro-polished, Carapella's etch. 100X.

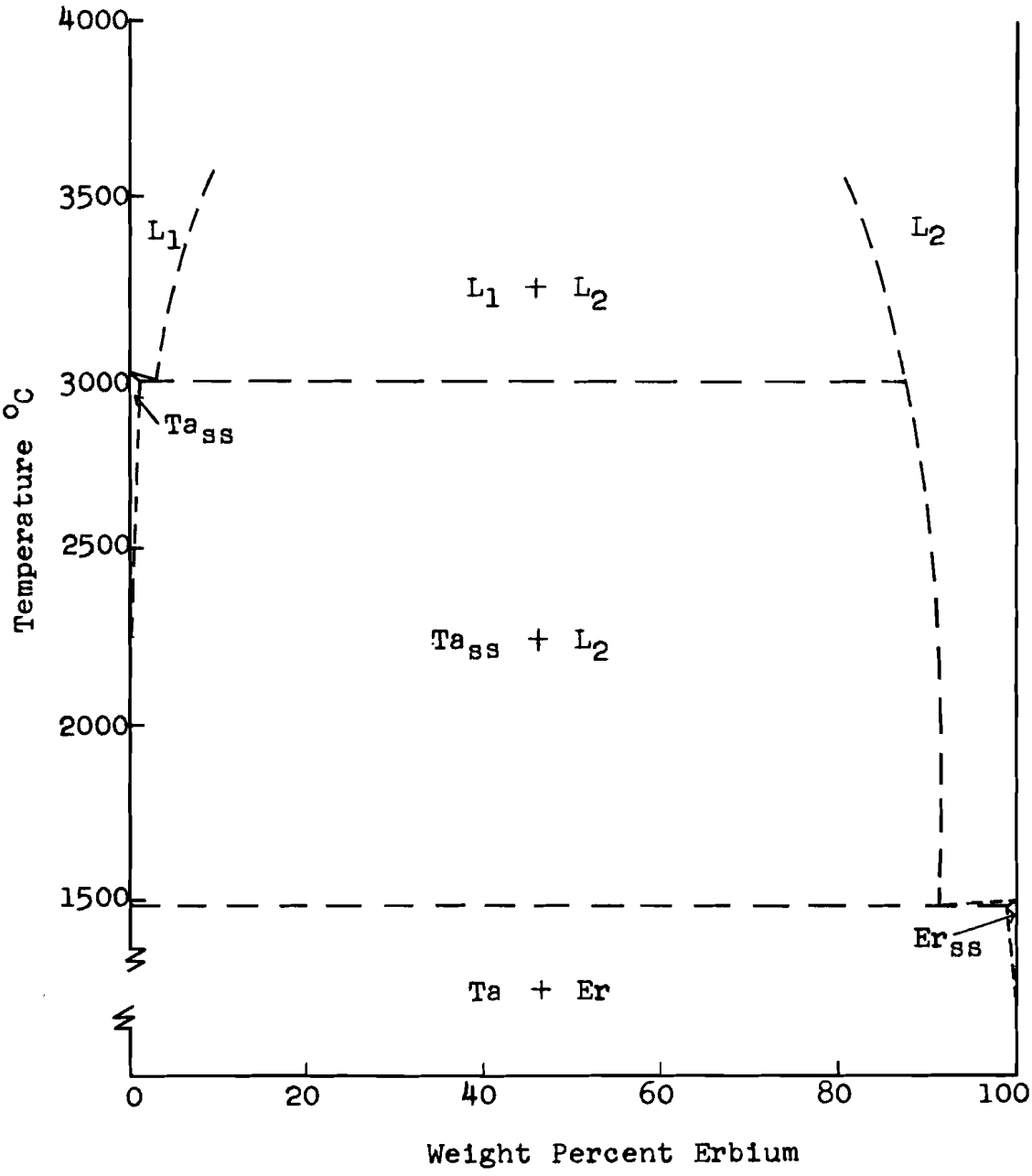

Figure 110. Tentative Constitutional Diagram for the Tantalum - Erbium System

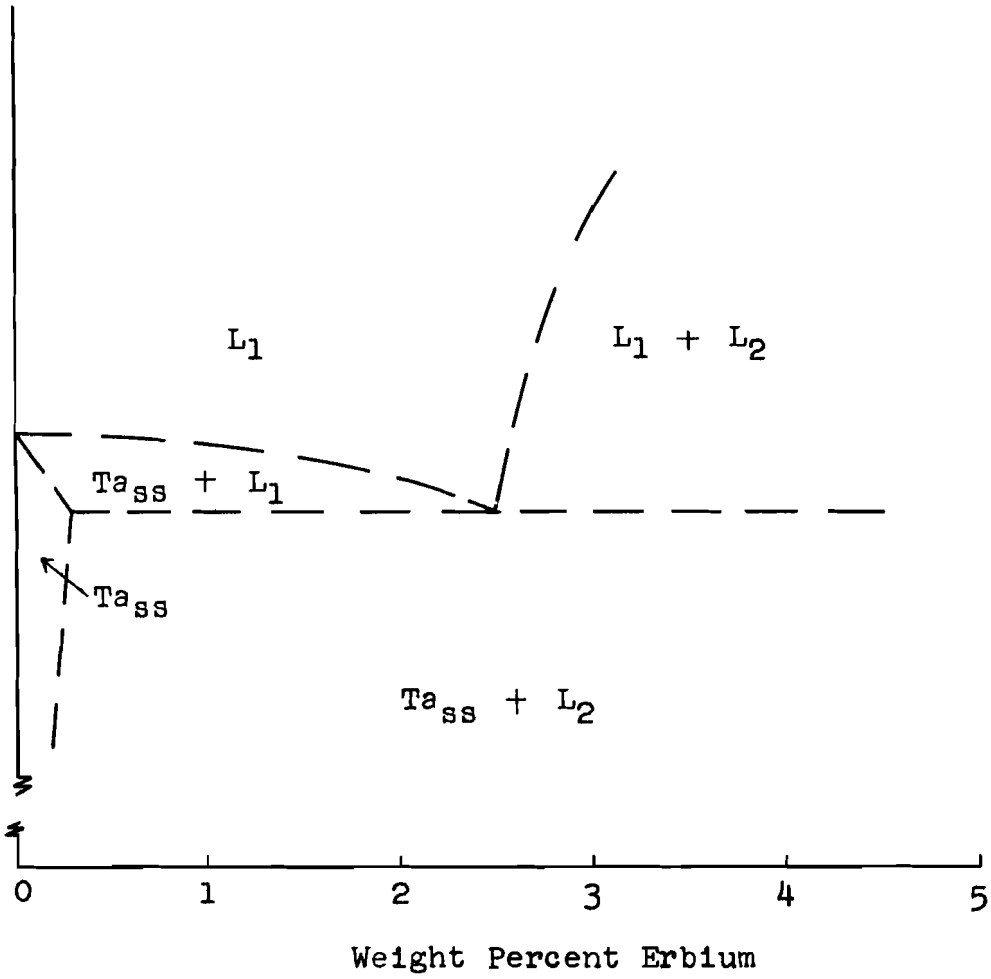

Figure 111. Tentative Constitutional Diagram for the Tantalum - Erbium System, Monotectic Detail

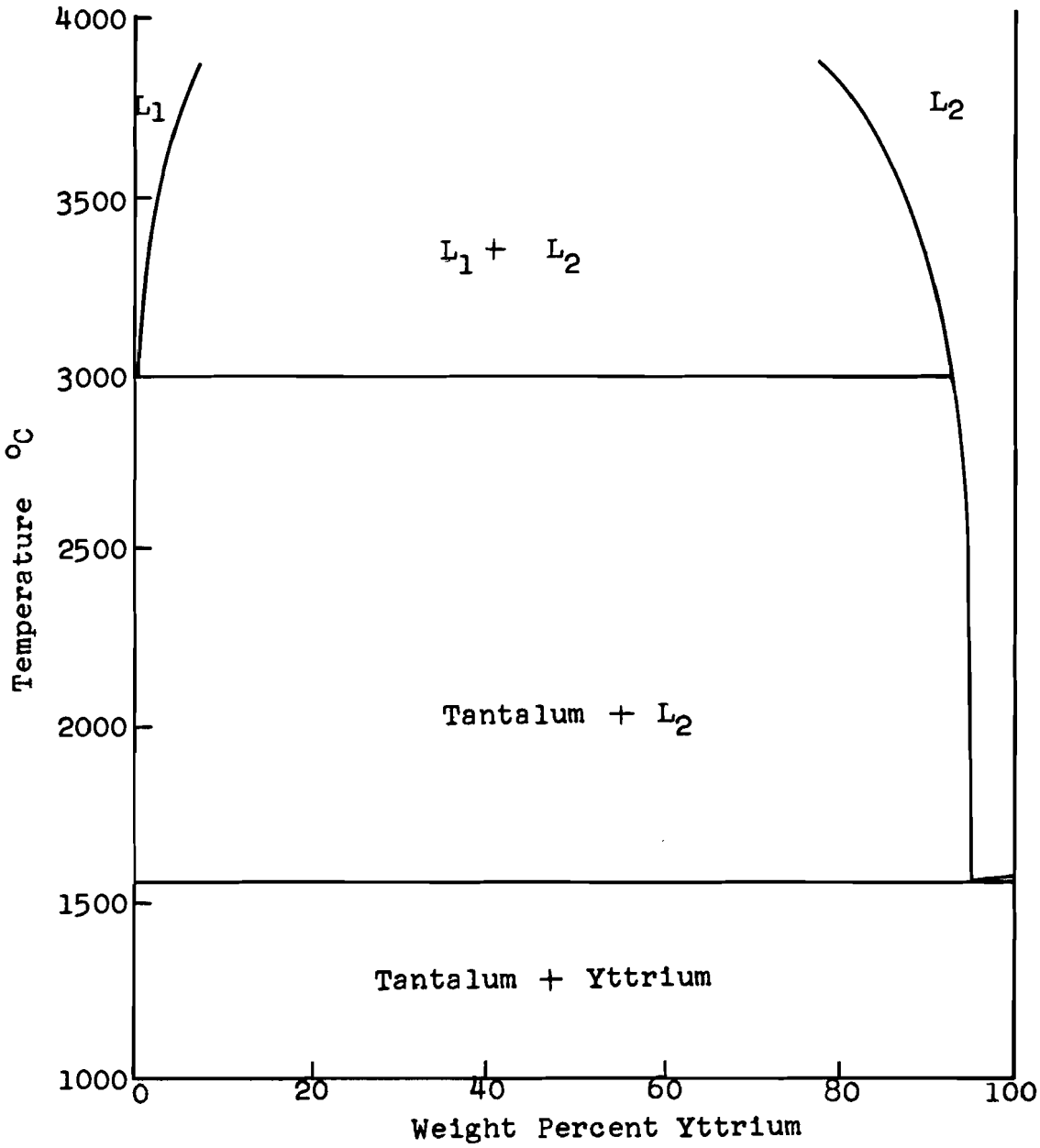

Figure 112. Constitutional Diagram for the Tantalum - Yttrium System. From Lundin (29).

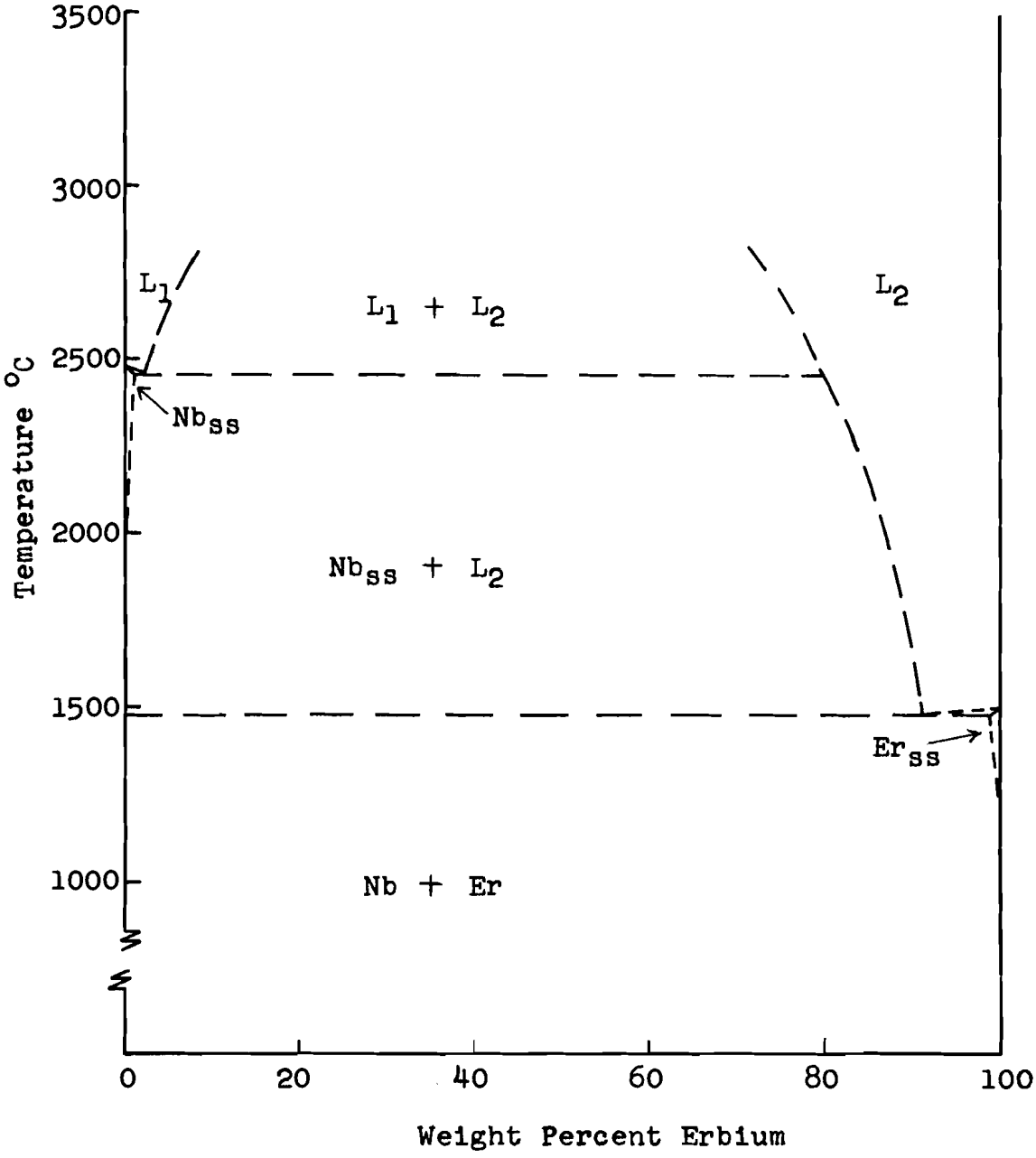

Figure 113. Tentative Constitutional Diagram for the Niobium - Erbium System

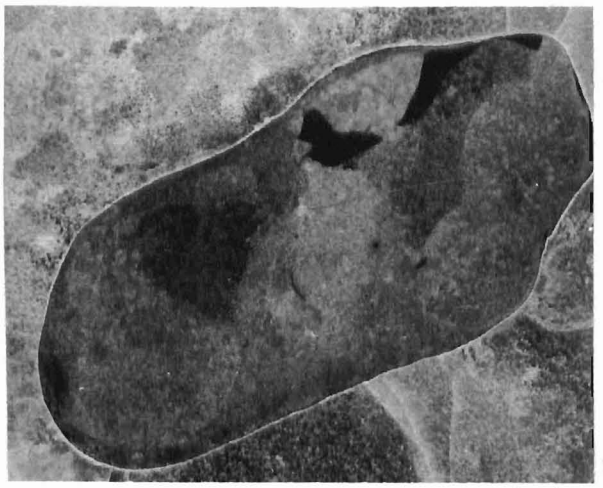

3291

Figure 114. Niobium-20% erbium (in "Lucite") as arc-melted. Black area is unmelted niobium. Light gray areas are erbium rich, dark gray areas are niobium rich. Oblique illumination. Unetched. 5X.

3322

Figure 115. Tantalum-25% erbium, as arc-melted. Interface between tantalum rich phase (light) and erbium rich phase (dark). Lactic acid chemical polish. 500X.

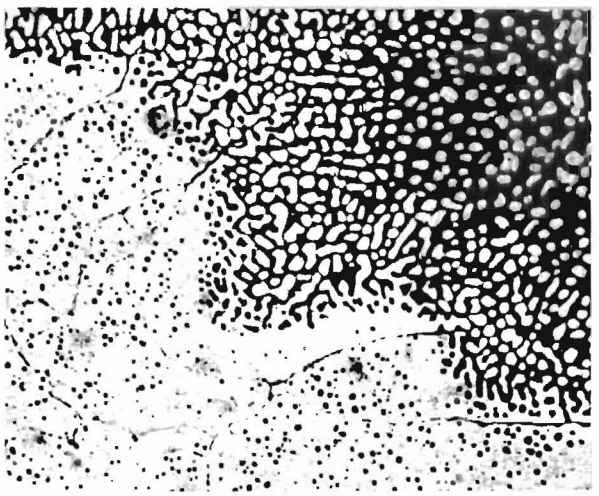

3227

Figure 116. Niobium-10% erbium, as arc-melted. Interface between niobium rich phase (light) containing entrapped erbium, and erbium rich phase (dark) containing entrapped and precipitated niobium. Unetched. 250X.

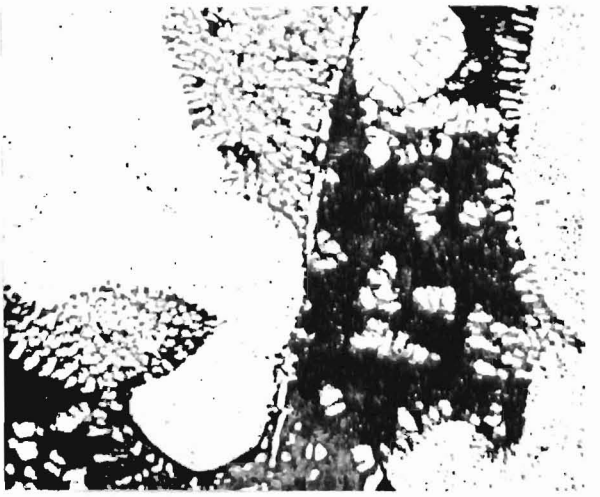

3219

Figure 117. Niobium-50% erbium, as arc-melted. Interface area showing niobium precipitated from erbium rich (dark) phase. Unetched. 250X.

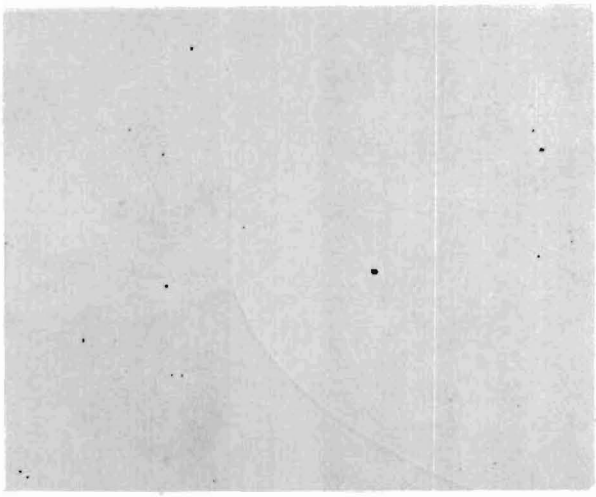

3507

Figure 118. Tantalum metal, as arc-melted. Large grains with small amount of impurity as second phase. Lactic acid chemical polish. 100X.

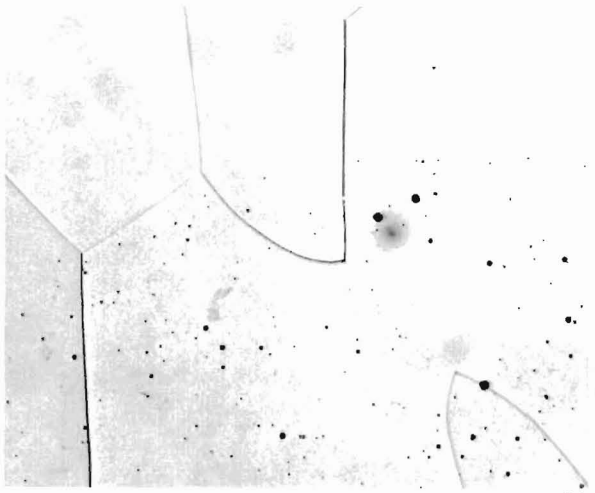

3284

Figure 119. Tantalum-0.07% erbium, as arc-melted. Large grains with erbium rich second phase. Lactic acid chemical polish. 100X.

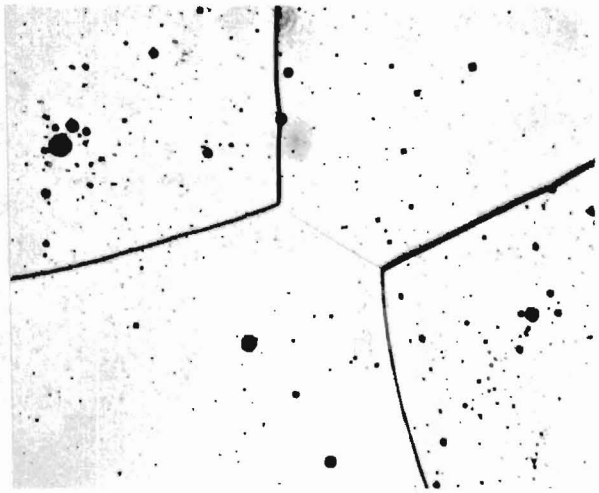

3285

Figure 120. Tantalum-0.8% erbium, as arc-melted. Large grains with erbium rich second phase. Bold grain boundaries due to physical relief between grains. Lactic acid chemical polish. 100X.

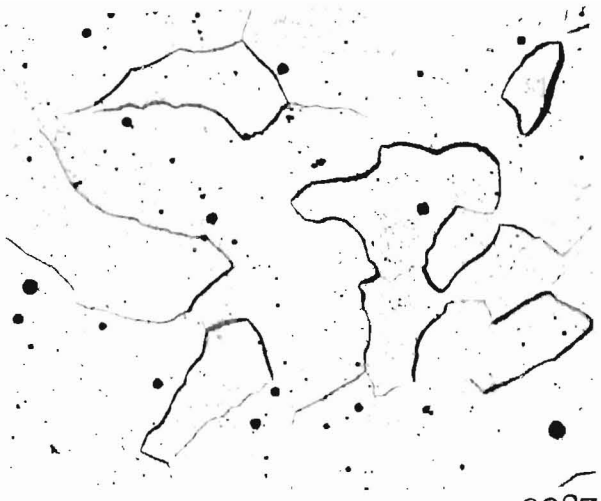

3287

Figure 121. Tantalum-1.0% erbium, as arc-melted. Grain refinement noted. Second phase observed as etch pits noted in Figures 119 and 120 and also as outlining subgrain boundaries. Lactic acid chemical polish. 100X.

3286

Figure 122. Tantalum-4% erbium, as arc-melted. Structure essentially similar to that in Figure 121. Lactic acid chemical polish. 100X.

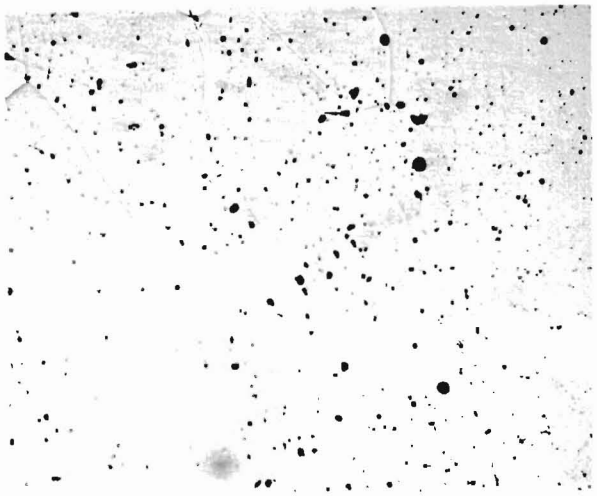

3319

Figure 123. Tantalum-4% erbium, as arc-melted. Another section of the same specimen seen in Figure 122. This portion has a structure more closely related to that observed for the lower composition alloys (Figures 119 and 120). Lactic acid chemical polish. 100X.

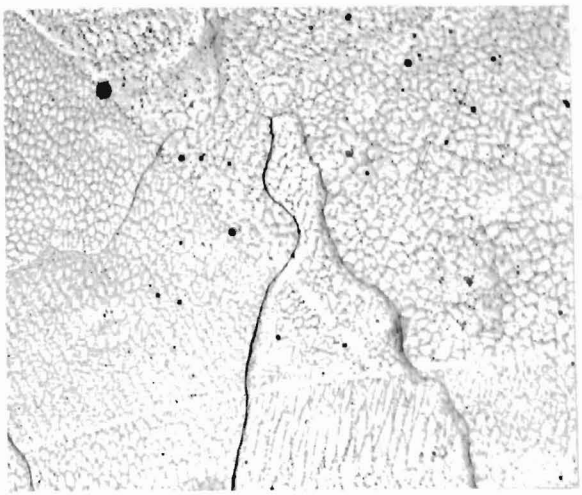

3288

Figure 124. Tantalum-15% erbium, as arc-melted. Tantalum rich liquid phase after monotectic reaction. Lactic acid chemical polish. 100X.

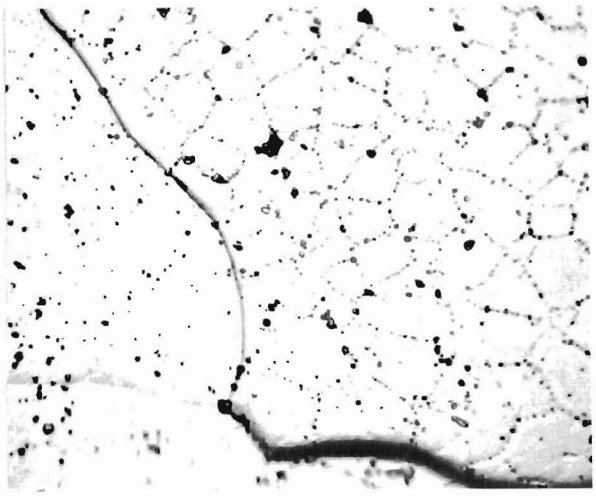

3314

Figure 125. Tantalum-15% erbium, specimen as in Figure 124. 500X.

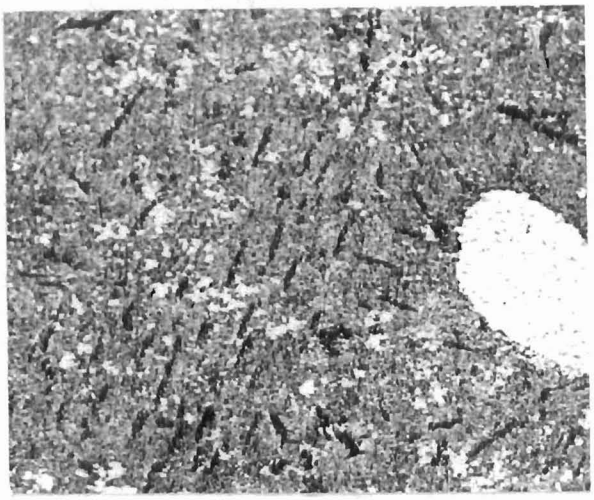

3322

Figure 126. Niobium-90% erbium as arc-melted. There is present in this structure grains of erbium metal (with oxide platelets), a globule of niobium, niobium which has precipitated either from liquid or from solid solution or both, and a structure which may be eutectic. It is not certain that this is an equilibrium structure. 500X.

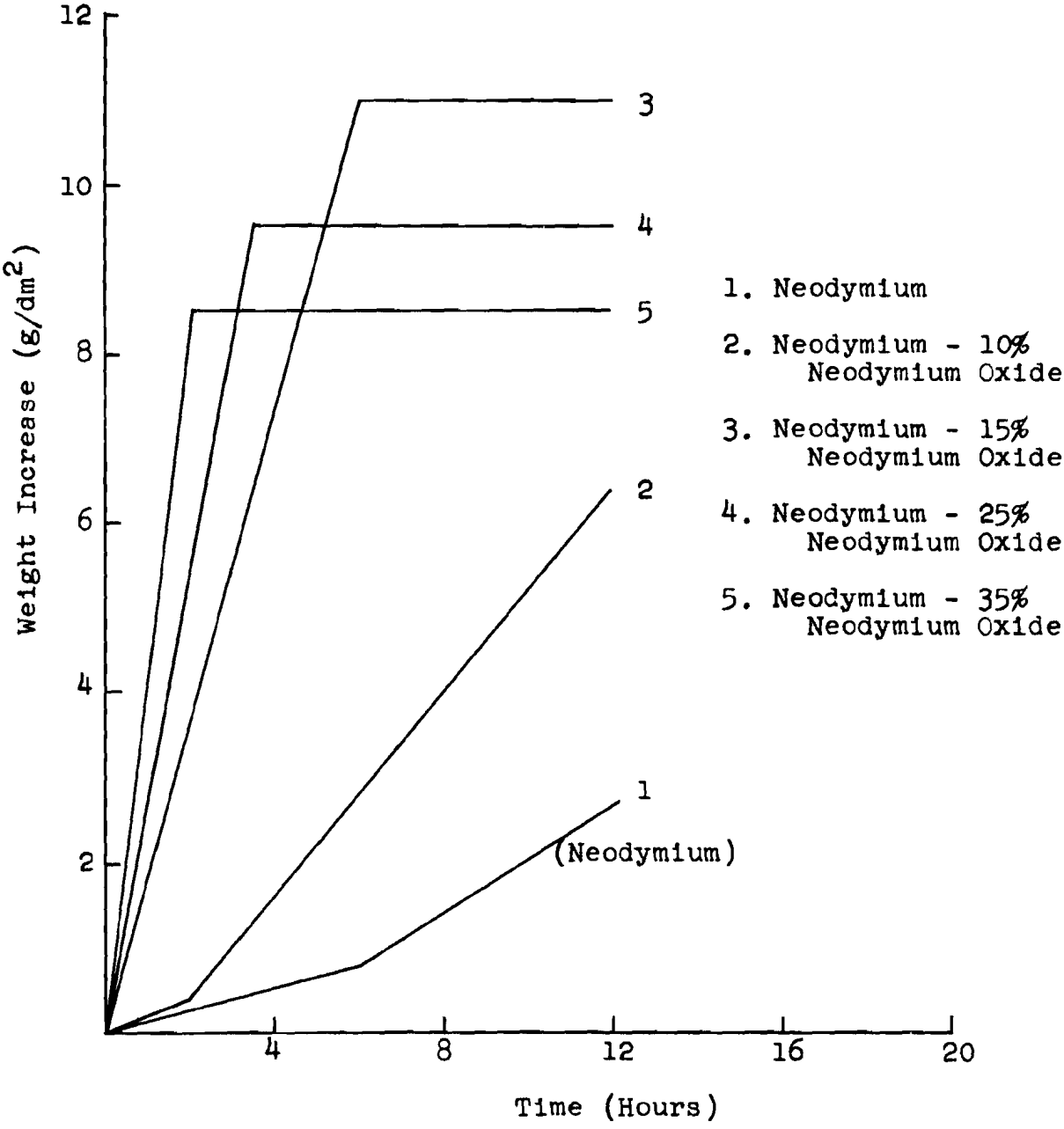

Figure 127. Atmospheric Corrosion in the Neodymium-Neodymium Oxide System. Dry Air at 600°C.

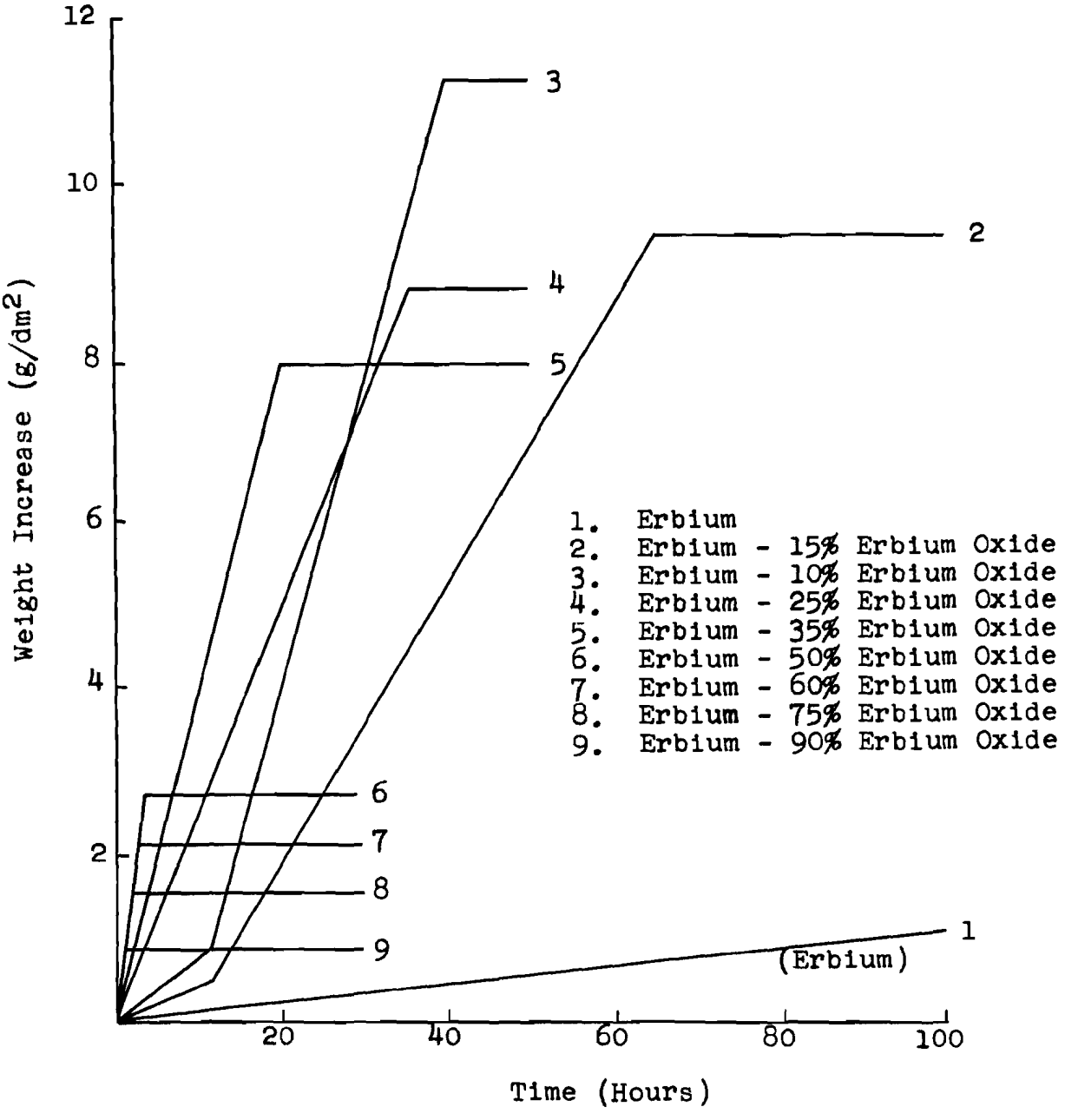

Figure 128. Atmospheric Corrosion in the Erbium - Erbium Oxide System. Dry Air at 600°C.

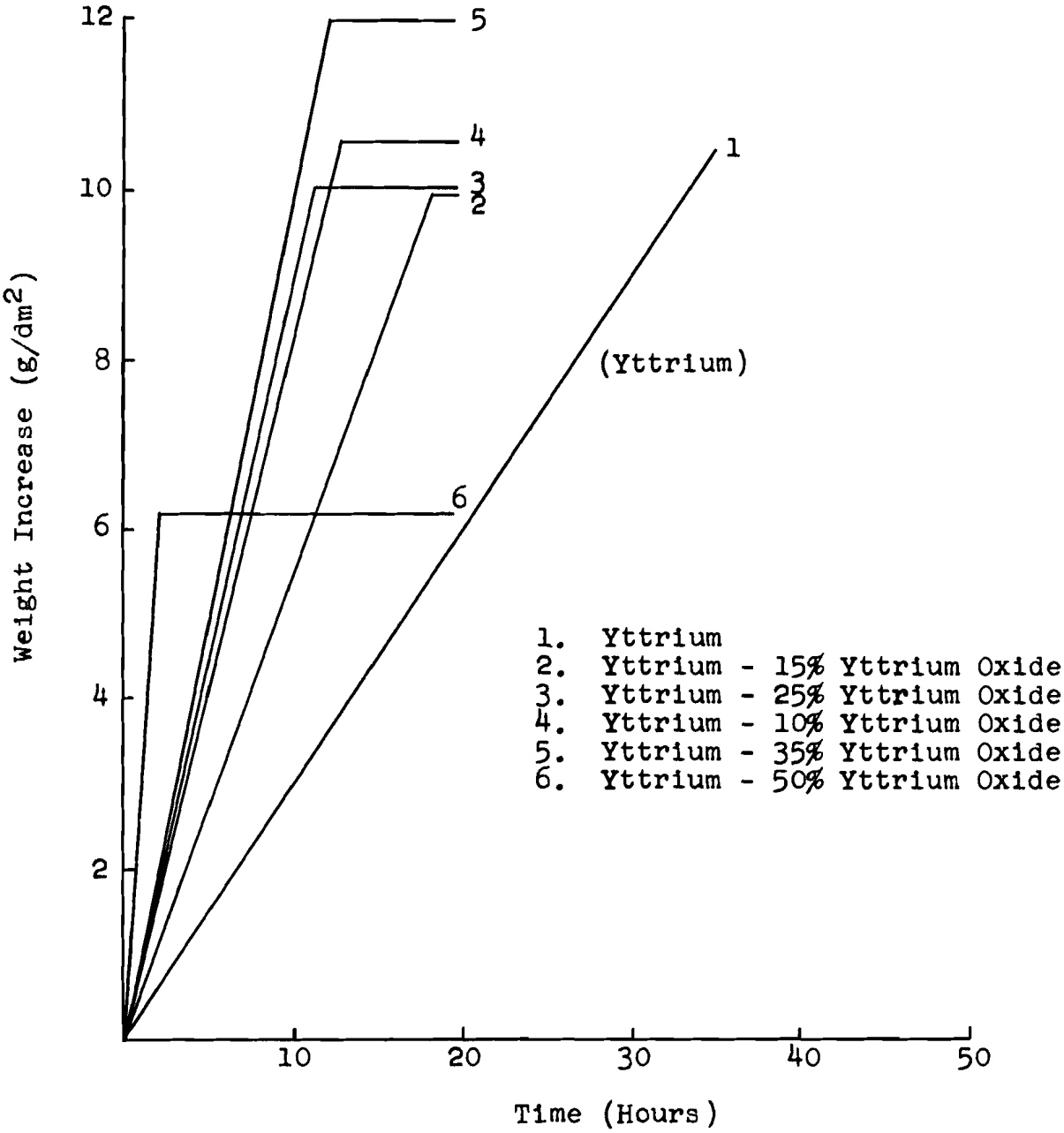

Figure 129. Atmospheric Corrosion in the Yttrium - Yttrium Oxide System. Dry Air at 600°C.

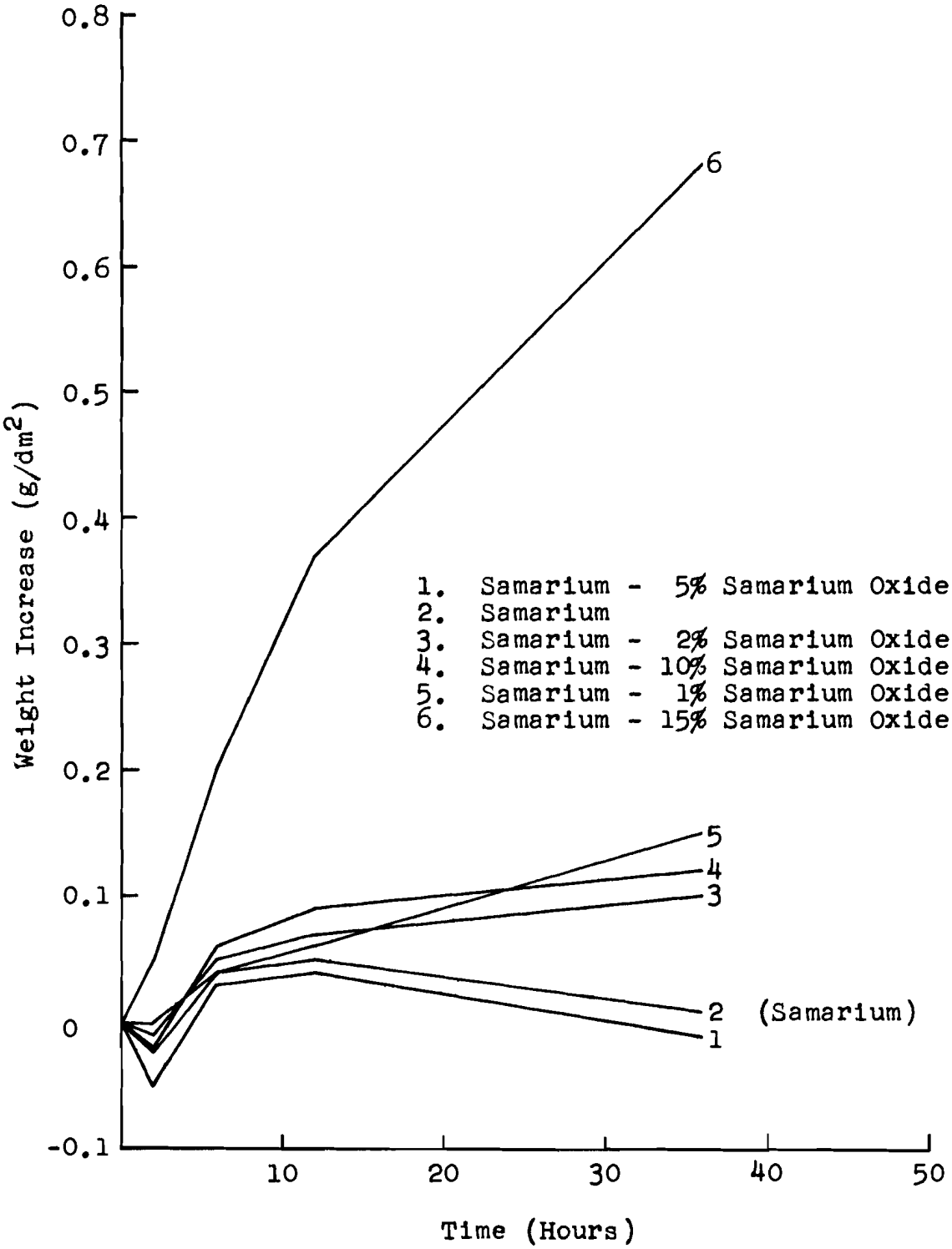

Figure 130. Atmospheric Corrosion in the Samarium - Samarium Oxide System. Dry Air at 600°C.

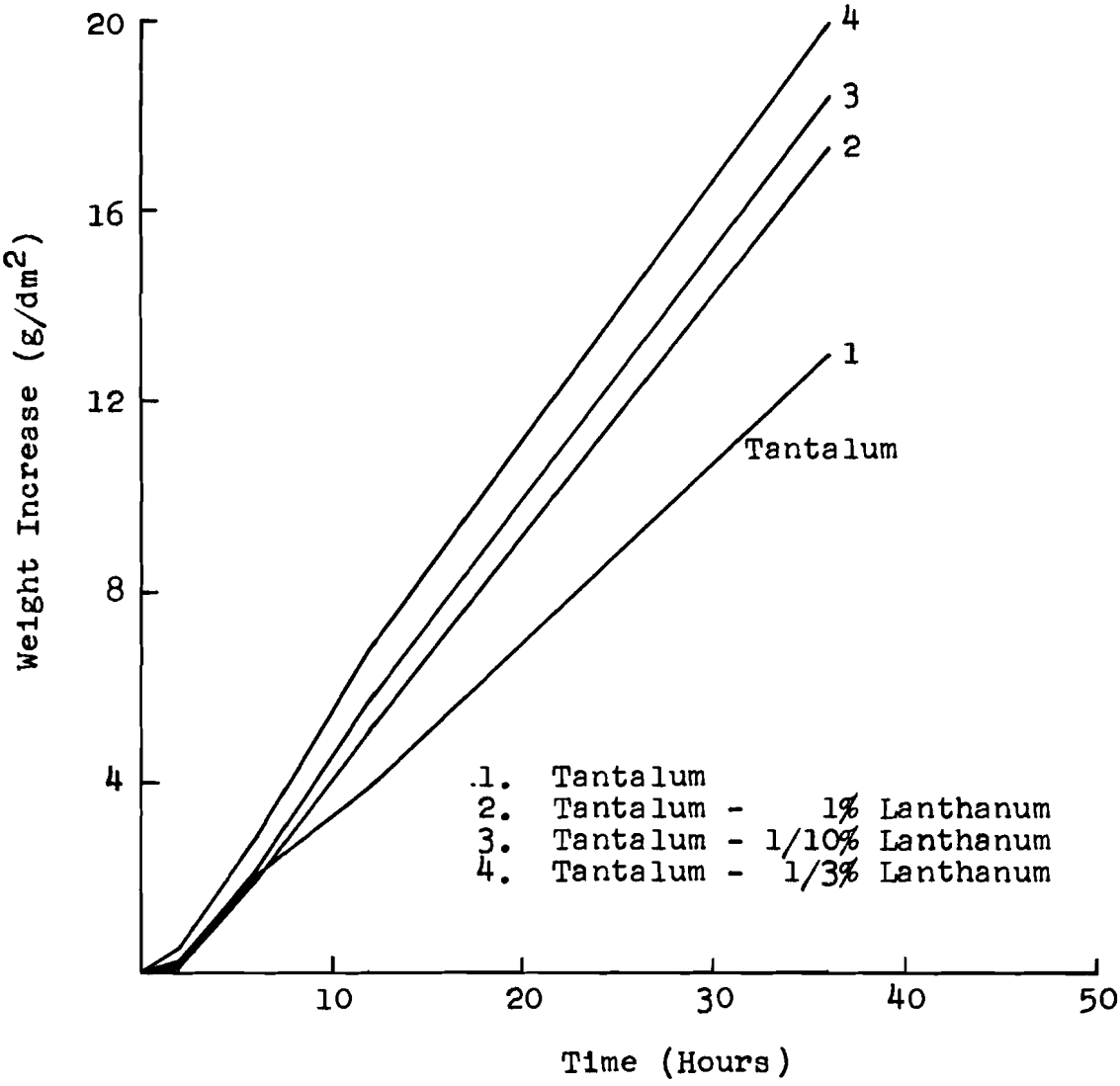

Figure 131. Atmospheric Corrosion in the Tantalum - Lanthanum System. Dry Air at 600°C.

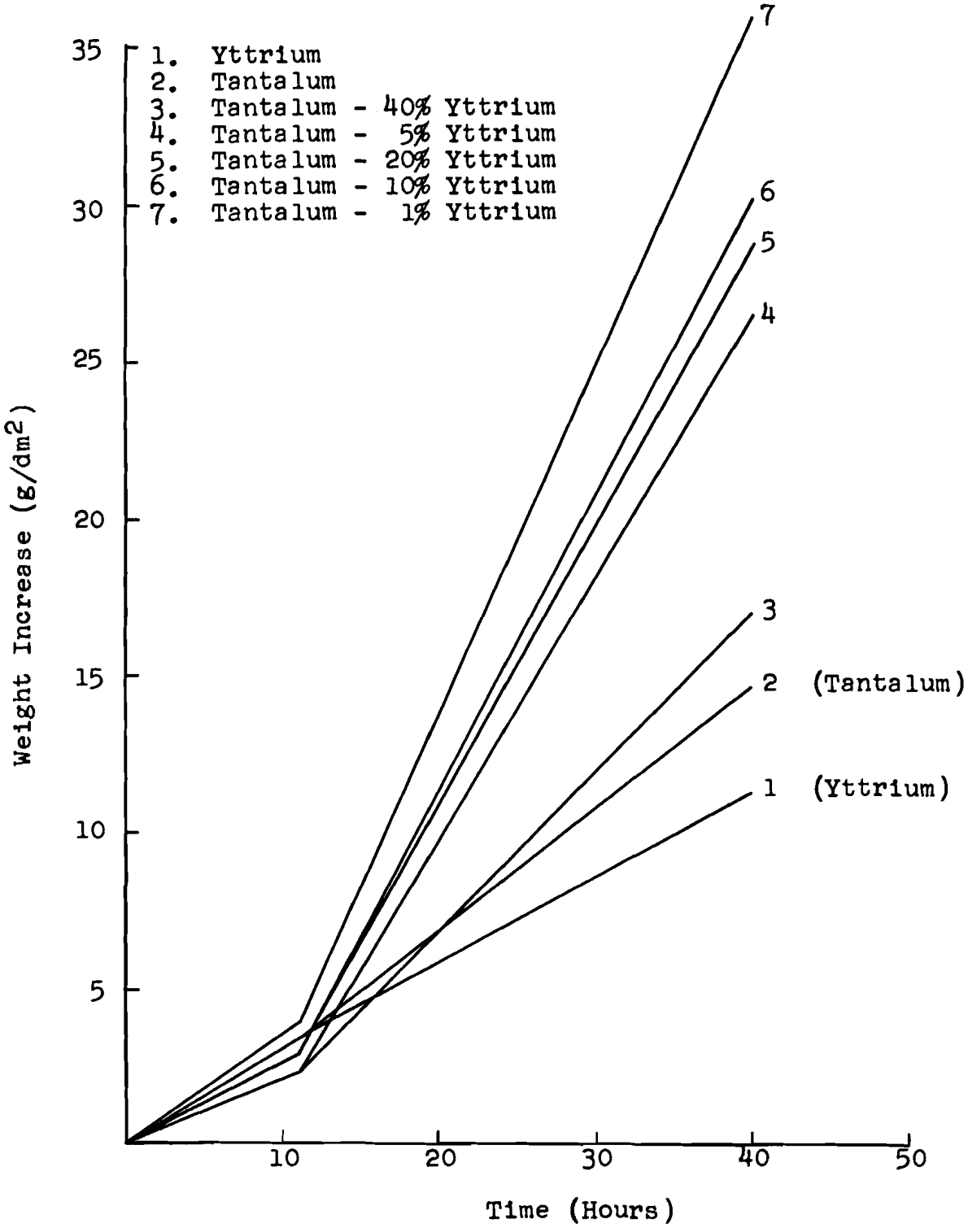

Figure 132. Atmospheric Corrosion in the Tantalum - Yttrium System. Dry Air at 600°C.

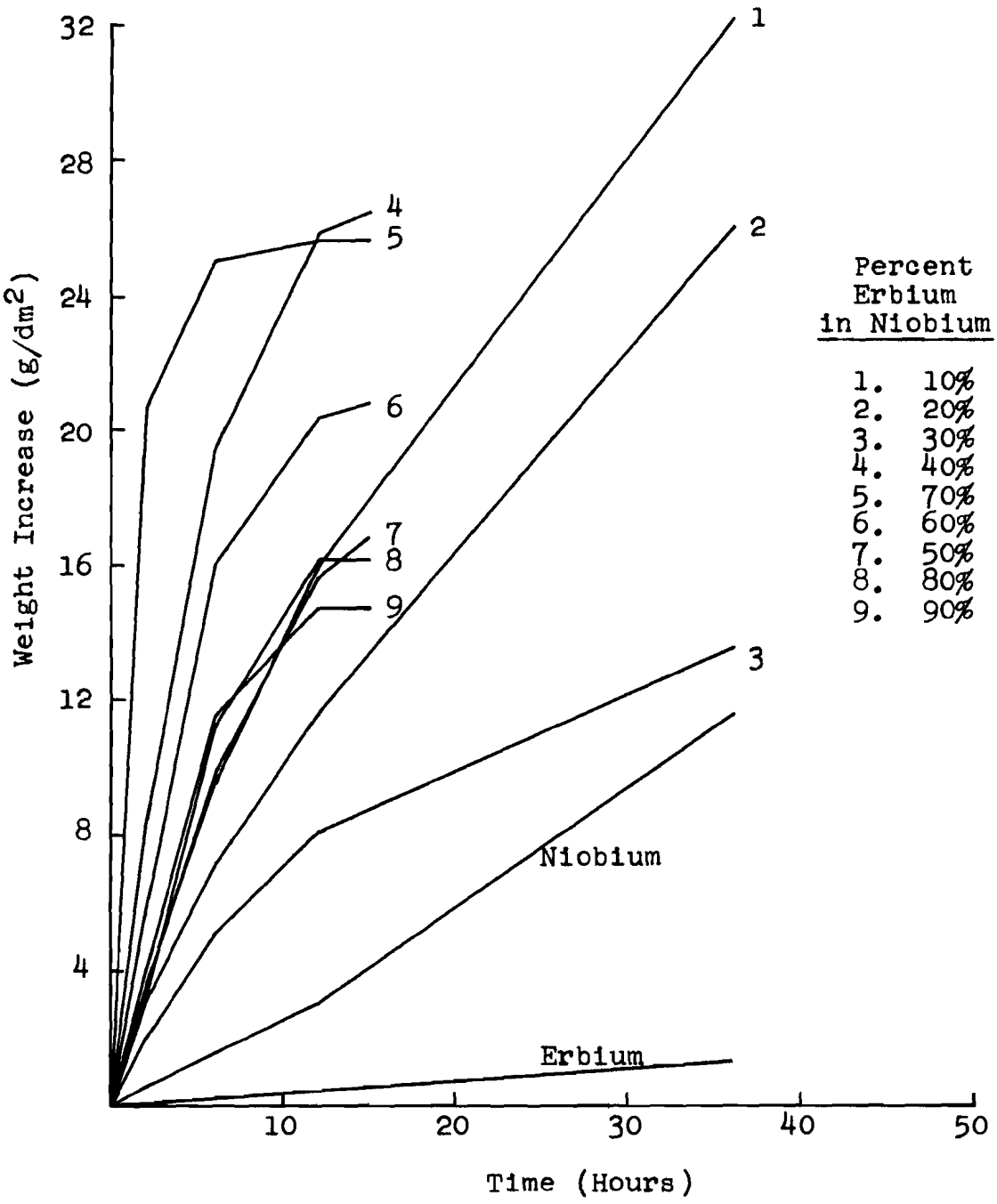

Figure 133. Atmospheric Corrosion in the Niobium - Erbium System. Dry Air at 600°C.

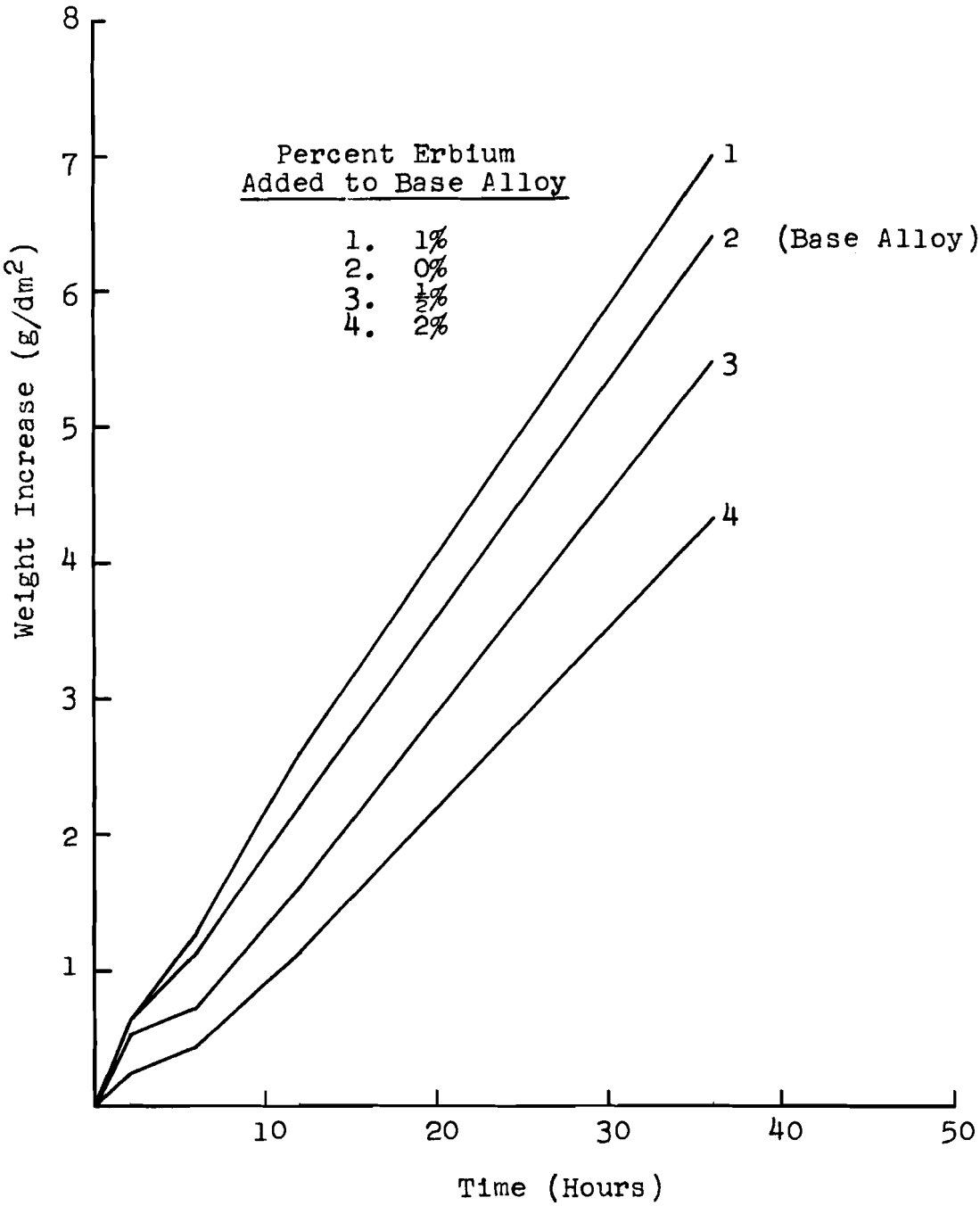

Figure 134. Atmospheric Corrosion of a Niobium Alloy Containing 15% Tungsten, 5% Molybdenum, and 2% Platinum with Erbium additions. Dry Air at 600°C.

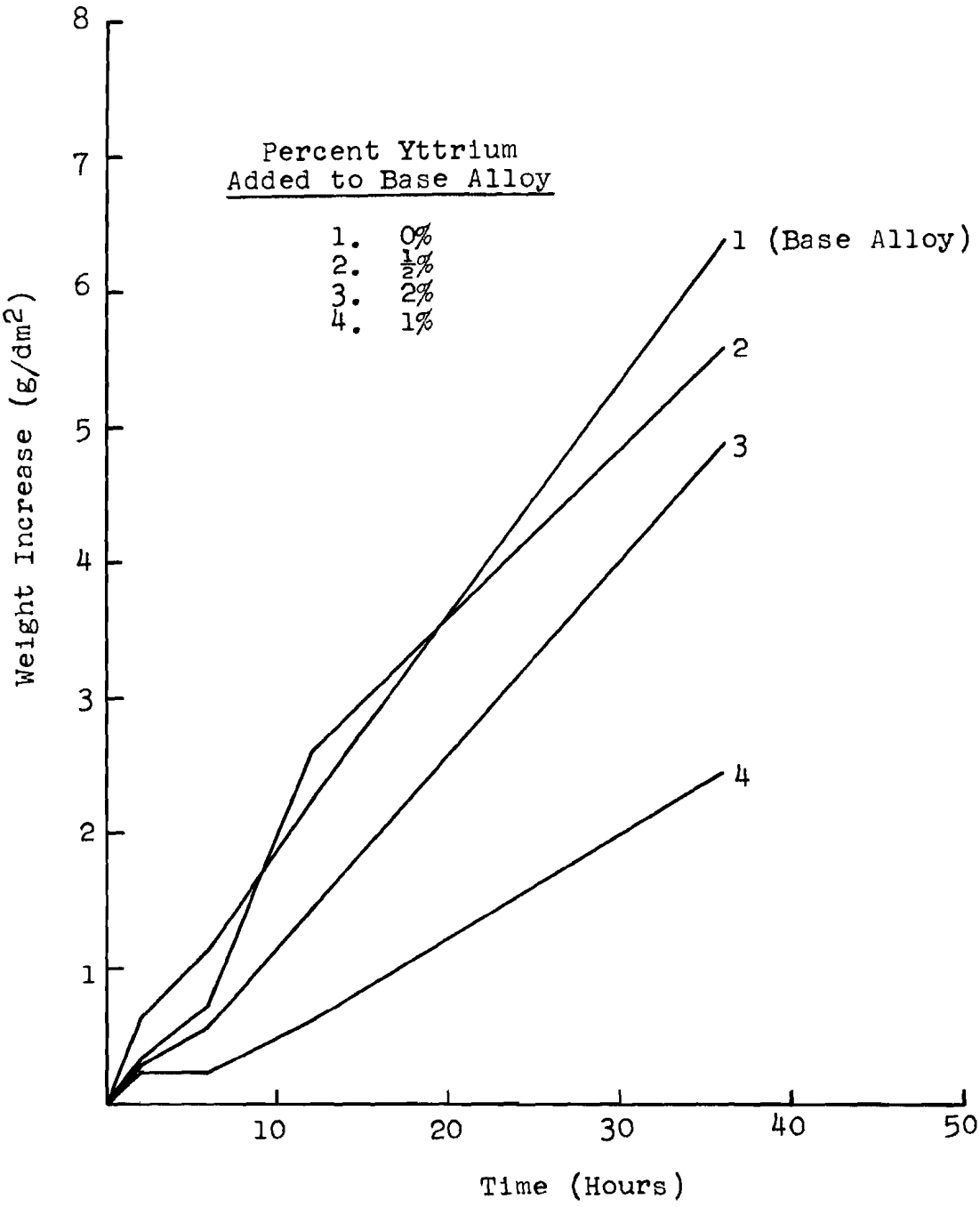

Figure 135. Atmospheric Corrosion of a Niobium Alloy Containing 15% Tungsten, 5% Molybdenum, and 2% Platinum with Yttrium additions. Dry Air at 600°C.

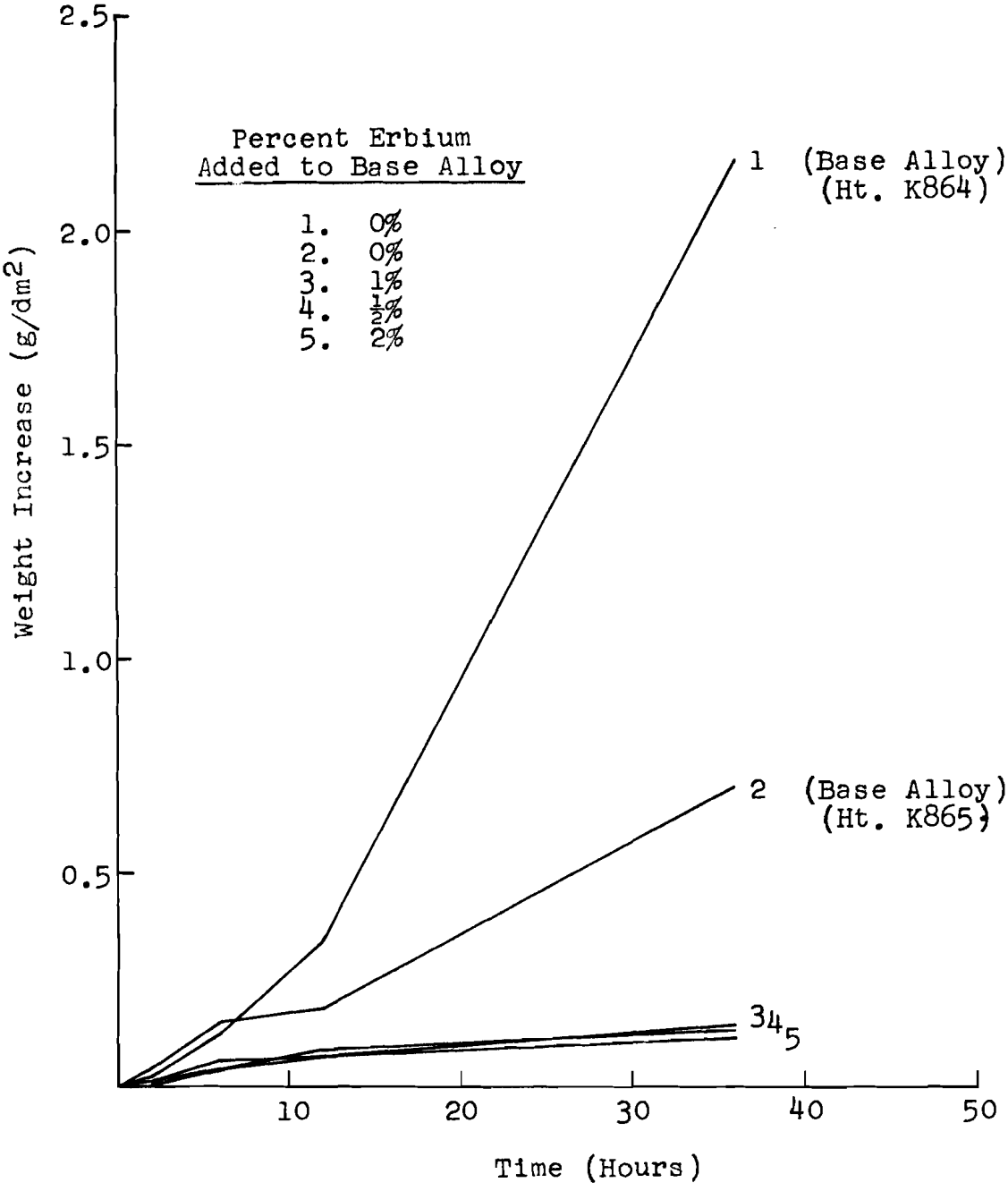

Figure 136. Atmospheric Corrosion of a Niobium Alloy Containing 20% Tungsten and 2% Titanium with Erbium Additions. Dry Air at 600°C.

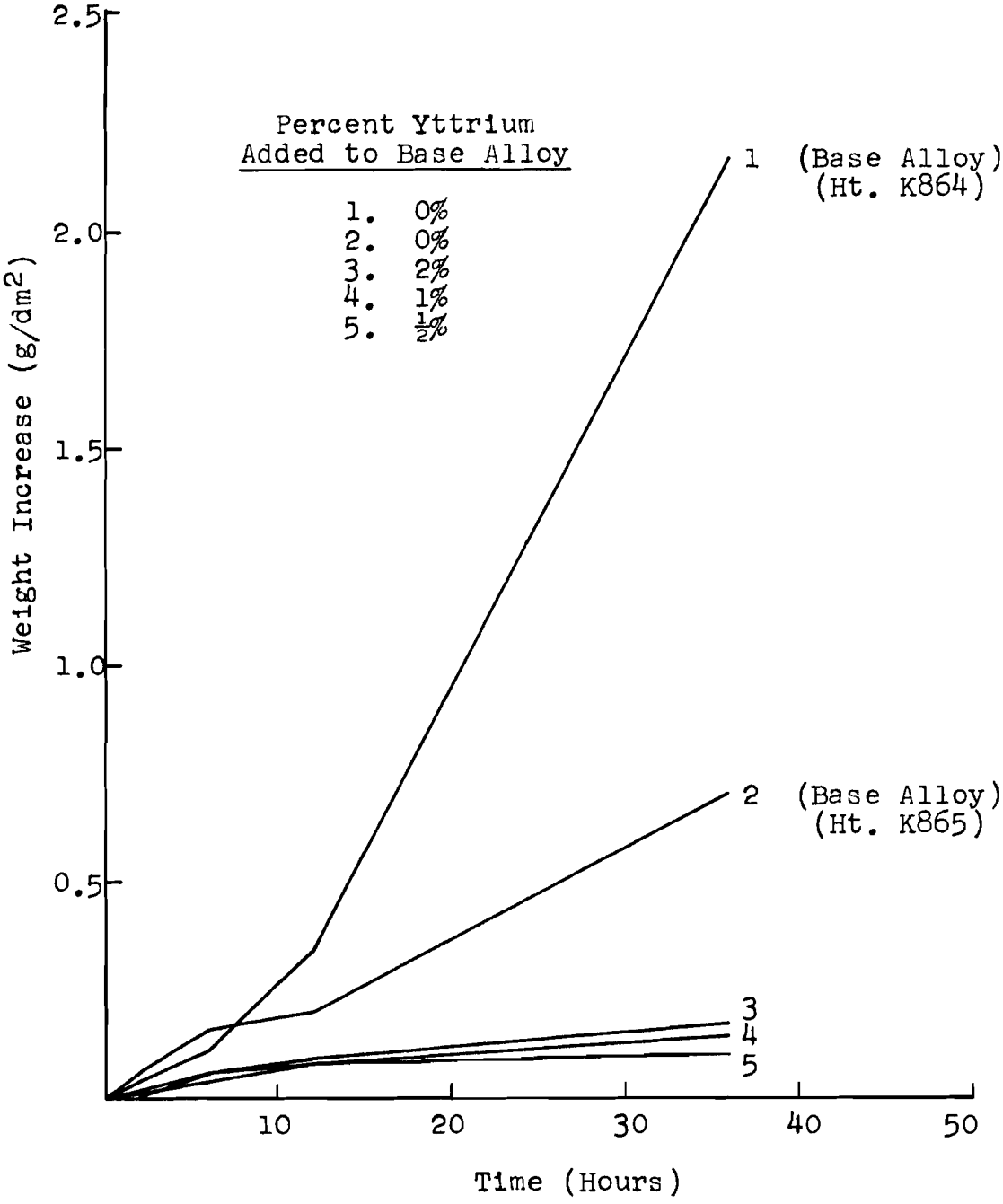

Figure 137. Atmospheric Corrosion of a Niobium Alloy Containing 20% Tungsten and 2% Titanium with Yttrium Additions. Dry Air at 600°C.

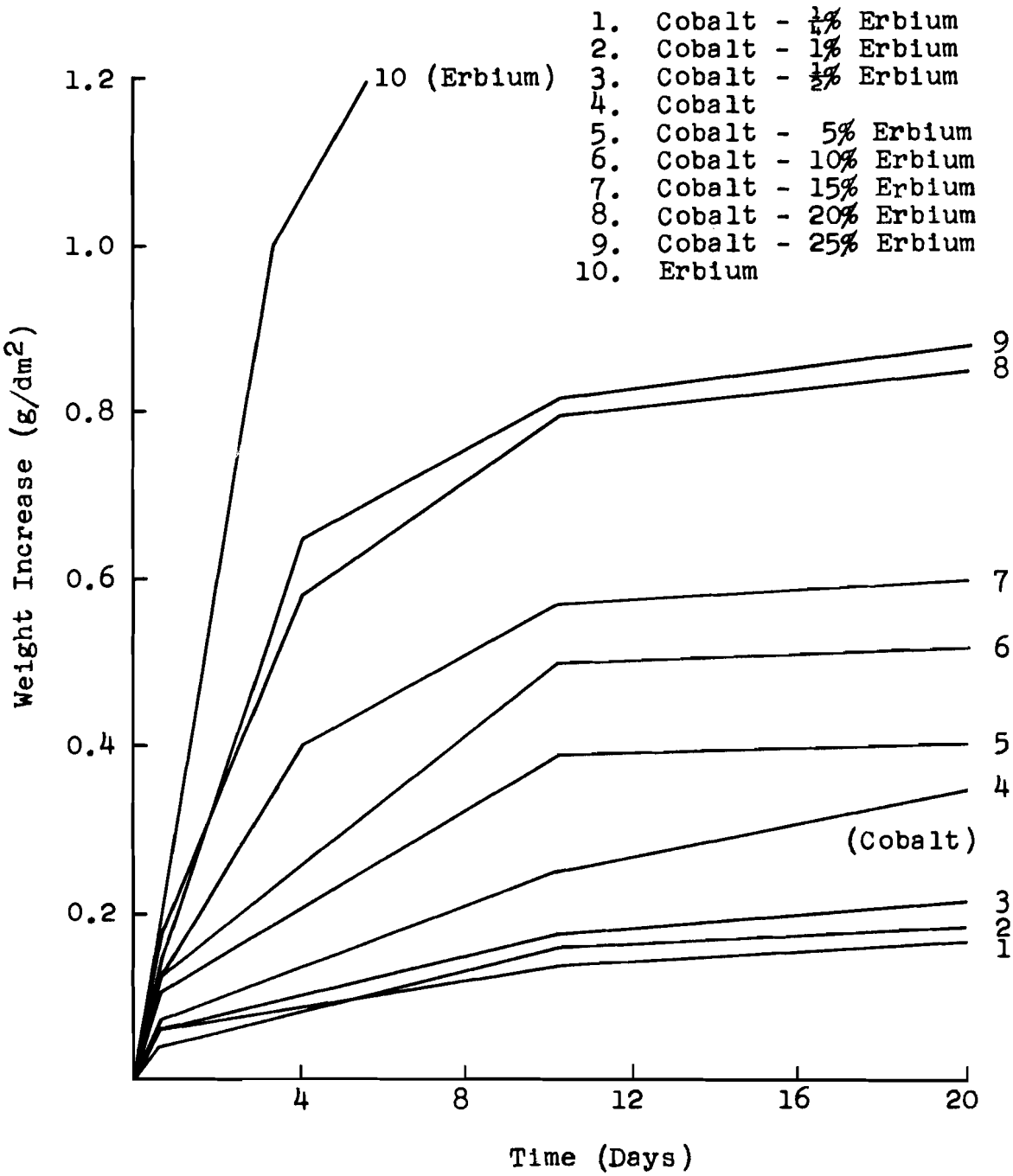

Figure 138. Atmospheric Corrosion in the Cobalt - Erbium System. Dry Air at 600°C.

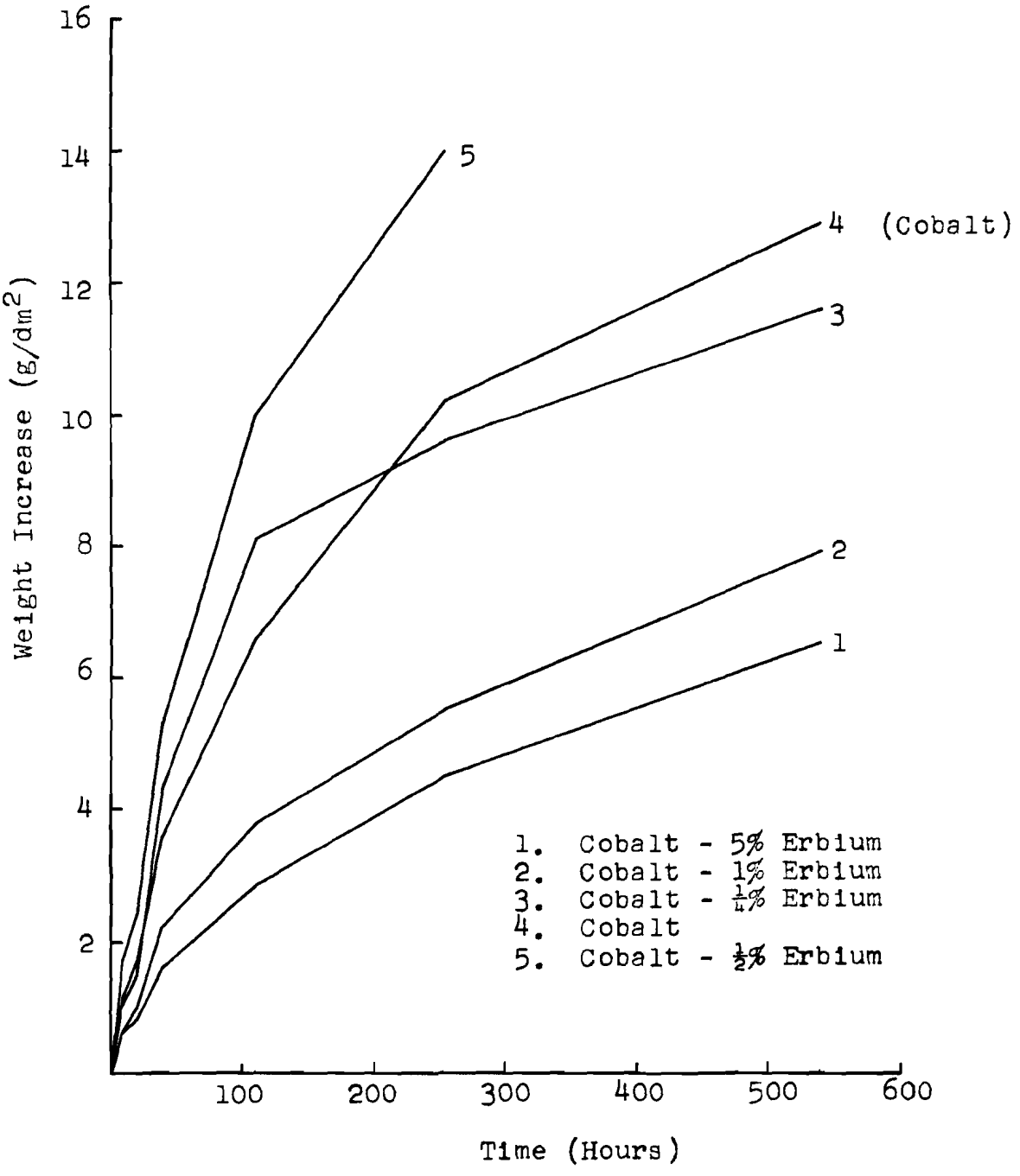

Figure 139. Atmospheric Corrosion in the Cobalt - Erbium System. Dry Air at 900°C.

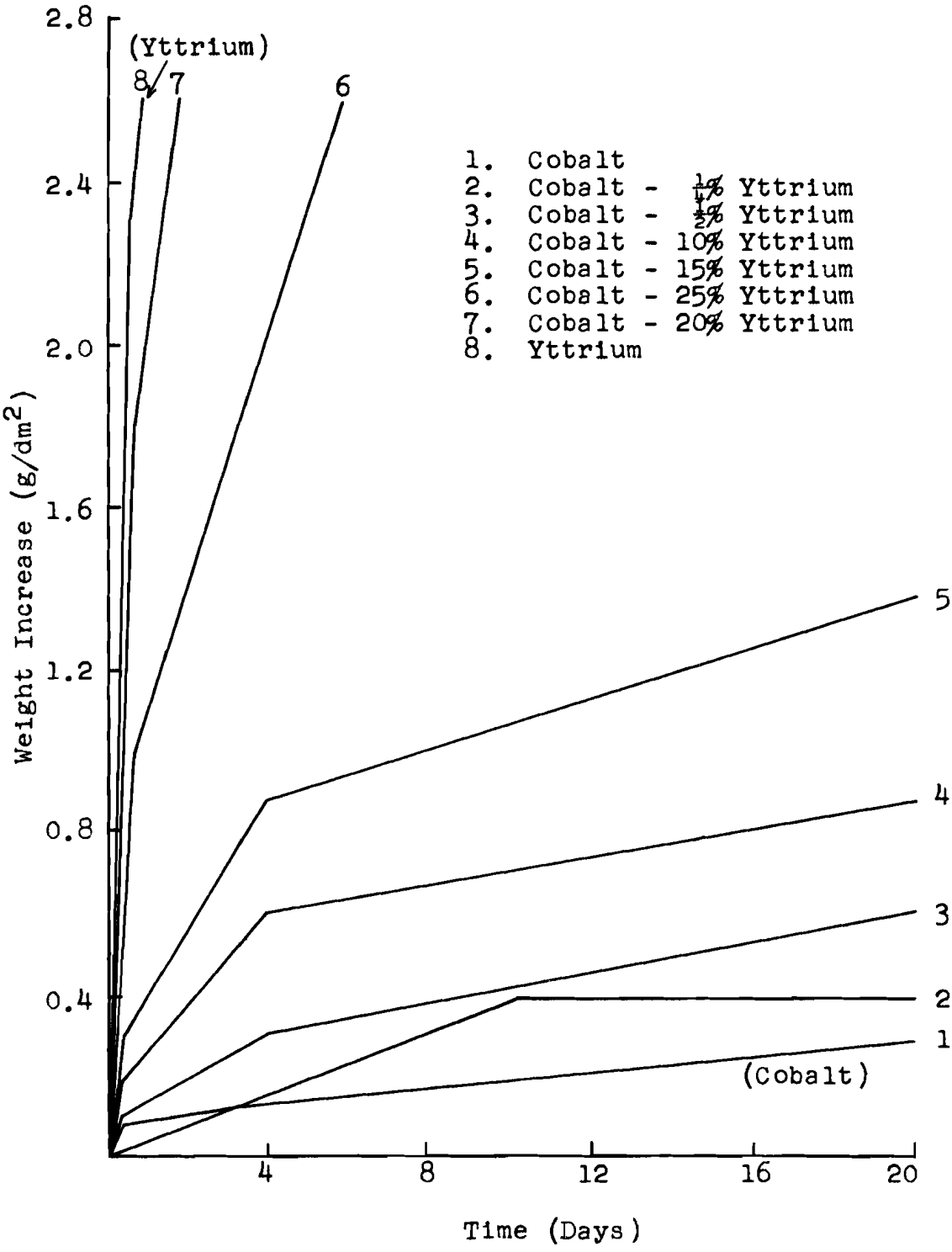

Figure 140. Atmospheric Corrosion in the Cobalt - Yttrium System. Dry Air at 600°C.

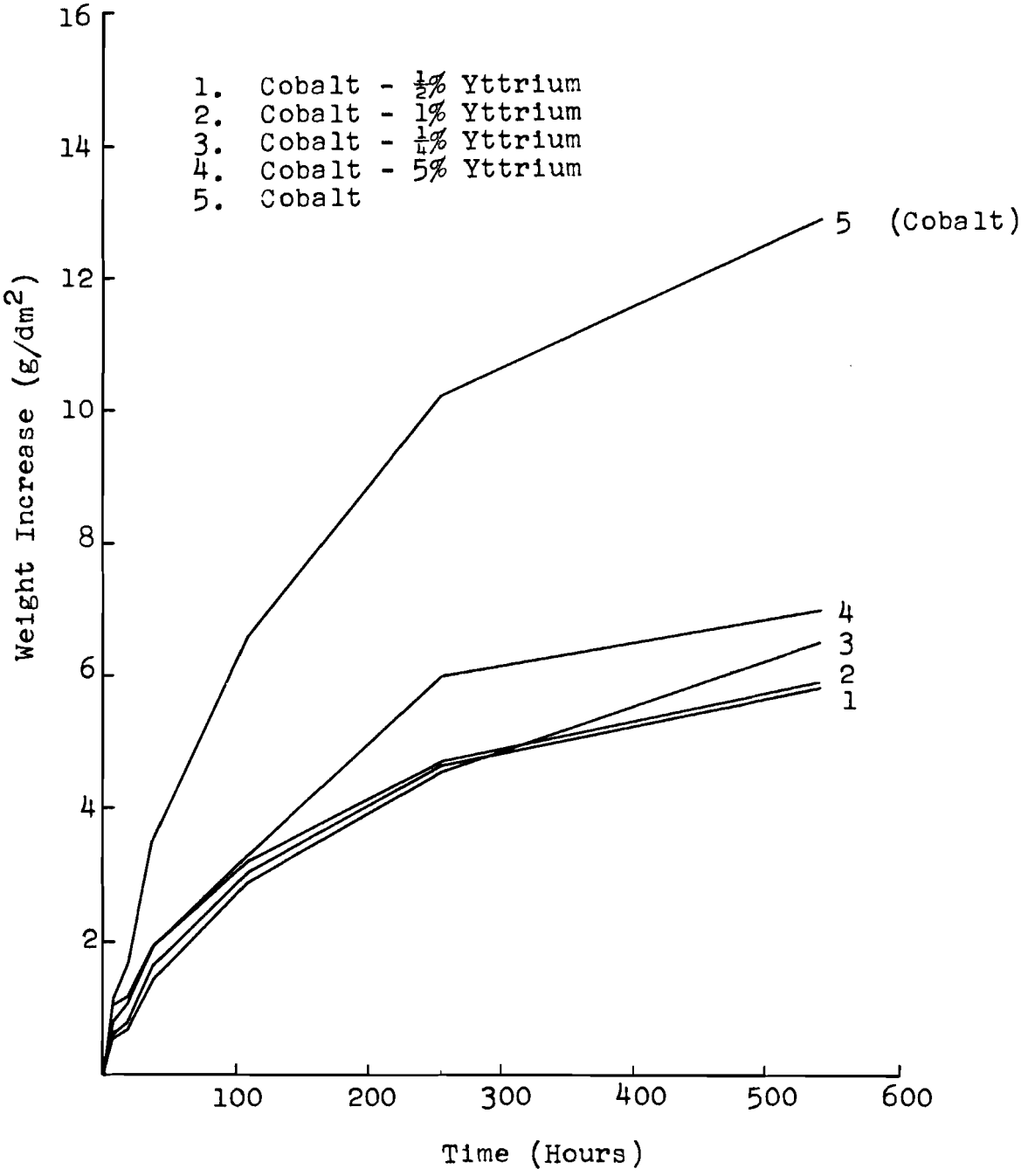

Figure 141. Atmospheric Corrosion in the Cobalt - Yttrium System. Dry Air at 900°C.

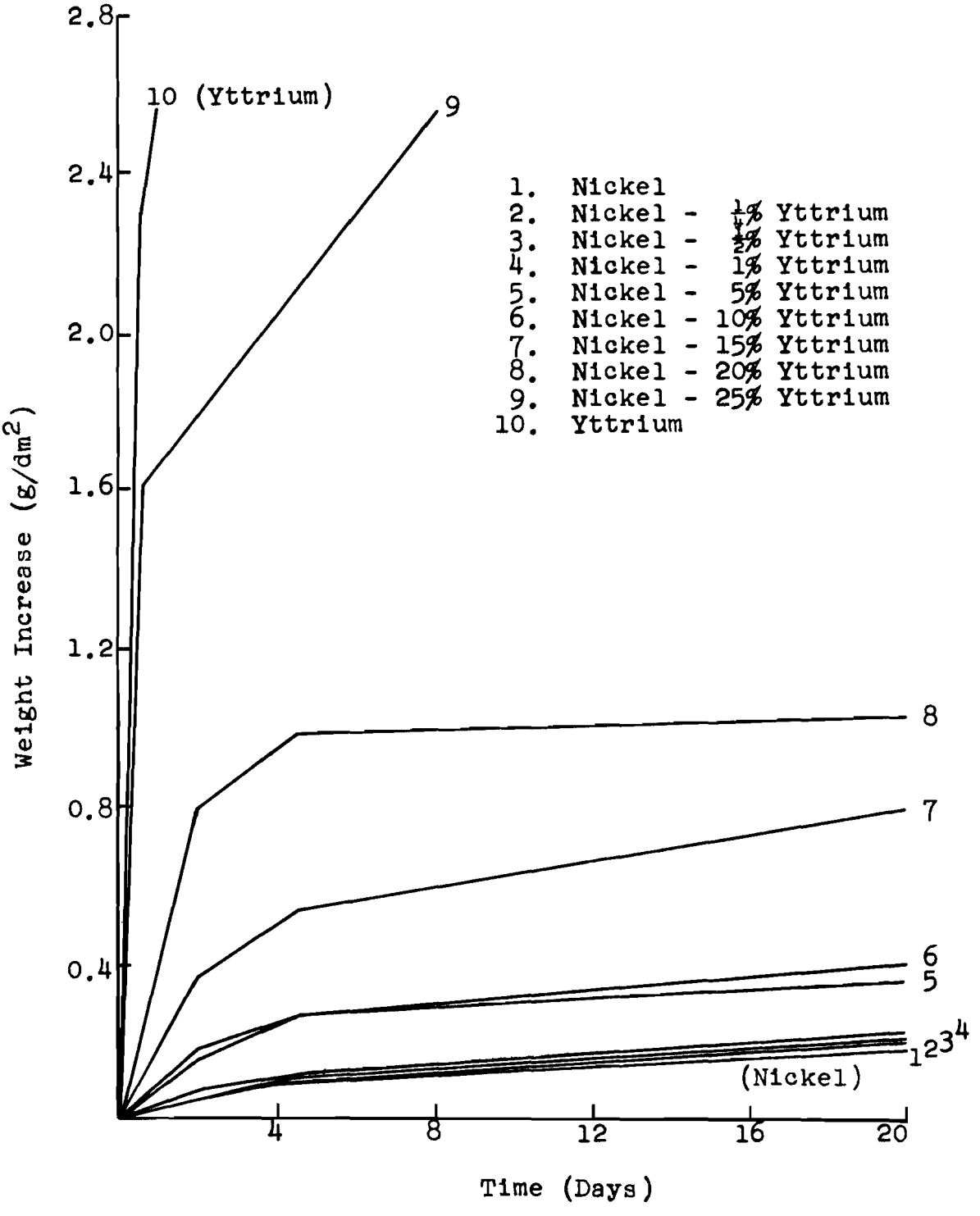

Figure 142. Atmospheric Corrosion in the Nickel - Yttrium System. Dry Air at 600°C.

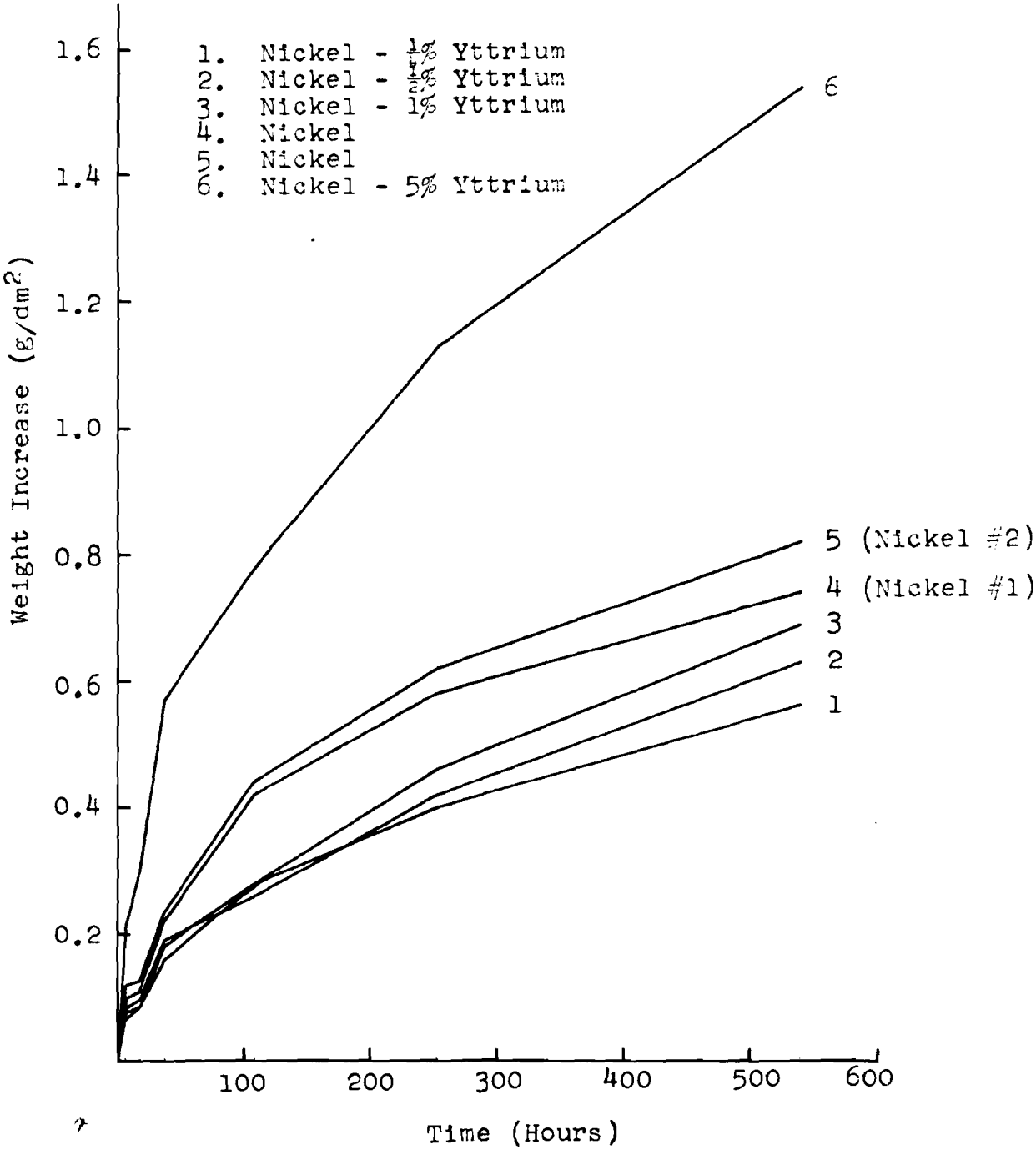

Figure 143. Atmospheric Corrosion in the Nickel - Yttrium System. Dry Air at 900°C.

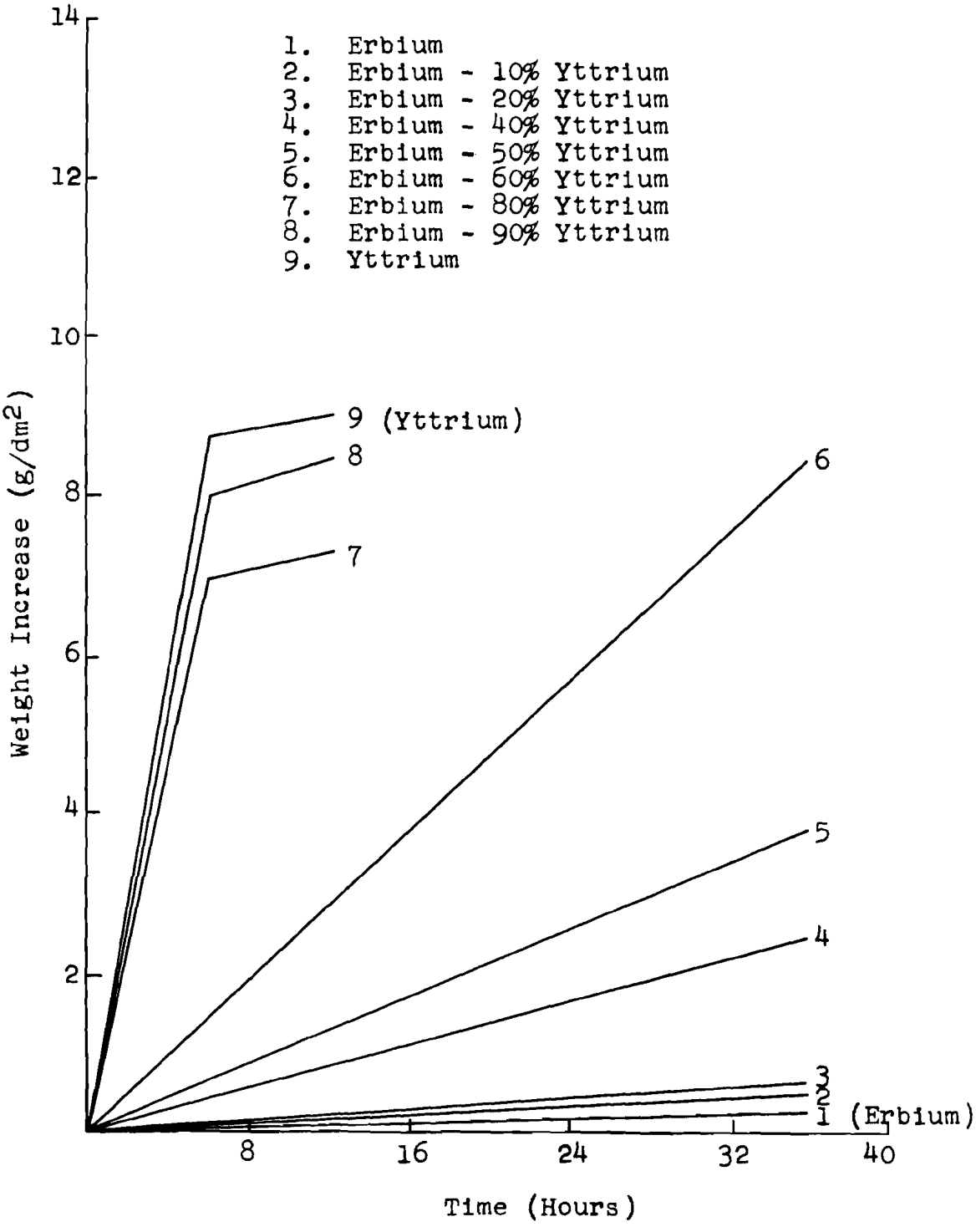

Figure 144. Atmospheric Corrosion in the Yttrium - Erbium System. Dry Air at 600°C.

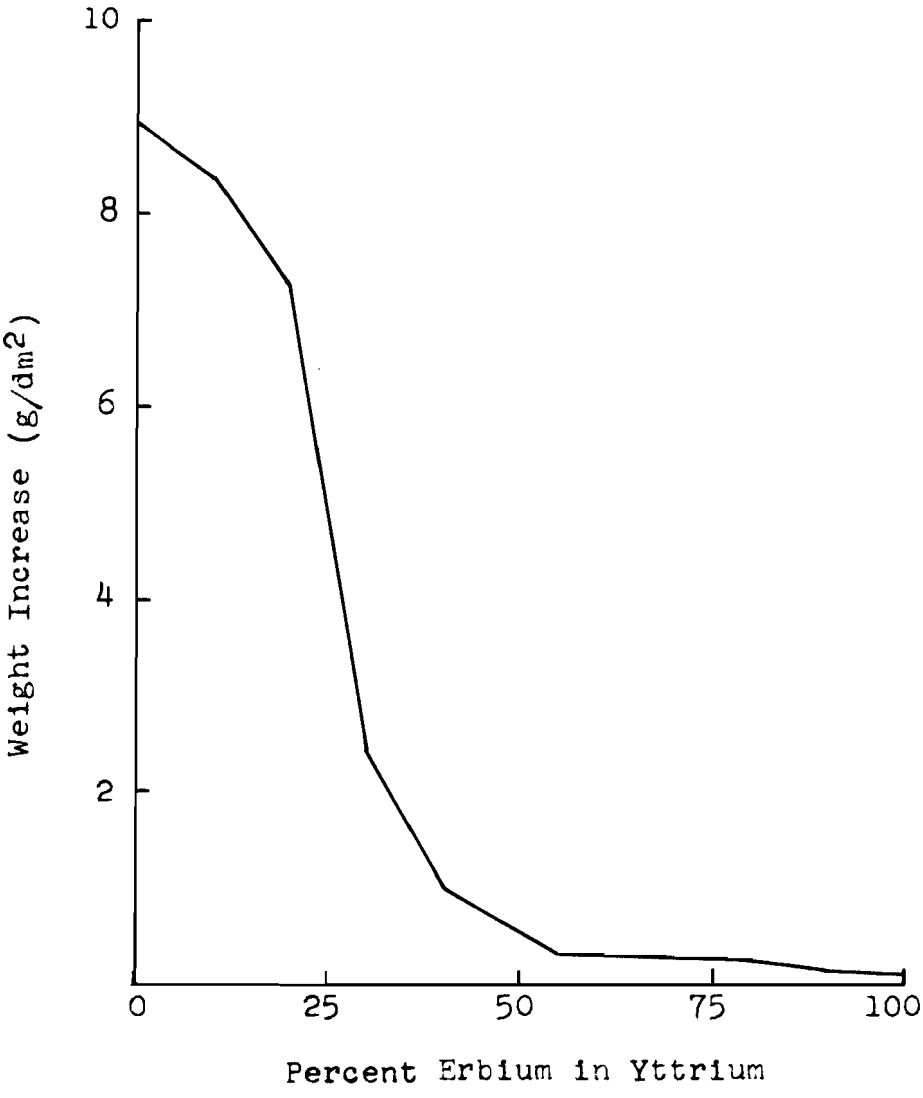

Figure 145. Atmospheric Corrosion in the Yttrium - Erbium System. Dry Air at 600°C after 12 Hours.

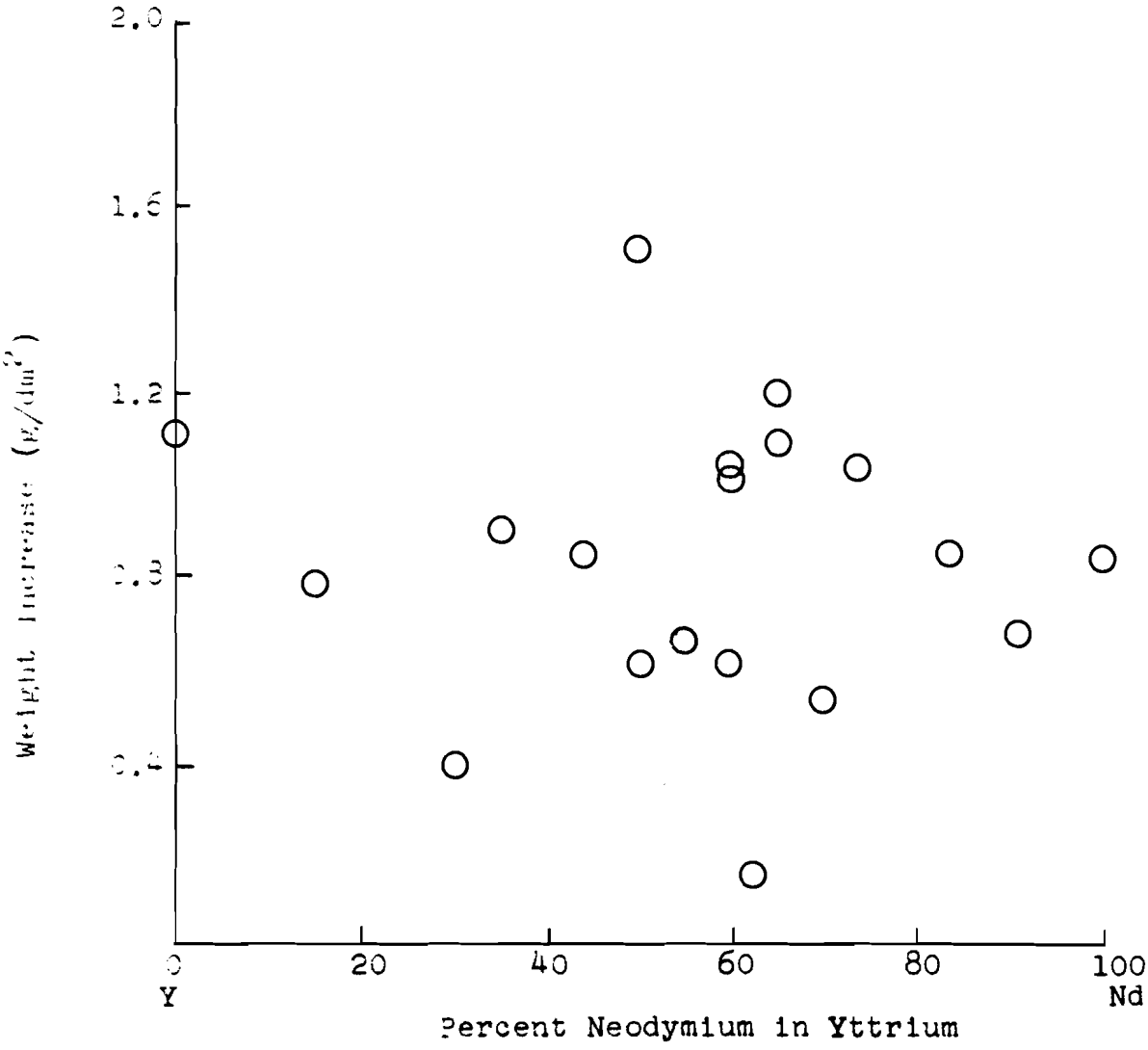

Figure 146. Atmospheric Corrosion in the Yttrium - Neodymium System. Weight Increase per Unit Area after Six Hours Exposure. Dry Air at 600°C.

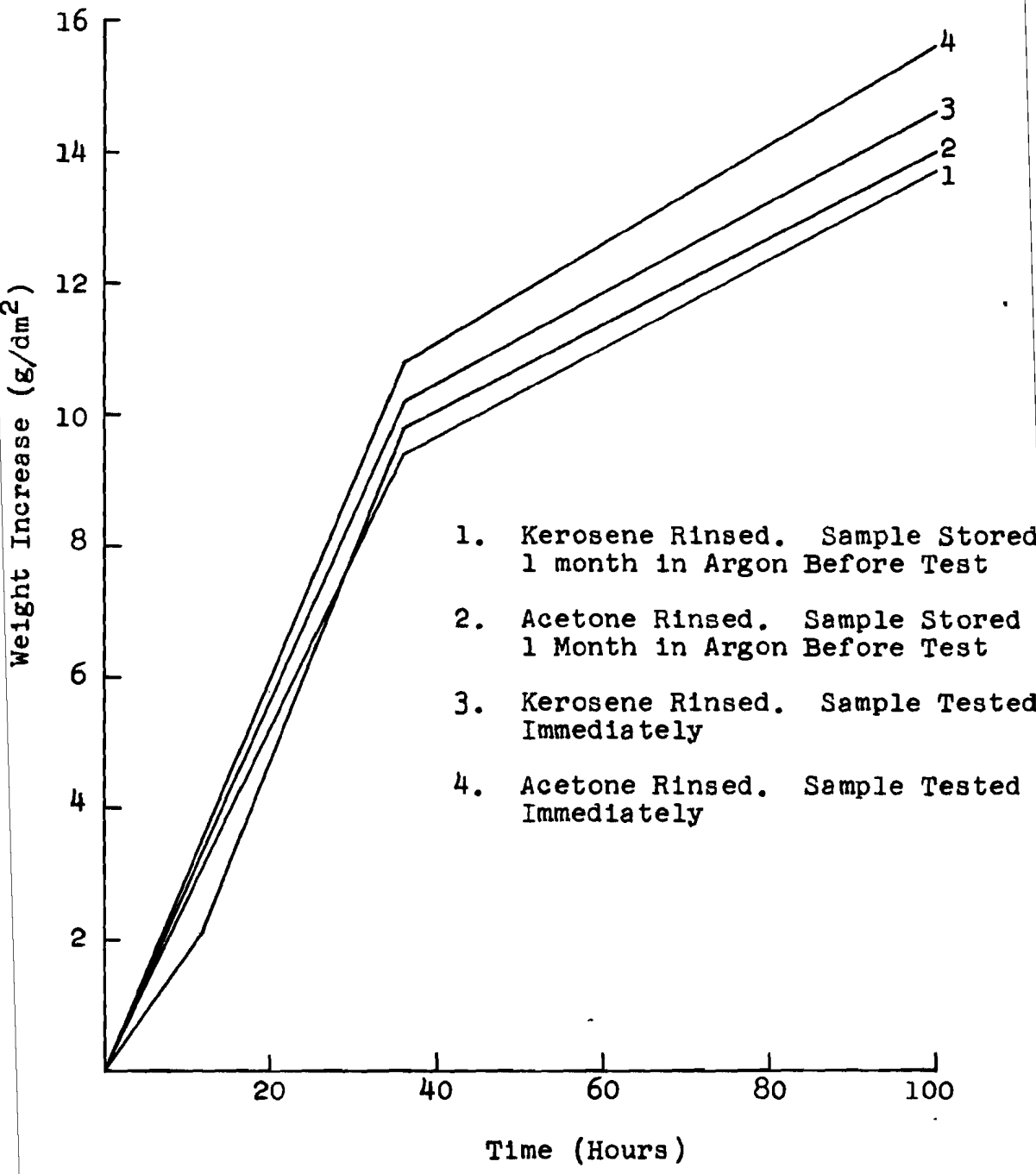

Figure 147. Atmospheric Corrosion of Yttrium Metal. Effect of Aging and Type of Solvent used in Final Rinse after Polishing. Dry Air at 600°C.

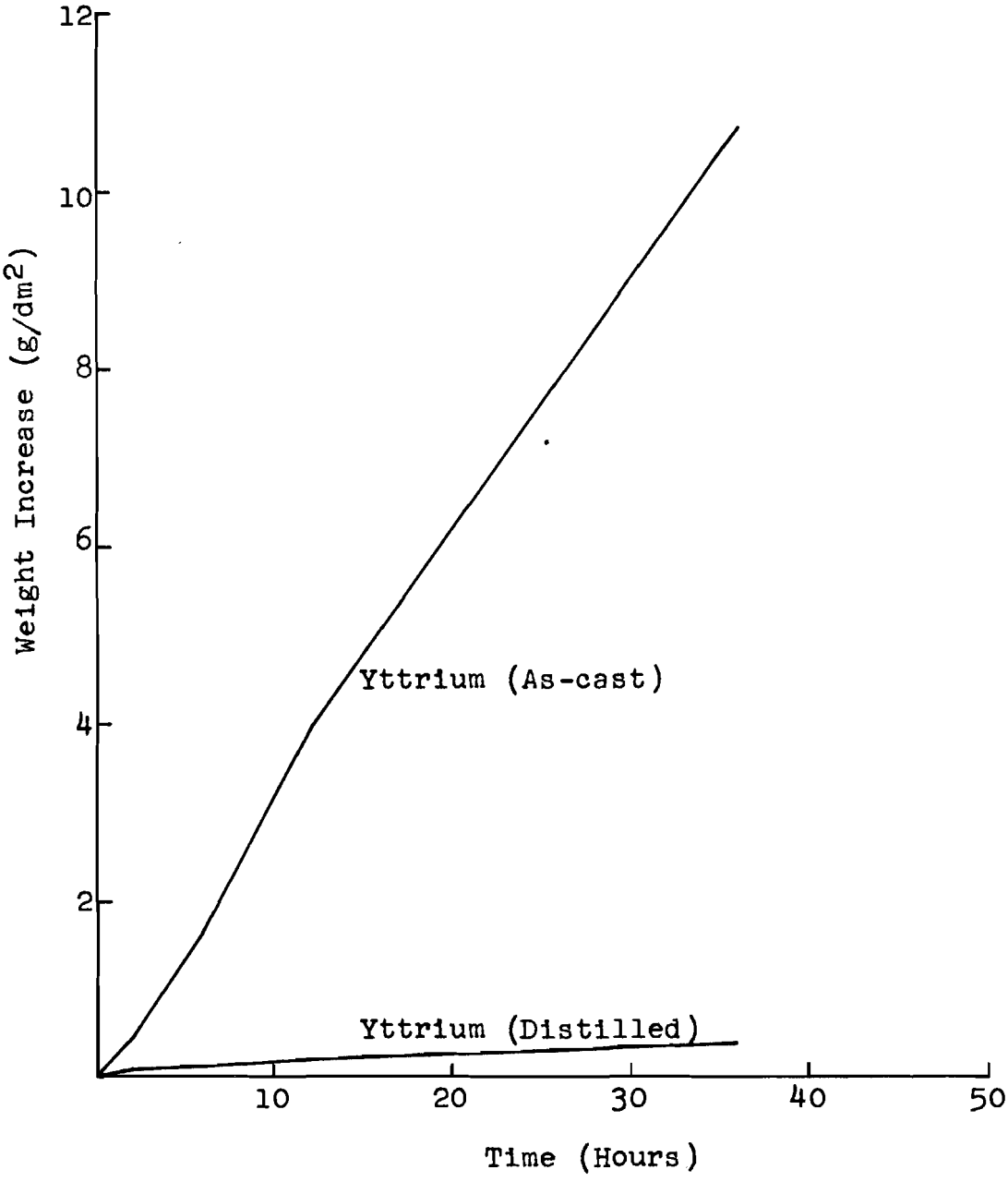

Figure 148. The Atmospheric Corrosion of Yttrium Metal. Dry Air at 600°C.

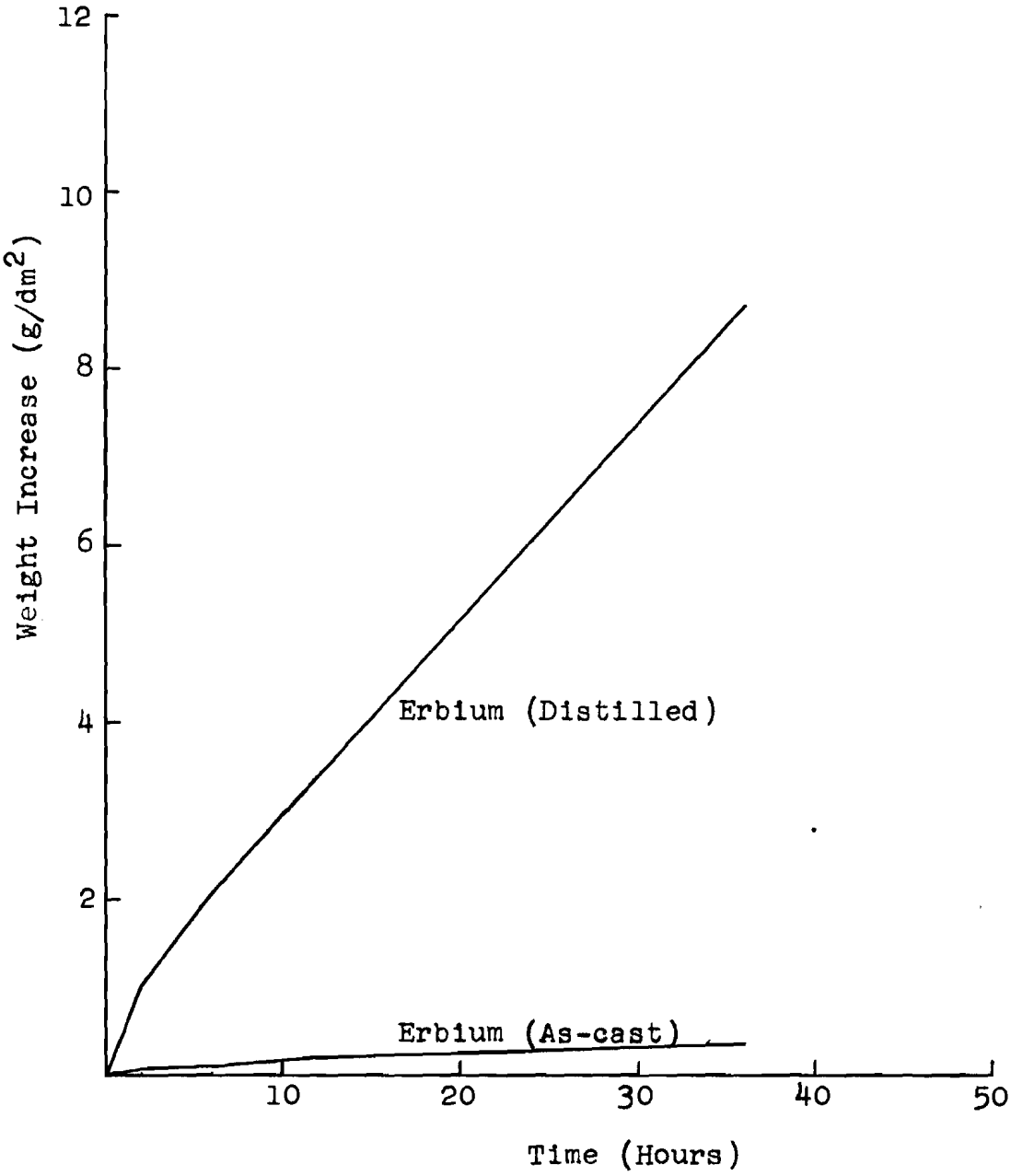

Figure 149. The Atmospheric Corrosion of Erbium Metal. Dry Air at 600°C.